Kinetic energy recovery system design and control of the braking vehicle system

A thesis submitted in fulfilment of the requirement for the degree of Doctor of Philosophy

By

Adnan Mohammed Saleem Alamili

B.Sc., M.Sc. Electronic

School of Engineering - Cardiff University

UK

December 2019

ABSTRACT

This PhD thesis presents a simulation of the dynamic energy recovery with an experimental-based model of the braking process. Accordingly, it describes the steps taken to develop a small-scale representation of the designed testing equipment, which was built within the laboratory boundaries to simulate the natural system. Moreover, it demonstrates the experimental probing and mathematical modelling of the system from an electronic perspective as well as in the mechanical perception as ready-made (black box) models. Meanwhile, the designed system shows an accurate representation in simulation, which was verified experimentally.

In this study, energy recovery with two distinct storage units, especially, ultra-capacitors (UCs) and battery energy storage systems (ESS) was considered as an alternative energy source with propulsion strategies to assess their effect on storing and generating electricity from the braking process. A simulation was determined to signal the system behaviour for different operating scenarios. Consequently, the voltage generated by a permanent magnet brushless direct current (PMBLDC) motor of the test network, when used as a generator in the braking operation, was used to study the impact of the uncontrolled charging loads (batteries and UCs) on the system performance in the braking process.

Furthermore, this research has proposed a new paradigm and regenerative braking (RB) algorithm. Taking the necessary information about the system from the flow rate correlated with two connected reservoirs to represent the charge flow rate in the RB mechanism. The dual tank's design was developed and used to describe the UCs' and the generator as a storage model. The variable generated voltage during the landing and braking process determines an important term, which is the generator capacity concerning the UCs' capacity. While modelling and analysis were primarily based on experimental results, many cases were examined to manage the best representation of the design. The outcomes were identified and discussed for both energy recovery

and downtime, which satisfy the design requirements and provide an accurate result regarding system performance.

Keywords

Regenerative braking (RB); Experimental-based model; Energy storage unit; Ultracapacitors (UCs); Battery energy storage unit; Ready-made (black box) models; Correlated tanks.

PUBLICATIONS

1- Alamili, A. et al. 2019. An experimental and analytical study of the ultra-capacitor storage unit used in regenerative braking systems. Energy Procedia 159, pp. 376–381. Available at: https://linkinghub.elsevier.com/retrieve/pii/S1876610218313687.

2- Alamili, A. et al. 2020. Laboratory-based examination of the effect of rotational inertia on energy recuperation in the regenerative braking process. Energy Reports 6, pp. 43–52. Available at: https://doi.org/10.1016/j.egyr.2020.02.026.

DEDICATION

To the memory of:

My Parents

And

My mighty martyrs

Salam & Mohammed Abdulridha Al-Asadi

Their souls have paradise and satisfaction

ACKNOWLEDGEMENTS

In the Name of Allah, the All-Merciful, the All-Compassionate

Above all else, I would like to give my gratitude to Allah the mighty, the all great without whom I could not have finished this instructive undertaking. Also, this research would not have been possible without the prayers of my deceased mother for her spirit of mercy and forgiveness.

Secondly, I owe the fatwa of Jihad and the martyrs of the Iraqi army in all its sectors and people's mobilisation **"Al-Hashd Al-Sha'abi"** who defended the homeland against the fanatical militants (ISIS). Without them, this work would have been not conceivable. Give this thesis to their noble souls.

I stretch out my sincere thanks and appreciation to the Ministry of Higher Education and Scientific Research/University of Kufa in Iraq for providing the opportunity to complete my higher studies and sponsoring and funding this research.

Thirdly, my genuine appreciation to Dr Yiqin Xue, for giving me confidence in this field of research. He is generous and patient, provides me with advice wherever I need, and to Dr Fatih Anayi to endorse the supervision in the third years, his collaboration and support gave me the tips that enhanced the progress and completion of this research. Also, my sincere thanks to Cardiff University, particularly all administrator staff in the research office, and I am appreciative to the IT the specialised staff of the School of Engineering for their help and support.

My heartfelt thanks to Dr Ali Al-Khafaji from the Southern Technical University in Iraq for his technical and scientific advice, and to Dr Raheem Al-Musawi from the University of Kufa for his generous support during my study.

My sincere thanks to Dr Ghanem Hamdan Lafta, previously he was the Directorate of Scholarships and Cultural Relations at the Ministry of Higher Education in Iraq to put on the first steps to complete my postgraduate study.

A special thanks to my dear colleague, Dr Bahaa Al-Mousawi from the University of Kufa, for encouraging me to undertake this challenge. Also, my thanks and appreciation to lecturer Ameen Al-Mudaffar, lecturer Gufran Habeeb, and Dr Osama Al-Hussaini from the University of Kufa. Also, special gratitude to my dear friends' Dr Yahya AL-Karagoly from the University of Babylon and Dr Safaa Al-Obaidi from the University of Baghdad for the cooperation and support. The words cannot reveal my sincere appreciation to them.

At long last, this research would not have been conceivable without the endless help of my family; my wife I would like to make you proud, and the debt of gratitude is for your understanding, sympathy and backing over the past troublesome years. Thank God for his grace; my adored sons Ali and Hassan, my dear brothers Akeel, Ali and Dr Ihsan and my sisters, my dear ones, and to anyone who did not forget me of supplication, my thanks and gratefulness for your support.

TABLE OF CONTENTS

Contents

LIST OF FIGURES

LIST OF TABLES

LIST OF ABBREVIATIONS

AI	Analogue Input
AC	Alternating Current
ACS712	Current Sensor
AO	Analogue Output
BB	Baghdad Battery
BCI	Battery Council International
BL	Brushless
Btu	British thermal unit
CC	Constant Current
CP	Constant Power
CSP	Concentrated Solar Power
CV	Constant Voltage
CW	Clockwise
CCW	Counterclockwise
CO_2	Carbon Dioxide
DAQ	Data Acquisition
DC	Direct Current
DIO	Digital Input/ Output
DoD	Depth of Discharge
DVSA	Driver and Vehicle Standards Agency
EBPMS	Electronic Braking Performance Monitoring Systems
EDLC	Electrochemical Double Layer Capacitor
EFVs	Environmentally Friendly Vehicles
EIA	Energy Information Administration
EM	Electric Motor
EMS	Energy Management System
EPA	Environmental Protection Agency
EVs	Electric Vehicles
ESS	Energy Storage Systems
ESU	Energy Storage Units
FESS	Flywheel Energy Storage Systems
FESU	Flywheel Energy Storage Units
FLC	Fuzzy Logic Control
GB	The Great Britain

GCE	Guidance of Community Energy
GUI	Graphical User Interface
GWe	Gigawatt electrical
GWh	Gigawatt-hours
HEVs	Hybrid Electric Vehicles
HWFET	High-Way Fuel Economy Test
ICE	Internal Combustion Engines
IEA	International Energy Agency
IEO	International Energy Outlook
IPM	Interior Permanent Magnet
ITC	Inland Transport Committee
JISHA	Japan Industrial Safety and Health Association
KCL	Kirchhoff's Current Law
KER	Kinetic Energy Recovery
ktoe	Kilotons of oil equivalent
KVL	Kirchhoff's Voltage Law
LabVIEW	Laboratory Virtual Instrument Engineering Workbench
L.S.b	Least Significant bit
LSR	Laser
M.S.b	Most Significant bit
MWh	Mega Watt-hours
NI	National Instruments
Non-OECD	Non-member Organization for Economic Cooperation and Development
OCV	Open Circuit Voltage
OECD	Organization for Economic Cooperation and Development
OGJ	The Oil and Gas Journal
OLEV	Office for Low Emission Vehicles
PEL	Programmable electronic load
PID	Proportional Integral Derivative controller
PMBLDC	Permanent Magnet Brushless Direct Current
PV	Photovoltaics
PWM	Pulse Width Modulation
RB	Regenerative Braking
Rb	Braking resistance
RE	Renewable Energy

SA	Simulated Annealing
SE	Sustainable Energy
SG	Specific Gravity
SoC	State of Charge
SPM	Surface Permanent Magnet
SUs	Storage Units
UDDS	Urban Dynamometer Driving Schedule
UK	The United Kingdom
ULEVs	Ultra-low Emission Vehicles
UN/ECE	United Nations Economic Commission for Europe
USB	Universal Serial Bus
VLS	vapour-liquid Solid
VR	Variable Reluctance
VV	Variable Voltage
WP.29	World Forum for Harmonization of Vehicle Regulations (a working party)

LIST OF NOMENCLATURES

A	A cross-sectional area of the tank, mm^2
Ah	Ampere-hour (1 Ah = 3600 C)
a_av	Average acceleration (m/s^2)
acc_nr	Number of acceleration (unitless)
acc_rate	Acceleration per km (/km)
a_neg_av	Average negative acceleration (m/s^2)
a_pos_av	Average positive acceleration (m/s^2)
a_pos_sd	The standard deviation of positive acceleration (m/s^2)
a_sd	The standard deviation of acceleration (m/s^2)
Btu	British thermal units (1 Btu = 1055 joules)
b	Viscous friction coefficient (Nms. /rad)
C	Damping coefficient (Ns/m)
C_d	Discharge coefficient
C_{ro}	Rolling resistance coefficient
dist	Total driving distance of the driving pattern (m)
E_{back}	back (or counter) electromotive force (emf) (V)
E_{gen}	Generated voltage (V)
E_{kin}	Kinetic energy (J)
E_{th}	Thermal energy (J)
E_{UCs}	Stored energy in the UCs (J)
$i_{UC(t)}$	UCs current (A)
$i_{UC(t)/char}$	UCs charge current (A)
$i_{UC(t)/disch}$	UCs discharge current (A)
m	Mass (kg)
Stop_rate	Stops per km (/km)
stop_T_av	Average stop duration (m)
F_f	Friction force (N)
GWe	Total capacity (Gigawatt-electric)
GWh	A measure of electrical energy, 10^9 watt-hours
I	Electric current (A)
i_a	Phase current of rotor winding (A)
$i_{a,b,c}$	Phase current vector
J	Moment of inertia (kgm^2)

K_a	Motor constant (Nm/A)
$L_{a,\ b,\ and\ c}$	Phase a self and mutual inductance of the rotor (H)
M	Mutual inductance between rotor-rotor windings (H)
p	Number of poles
P_{batt}	Input power to the battery (W)
P_{rot}	Rotational power (W)
PKE	Positive kinetic energy (m/s^2)
r_a	The resistance of the rotor winding (Ω)
$R_{a,b,c}$	The phase resistance (Ω)
RPA	Relative positive acceleration (m/s^2)
RCS	Relative cubic speed (RCS) (m^2/s^2)
RPCS	Relative positive cubic speed (m^2/s^2)
RPS	Relative positive speed(unitless) (m^2/s^2)
RPSS	Relative positive square speed (m/s)
RRCS	Relative real cubic speed
RRS	Relative real speed (unitless)
RSS	Relative square speed (m/s)
RMSA	Root mean square of acceleration (m^2/s^2)
$L_{a,b,c}$	The self and mutual inductance (H)
S_1	Speed at which the UCs stope charging (rpm)
Stop_nr	Number of stops (unitless)
T	Time (s)
T_{acc}	Drive time spent accelerating (s)
T_{brake}	Time spent braking (s)
T_{charge}	Charging time (s),
T_{cruise}	Cruise time (s)
T_{dec}	Drive time spent decelerating (s)
T_{drive}	Driving time (s)
t_e	The electrical time constant (s)
T_{em}	the air gap torque (electro-mechanical) (Nm)
t_m	The mechanical time constant (s)
T_{stop}	Standing time (s)
T_{total}	Total time (s)
UCs	Ultra-Capacitors (F)

t_1	The initial time of each braking interval (s)
t_2	The final time of each braking interval (s)
Td	Derivative time of PID controller (min)
Ti	Integral time of PID controller (min)
T_l	Load torque (Nm)
toe	A tonne of oil equivalent (equal to 11.63 MWh)
T Wh	A measure of electrical energy, 10^{12} watt-hours
U_{DC}	DC link voltage of the inverter (V)
v	The velocity of the object (m/s)
V_1	Initial vehicle speed of each braking interval (km/h)
V_2	Final vehicle speed of each braking interval (km/h)
$\overline{v}_{drive}$	Average driving speed (km/h)
Vs	The supply voltage (V)
v_sd	The standard deviation of speed (km/h)
$\overline{v}_{trip}$	Average speed (trip) (km/h)
$v_{UC(t)}$	UCs voltage (V)
V_{UC-ini}	UCs initial voltage (V)
V_{UC-fin}	UCs final voltage (V)
ω_m	Rotational speed (rad/s)
W	Electric energy (J = W s)
% acc	% of time accelerating
% brake	% of time braking
% cruise	% of time cruising
% dec	% of time decelerating
% drive	% of time driving
% stop	% of the time standing
τ	The RC time constant (sec)
η	Efficiency ($\eta = p_o/p_{in}$) (unitless)

Chapter 1
Introduction

In recent years, there have been growing concerns about issues related to global warming and limited fuel resources (Ehsani et al. 2009; Erdinc and Uzunoglu 2012). The environmental impact of the oil transport infrastructure combined with the sudden depletion of oil reserves has raised institutional interest and led to the trend of rising demand and dependence on electricity and sustainable energy on account of carbon dioxide emissions. Also, an alternative form of sustainable energy has prompted broader interest, especially in the recovery of energy from wasted energy. This interest has been reflected in an increased focus on various industrial applications, for example, utilising electric transport, which uses the electric motor as a propulsion engine (Nehrir et al. 2011; Tie and Tan 2013). One of the essential characteristics of using the motor as a propulsion engine in electric vehicles (EVs) and hybrid electric vehicles (HEVs) is low maintenance, low noise, and no carbon emissions (Clarke et al. 2010). Therefore, the demand for batteries in EVs and HEVs has widely increased as an alternative energy source compared to fuel to mitigate the environmental pollution problem and fuel crisis (Muradov and Veziroglu 2012). Subsequently, there has been an expanding need to supplant the traditional mechanical, hydraulic, and pneumatic braking with electronic systems that depend on power electronic converters and electric motor drives (Chicurel 1999; Bao 2015).

1.1 Background

The concept of using electric motors for driving was created after the invention of the motor itself. Robert Anderson, between 1832 and 1839, invented the first electric car model, which worked with primary non-rechargeable cells (Guarnieri 2011a). Then, Gaston Plante invented the first rechargeable lead-acid battery in 1859, and around 1881, Camille Alphonse Faure made it a marketable product (Guarnieri 2011b). The first commercial vehicle put on the market, for example, in New York City was an electric taxi in 1897. After three years, EVs accounted for 28% of road vehicles and were the preferred type (Yong et al. 2015). However, EVs confronted a significant challenge after a decade of use. In 1908, fuel-powered vehicles, such as the

Ford T-Series by Henry Ford, emerged onto the market. In 1912, the development of the electric starter by Charles Kettering prompted the end of the requirement for an arm to start the fuel-powered vehicles (Denton 2004). Besides, the accessibility of cheap petroleum resulted in the lower utilisation cost of fuel-powered vehicles compared with EVs.

On the other hand, EVs could travel only relatively short distances, and there were limited charging stations. Because of these aspects, fuel-powered vehicles were generally accepted. Thus, by around 1935, there were no EVs on the road (Yong et al. 2015; Un-Noor et al. 2017). However, a few decades later, the issue of emissions of fuel-powered vehicles and rising oil prices lead to renewed interest in EVs. Therefore, governments were implemented regulatory actions to reduce air emissions and promote the development of EVs and HEVs.

The regenerative braking (RB) process was increasingly being used as an energy recuperation system for a variety of applications, including elevators and conveyor belts as well as in the transport and automotive sectors (Zhou 2008). RB was a procedure to restore energy, depending on slowing down the vehicle or an object by transferring the kinetic energy into another form adequate for storing until needed. In this circumstance, for instance, vehicles were driven by electric motors do most of the braking by utilising the motor as a generator to produce electricity that was then fed into the onboard vehicle's energy storage systems (ESS) (Bolund et al. 2007; Clarke et al. 2010; Yoong et al. 2010). This process was an improvement on conventional braking systems, where the surplus kinetic energy was turned into heat by friction and therefore squandered (Tur et al. 2007; Midgley and Cebon 2012). ESS was one of the essential innovative fields of work in numerous industries. However, additional information is required on the behaviour of ESS at different operation states to broaden the range of applications for RB as an alternative energy source, which could then be used to utilise the generated electricity. Likewise, generator modelling as the primary source of generated power should be tested in an efficient representation in the RB application to fulfil its operation (Gupta et al. 2008). While batteries gave the tremendous advantage of high energy density (Yuan et al. 2011), their restricted life

cycles, charge and discharge cycle, and management constraints reduce their adequacy in a specific application.

In contrast, ultra-capacitors (UCs), which were devices with much-extended life cycles where the power density runs through charging and discharging sequences, were frequently used with high currents and over a short period to assist the battery in accomplishing the energy density of the cells. The UCs offer extended lifespans and no environmental issues (Grbovic 2011). The feasibility study has been involved in modelling the overall design and building of a test rig to represent the RB process, which was one of the main contributions. Also, studying and modelling of the generator and the UCs as an energy storage unit in the braking analysis. The priority has been given to charging UCs in ESS through a variable voltage generated by braking and power management to enhance efficiency as recommended by this research.

1.2 Community energy project

As directed by the guidance of community energy (GCE) of the UK government, who were interested in developing a community energy project, there were various aspects to tackling challenging the issues around energy, including the collective effort to reduce, manage, and generate power (EIA 2017). Therefore, it was used to determine the reason for its evaluation to add a global perspective to its mission and programs, which can be carried out as follows:

1.2.1 Fleet management essentials

One key segment of a growing knowledge base was the comprehension of common issues, which was viewed as vital for sustainable fleet management and included a range of simple strategies. These strategies have been added knowledge for different aspect such as managing the fleet sustainably, encouraging alternatives, and driving cleaner ultra-low emission vehicles (ULEVs) (Office for Low Emission Vehicles 2013). There were many case studies of the online self-service tools offered by in-depth consultancy services in England and Scotland, which has covered the various approaches,

such as mileage management, vehicle choice, and managing vans and light commercial vehicles.

1.2.2 Electric cars and vehicles

There was government support for EVs, in addition to programs to meet organisational goals, in the form of additional vehicle grants to achieve a global perspective or global awareness. The office for low emission vehicles (OLEV) has a list of eligible vehicles based on their carbon dioxide emissions for proficient driving in electric and low discharge (Office for Low Emission Vehicles 2013). On the other hand, the guidance on electronic braking performance monitoring systems (EBPMS) can be used to observe the braking performance of commercial vehicles and to measure the development of drivers from a global perspective (Agency [no date][a]). Furthermore, the driver and vehicle standards agency (DVSA) has prepared a general determination and foundation which traces the best testing administration for commercial vehicle braking performance. This testing was utilised to overcome a number of the challenges and constraints of the current service brake guidance for trailers in the UK that meet the goal (Agency [no date][b]).

1.3 Motivation

Compared with the 336 TWh electricity produced in the UK in 2016, there were 324 TWh supplied to the grid. Gross production comprised 21.4% nuclear, 42.5% gas, 9.2% coal, 0.5% oil, and 24.5% from renewables (11% wind, 3% solar PV (a technology for converting sunlight into electricity), 2.3% hydro and pumped storage, and 8.9% biofuels including waste). Increased renewables generation capacity was depending on less favourable climate conditions for solar and wind generation (Association 2018).

There was a significant difference between developed and developing countries. For example, in Iraq, the primary source of energy relies heavily upon oil reserves, with approximately 94% of its energy needs to be met by petroleum, which was the pillar of the economy. The total installed electricity

capacity in 2008 was 7.20 GWe with 51% thermal, 26% gas turbine, 21% hydroelectric, and 2% diesel plant (Information Portal - reegle 2012). Meanwhile, in 2009, Iraq produced 46,063 GWh of electricity and consumed 33,223 GWh; in the same year, the renewable share of electricity production was 0.8%. Furthermore, the total primary energy supply in 2009 was 32,175 ktoe (the international energy agency (IEA) defines one tonne of oil equivalent (1 toe) as 11.63 MWh), with 96% oil, 3.0% gas, 0.9% hydro, and 0.1% biofuels and waste. With these ratios, alternative energy, and the exploitation of wasted energy have not been used.

Concerning to the oil and gas Journal (OGJ), Iraq ranked fifth in proven crude oil reserves at the end of 2017. It had approximately 149 billion barrels, accounting for 18% of proven reserves in the Middle East and about 9% of global resources (World Oil Review. 2018). Furthermore, the burning of natural gas due to insufficient pipelines and the other intermediate infrastructure associated with the extraction process, although needed, was imported from abroad to address the issue of part of the power plants, which were the basis of its work. Iraq burns crude oil directly at power plants to compensate for limited raw materials from other types of power generation. Figure (1.1) shows the electricity generation and distribution losses in Iraq in the years 2000-2015 (U.S. Energy Information Administration (EIA) 2019).

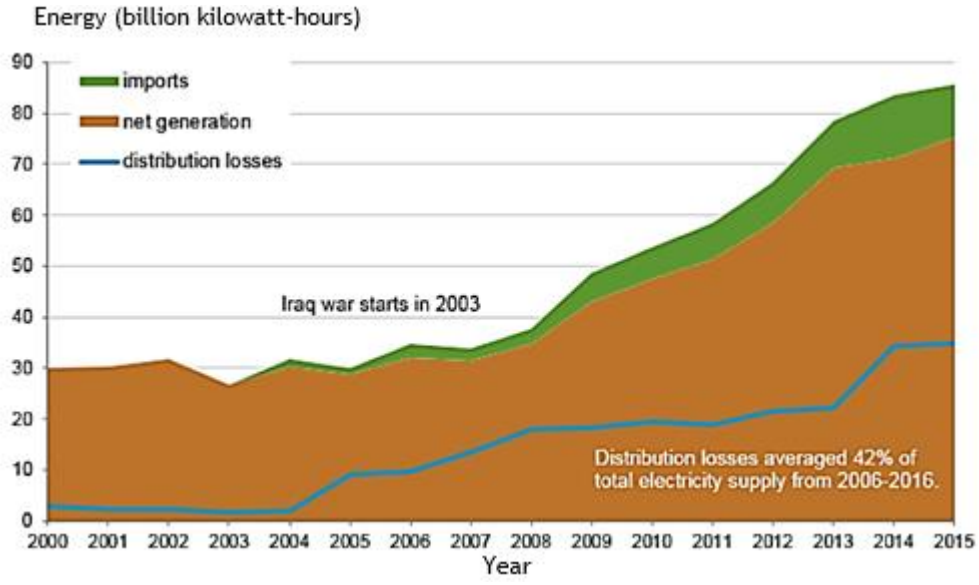

Figure 1. 1: The net electricity generation, imports, and distribution losses in Iraq

Therefore, despite all challenges (due to the depletion of the global strategic oil reserves), there it was still an aggregate reliance on oil as a leading source of power. Also, studies in this area, despite their importance, rarely reach the level of ambition. This research used to delve into the analysis (as in the developed countries), of various fields of studies. Also, for investment and for deriving benefit in particular of one form of energy, which was represented as the energy generated by the braking process, used to reduce oil consumption and mitigate global warming.

The kinetic energy recovery (KER) system was an automatic system to restore the kinetic energy of a moving vehicle during braking. The recovered energy was stored in the storage units (SUs) (e.g., flywheel, UCs, or batteries) for later use with acceleration. There was an urgent need to represent this application within the limits of a laboratory that can simulate the natural system. Thus, the different components have been utilised to implement the braking system in the designed test rig.

The most economical scheme of recovered energy in the automotive industry was with the RB system (Chishty and Melis 2012; Long et al. 2014). The simulation must be validated by experimenting with the designed test rig so that the model can be upgraded to represent the actual behaviour of the performing system. These components were being generally used for different applications, such as in a sustainable energy infrastructure, which benefits from specific SUs applications and energy management (EMS) (González-Gil et al. 2013). The EMS system operation aims to invert and monitor the movement of current from and to different SUs (Herrera et al. 2016). This research has attempted to highlight the overall system performance of the complete building test rig and to verify the designed circuit to ensure the capability of using the RB system approach efficiently in the subsequent stages.

1.4 System under analysis

The most widely recognised type of RB has included an electric motor as an electric generator. The power generated was bolstered once more into the supply system such as being stored chemically in a battery, electrically in the UCs, mechanically in a turning flywheel, and in other different forms. A test rig was modelled and constructed to be used to satisfy these research purposes. At the first stage, the existing platform suffered from a different deficiency, which led to it being redesigned following the steps to develop it starting from the model. This model has contained two types of electrochemical storage units and a permanent magnet brushless direct current (PMBLDC) motor connected with the flywheel and other components. From the experimental data and calibration equations of all elements, the construction of an entire simulation was done under the "LabVIEW" environment to represent the system.

Furthermore, an energy storage unit must be durable and able to handle high power efficiently, and any additional energy transmission or conversion equipment must be efficient, compact and cost-effective. The proposed framework should be able to customise and highlight different characteristics based on the control objective and the nature of the system's behaviour. If there was enough empirical or operational data, an alternative to physically-based modelling was a data-based "identification system" that can be applied to virtually any system. This identification system generally provides relatively simple models that can describe well system behaviour within a specific operating condition. These models can be "black box", which only represents the behaviour of input and output or other descriptive interiors, such as state-space equations, which can explain physically meaningful judgments. The primary objective task of modelling was to obtain a useful and reliable apparatus that can be used for the requirements of analysis and control of the RB process. Moreover, the full circuit test was utilised to assess the feasibility and evaluation of the energy recovery process. Therefore, there was a more significant effort to define further analysis of the power management scenario to determine the improvement in system efficiency.

1.5 Significance of the study

Due to the energy crisis and the climatic conditions, many researchers have dealt with this topic (Ahn et al. 2009; Midgley et al. 2013; Papanikolaou et al. 2013). The feasibility and leverage of the implementation of RB systems and renewable energies that can reduce fuel consumption and reduce gas emissions associated with urban vehicles had been explored. The study has taken two axes: firstly, to circuit design, and secondly to realise for KER. The research findings had added the knowledge and the understanding of the subject of the design and control of energy transfer through different SUs from a recovered energy resource. The RB system should have the necessary attributes to succeed and should be significant in the sense that it has to cover many aspects, including the following:

- increased awareness between the integration of the system design methodology and the hypothetically designed system that represents the actual behaviour of the system
- a system identification concept for the framework of the energy manipulation system
- support and enrich the theory and model of the controlling objective
- useful knowledge of the factors that could influence and contribute to the successful adoption of an EMS system design and control strategy
- simple control system for connection to transmission bus
- energy transformation proficiency
- high capacity with energy storage units
- high performance: In a short time, large amounts of energy can flow
- the smooth flow of electricity from the regenerative equipment, and
- absorbing and storing of braking power that is directly proportional to the braking with minimal delay and loss over a wide range of road speeds.

1.6 Thesis aims and objectives

The energy recovery system was recognised as a useful introduction to problem-solving related to global warming as well as a shortage of energy resources. Hence, an increased effort in determining the basic structure of energy harvesting from descending and braking was a crucial determinant of system power enhancement. An efficient representation was provided for each circuit component, considering its operation, from the experiment, and it was implemented in a simulation.

1.6.1 Research questions

1. When designing and building the RB test rig, the following questions were raised:
    - What factors need to be considered to represent an ideal system?
    - What is the best way to determine the required level of accuracy for the designed system?
    - How to represent the variation in the generated voltage in the braking system?
    - How can KER be represented in the system? What is the factor that affects their behaviour?
    - What is the impact of the SoC variation in the storage units due to driving characteristics (acceleration and speed) on the energy absorption of the vehicle?
2. What techniques should be used for EMS to enhance the recovered energy, and what is the level of efficiency?
3. What are the values of the maximum recovered energy and the minimum stopping time in the design stage?
4. How can regularly drive cycles (UDDS, UN/ECE, etc.) be represented in the test rig to emulate the entire system?

To ensure that these questions are answered regarding the required recovering energy and stop times, this research focuses on the designing an

efficient system which can handle the energy generated from the braking resource and stored in different SUs.

1.6.2 Research aims

The fundamental aims are:

1) To develop a practical test device capable of representing the system under study, which serves to harvest energy from brake loss and bridge the gap in the literature.
2) To simulate the system using mathematical equations and to find the best and more straightforward representation.
3) To exploit system data obtained from the experimental tests, to represent the behaviour of system components. Also, it is likely to be of increasing interest and significance in the future.

1.6.3 Research objectives

In doing so, the research objectives can be summarised as follows:

- The establishment of a test bench for the EMS and the RB system used to meet the requirements of the application for which it was designed.
- Capture the available brake power and store it in the energy storage units as needed to accelerate the vehicle (motor in the test rig).
- Create a virtual system within the "LabVIEW" simulation environment.
- The development of a comprehensive analysis of recovered energy was introduced.
- Ensure that the system was safe, lightweight, cost-effective, easy to execute and accumulates.
- Achieving the required level of performance that necessitates new developments in both the design system and the associated control electronics, and thus answering the research question (1).
- Specific factors that contribute to the designed system and see how these factors can be organised, thus answering research questions (1 and 2).

- Highlighting any other results of interest and contributing to the topic, and thus answering the research question (3).
- Applying regular driving cycles to the designed test rig, thus answering the research question (4).

1.6.4 Assumption and Limitations

The research assumption and limitation can be summarised as follows:

A direct model of interaction with the dynamic differential equation of the system (represented by the designed flywheel, which acts as a hollow cylinder directly connected to the shaft of the DC motor) used to service the system under study. Presumably, the ideal situation was that the linear motion of the motor has not considered. And it was also accepted that the vehicle has one motor connected with the gear transmission and that the ratio can be specified. Additionally, there was no friction brake for the blended braking strategies, which was recommended for future work.

1.6.5 Delimitations

The energy recovery system works only when the vehicle (motor) is in motion. Also, RB is of great benefit only during frequent braking, and the same electronic control unit must control the recovery system.

1.7 Thesis contributions

The motivation behind the examination displayed in this thesis was to contribute towards the better understanding and prediction of electricity generated based on the RB process and energy recovery enhancement by considering the system operation as a black-box model. It was necessary to predict and to monitor the storage units during the braking process to achieve this objective. Also, this thesis has been provided knowledge of the way the generated electricity, which affects the stored energy. Modification of a system should be considered to simulate and to enhance the process. Following the better understanding of the mechanical (such as the flywheel

stored energy) and electrical perspective of the designed test rig, a newly proposed technique was used. This technique relies upon to measure the generator capacity during the process, as current approaches show compatibility with system behaviour as has been presented in the following chapter. Lastly, it was also necessary to investigate the influence of the battery SoC on the electricity generated by the system.

The following research tasks have been identified to achieve the overall objectives,

Task 1: Designing and building test apparatus.

Task 2: Development of a mathematical model of energy storage systems (i.e., the UCs and the batteries).

Task 3: SoC monitoring.

Task 4: Measurement of KER from the mechanical storage unit.

Task 5: Investigation of the enhancement of the recovered energy.

1.8 Thesis structure

The organisation of the dissertation can be presented as follows:

Chapter (2) begins with a review of the literature, which provides a basic understanding of energy harvesting from braking and prose in modern transportation. Besides, the evolutionary history of EVs and HEVs was briefly reviewed, including primarily a review of the current trends and research in energy recovery associated with the development of the RB process. In this chapter, the current knowledge gaps that affect the representation of the process being analysed. Finally, the results were informative for the future development strategy of existing methods allowing the determination of recovered energy, and their limitations were described in the context of the designed test bench.

Chapter (3) presents the driving train used in the drive system with an analytical analysis of electric propulsion systems and the theory identified with the test apparatus used to meet and validate the designed circuit.

Furthermore, regular drive cycles were addressed to emulate real system behaviours. Besides, an introduction to various drive cycles was processed with the kinematic measurement developed to measure the RB process. The utilisation of monitoring signals was analysed, which can be used to study the mechanical behaviour of the machinery during the regenerative process. A complete understanding of the power system hardware, including an explanation of various power electronic converters, was required to design the test bench with a summary of the component configuration described in the next chapter.

Chapter (4) explains the core information for the experimental setup; in particular, the electric propulsion system, PMBLDC motor drives, which were provided with a case of RB application case were studied. The basic construction, operating principles, control and handling characteristics were described from an application that analyses the operating principle of the flywheel energy storage systems (FESS) as a mechanical SUs. The principal purpose of this chapter was to provide the basic knowledge of the circuit components of the designed test rig that were essential for understanding the vehicular drive train design and RB analysis. Also, it involves power and an energy analysis study to estimate and manipulate the energy saved during the braking process. The different case was used to describe the actual value of the reasonable stopping time and the recovered energy.

Chapter (5) focuses on identifying and modelling various energy storage technologies, including batteries and UCs, which extend the conventional approach in the literature, to assess the use of this data extracted from experiments. Subsequently, experimental work was reported to discuss the implications of the proposed formula for determining the generator capacity in terms of SUs capacity. Next, theoretical, and empirical studies were conducted which illustrate the conventional method of determining the energy recovered during RB.

Chapter (6) provides a summary of the research work completed in this thesis. The main findings and the original scientific contributions of this thesis were also highlighted, and the recommended areas for future work were outlined.

Chapter 2
Literature Review

The purpose of the vehicle's brake system, as an example, was to slow down and stop the moving vehicle and keep it plugging hard. The designed brake system must meet the standards, expectations, and the regulations to provide maximum confidence that it was safe in any situation with minimal environmental impact. The literature review was intended to identify information on the design and operation of regenerative braking (RB) systems, to obtain the benefits of the kinetic energy stored in the rotating object during stop rather than wasted as heat. The RB was aimed at recovering part of the kinetic energy and converting it into electrical energy which can be reused and stored for later acceleration purposes. This chapter covered the revision of the literature to manage the gap in energy harvesting and held from the braking activity. The main parts of this chapter aim and objectives focused on reviewing the various methods of energy resources used for electricity generation including braking and gave the advantage and disadvantages of each approach to determine the best economic procedure. Also, it was implemented to represent and to study the storage units used to store the energy generated by different strategies, including the brake system in terms of circuit modelling and analysis. Furthermore, by the laboratory design test rig, information was used to achieve the desired research objectives for the RB and energy saving.

2.1 Background

As claimed by the U.S. energy information administration (EIA), the international energy outlook (IEO) 2017 energy consumption, divided the world regions according to the organisation for economic cooperation and development (OECD) members, and (non-OECD) non-members. The world energy utilisation has increased by 28% between 2015 and 2040 with more than a half attributed to Asia non-OECD (including China and India) due to economic growth, as shown in Figure (2.1) (EIA 2017).

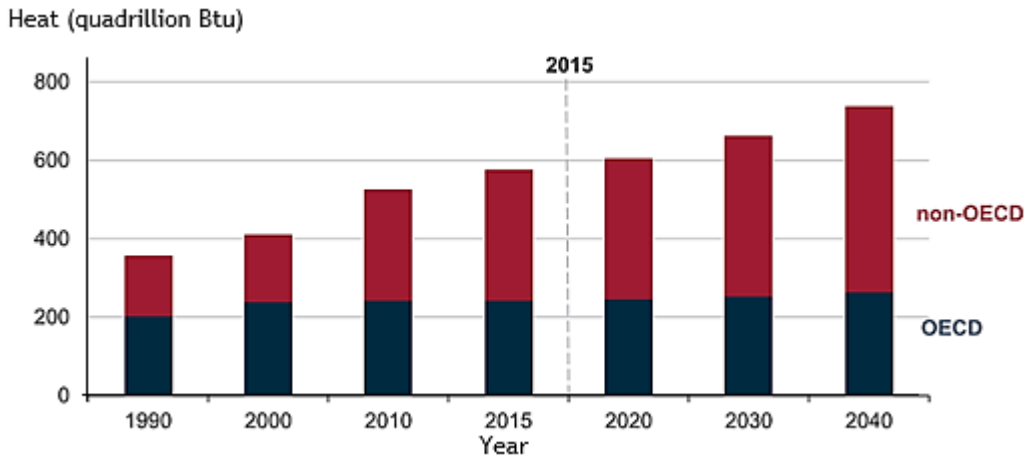

Figure 2. 1: Word energy consumption

The world energy consumption raised from 575 quadrillion British thermal units (Btu) in 2015 to 663 quadrillion Btu by 2030 and after that to 736 quadrillions Btu by 2040, as shown in Figure (2.2) (EIA 2017). In non-OECD regions, Asia leads the most world energy consumption for fifty years time duration.

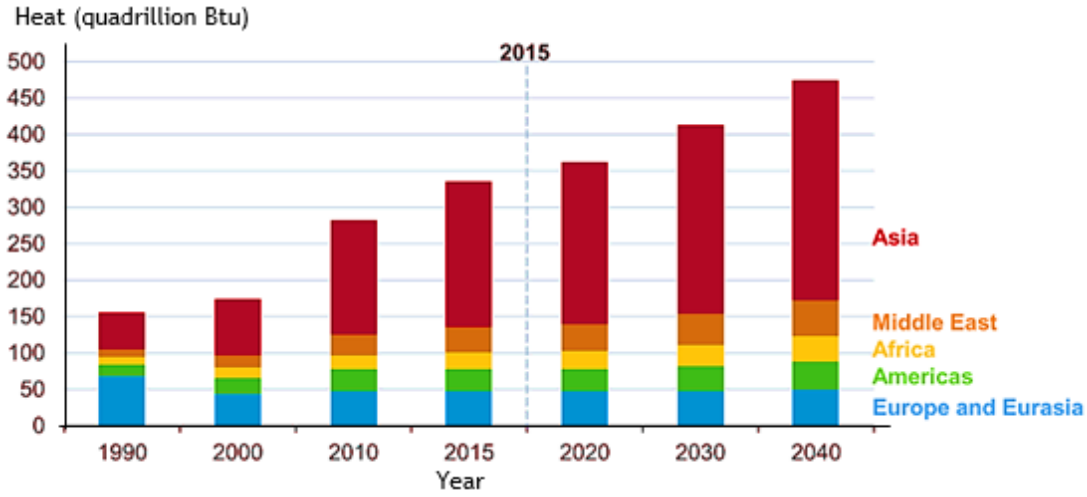

Figure 2. 2: Energy consumption by sector

The automotive industry has been distinguished as having the speediest development among ventures in the current industrial applications. However, different technical regulation concerning vehicle emissions and environmental measures have been introduced to improve vehicle fuel efficiency, promoting low exhaust emission, and reinforcement to the development of next-generation environmentally-friendly vehicles (next-generation EFVs) (UNECE 2012). Different approaches achieved this constraint that has been proposed to accomplish this goal.

Furthermore, the United Nations economic commission for Europe (UNECE) concerned with economics, statistics, transport, trade, environment, habitat, and sustainable energy which offered a regional framework for the preparation and coincidence of conventions, norms, and standards. The UNECE inland transport committee (ITC), supports the international movement, aims to improve safety, energy efficiency and security in the transport sector which provides rigorous information on the world forum for harmonisation of vehicle regulations (WP.29) (UNECE 2012).

On the other hand, from the electronic perspective; studying the designing of the electronic circuit has become an essential part of electronic subsystem dominated automotive improvement and contribution in this field (Chong 2010). Electronic engineering proceeds at a quick rate where researchers have been anticipated to preserve their knowledge and practical experience to incorporate with the new subject areas such as in industrial transport application (Delsing et al. 2016; Enterprise and Munich 2016). So, there have been many papers about this topic showed that the internal circuitry has an essential functional parameter in the system performance, and significantly affected by the influence of the circuit operations (Hanselman 2006; Ehsani et al. 2010; Roscher and Sauer 2011; Un-Noor et al. 2017). Though, some of them investigated the general idea without dealing with its paramount in the overall system design tool. The use of appropriate analysis strategies and connected research has depicted as a need. Review all useful data available in braking configurations, power sources, electrical machines and charging techniques, provides an overview of existing technology and future development forms to assist future research.

2.2 Types of energy resources

The law of energy conservation expresses that the total energy of an isolated system cannot be changed; it was said to be maintained over time. Energy cannot be created nor destroyed but can be changed from one form to another (Moran et al. 2018). Therefore, the braking was a complete loss; when generating heat, it becomes difficult to reuse. The energy recovery mechanism slows vehicles or objects down by converting its kinetic energy

(E_{kin}) into another energy form, which can be reused or stored until needs (Clarke et al. 2010). Also, the efficiency in the RB process can be enhanced if it was possible to restore maximum energy from vehicle brakes to the energy storage units (ESUs), which has improved vehicle efficiency and also tackle gas emissions (Chiara and Canova 2013; Li et al. 2016). While the rechargeable energy storage system (ESS) has been taken as a problem-solving for the lost energy, has a wide variety of uses in propelled the EVs and HEVs (Sakka et al. 2012; Fleurbaey et al. 2014).

Most of the literature focused on restored energy and controlled topology. RB can be considered a set of different subsystems. The essential parts of these subsystems interact with each other, and their contribution to the total system was clarified (Emadi and Ehsani 2001; Chiara and Canova 2013). So, there was a gap in the circuit performance of the designed circuit in the operating conditions. Therefore, to verify its activity and to meet the required accuracy, a new procedure (dealing with the system as a black box) was proposed to model different components in this research.

In the next section, an introduction to a different type of energy resources used for electricity generation and the critical issue related to conservative energy from braking energy strategy was discussed.

2.2.1 Sustainable energy (SE)

Environmental impact and climate change through the use of traditional fossil fuel-based energy technologies have had a significant effect on the local and regional environment (Basha et al. 2009; Joerissen and Frey 2009). It has mainly explained by the considerable growth of carbon dioxide in the atmosphere (Midgley and Cebon 2012). Instead, alternative energy-efficient technologies from natural flows such as solar radiation and the wind have been considered environmentally neutral and may provide clean energy for an indefinite period (Ekren and Ekren 2010; Singh 2013). Also, so far, we do not have technology without harmful effects on the environment; some of them have much fewer undesirable results and more control. By moving from the use of firewood as a source of cooking and the provision of heat to the use of wind energy in transport, and later, as a source of mechanical energy in the

first machines, renewable energy (RE), played a vital role in the development of the pre-industrial era (Turkenburg 2010).

Several studies have tended to the analysis of various regions related to the RE. Each source of RE system (solar, hydroelectric, biomass, wind, ocean and geothermal) has the characteristics that make it especially appropriate for some load types in different applications. Also, several topics have always been put together to find the variance between RE being dispatchable (with a high conveyance capacity if necessary) and being variable (low conveyance capability). From these studies, several types were covered by the SE resource, which was energy production that can continue for the prospective future.

2.2.1.1 Solar and wind energy

An assortment of solar energy, such as solar heat, solar photovoltaic (PV), solar thermal energy and solar fuel, provides a clean, highly abundant and comprehensive resource for humanity (Dufo-López and Bernal-Agustín 2005; Singh 2013). Solar energy was the transformation of sunlight into electricity, either directly using PV power or using indirect concentrated solar power (CSP). The control programming method was used to control the solar tracking system. Singh (2013), in his study, suggested that the two-axis tracking program, for an instant, produces an increase in the daily collection of 41.34% compared to 32^0 fixed surfaces (Singh 2013).

Further, wind turbines were captured the kinetic energy of the wind and convert it into a usable form of energy. Wind power systems can be categorised as follows; independent (stand-alone), mixed (hybrid), grid-connected (Rashid 2018). Small-scale combination, as an example, including small wind turbines, and PV solar panels with a rechargeable battery can supply a reliable source of electricity to a commercial building or home (Fernando et al. 2019). Different factors affect power generation (p), such as an increase in wind speed (v), which can be calculated as $\mathrm{p} = 0.5\,\rho \mathrm{A} \mathrm{v}^3$ (Masters 2004; Zhou 2009). According to Díaz-González et al. (2012), which pointed out several benefits for the operation of the power system,

considering wind power plants that can be achieved (Díaz-González et al. 2012).

2.2.1.2 Ocean waves energy

Ocean power (hydropower) was another form of SE that uses large amounts of energy within the ocean's tides to generate electricity. It can be classified into three main ways: ocean wave, tidal and ocean thermal energy. All three methods can be installed as land or marine applications (Rashid 2018).

Zuo and Tang (2013) covered the importance of capturing energy from the ocean waves with an extension of kinetic energy from surface waves and potential energy in the natural oscillations of ocean waves which have been converted into electrical energy (Zuo and Tang 2013). The mechanical kinetic energy absorbed by the waves was moved to the turbine to push the shaft of an electric generator (rotary generators) in different ways. The linear motion generator, which can be driven directly by energy absorption or by device movement, and rotary generators produce variable frequency and alternating voltage with varying capacity (Khaligh and Onar 2010). Besides, ocean wave energy (thermal gradient) technology have been examined in terms of energy converter by O'Sullivan et al. (O'Sullivan et al. 2011). With the theoretical and experimental studies indicate that up to 90% of wave strength can be extracted under certain conditions (Khaligh and Onar 2010). Therefore, the energy of ocean waves can be converted efficiently into electrical energy.

Although energy production has been intermittent, the tidal power scheme produced by the surge of ocean waters will slightly reduce the need for a thermal station (A.Laughton 2003). Furthermore, the tidal current was not influenced by the variation of climate, lack of rainfall or melting. Therefore, harvesting energy from the tides was practical due to the predictable and uniform flow (Roberts et al. 2016). Also, the environmental and physical effects and pollution problems were negligible. Tidal energy, in combination with the electrolysis of water, can be used for hydrogen production and desalination applications. However, tidal power generation was an immature technique that needs further research and development (Rashid 2018).

2.2.1.3 A mixed combination of power generation

One form of energy enhancement was by considering the combination of different energy topology. Nehrir et al. (2011), employed a blend of two or more related power generation technologies in the design and power management with storage units. Due to the intermittent nature of many RE resources such as wind, solar, and ocean wave have been used to enhance system performance, and reduce system cost (Nehrir et al. 2011). Hybrid PV panels and wind were the most profitable solution to consolidate traditional energy sources. The attributes of these sources of being productive and stable are possible because of their complementary nature compared to independent energy systems (Sawle et al. 2017).

Protogeropoulos et al. (1997) provided a general methodology for the size and improvement of RE supply systems, including hybrids such as those containing PV and wind power components (Protogeropoulos et al. 1997). Later that studies on the simulated annealing algorithm (SA) is implemented to optimise the size of the hybrid PV and wind power system with battery energy storage (Ekren and Ekren 2010). Moreover, according to Erdinc and Uzunoglu (2012), the optimal size of these hybrid systems based on RE has significantly improved the economic and the technical performance of energy supply, as well as promoted the widespread use of these environmentally friendly sources (Erdinc and Uzunoglu 2012). In (2014), Kusakana, in his study, analysed a detailed analysis of the optimal sizing approaches for enhancing system economy (Kusakana 2014). Consequently, an optimal mixed configuration of the colony of ants was presented with an artificial bee colony an algorithm called the ACO-ABC hybrid algorithm to determine the optimal location and size of distributed energy resources in the distribution systems (Kefayat et al. 2015). In contrast, Maleki et al. (2015) described the performance of various particle swarming algorithms to determine the optimal size of the hybrid system (PV, wind, and battery), based on the repulsions factor with the constriction factor, and the inertial inertia weight (Maleki et al. 2015).

Intelligent control systems, backed by adequate energy storage systems and energy transmission infrastructure, help the RE to meet energy requirements

in different sectors (Passino 2001). However, asymmetry in wind, sun, and clean energy resources can create technical barriers or costs to integrate with the grid at high penetration levels (20% or more) (Turkenburg 2010). To reduce or overcome these barriers, critical approaches in the electricity sector include improvement of network infrastructure, increased transport capacity, use of demand measures to move loads, and the development and implement of energy storage technologies (Turkenburg 2010).

Furthermore, design of hybrid systems used to solve complexity due to the uncertainty of the RE supplies; the load requirements and the nonlinear properties of several components were provided using optimisation methods that use the genetic algorithms (Dufo-López and Bernal-Agustín 2005). Gupta et al. (2011) analysed an integrated economic, technical analysis of the model hybrid of the energy system to supply the load of remote rural areas (Gupta et al. 2011). Meanwhile, Sangpanich (2013), addressed the potential optimisation of wind-solar energy systems by using low-speed wind turbines to improve rural electrification optimisation of weak wind speed turbines. Solar system technique has also been used to enhance rural electrification (Sangpanich 2013). System integration studies have not revealed a baseline for the share of renewables in local, regional or global energy supplies (Sen et al. 2017).

2.2.1.4 Geothermal energy

The use of geothermal energy at high temperatures to produce electric power began experimentally in Larderello, Italy, in 1904; the first commercial station (250 kW e) was available in 1913 and connected to the grid (Turkenburg 2010). Thermal energy was renewed from the deepest layers of the earth; therefore, it was not depleted (Rashid 2018). Some geothermal power plants have utilised the steam from a tank to power a turbine/generator. At the same time, different stations have used high temp water to boil fluid that evaporates and afterwards runs the turbine. High temp water can be used near the ground surface directly to warm the buildings, the plantation in greenhouses, drying crops and various industrial processes (Geothermal. 2013).

2.2.1.5 Biomass energy

Another type of SE is biomass. Wright et al. (2010) examined biomass based on hydrogen fuel production, which affords various categories and measures of cooling and heating services (Wright et al. 2010). However, there were some significant problems in adding biomass to the hybrid system as an energy source. The first obstacle was defined as providing fuel and a continuous supply of this system. The second most important was pollution and emissions from burning biomass fuels. The biodiesel produces, for the most part, carbon monoxide, carbon dioxide, nitrogen oxides, sulphur oxides and fume. It was concluded that the tests with oil-bearing crops; the emission of non-burning hydrocarbons and the emission of nitrogen oxides from the engine were more significant in all fuel mixture than diesel (Basha et al. 2009).

2.2.1.6 Hydroelectric energy

Hydroelectric power has great potential to provide energy management to the world (Khaligh and Onar 2010; Upadhyay and Sharma 2014). Hydropower generators can be utilised as motor pumps to force water from the tail tank to the head tank and store it at a high level using the off-peak power grid. During peak demand, headwater has run generators to meet demand. The typical cycle of energy efficiency can be 75%. There are more than 90 GW of storage facilities that are supplied all over the world (Abu-Rub et al. 2014).

2.2.2 Energy recovery from vibration and vertical movement

Waste energy Recovery and use (conservation) was a significant opportunity to reduce primary energy, improve energy efficiency, and to reduce emissions for the global industry. Zhu (2011) presented that the harvesting of machine vibration energy, which includes electromagnetic, piezoelectric, electrostatic, and tuneable vibration energy harvesters, was based on spring-mass damping, and was linear energy collectors (Zhu 2011). On the other hand, the different technology consists of collecting energy from the vertical movement of the vehicle which can be achieved from the throw during acceleration and deceleration, the movement of the wheels when crossing

the pits, and the unevenness of the road. However, it was not as large as the horizontal kinetic energy. Research has devised the automotive suspension system to capture the vertical motions (Hoo 2013). Zhang et al. (2016) developed a simulation model and applied energy analysis to capture kinetic energy for vehicle suspension vibration (shock absorber) (Zhang et al. 2016b).

2.3 Braking methods in the drive system

Braking was the process of controlling the speed of an object by preventing its movement (Liudvinavičius and Lingaitis 2007). A moving object has kinetic energy (E_{kin}), which must be eliminated by dissipating it into the outside through friction or by transferring it into another form of energy at stopping, followed energy conservation principle. There were several solutions to integrate brake control into the application (Han et al. 2011). Sangtarash et al. (2008) discussed three main brake control strategies, which including sequential braking with a better sense of brake, subsequent braking with optimal power and brake recovery, and parallel braking. Next, brake performance and fuel economy were studied for each method and compared to the other products in the driving cycle. In contrast, in a drive cycle such as Nuremberg, the use of these strategies can restore 30%, 36% and 15% of the total electric power produced (Sangtarash et al. 2008).

The braking of machines driven by electric motors, such as in EVs and HEVs, was necessary to reduce or cease the speed of engines for system correction and safe operation (Murthy et al. 2015). Most functional braking was achieved by using electrical braking to ensure smooth operation by following the speed time profile and allowing restoration of the E_{kin}. However, for safety and emergency brakes, mechanical brake systems remain essential brakes to ensure system stability when not in use (Gao et al. 2007; Liu et al. 2011; Mutoh and Akashi 2011; Murthy et al. 2015).

Depending on a different type of engines, and regarding their properties, there are various methods of braking. The structural classification of braking systems of electric motors has been mainly completed through two strategies according to different researches (Davis et al. 1990; REN 2010; Mutoh and

Akashi 2011; Chishty and Melis 2012; Xie et al. 2012; KELJIK 2013; Alamili et al. 2019). The methods of braking can be categorised as:

- non-regenerative, where the source supplies electric energy to give braking, or,
- regenerative, where the E_{kin} of the rotor was transformed into electricity and get back to the power source.

In the following section, different approaches have been studied and analysed to get an exceptional understanding of the study involved in this research.

2.3.1 Mechanical (friction) braking systems

Most EVs and HEVs braking systems depend on hydraulic braking technology in which the E_{kin} was converted into heat during braking, resulting in an energy waste (Kapoor and Parveen 2013). The essential operation of the conventional braking system was depended on friction to counteract the forward momentum of a moving motor. The E_{kin} dissipated as thermal energy (E_{th}) into the air by applying resistance to the moving parts of the system using the usual brake disc with shoes that were employed by weights, springs, and electromagnetic or pneumatic power as shown in Figure (2.3), squandering motor's produced energy (Tushnet 2000).

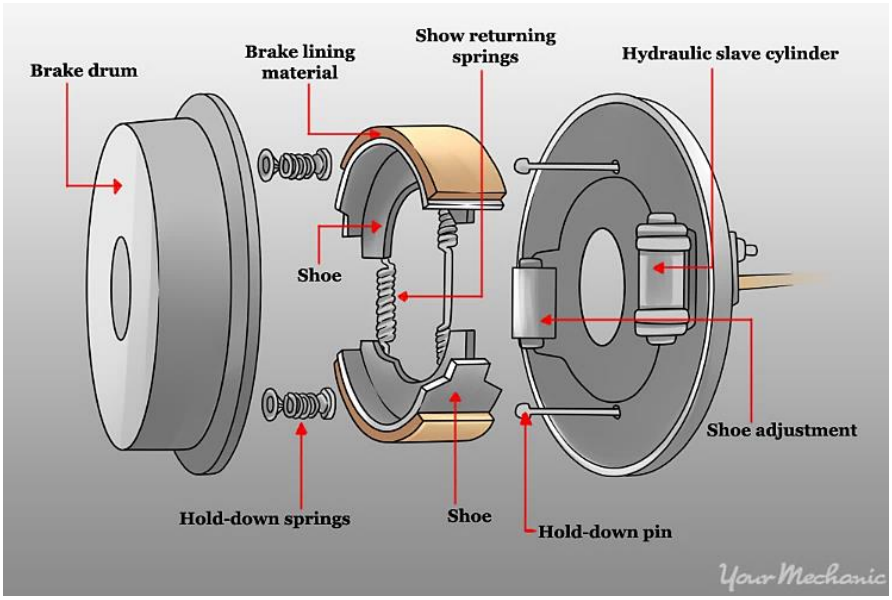

Figure 2. 3: Drum brake system (adapted from (Engineering Insider. 2017))

Furthermore, the energy obtained from the system was consummated through the following formula:

$$E_{th} = F_f \, d \tag{2.1}$$

Where; F_f, is the friction force in (N), d is the stopping distance in (m), and E_{th}, is the thermal energy in joules (J). Also, the E_{kin} found in an object in motion is implemented as,

$$E_{kin} = m \, v^2/2 \tag{2.2}$$

Where; m is the mass of the rotational object in (kg), v is the velocity of the item in (m/s), and E_{kin}, is the kinetic energy in (J).

By the application of energy conservation of the two previous equations, the thermal energy produced must be equal to the kinetic energy wasted ($E_{th} = E_{kin}$), so that, the friction force will be:

$$F_f = m \, v^2/2d \tag{2.3}$$

From equation (2.3), when speed or mass increased, the applied friction force must be increased to make the body stop at the same distance.

2.3.2 Review of electric (dynamic) braking

The evaluation of braking need starts from the electric motor, which was connected to the supply voltage out of an inverter that converts the DC voltage to the AC voltage feeding motor at the desired frequency. The basics condition of electric braking in an industrial application was to shut down the mechanical system within a specified period. Dynamic braking method of the motor was achieved by controlling the engine current during deceleration. During the brakes, the brake motor turned to be as a generator through the short process, driven by the kinetic energy of the load. The output was dissipated as heat in brake resistor or back in the supply line or dissipated as heat in the same engine (Tushnet 2000; Mutoh and Akashi 2011). The benefits of dynamic braking were to reduce corrosion of braking components based on friction, while the replenishment reduces net energy consumption. Typical examples of brake applications are cranes, lifts, vehicles, conveyors and test benches (KELJIK 2013).

Electric brakes, according to the literature, can be classified as follows:

2.3.2.1 D.C. injection braking

For most applications, quick stopping of high inertia motor loads can be achieved with DC injection braking, which has not added to system cost or complexity. The DC Injection braking was a strategy for slowing down AC motors without the applying of a frictional brake or an additional braking source such as a dynamic braking resistor (Senty 2013). The unit used was an electronic device that provides frictionless braking for the three-phase induction AC motors (Guideline 2011). In this process, there was no component in contact during braking. If a DC braking was required, a separate source of DC excitation has been inserted into two of the windings of the motor, creating a fixed magnetic field that applies a steady torque to the rotor, (switch K1 was closed). After the supply voltage has been switched off (K2 wass opened), meanwhile, the two switches (K2 and K1) cannot be closed at the same time. A DC voltage was obtained in a thyristor-controlled injection brake unit which was then fed into the stator of the motor by rectifying the supply voltage, as shown in Figure (2.4) (Rajashekara, Ashoka K. S. Bhat 2000).

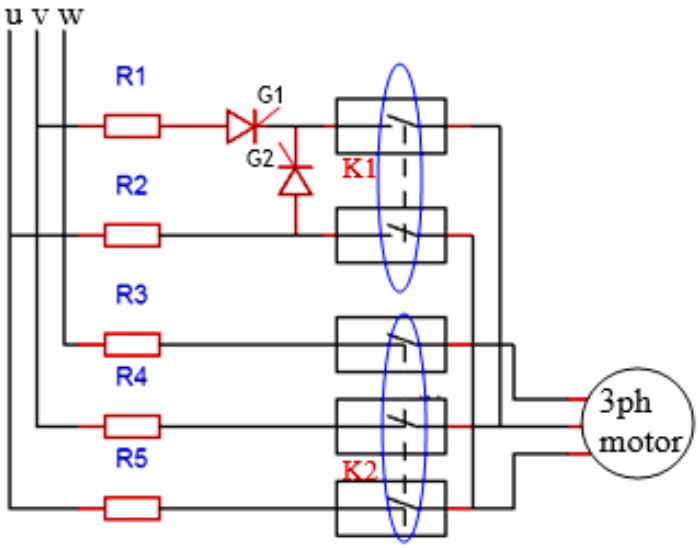

Figure 2. 4: DC supplied by a half-wave rectification

The braking torque has depended on the current magnitude, which can be changed by controlling the phase (G1, and G2) of the thyristor. The engine will stop for a while since there was no induced field to keep it rotating. However, the coasting time after the voltage removal may be unacceptable, especially in an emergency, with a controlled DC voltage providing the motor winding. According to the guideline and the technical guide No.8- electrical braking, the current injection must be 3~4 times the engine rated current when passed through the stator windings to provide more immediate stops (Guideline 2011; *Technical guide No. 8 - Electrical Braking* 2018).

Moreover, the current injection can also be maintained after the motor stops to keep it in place. For the rapid and repetitive brake of the generator, the power electronics adapter must deal with the power generated either by the controlled dynamic brake switch (with brake resistor) or by bidirectional energy flow. The loss of power in the converter can also be helped with dynamic braking (Rashid 2018). This type of brake was usually used with light loads, and this prolonged use can cause engine damage.

2.3.2.2 Plugging braking

In plugging (reversing current flow) braking, mainly used in controlling elevators and rolling mills, the changing of armature terminal or supply polarity of a separately excited or shunt wound DC motor, and hence the back electromotive force (E_{back}) starts acting in the same direction with the supply voltage (Serteller and Ustundag 2017). The adequate techniques across the armature will be the supply voltage plus the E_{back}, which was almost twice the supply voltage. Thus, the armature current was changed, and the motor has developed a counter torque and exerting a hindering (retarding) braking torque. The plugging process reverses energy temporarily and thus turns off the engine quickly (KELJIK 2013). Tushnet (2000), stated that the main downside of this scheme was that the supply must be detached at the precise moment; otherwise, the braking force may stop before the motor has ceased, or the engine may start to run in the reverse direction (Tushnet 2000). The current limit resistor was connected in series with the armature to reduce the

armature current to a safe value. The DC separately excited motor connection diagram and its characteristics are as shown in Figure (2.5).

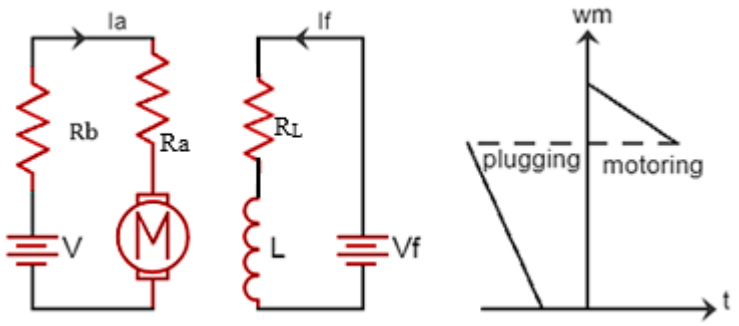

Figure 2. 5: Separately excited DC motor

In rheostat braking, the overturning of the direction of the torque was controlled by detaching the motor from running from the supply and then connected to a variable braking resistance. Rheostat braking of motors was possible for both high and low armature speed (Liudvinavičius and Lingaitis 2007). In this situation, the field winding remains connected across the source. At the same time, the armature was driven by the inertia so that the engine was being made to operate incidentally, as a generator driven by the kinetic energy of rotating parts and the load to produce the braking torque (Serteller and Ustundag 2017). The generated voltage from this generator was then supplied to a braking resistance (Rb) which dissipated it as heat and scattered throughout the motor armature resistance (Ra) as shown in Figure (2.6), as an example of two types of motors. The braking was inefficient because it cannot recover the generated electricity, and it might be used just in a specific case (Guideline 2011).

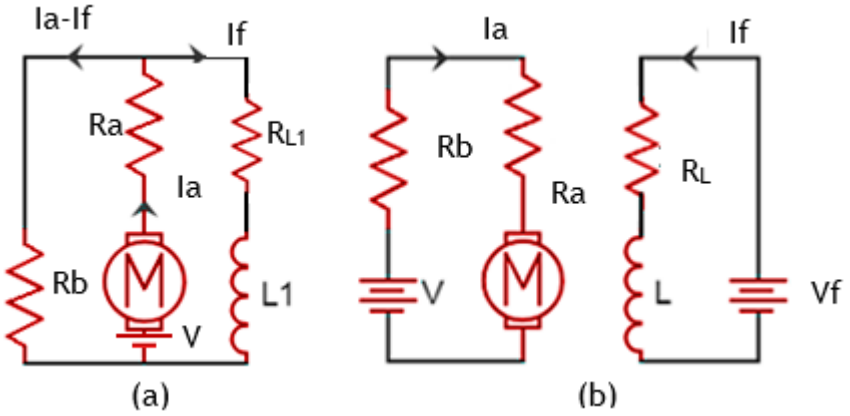

Figure 2. 6: Braking with (a) self-excitation, and (b) separate excitation

2.3.2.3 Motor flux braking

Flux braking was a strategy, mainly useful in low-power motors, dependent on motor losses that can be actualised in the system drive with field-oriented control units, or flux vector control units. While braking was required, the frequency was decreased, which significantly increases the flux generating and the current magnetising component of the motor increasing motor losses. Likewise, with many past techniques, flux braking was turning systems energy into heat at the motor and should be used sporadically to prevent motor harm. The control of flux carried out through the direct torque control (DTC) principle. The flux braking method based on DTC enables the motor to shift quickly from braking to motoring power when requested (*Technical guide No. 8 - Electrical Braking* 2018). Figure (2.7) displays full diagram for DTC contains two main parts; the torque control loop and the speed control loop (Erno Pentzin 2013).

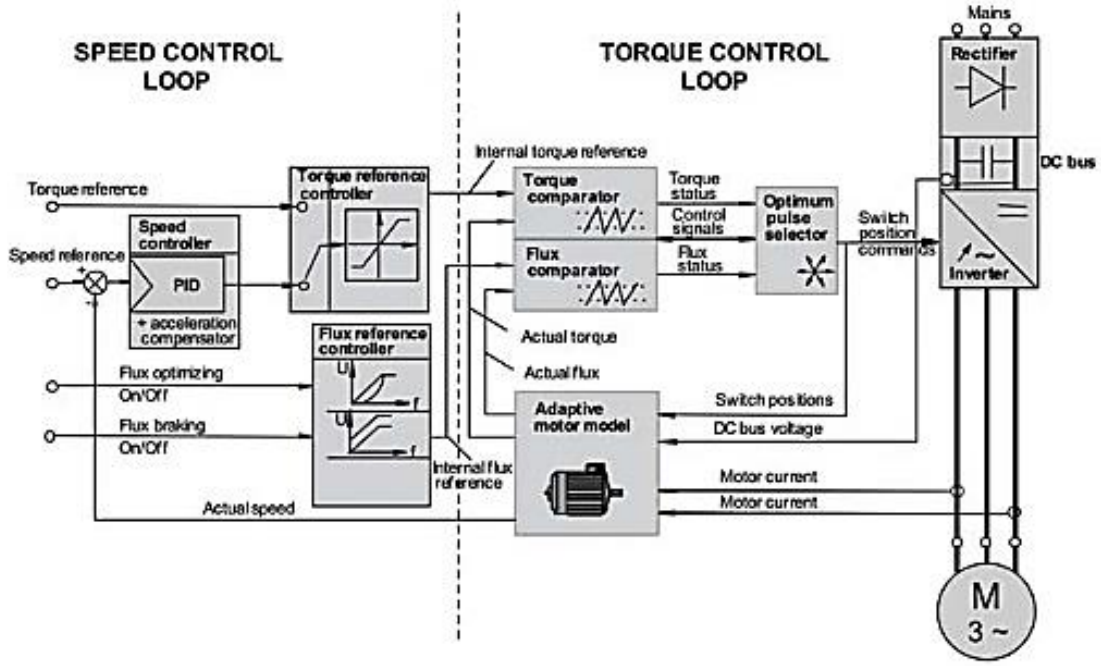

Figure 2. 7: DTC block diagram (adapted from (Erno Pentzin 2013))

2.3.2.4 Magnetic and Eddy current braking

Kitanov and Podol'skii (2008) stated another viable strategy for braking. The braking scheme was by using two types of brake suitable for high-speed trains, including a magnetic brake and an eddy-current brake. The braking activity of a magnetic rail brake, for instance, was expected to adhesion force between the curb and the track. Furthermore, the magnetostatic relies upon the magnetic field strength and the contact region of the brake and the rail. Besides, the braking action of an eddy-current brake originates from the way that a conducting body slows down when crossing an area of changing the magnetic field (Kitanov and Podol'skii 2008).

Moreover, a separate device coupled to the shaft of the motor comes about when electromagnets were actuated, and they induce eddy currents in the rotating metallic disk. However, the eddy currents produce magnetic fluxes contradict the flux generated by the electromagnets and in this manner result in a braking torque on the motor. The energy was dispersed as heat in the turning hard disk (Ma and Shiau 2011; Al-sharif 2016). Figure (2.8) illustrates an example of the integrated brakes combine the friction brakes and eddy-current brake on the same calliper (GAY 2005).

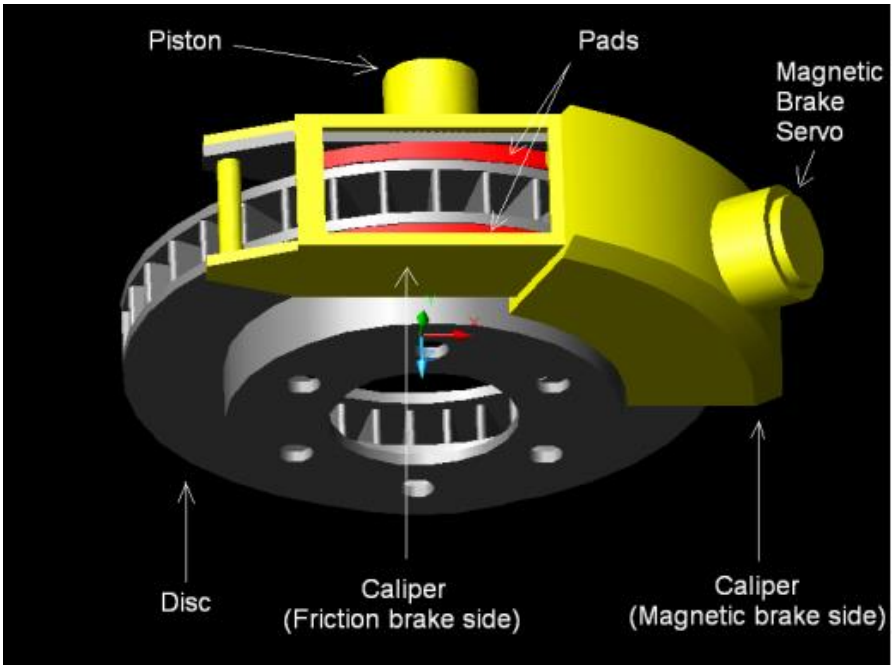

Figure 2. 8: Eddy-current and friction brake integration

2.3.2.5 Capacitor excitation braking

Braking systems for three-phase induction motors, which use the self-excitation of the capacitor after supply shutdown, were used for dynamic braking (Murthy et al. 1984). The principles of capacitor excitation braking, as shown in Figure (2.9), can be applied when connected in a delta connection to a so-called capacitor bank used to achieve instant braking. In the regular operation of the motor, the capacitor bank remains massively open (K2 switches were opened), and switches K_1 were connected. The three-phase star-connected stators coils were connected directly to the three-phase terminals. While when the braking was required, the supply of the engine was turned off (K1 switches were opened), and concurrently the capacitor bank was connected to the motor terminals (K2 switches were closed), which causes the capacitors to be connected in delta formation (Tushnet 2000). The value of capacitive reactance increases as the stator frequency falls, though the inductive reactance reduced. If the capacitive reactance esteem was much lower than that of the magnetising reactance; the capacitance can absorb all energy in the magnetic field. Meanwhile, the flow of AC was maintained. For low-frequency values, the capacitance cannot absorb all energy in the magnetic field and thus stop the AC as well as the effect of the capacitive braking.

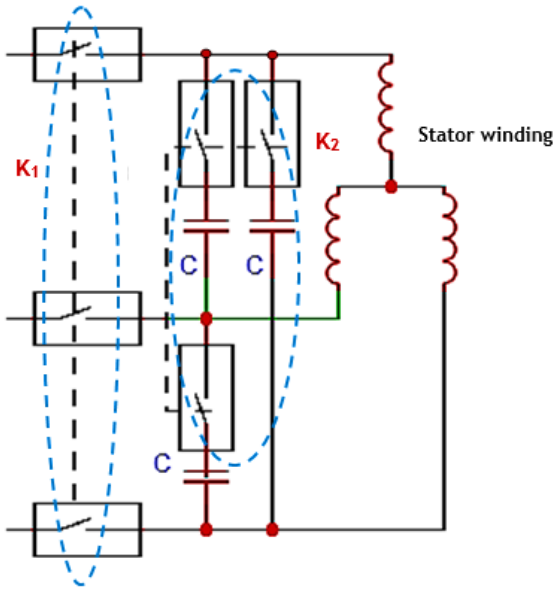

Figure 2. 9: Capacitor braking circuit diagram

2.3.2.6 Regenerative Braking (RB)

Because EVs carry a limited amount of electrical power on their energy storage systems, it was critical to maintaining the highest electrical power possible to increase the range of travel. Research studies gave an excellent opportunity for understanding the principles of the RB system, which was the subject of this research. The form of electric braking involves recovering the kinetic energy of a moving object by converting it into valuable energy. For instance, the converting energy was stored in various storage units likes a battery or ultra-capacitors (UCs), pneumatic, or mechanical energy in the flywheel. In EVs, the utilisation of RB can increase the overall efficiency by maintaining a portion of kinetic energy that would then be able to be accustomed to conveying the vehicle to speed (Clarke et al. 2010; Yang 2012). This type of braking was conceivable when the driven load forces the motor to run at a speed higher than its no-load rate with a fixed excitation. As a result, the motor induced voltage (back electromotive force emf) $\mathrm{E_{back}}$ has become more than the supply voltage, which leads to reverses the armature current direction and then to work as a generator that produces the braking torque.

Moreover, the kinetic energy stored in the rotating parts of the engine and a connected load was turned into electrical energy and were stoked into the power supply (Yeo et al. 2006; Lv et al. 2015). When the speed remains to land, consequentially, the $\mathrm{E_{back}}$ was reduced until it becomes lower than the supplied voltage and then the armature current returned to opposite the induced voltage $\mathrm{E_{back}}$. In this case, the other electric or the standard friction braking might be used to stop the engine safely. Due to the maximum recharging rate of the circuit and the storage unit (battery) capacity, the electromagnetic RB braking force was always limited. Therefore, the traditional friction brake system was required to convert excess power from the vehicle (Davis et al. 1990; Ko et al. 2014). Friction brakes can also be prevented the loss of braking ability if the RB was failed. Therefore, the concept of RB was vital for such vehicles because operating in this mode during the braking event restores the energy to the energy storage system (ESS). Also, it has helpd by reducing the corrosion of components within the

mechanical friction braking system. To achieve braking in mixed mode, the two systems (regenerative and friction) need to be combined. In the brake configuration, the motor/generator (M/G) and the hydraulic drive pressure were controlled together to meet the driver's demand for braking. Zaini (2012), stated a blended mode control slowing mechanism dependent on the extent of braking combination of regenerative and hydraulic braking. His study presented to understand the method that can be used to measure systems kinetic energy that can be stored for enhancing energy recovery (ZAINI 2012).

2.4 Concluded remarks

Of all the renewable technologies mentioned above, and due to climatic, political, and natural conditions, it was evident that research was needed in these sectors so that they can be implemented in practice in Iraq which can be used in the future. Meanwhile, the benefits of electrical braking compared with mechanical braking can be listed as follows:

- For mechanical brakes, due to excessive wear on brake blocks or braking linings, need frequent and costly replacement and maintenance cost,
- In some electric braking situations, the kinetic and potential energy can be returned to the system, such as in RB process, which was not possible with mechanical braking,
- The capacity of the system can be raised using higher speeds and the transport of heavy loads,
- The electric braking was smooth compared to mechanical braking.

From all the points mentioned above, it can be observed that the benefits of RB braking compared to other technologies was the most suitable for EVs and HEVs application. Therefore, the underlying technology was proposed in this study to harvest the kinetic energy of the vehicle deceleration and to reduce gas emissions and fuel consumption that may be amenable for application in Iraq in the current circumstances.

2.5 The components of the RB system

2.5.1 Power train configurations

According to the literature, different settings of power train group designs, such as serial, parallel, and series-parallel connections were available (Lee 2011; Park et al. 2014). Ehsani et al. (2010), provide the HEVs structure, according to the characteristics of coupling or separation of power which can be implemented in the designed test rig with two different voltage sources, such as electric coupling, mechanical coupling, and mechanical-electrical coupling drive trains (Ehsani et al. 2010). The electrical, hydraulic, and mechanical links have been used in a system with batteries, electric motors, generator and second torque source with a hydraulic link to pump fuel source to the fuel-powered internal combustion engine (ICE), as in Figure (2.10). The series structure HEVs was suitable for city driving, where it can be handled the frequent stop and run a driving pattern.

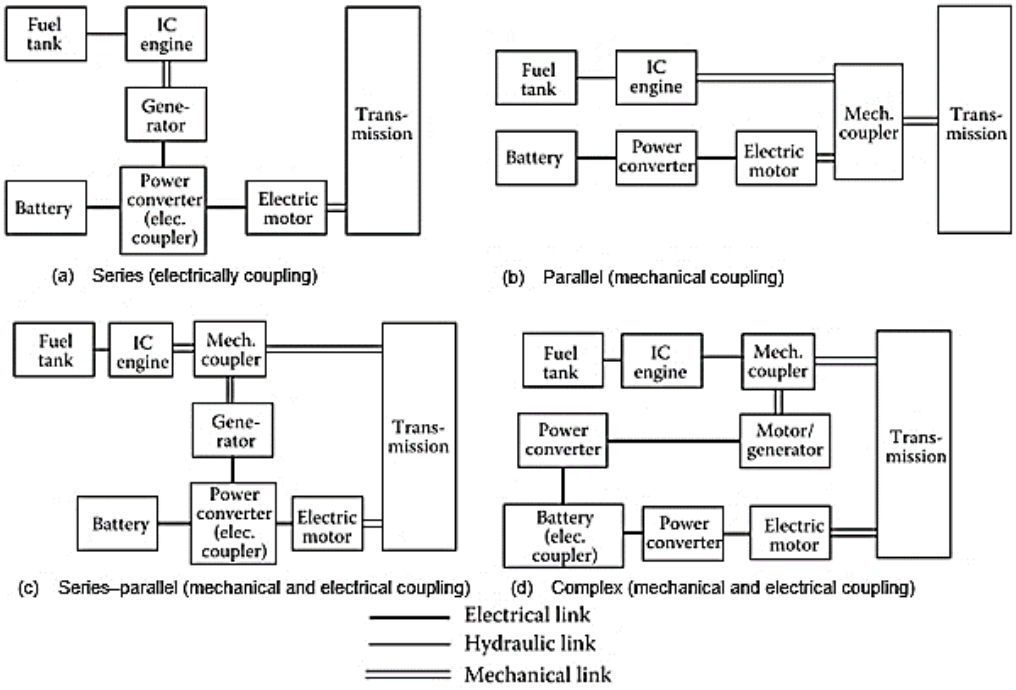

Figure 2. 10: Hybrid EVs configurations

Tie and Tan (2013), argued that the series hybrid type of HEVs has reduced the overall efficiency of the vehicle to about 25.7% but retains and stores most of the RB energy in the ESS (Tie and Tan 2013). Figure (2.11) shows the configuration of a series of hybrid electric transmission in detail.

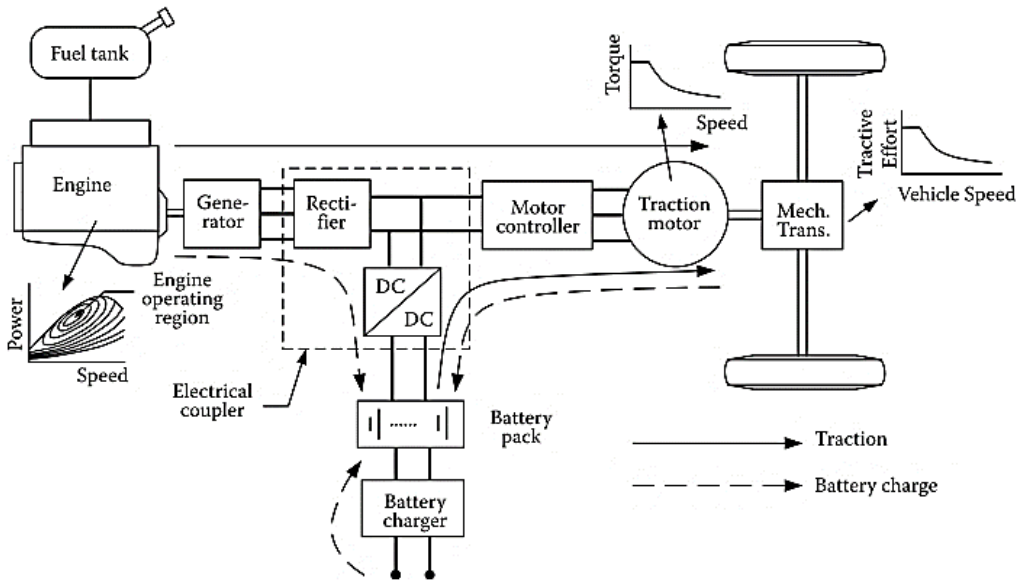

Figure 2. 11: Series hybrid power train structure (adapted from (Ehsani et al. 2010))

On the other hand, in the parallel structure Figure (2.10b), two mechanical powers are added in a mechanical coupler. The HEVs parallel structure can improve the overall efficiency to 43.4% (Tie and Tan 2013). It was more desirable on the highway and city driving conditions.

The distinguishing feature of Figure (2.10c) configuration was the use of two power couplers that were mechanically and electrically powered, although it was relatively more complicated and expensive. The only difference between Figure (2.10d and 2.10c) was that the electric coupling function moves from the power converter to the batteries and that the additional power converter was included between the motor/generator and the cells, which was the most complex (Ehsani et al. 2010). The modern electric propulsion train has consisted of three main subsystems; electric motor propulsion, power source, power converters and electronic controllers (Ehsani et al. 2018). Figure (2.12) shows an illustration of the general EVs configuration, which can be represented in the laboratory environments.

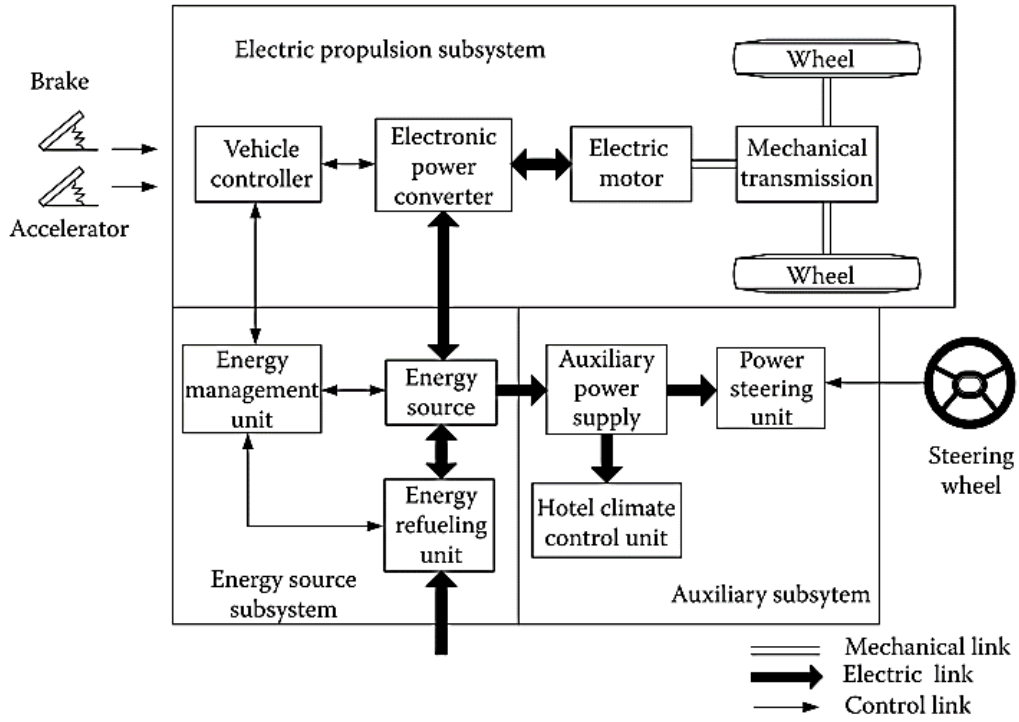

Figure 2. 12: EVs configuration (adapted from (Chan and Chau 2001))

2.5.2 Energy storage units (ESU)

According to the literature, the EVs require a transmission that can efficiently hold torque and speed requests and smoothly control the flow of energy in the vehicle's wheels (Ehsani et al. 2018). Brake controls were an electronic device that can control brake demand, determine brake end time and how quickly brakes were applied. For EVs related to the transmission, most designs have utilised a fixed ratio transmission. REN (2010), in his study, investigated the challenge of whether the use of the electric motor can be improved in its highly efficient area by controlling the transmission. The simulation results demonstrate two examples of EVs that the benefits of energy consumption were genuinely achievable between 7% and 14%, depending on the driving cycle (REN 2010). In the designed test rig, a direct-coupled flywheel was jointed with the PMBLDC motor.

During braking, the controller directs the electricity generated by the generator to batteries or the UCs storage units (Pay and Baghzouz 2003; Li et al. 2005; Chen et al. 2009; Clarke et al. 2010; Dixon et al. [no date]). The

need for a medium to store generated energy and the surplus energy was essential for industrial applications. Although, energy can not be stored in the form of electricity; it was possible to convert into another condition that can be saved and then turned back to electricity if desired. Therefore, there were a variety of possible ways that energy can be stored depending on the circuit designed and the level of performance required. The classifications of energy storage systems (ESS) based on technologies is as shown in Figure (2.13).

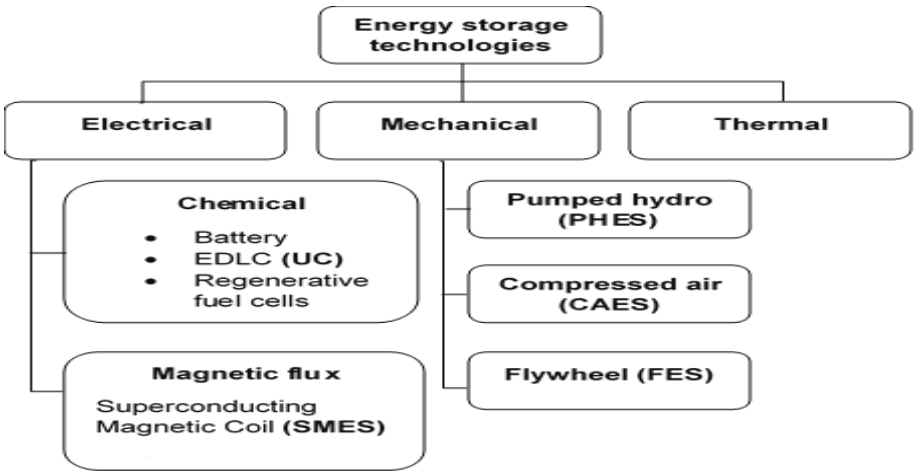

Figure 2. 13: Classification based on technologies of ESS

Concerning mechanics; The ESS selection for expenses and environmental situations have considered the kinetic energy transfers to the rotating mass using the flywheel (FES) as the most proper technology (Hedlund et al. 2015; Ren et al. 2015; Rashid 2018; Alamili et al. 2020). It can be easily justified because it provides high density, high efficiency, low cost, high life cycle, and does not mean any adverse environmental effect (Barin et al. 2011). While in the pumped hydroelectric storage (PHES), which stored the energy in gravitational form by transferring a water mass from low to higher ground level has played an essential role, as an example, in the United States electrical grid (Rachel Carnegie et al. 2013). Also, it can be stored in the compressed air (CAES), which has started in the 1970s when the oil and gas prices have increased (Rachel Carnegie et al. 2013). Ribeiro et al. (2001), stated that energy could be stored in the electromagnetic energy storage (EMES) in the form of magnetic fields using superconducting magnetic energy storage techniques (SMES) (Ribeiro et al. 2001). While in the electrostatic energy storage (EES), the energy stored in UCs using electric charge (Dixon et

al. 2009). Also, the electrochemical storage unit (ESU); had used hydrogen produced by water electrolysis and combine it with oxygen in fuel cells to release energy (Rachel Carnegie et al. 2013). Hence, battery energy storage unit (BESU) has utilised the chemical components built into them to store and release energy (Glaize and Genies 2013; Sakka et al. [no date]).

Furthermore, energy storage systems (ESS) can be classified according to characteristics, as shown in Figure (2.14) (Chatzivasileiadi et al. 2013).

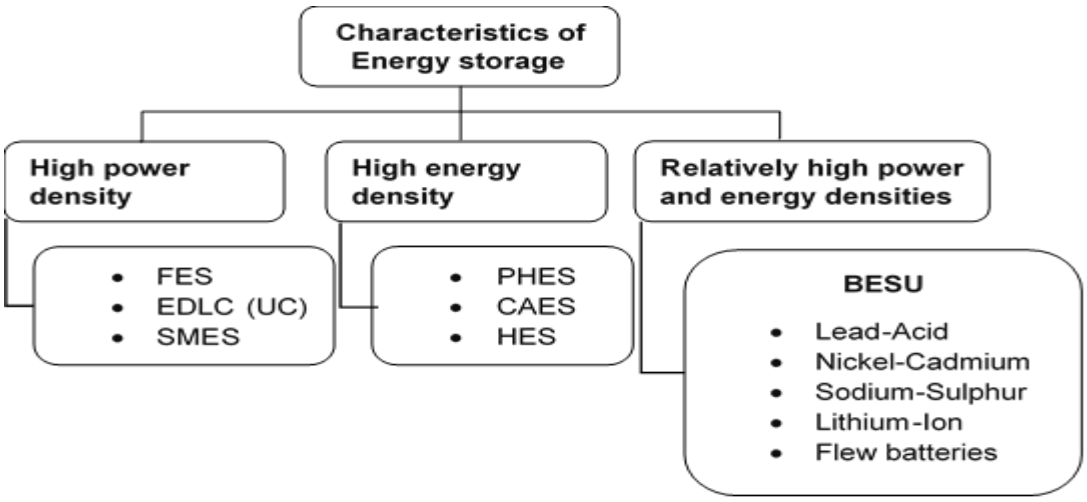

Figure 2. 14: Classification based on attributes of ESS

Also, ESS can be classified based on the power and energy rating or densities available since these criteria often reflect the use of ESS. This ESS includes FES, SMES, and UCs, which can provide high power output for a short period (for example, minutes) and could be committed in a short time (for example, seconds). Meanwhile, ESS that includes the PHES, CAES, and HES can be provided low output power for a more extended period (i.e., hours) and require some time before starting the deployment or storage energy (for example, minutes). Finally, ESS has had both high power and energy densities relatively, as shown in Figure (2.14). The BESU was located between the two previous groups, depending on the type of battery used (Lead-Acid, Nickel-Cadmium, Sodium-Sulphur, Lithium-Ion, or flew batteries) (Rachel Carnegie et al. 2013).

The most challenging part of designing electrical KER was how to store the electrical energy and how to manage it. Many modern EVs and HEVs included power conversion technique to extend the range of the battery pack (Ribeiro

et al. 2001; Lukic et al. 2008; Kapoor and Parveen 2013). The selection criteria for adequate energy storage has included high specific energy storage density, high energy transfer rate, and small space requirement. Figure (2.15) shows the ESS classification according to power density (Abu-Rub et al. 2014).

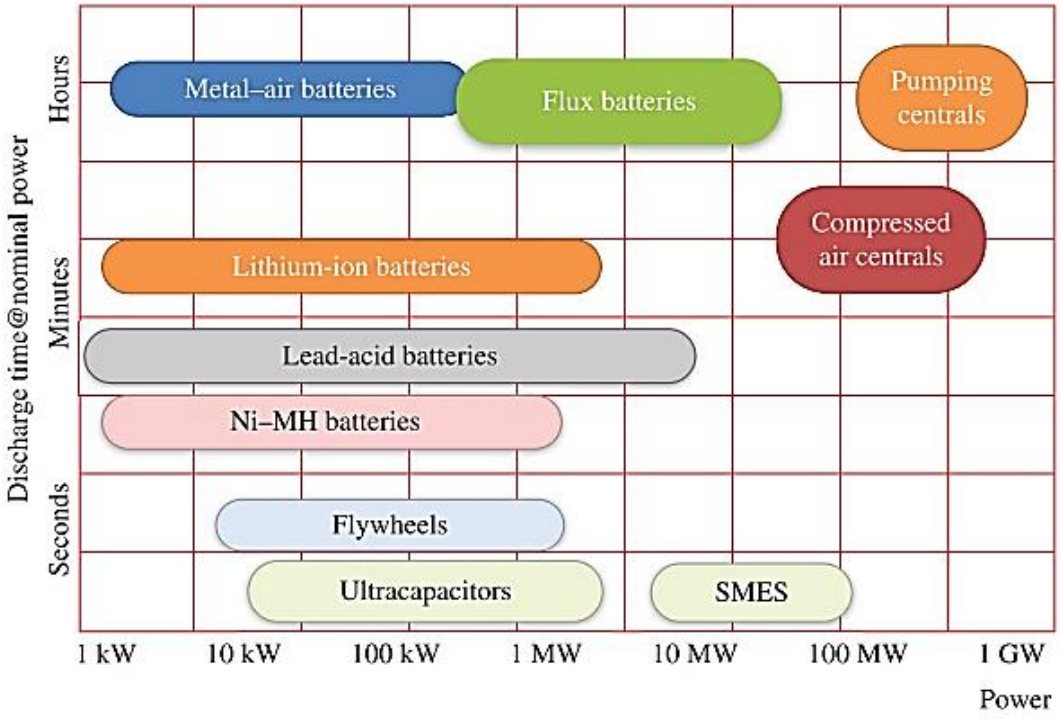

Figure 2. 15: Classification of the ESS

2.5.3 Application of ESS for energy recovery

In RB form, the primary distinction between various storage units was that in the way they convert the energy and the way that energy was stored. These types of storage units include the CAES, for an instant, was technically efficient and economically attractive for energy management. During acceleration, the pressurised hydraulic fluid in the accumulator drives the variable axial displacement unit, which then works as a motor, as shown in Figure (2.16). When braking, the variable axial piston unit converts kinetic energy into hydraulic energy and pumps hydraulic fluid into a bladder accumulator filled with Nitrogen. Zhang et al. (2007) suggested that the system provide 10% of the energy using a brake regeneration (Zhang et al. 2007).

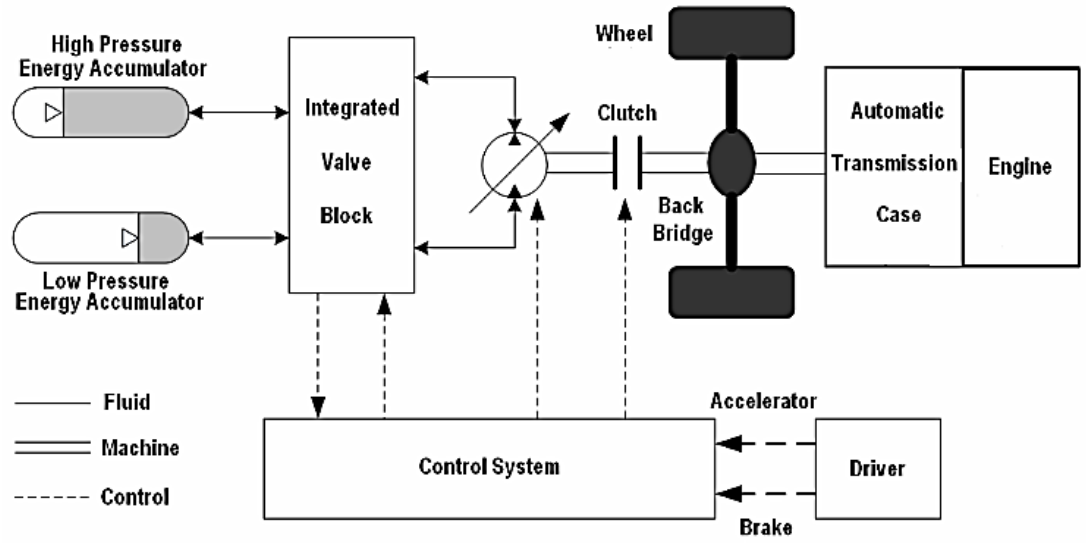

Figure 2. 16: Compressed gas brake system (adapted from (Zhang et al. 2007))

Meanwhile, physicist Richard Feynman has postulated the concept of transferring the vehicle's kinetic energy using flywheel energy storage in the 1950s. Unlike electrical KER system, this method of storage prevents the need to transform energy from one type to another. The E_{kin} of the vehicle ends up as E_{kin} of a rotating flywheel (only a mass rotating about an axis) through the use of shafts and gears (Cibulka 2009). The benefit of using flywheel technology was that more of the forward inertial energy of the car could be engaged even during relatively short intervals of braking and acceleration (Mirabadi and Najafi 2011; Farahani 2012).

Hydraulic RB used to improve the fuel economy of the vehicle, which was an alternative form of RB system (Chu et al. 2009). Ford Motor Company and Eaton corporation developed hydraulic power-assist (HPA) (Pochiraju 2014). In this system, during acceleration, the fluid in the high-pressure collector was driven to operate the pump as a motor. This system can be produced with a fuel saving of 21.7% in a perfect shutdown cycle (Midgley et al. 2013). Also, Zhang et al. (2012) concluded that the fuel economy has improved by more than 25% of the RB system (Zhang et al. 2012).

BESU in EVs and HEVs has been used to supply energy at motoring operation, and in braking action. The motor works as an electric generator to generate electricity that can be fed back into batteries (Michalczuk et al. 2012; Andre et al. 2013). The significant characteristics of the UCs ESU have used to perform higher acceleration and deceleration of the vehicle with a minimum

waste of energy, and minimum degradation of the main battery (Dixon et al. 2009). Energy storage devices like UCs typically have used along with batteries to compensate for the limited battery power capability, as shown in Figure (2.17).

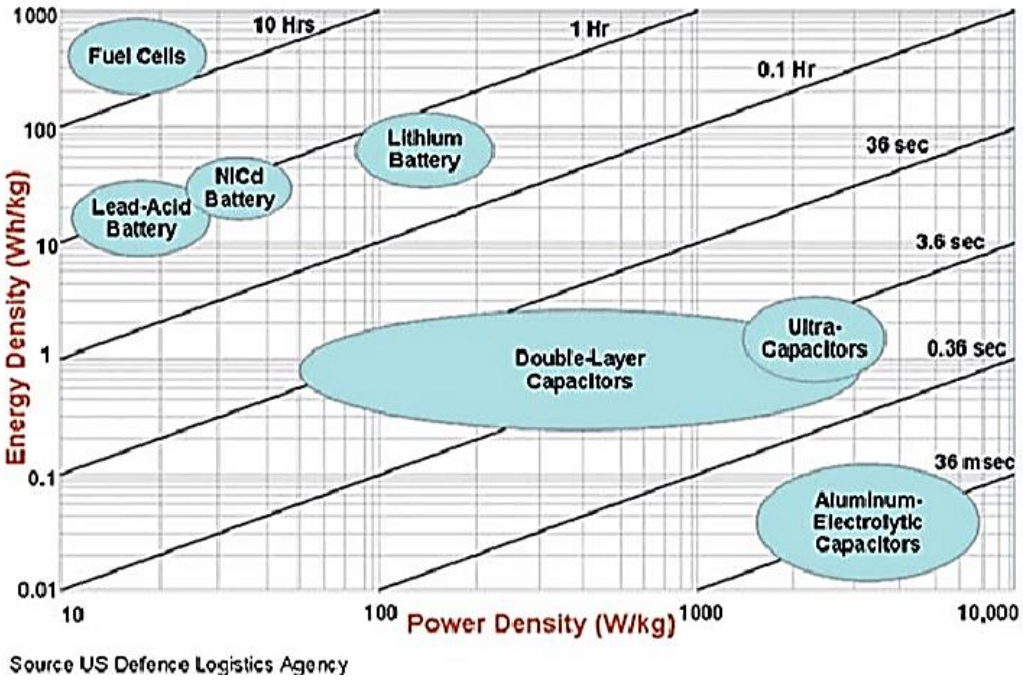

Figure 2. 17: UCs vs batteries power density and energy density graph (adapted from (Zhao et al. 2011))

The proper control of the ESS has presented a challenge and an opportunity for the power and energy management system (EMS). The UCs can be discharged and recharged many more times and with far deterioration than a battery as it accepts and releases charge much more quickly.

Most importantly, these technologies have vigorously relied on battery packs as the central storage unit. In this way, it was critical to creating an accurate cell model that can advantageously be utilised with a simulation of the EMS (Ostadi and Kazerani 2015; Xu and Cao 2015). However, to operate safely and efficiently, batteries ESS should be used within the safe temperature and voltage ranges. In this case, the UCs that were undergoing charging and discharging cycles frequently in high current and short duration were used to assist the battery. Furthermore, it can be used to store energy that has additionally made fundamental advances into the electric power system (Karden et al. 2007; Sangdehi 2015). Based on the proposed developing of the hybrid ESUs, improvement of properties can be taken advantage of the

combination of batteries (higher energy density) with UCs (higher power density) (Ren et al. 2015; Itani et al. 2017). The best battery performance can be accomplished with additional UCs. The UCs were being assisted in achieving the energy density of cells, offering almost unlimited lifespans, widen temperature run and no environmental issues. Additional consolidate it has used UCs to transmit of high current on acceleration and to accept RB energy on descending to disconnect the electric motor from the battery through the electronic control unit. This fact has made it ideal as energy storage for the designed test rig and in EVs and HEVs power applications.

2.6 Sustainable energy (SE) control strategies

In EM, the control unit was necessary for hybrid RE resources used to monitor and control the various variables according to the load requirements to maximise system reliability and operational efficiency at the desired level of performance. In general, researchers consider four classes of controllers have used to manage the operation of hybrid RE. The controllers have classified as; centralised, distributed, combined hybrid, and multiple control (Nehrir et al. 2011; Lodha and Shukla 2016; Sawle et al. 2017). In all cases, each power supply must have had its own (local) controller that can determine the optimum performance of the corresponding unit according to the current information. Bala and Siddique (2009) implied the centralised control, in which a central control arrangement manages the signals from the power supply. This form has a drawback because it has taken more time to implement (Bala and Siddique 2009). While during distributed control, which has one power source to manage, it was more useful as a minimum for the account to be achieved without any failure. It was flawed in multiple communications, which can be overcome using the most appropriate artificial intelligence techniques available, such as multi-agent systems (Nagata et al. 2002).

Meanwhile, the hybrid control technology has combined distributed and centralised control units, using local and global improvements and energy management. The inadequacy of this method was one of the main complications of the information transfer system. However, the latter

approach was the multilevel method in which the operation principle equates the hybrid control technology for better control of the system based on the current information (Sawle et al. 2017).

2.7 Energy management system (EMS)

EMS treated as one of the useful management tools used to enhance performance by recovering sufficient energy from the brake system. ESS studies have provided high energy density (PHESU, CAESU and BESU) with long-term charging/discharging duration. The higher penetration of intermittent energies due to electrical system intrusion highlights the need to maintain a certain level of energy reserves to compensate for power loss.

Therefore, the using of ESS opened a promised opportunity to the possible use of these units beyond the electricity industry to include other sectors such as an EVs and traction system, where ESS uses brake energy to accelerate the speed and to provide continuous and pulsating power for the EVs. There was a wide range of arrangements for consolidating hybrid ESS, for example, batteries and UCs (Gao et al. 2005; He 2014; Sangdehi 2015). Various hybrid active, semi-active and passive approaches have been adopted and summarised by multiple researchers (Omar et al. 2012; Song et al. 2014; Castaings et al. 2016; Zhang et al. 2016a; Song et al. 2017). Chapter 5 extends knowledge about EMS for more details and analysis.

Finally, Figure (2.18) illustrates the flowchart used to describe the research objectives/questions and contributions within all the chapters.

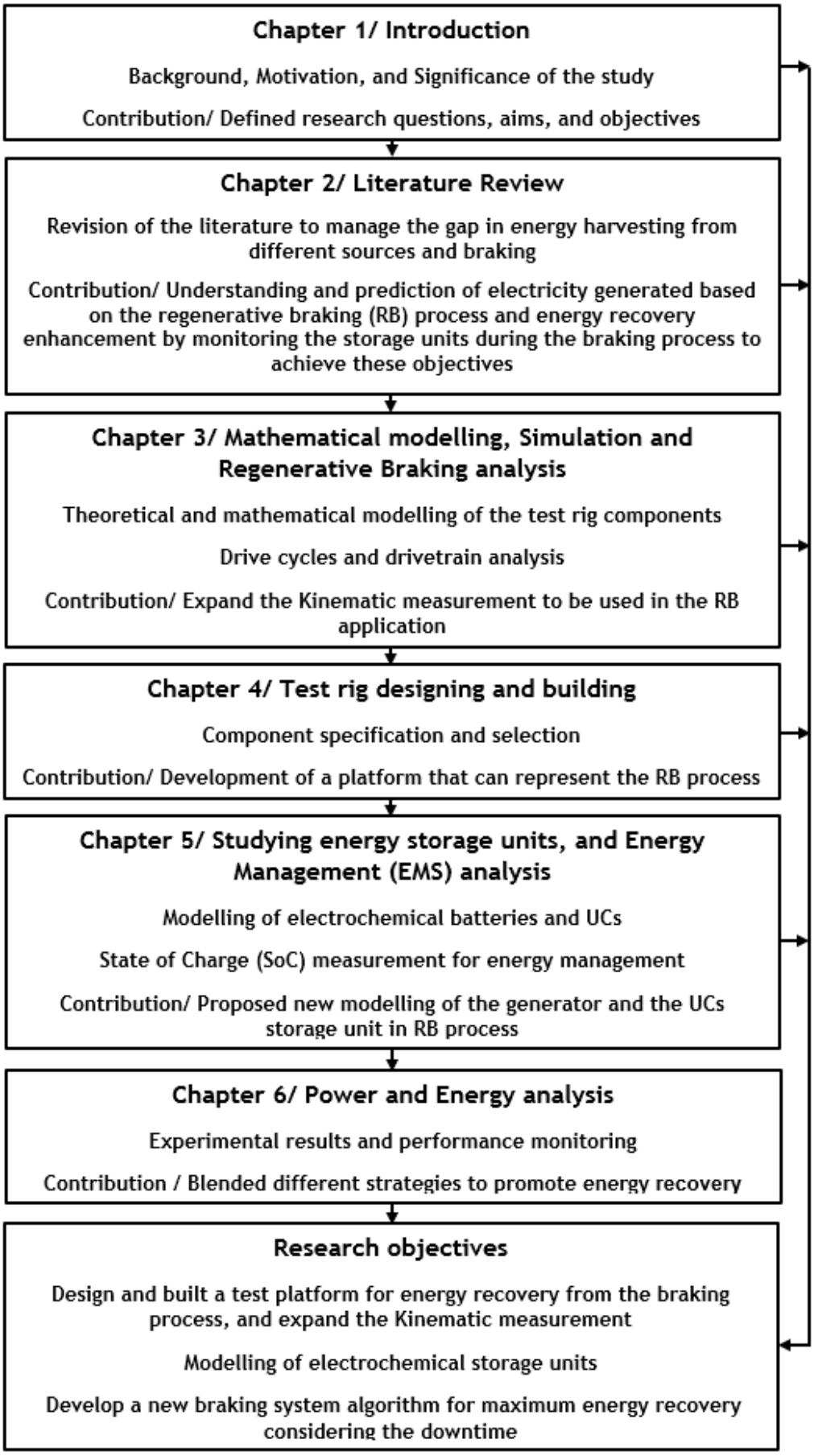

Figure 2. 18: Thesis outline flowchart with contributions within all the chapters

2.8 Conclusions

RB has a significant impact on the reduces the environmental impact and cost of many industrial systems. Most of the literature highlighted and focused on renewable energy as an alternative to fossil energy. The lack of necessary tools and due to the climate conditions, such as high temperatures in summer and drought in Iraq necessitated research on the restoration of waste energy. As a part of this research, to cover the gap, it was noteworthy that in the waste energy recovery to the design of a test platform to represent the real behaviour of the system. It was necessary to adopt the approach and serve it as a black box to compensate for the lack of design representation for some components of the circuit through which the system can be optimally represented. Different strategies should be considered to enhance system performance on the current platform. Specific knowledge gaps can be summarised as follows:

The system must be strictly designed to deal with several limitations to reduce energy loss due to friction in the braking process. Besides, system components must be compatible with each other for more exceptional durability and performance. The elements must be tested experimentally to emulate the real behaviour of the system. Also, the total cost should be minimal, and the life of the system should be maximally beneficial since it affects the overall benefits in the industrial sector. Control strategies should be as simple as possible to use in EMS and improve efficiency.

The next chapter (Chapter 3) provides an introduction and the necessary information about the mathematical description and modelling of energy recovery for the designed test rig. Also, it gives a review of the system components, for which the characteristic equations were prepared experimentally to build the virtual system and compare its behaviour with the actual functioning of the system. Furthermore, it introduces a driving cycle as a representative of the road, and the set of data points for vehicle speed with time travelling at a specific path with the kinematic measurement in the RB process.

Chapter 3

Mathematical modelling, Simulation and Regenerative Braking analysis

These chapter aims were to demonstrate the drive train used in the driving system and to exhibit the practical application of each type. Moreover, with a large extent, it can be analysed to study every component to satisfy the requirement as needed. Also, to dissect a theoretical probing and mathematical modelling of every reasonable part used in power conversion scheme due to the RB process that might be used in the accompanying sections. Moreover, to understand the operation of the RB, the essential terms and components have been described and defined to pack up test rig modelling and simulation regarding these requirements.

The outline of this chapter was partitioned into different sections. In the first part, the unique type of drive train was discussed. Throughout the revision of different kinds of DC motor from which it was possible to determine the importance of the research subject from both theoretical and practical aspects. In the second part, theory identified modelling of all elements has been implemented in the RB process. Also, an introduction of different drive cycle available with the kinematic measurement has been developed to measure recaptured energy, which set as the main contribution in this chapter.

Furthermore, an introduction to power systems devices, including an explanation of various power electronic converters and other element used or projected to be utilised in the testing appliance, has been clarified. The necessary information about the proposed model of the main and the auxiliary rechargeable energy storage system has been described in chapter five. At last, the conclusion has been given at the end of this chapter.

The following section describes the basic idea of different types of electric motors and part of the user in a separate application. Also, it has offered a necessary background of the most central drive system used in the RB process, which can be chosen in test apparatuses.

3.1 Electric drive system

The features of the electric drive of the electric motor have been included; the transmission shaft and control unit, which adjusts the motor

characteristics when adapting operating conditions to mechanical load requirements (Pillai 1989). For the correct drive specification, the design specifications have been reflecting operating conditions and the environment concerning the type of application focuses on a specific load property. Applications can access four basic sets of motor drives: appliance drives, general-purpose drives, system drives, and servo drives. Table (3.1) shows the natural forms and the main sections of these groups (Vodovozov 2012).

Table 3. 1: Classification of electric drive

Feature	Appliances drives	General-purpose drives	System drives	Servo-drives
Applications	Home appliances	Fans, pumps, compressors, mixers	Test benches, cranes, elevators, hoists	Robots, lathes, machine tools
Performance	Middle	low	High	Very high
Power rating	Low	Whole range		Low and middle
Motor	Mainly induction motors		Mainly servomotors	
Converter	Simple, low cost	Open-loop ac and dc	Expensive, and high quality	
Typical feature	Home and mass production	The process cost-sensitive, and low - performance	High precision and linearity, high accuracy and high dynamic	

The motor drive specifications must meet the requirements of the machine in all working conditions, especially in terms of torque and power. Motor overload leads to rapid insulation and mechanical damage (*Variable Speed Drives and Motors - Installation Guidelines for Power Drive Systems* 2012). At the same time, an unjustified reduction leads to an increased in the size of the framework, costs, and deterioration in loss of performance. Therefore, it was necessary to adjust the engine consumption with the potential next load demand (Fontaras et al. 2017). Meanwhile, motion control was accomplished in many industrial applications in which the system employed was named as a driver of the prime movers for supplying mechanical energy for motion control (Dubey 2002; Krishnan 2010; Vodovozov 2012).

3.2 Review of electric drives

The propulsion system consists of an engine or motor as an energy source. From a distinct point of view, there was no perfect engine, because a nominated engine may have a feature in each application but with a flaw in another form. This disparity can be due to different drivers has unique features that make it fit for specific applications being used in an industrial application (Microchip Technology Inc. 2017). The classification can be made according to the principle of conversion, such as; electromagnetic, electrostatic, and ultrasonic (Briand et al. 2015). Additionally, it might be arranged depending on the power supply as a direct current (DC) power supply, and single or three-phase alternating current (AC) power supply, as shown in Figure (3.1) (*Global Power Solutions, Power Supply Technical Guide 2010/11* 2010).

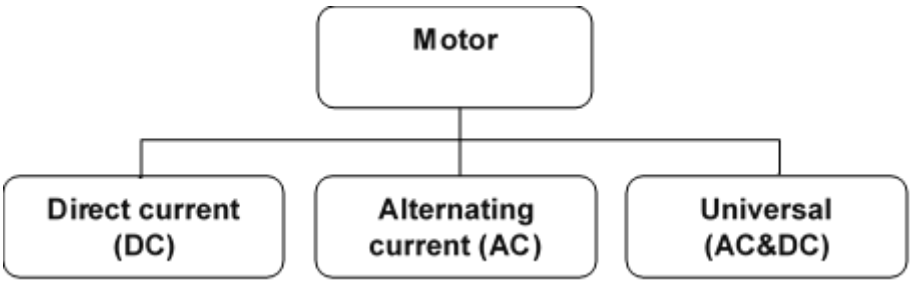

Figure 3. 1: Classification of an electric motor according to the power supply

Besides, the classification can be made by the rotation manner (a unit that characterises the rotating speed or the direction of rotation), or by the structure (a group of rotating and static parts) (Nidec Corporation 2019).

3.2.1 DC motor

The DC motor can be classified according to commutation types as brushed and brushless (BL) DC motor (Yedamale 2003; Reston Condit 2004; Zhao and Yangwei 2011). The BLDC motor was extensively used in an industrial, automotive application, aerospace, and automation devices. By taking full advantage of these motors, the BLDC motor was widely used in different forms as in refrigerators, washing machines and other household appliances (Rodriguez and Emadi 2007; Miyamasu and Akatsu 2011; Milivojevic et al.

2012). Also, the BLDC motor has several features that combined its benefits in the areas of low noise, high efficiency, more significant dynamic response, energy-saving, and robustness (Gamazo-Real et al. 2010). For instance, the stepping (stepper) motor was a BLDC motor that divides the full rotation into several equal steps defined as a steps angle suitable to be used within computer-controlled systems and in the numeric control of machine tools. The motor position can then be ordered to move and continue in one of these steps without any position sensor for feedback which minimises sensing devices (Bishop 2002). This motor was a combination of a six-coil concentrated winding stator and a salient pole lamination rotor to make it ideal for position applications (Reston Condit and Jones 2004). In this motor, a rotary switch was used to switch the current between the windings. It can be classified into three main kinds, as shown in Figure (3.2) (McComb 2007).

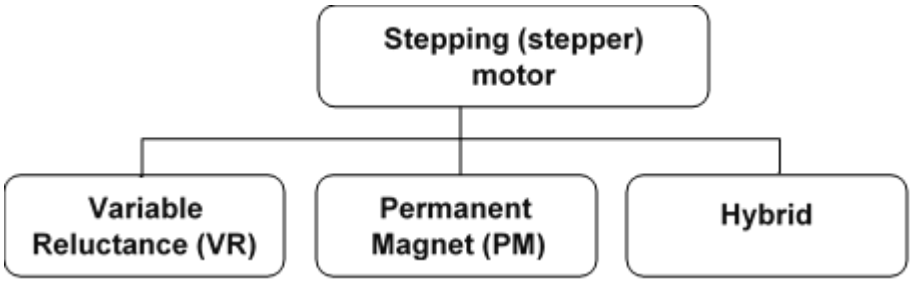

Figure 3. 2: Classification of stepper motor

The variable reluctance (VR) motor has replaced the magnetic rotor with a geared, not-magnetised soft-iron rotor. It was utilised in machine tools and computer device peripherals (Manzer et al. 1989).

Meanwhile, the permanent magnet (PM) motors were characterised by the fact that they have low power consumption when built-in PM. Finally, the hybrid motor has a combined characteristic of the last two types, consolidates VR and PM features. The hybrid refers to the VR structure, which has a precisely notched stepping angle, and the utilisation of PMs which expands torque combination. The three types of stepper motor have been offered very high rotational resolutions and improved torque (McComb 2007). Table (3.2) gives a comparison of the characteristics of the three types of stepper motors.

Table 3. 2: Comparison of three different stepper motors (adapted from (McComb 2007)**)**

MICROCHIP WebSeminars

PM vs. VR vs. Hybrid

Characteristic	Permanent Magnet	Variable Reluctance	Hybrid
COST	Cheapest	Moderate	Most Expensive
		More expensive due to manufacturing processes	
Design	Moderately Complex	Simple	Complex
Resolution	30° - 3 °/step	1.8 °/step and smaller	
Torque vs. Speed		Less pronounced torque drop at higher speeds	
Noise	QUIET	Noisy no matter what type of excitation	QUIET
Stepping	Full, Half and Microstepping	Typically run in Full-Step only	Full, Half and Microstepping

It clears that from the table, the PM was the most suitable motor regarding cost and noise characteristics.

Furthermore, switched reluctance motor (SRM), was a type of stepper motor with closed-loop commutated and variable-speed controlled, used in wind energy systems and EVs. It has a robust and reduced pole count structure utilises a stator of concentrated winding and a salient pole lamination rotor. The power was delivered to the winding in the stator with electronic devices can precisely time switch, facilitating SRM configurations (Hughes 2006; Bouiabady et al. 2017).

Moreover, DC motor can be classified according to its construction as an inner or outer rotor design as; surface permanent magnet type (SPM), and an interior permanent magnet type (IPM) (Ozcira and Bekiroglu 2011). The IPM motor has been built from two forms as concentrated and distributed winding and used for vehicle traction due to its constant torque at low speeds and its broad, consistent power at high rates (Choe et al. 2012).

Furthermore, the DC motor can be classified by the excitation types as:

3.2.1.1 Permanent magnet (PM) exited DC motor

There were several types of DC motors such as the PMBLDC motor offers simpler drive schemes which eliminate problems correlating commutation represented in a different strategy (Krishnan 2010; Milivojevic et al. 2012). The PMBLDC motor has performed the commutation electronically using rotor position feedback to determine when to switch the current to each coil depending on input from a connected Hall sensor or a rotary encoder. The stator coils have worked in conjunction with a PM in the rotor to generate an almost uniform flux density in the air gap. This representation has permitted the stator coils to be driven by a constant DC voltage, which switches from one stator coil to the next to create a waveform of the trapezoidal AC voltage (Zhao and Yangwei 2011). The classification, according to the armature types depending on application needs, is as shown in Figure (3.3) (Fei 2011).

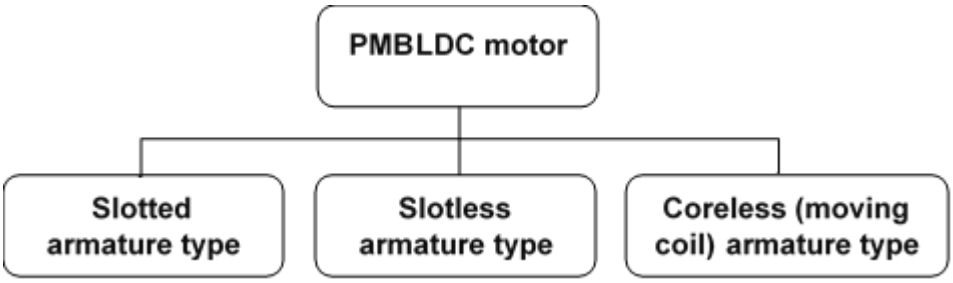

Figure 3. 3: PMBLDC motor types

The PM switching motors with a slotted and slot-less armature (rotor) has armature windings fixed to the laminated core and shaft make one essential part. Also, the moving coil DC motor has the armature windings joined to the insulating cylinder that turns between PMs or PMs and laminated core (GIERAS 2010).

3.2.1.2 Field winding (self-excited) DC motor

The motor was used mainly for a medium and large application within a power range about (1hp =~ 750 watts). In this type, the field winding of a self-excited DC motor was connected in series, parallel or partially in series/parallel with the armature winding that produces the main magnetic field in a machine (Chapman 2012). Accordingly, DC motors can be classified into three types, as shown in Figure (3.4).

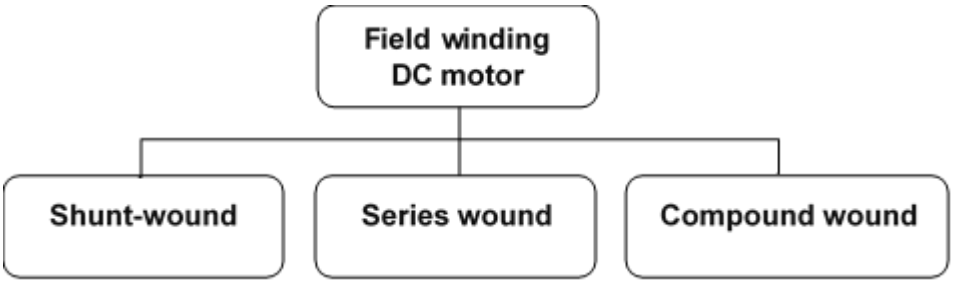

Figure 3. 4: Winding field DC motor types

Each class has characteristics depending on the load connection that make it used in specific applications, for example, cranes, electric trains, and elevators (Khajepour et al. 2014).

3.2.1.3 Separate field (separately exited) DC motor

This type of motor was used mainly as actuators in trains and automotive applications. The armature and field winding are electrically separated from each other, and a separate DC source activates the field winding. It was described that there is a wide range of speed control by independently controlling the amount of current for the two windings (SEN 2013).

Serteller and Ustundag (2017) have examined the models of the three types of the DC motors described above according to dynamic behaviour during starting and stopping time (electrical braking) and steady-state for electromechanical energy conversion. They have concluded that the power consumption does not change linearly with braking time; it depends on the energy stored in the load, while the motor acts as a generator during the brake (Serteller and Ustundag 2017).

3.2.2 AC motor

In this type, the rotational speed was determined by the rotating magnetic field generated by the application of multi-phase alternating current to the stator winding. The rotational speed was obtained by the frequency of the multiple-phase alternating current (Theraja and Theraja 2005). The AC motors are classified by the rotation method, as shown in Figure (3.5).

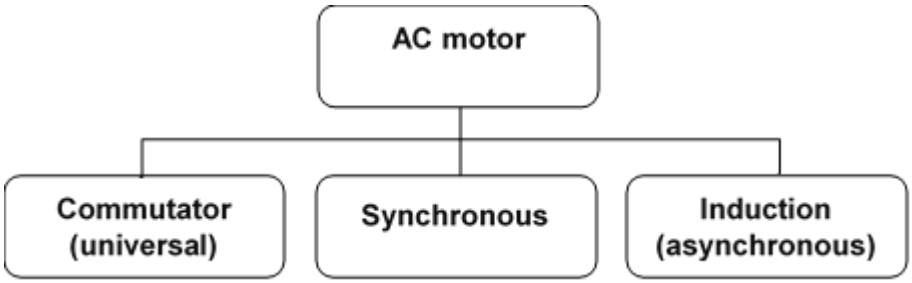

Figure 3. 5: Classification of AC motor

The commutator (universal) was a linear motor utilised in an application where it was necessary to rotate at high speeds using a single-phase AC or DC source, for example, in vacuum cleaners and power tools (Theraja and Theraja 2005). Furthermore, the synchronous motor refers to motors whose speed was equivalent to the synchronised rate (Chapman and Ninni 2004). They have incorporated the accompanying three types, as shown in Figure (3.6).

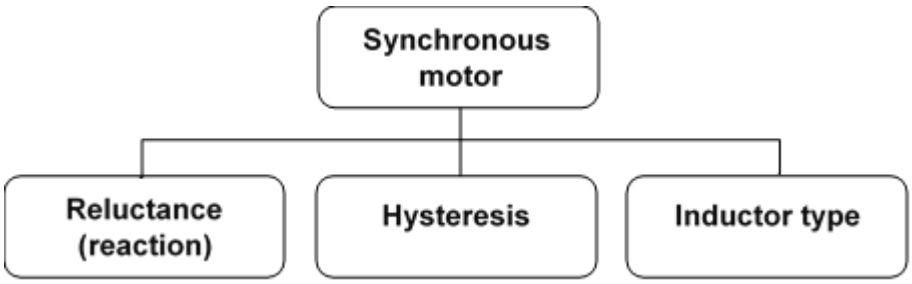

Figure 3. 6: Classification of synchronous motor

This classification has been implemented depending on the principle of its operation. The reluctance motor principle of operation was that it initially rotates as an induction motor, then alternates synchronously with the frequency of the power supply during the process (Theraja and Theraja 2005).

While the hysteresis principle of operation was that it rotates using the hysteresis characteristics; it has minimal rotational abnormalities or vibrations (Theraja and Theraja 2005). Additionally, because there was no distinction between the start-up and stop torques, it ought to preferably be worked under a constant load condition.

Finally, the Inductor type motor principle of the operation has utilised to synchronise the movement of the rotor with the current frequency applied to the stator coil and converted the input energy into rotational motion by repeated attraction and repulsion process. This motor can be classified

depending on the rotor structure as claw-pole motor and hybrid stepper motor (slow synchronisation engine) (Corporation 2019).

On the other hand, the Induction (asynchronous) motor, which was designed to spin at speed slightly lower than the synchronous rate can be subdivided into three main types as shown in Figure (3.7) (Parekh 2003).

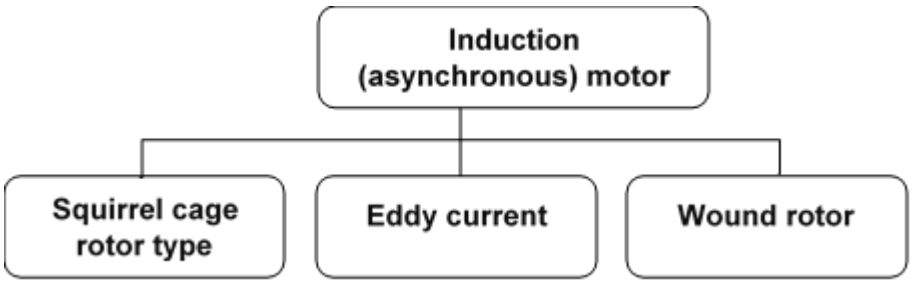

Figure 3. 7: Classification of asynchronous motor

The squirrel cage motor was a general-purpose three-phase motor with four design kinds as (A, B, C, and D), used for industrial applications. Approximately 90% of the three-phase AC induction motors (IMs) lie on this type (Parekh 2003). It can be designed with fully sealed motors to operate in dirty and explosive environments. The single-phase was utilised in the household and small-scale applications that require fractional horsepower (Stephen L. Herman 2010), and it can be classified as:

- ❖ Split phase-type, which can be classified into:
- ➢ Capacitor starting motors: It was utilised in compressors, oil burners, and small machine equipment. Aside from other applications requiring strong starting torque in which the capacitor was only introduced at start-up (KELJIK 2013),
- ➢ Capacitor run motors, in which a constant capacitor was included from the start time. The power factor in the nominal load was approximately 100% or unity because of that the capacitor was used at all the times (KELJIK 2013).
- ➢ Binary capacitor motors that minimise the capacitance by mutating the capacitor when the motor has a stable operating status (ANDREA 1970),
- ➢ Permanent split capacitor (PSC); in which it has a run type capacitor perpetually connected in series with a start winding. The PSC motor starting torque was from 30% to 150% of the nominal torque. The PSC's

drives have a low start current, which was typically less than 200% of nominal current, making them magnificent for applications with high on/off cycle rates (Parekh 2003),

- Resistance starts motor; in which, the start winding seems more resistive and less inductive than the run winding, causing the start windings current to be less out of phase with the applied voltage (Grundfos Motor Book/ Single-phase motors. [no date]).
- Shaded-pole type; this motor was utilised in fan and other small gadgets due to its simple construction. These motors are usually, fractional horsepower ratings and were used in applications that have not affected by the starting torque (KELJIK 2013).
- Variable reluctance; constructed with the teethed ferromagnetic rotor with stator windings. The rotor movement was the result of reducing the magnetic reluctance between the rotor and the stator poles (Bishop 2002).

Moreover, there were many kinds of IMs utilised in a specific application.

3.2.3 Universal motor

The universal motors have had high torque and can operate at high speed, lightweight and can be operated on AC or DC voltage. AC was more common for use as a supply in most applications. This type of machine was preferred when a high power/weight ratio was required. The speed of the universal motor can usually be in the range of 200 to 5000 rpm. They were typically used in portable tools and equipment, as well as in many devices (Stephen L. Herman 2010).

3.3 Concluded remarks

The motor selection has lied within performance limits. The comparison of several aspects of each motor can be facilitated the identification of the motor that fits the intended application. The motor torque, power, and speed must exceed the load values involved. Usually, the motor moment of inertia was commonly higher than the load inertia. However, the low dynamic machines have accepted smaller quantities, and the high-dynamic machines have taken the most top. Also, every gear associated with all possible motors, in which the power and torque should meet the load requirements as well as the speed, have met the transmission conditions.

The DC motor, built from high-energy PM, was used in many industrial applications and studies due to the flexibility of speed torque properties, high efficiency, and low maintenance (Yedamale 2003; Nian et al. 2014; Naseri et al. 2017). The rates can vary, and full torque can be reached in the operating speed range. Not only such machine has used on fixed torque loads such as elevators and cranes, but also in an electric vehicle application. Moreover, automation and the requirement for controller and driver, controlled speed and torque have realised a resurgent enthusiasm for the utilisation of such DC motors. The advantages of utilising PMs in the electrical machines can be given as (GIERAS 2010);

- The excitation field system does not consume electric energy, so that, a significant increase in efficiency achieved because there were no excitation losses.
- Higher power density and torque density can be achieved when it contrasted with electromagnetic excitement,
- Better dynamic execution (higher magnetic flux density in the air gap) has been accomplished than electromagnetic excitation motors, and
- Streamline designed and easy maintenance

From all the benefits mentioned, the PMBLDC motor was considered in the designed test rig. In the following section, the PMBLDC actuators and its control conjunction, assemblies are explained.

3.4 Permanent magnet brushless direct current (PMBLDC) motor

According to the literature discussion, the PMBLDC motors were one of the leading actuators in control systems, with high-performance and capabilities. It can provide rotating movement along with wheels or drums that can access transitional motion.

All types of DC motor had worked under the fact that when a current-carrying conductor was placed in a magnetic field, this conductor experienced a mechanical force. So, it was essential to build a magnetic field when making a DC motor. The PMBLDC motor was a modified type of DC motor that uses a permanent magnet to generate the magnetic field required to operate a DC motor. However, the AC output has powered the PMBLDC motor at a controlled time throughout the configuration of each coil using the Hall sensor described in the next paragraph. The BLDC motor was being widely electronically commutated, used in industrial and automobile applications (Niapour et al. 2015). The significance of these engines has accompanied the one-of-a-kind attributes of the DC motor such as high starting torque for traction application, or where portable equipment must be kept running from a DC battery power supply. Furthermore, an integrated inverting switching circuit was utilised to achieve unidirectional torque. The free rotor body diagram can be represented as in Figure (3.8).

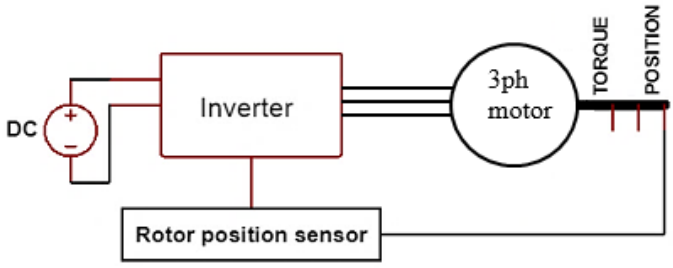

Figure 3. 8: Topology of PMBLDC motor

Contrasted with other types of motors, the PMBLDC was excited by a square wave, providing with many advantages, such as the use of higher permanent magnets, smaller dimensions, higher torque, high efficiency and reliability. Therefore, the PMBLDC motor has played an essential role in improving product quality, longevity, and energy-saving (Xia 2012).

3.4.1 PMBLDC construction

The PMBLDC motor structure has included a stator with armature winding and rotor with a permanent magnet. Figures (3.9, and 3.10) shows a sectional diagram and the construction of stator winding PMBLDC motor which consists of the fundamental element.

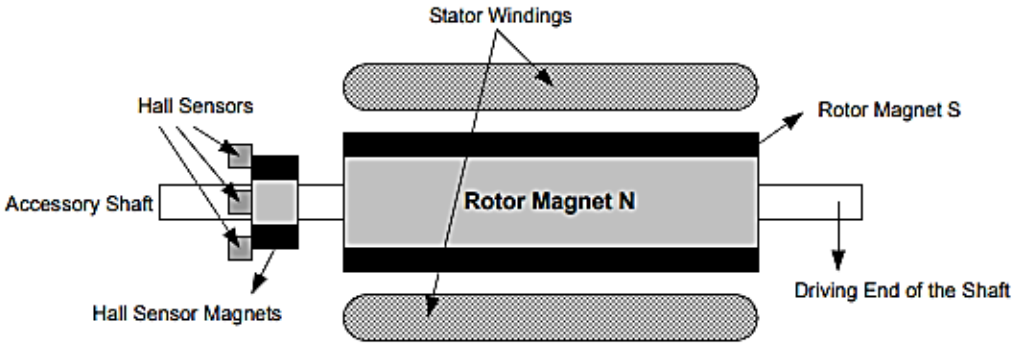

Figure 3. 9: PMBLDC motor transverse -section (adapted from (Yedamale 2003)**)**

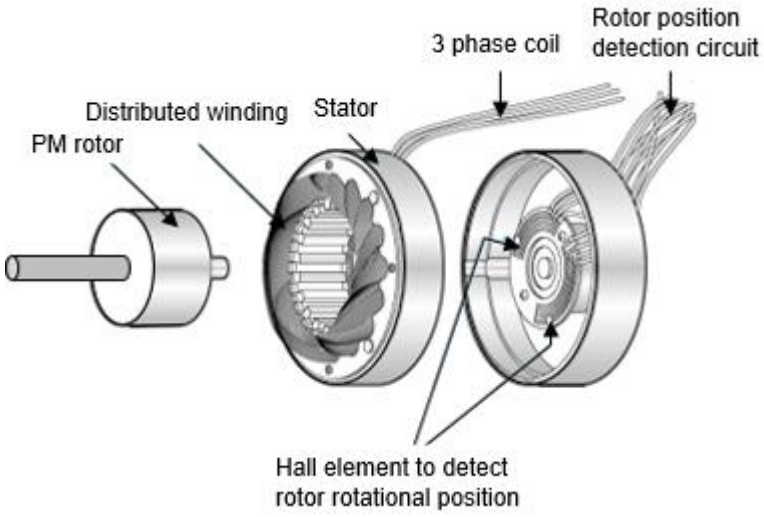

Figure 3. 10: Structure of PMBLDC motors (adapted from (Nidec Corporation 2019)**)**

- The stator cores: The structure of the BLDC motor was like that of a general synchronous motor or even an Induction motor shown in Figure (3.11). Single or multi-phase coils were implanted in the iron core, which can be set as star "Y" or delta "Δ" type connection. By considering the implementation and expense of the system, type Y was mostly used where three-phase windings were connected uniformly without a neutral point (Xia 2012). The stator windings can be classified as trapezoidal and sinusoidal motors. This separation was made based

on the coils' interconnection in the stator windings to allocate the various kinds of back electromotive force (E_{back}) in which the phase current has the same form accordingly (Yedamale 2003).

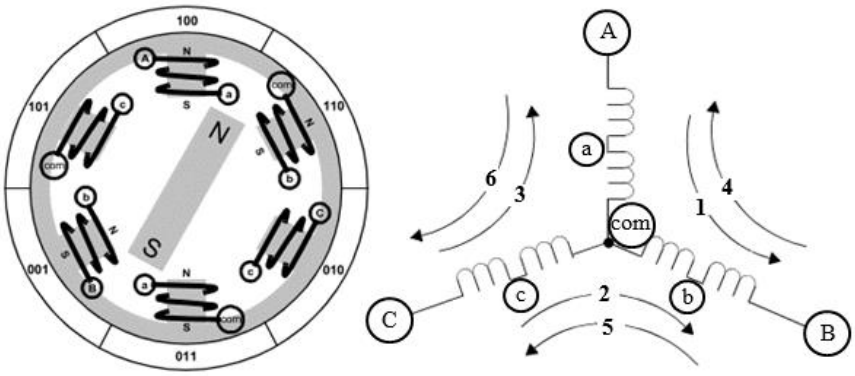

Figure 3. 11: The PMBLDC motor diagrams (adapted from (Brown 2002)**)**

- The PM rotor: the PMBLDC motor rotor consists of a PM with individual pairs of poles nestled in the surface or the inside of the iron core. Due to the magnetic field density needed in the rotor, the ferrite magnet is traditionally chosen as the appropriate magnetic material to make the rotor. The neodymium, ferrite and boron (NdFeB) was an example of rare earth alloys have the advantages of severe coercive, and remaining intensity (Xia 2012). The electrical energy was turned into mechanical energy by attractive magnetic forces between the PM rotor and the induced rotating magnetic field in the wound stator poles (Brown 2002).
- The position sensor: the installed position sensors in the motor can distinguish the rotor position and turn it into an electrical signal, indicating the correct commutation information for the logic gate circuit. Thus, the best possible switching of the coil was obtained through the rotor position information, and the PM rotor has continuously been rotated as a result of the persistent rotary magnetic field produced by the current in the air gap. There were different sorts of position sensors, and each has its attributes. Currently, a wide range of electromagnetic, photoelectric and magnetic sensors have been utilised in PMBLDC motors (Xia 2012). As a kind of magnetic sensor, the Hall sensor has minimal volume, low cost and convenient operation.

Therefore, it was generally utilised in PMBLDC motor control systems as the rotor position detector.

- Hall sensors: instead of the mechanical commutation for supplying the rotor with field and current, the design principle of a PMBLDC motor was to replace the mechanical commutator with the electrical switch circuit. The rotor position sensor, control circuit and power inverter should be included in the PMBLDC system to control motor speed and direction. The full-bridge (H-bridge for a single-phase PMBLDC motor) driving circuit was used to control transistor gates excitation, as shown in Figure (3.12).

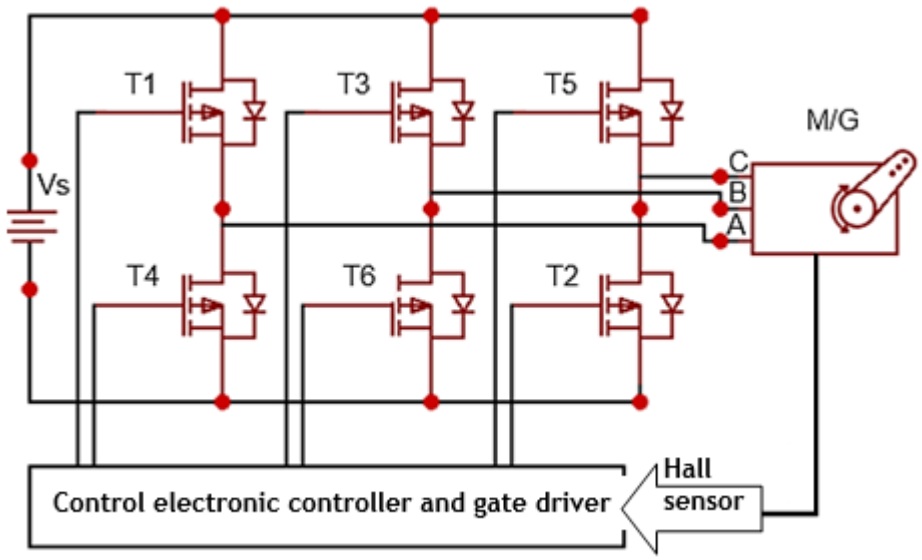

Figure 3. 12: Full-bridge driving circuit

- The control electronics can be used to change the stator field; the rotor utilises a PM so that no direct energy was supplied to the rotor. Detection devices must be used to determine the movement of the rotor to change the provided power of the field windings. When rotor speed increased or decreased; the sensor transmits information to the electronic switching source, which was adjusted continuously to provide the correct voltage to the right stator poles to maintain the speed and direction. Also, the dead-time control was a precaution measure against both drivers being active simultaneously. At the point when the drive output transition from the high to low state, more time was required for the upper side driver to switched off before initiated

the lower side driver. The drivers take more time to turn off than to turn on, so additional time must be enabled to pass, so both drivers were not conducting simultaneously.

- In the braking mode, the PMBLDC motor can be worked as a synchronous generator which converts mechanical power to ac electric power and then rectified throughout the same electronic controller to a DC electric power which can be used to charge the power supply (Vs).

3.4.2 PMBLDC motor working principle

The primary operation of the PMBLDC motor was that two windings operate simultaneously with equal and opposite polarities, with the rotor moving away from one of them. At the same time, the other draws the rotor towards him. This form has increased the overall torque capacity of the motor, and the Hall Effect sensor determines which two coils must be energised to achieve this strategy, as shown in Figure (3.13).

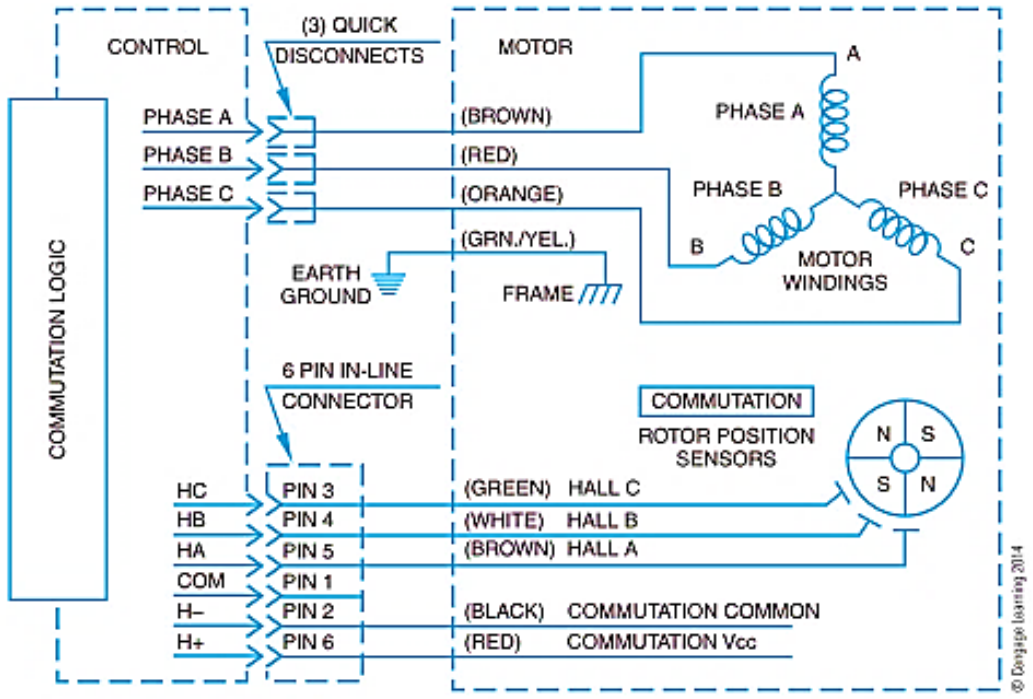

Figure 3. 13: PMBLDC motor the circuit diagram (adapted from (KELJIK 2013)**)**

Furthermore, an electronic controller continually excites each phase winding at a specific time in a pattern that rotates around the stator of the DC motor

to keep turning. The static alignment of the terminal voltage of each stator coils and Hall sensors feedback was shown in Figure (3.13), which was used to establishing an electrical current flow from terminal A to B, designated as a route (1), as shown in Figure (3.11) above.

3.4.2.1 Sensors commutation

Numerous PMBLDC motor manufacturers have provided motors with a three-element Hall Effect position sensor to detect the rotor's position. Based on the location of the Hall sensors, there were two types of output: 60° phase shift and a 120° phase shift. The combination of these three Hall sensor outputs can establish the exact communication sequence (Zhao and Yangwei 2011). The PMBLDC switch was used to detect the position of the rotor, then activate the phases that will produce the most torque. The rotor has travelled 60 degrees electric for each switching step. The current path of the appropriate stator was activated when the rotor is 120 degrees of alignment with the magnetic field of the corresponding stator. It was then deactivated when the rotor is 60 degrees of adjustment, at which time the next circuit was activated, and the process was repeated. Switching the rotor location, shown in Figure (3.11), follows the current route (2) and the beginning of the current path (3) to rotate clockwise (Brown 2002). The three sensors were counterbalanced from one another by 60 electrical degrees so that each sensor's output was in aligned with one of the electromagnetic circuits. For each step, there was one high state motor terminal, and the other one was in a low state, while the third terminal left floating. A timing diagram demonstrating the relationship between the sensor outputs and the required motor drive voltages is appeared in Figure (3.14) (Brown 2002).

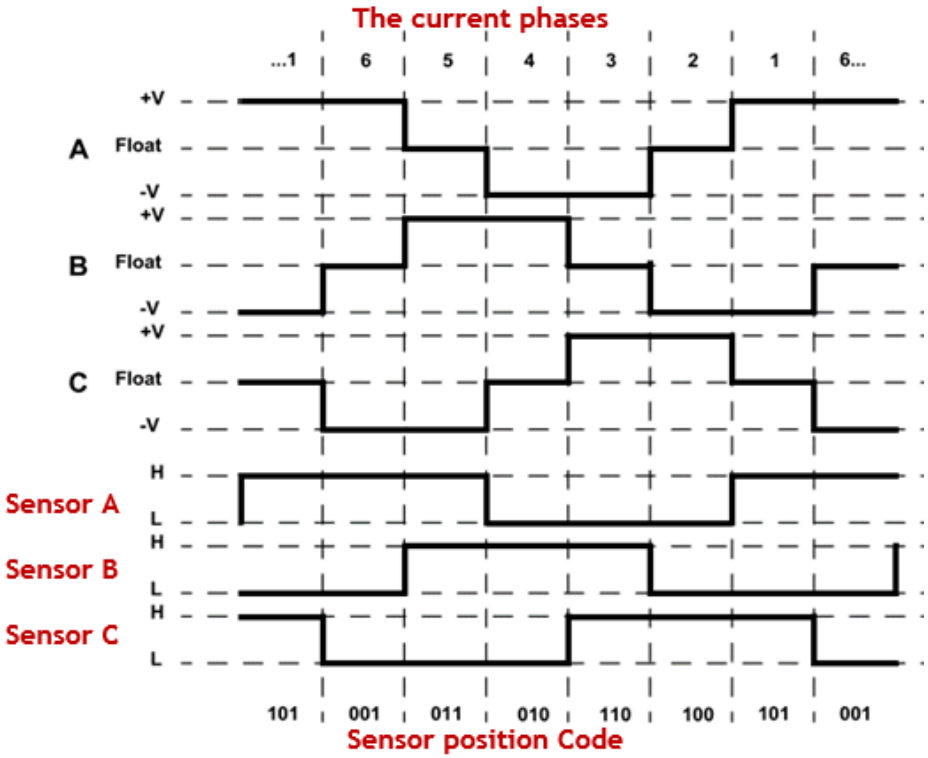

Figure 3. 14: Voltage time diagram of the PMBLDC motor (adapted from (Brown 2002)**)**

The commutation logic block was shown in Figure (3.14), which can be represented as appeared in Figure (3.15), which used to activate the metal oxide semiconductor field-effect transistor (MOSFET) gate signal.

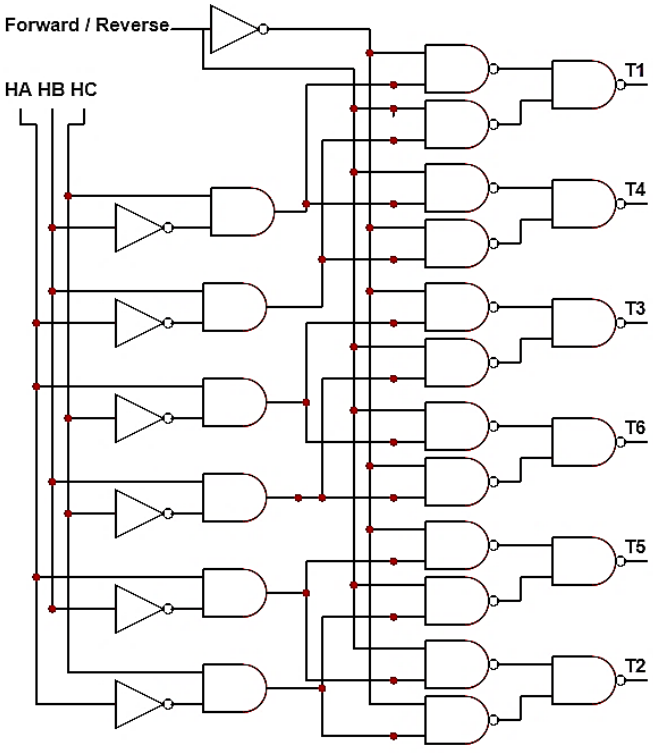

Figure 3. 15: Commutation logical signal circuit

The controller times commutation has indicated the speed of rotation (rpm) and the current waveforms produced to represent the torque. Three Hall sensors have used to detect the rotor position, each having a phase lag of 120º concerning the earlier one used to determine the location of the rotor field. Meanwhile, the next electromagnet stator was energised when the PM rotor begins to align with this active stator, and the rotor was continuously rotating. Also, from Figure (3.13), it was clear the internal feedback coming from shaft position (Hall Effect) sensors have given the desired information used in the drive electronics, and the characteristics of linearity (linear speed-torque) and high starting torque mimic the DC motor.

The simultaneous activation sequence of two windings starting from the first phase to the next and voltage timeline was shown in Figures (3.11, 3.14). The three sensor outputs were overlapping in such a way that six unique codes of three bits were generated corresponding to each of the drive phases.

Each drive phase has consisted of one high driven, one low driven, and one floating motor terminals. A single drive has controlled for the high, and low drivers allow for a high drive, low drive, and floating drive at each motor terminal. One of the vigilances to take with this type of driver circuit was to not activate the two high side drivers and the low side drivers at the same time. Also, when the output transitions from a high drive state to a low drive state, the appropriate time must be allowed for the high side driver to turn off before the low side driver is activated. Commutation consists of matching the input sensor state to the corresponding drive state, and the possible output drive codes list has shaped the state table (Brown 2002). The sensor states and motor drive states shown in Figure (3.14), can be represented, as shown in the following Tables (3.3-3.5).

Table 3. 3: Clockwise (CW) sensor and commutation drive bits by phase order

Current Phase	Sensor C M.S.b*	Sensor B	Sensor A L.S.b*	T5 High Drive C	T2 low Drive C	T3 High Drive B	T6 Low Drive B	T1 High Drive A	T4 Low Drive A
1	1	0	1	0	0	0	1	1	0
2	1	0	0	1	0	0	1	0	0
3	1	1	0	1	0	0	0	0	1
4	0	1	0	0	0	1	0	0	1
5	0	1	1	0	1	1	0	0	0
6	0	0	1	0	1	0	0	1	0

* The numbers are the sensor logic levels where the (M.S.b) represent the Most Significant bit, and (L.S.b) represent the Least Significant bit. Also, Phase A, phase B, and phase C were defined as (A, B, and C) in the Table.

The assortment of Table (3.3) according to the sensor binary-weighted code, is produced in Table (3.4). Activating the motor drivers, according to a state table built from Tables (3.3 and 3.4), will spin the motor clockwise.

Table 3. 4: CW sensor and commutation drive bits by sensor order

Current Phase	Sensor C	Sensor B	Sensor A	T5 High Drive	T2 low Drive	T3 High Drive	T6 Low Drive	T1 High Drive	T4 Low Drive
6	0	0	1	0	1	0	0	1	0
4	0	1	0	0	0	1	0	0	1
5	0	1	1	0	1	1	0	0	0
2	1	0	0	1	0	0	1	0	0
1	1	0	1	0	0	0	1	1	0
3	1	1	0	1	0	0	0	0	1

Counterclockwise (CCW) rotation is accomplished by directing current through the armature windings in the opposite direction to CW rotation. Table (3.5) was established by swapping all the high and low drives in the table (3.4). Energising the motor windings, according to the state table constructed from Table (3.5), will cause the motor to rotate CCW.

Table 3. 5: CCW sensor and commutation drive bits

Current Phase	Sensor C	Sensor B	Sensor A	T5 High Drive	T2 low Drive	T3 High Drive	T6 Low Drive	T1 High Drive	T4 Low Drive
/6	0	0	1	1	0	0	0	0	1
/4	0	1	0	0	0	0	1	1	0
/5	0	1	1	1	0	0	1	0	0
/2	1	0	0	0	1	1	0	0	0
/1	1	0	1	0	0	1	0	0	1
/3	1	1	0	0	1	0	0	1	0

The phase numbers in Table (3.5) were preceded by a bar indicating that the emf is opposite that of the phases in Table (3.4).

3.4.2.2 The practical drive modes

The control electronics of the electric drive depended on Hall sensor output to activate the excitation state of each gate in the designed test rig is as shown in Figure (3.16) and more specifically in Figure (3.17).

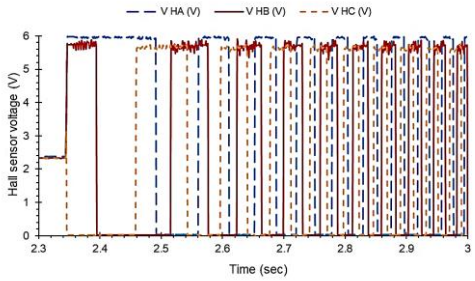

a- At starting operation

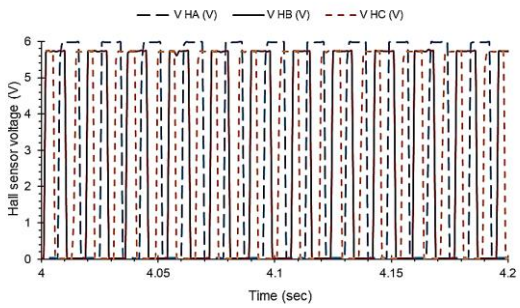

b- At steady-state operation

Figure 3. 16: Hall sensor control feedback practical signals measured

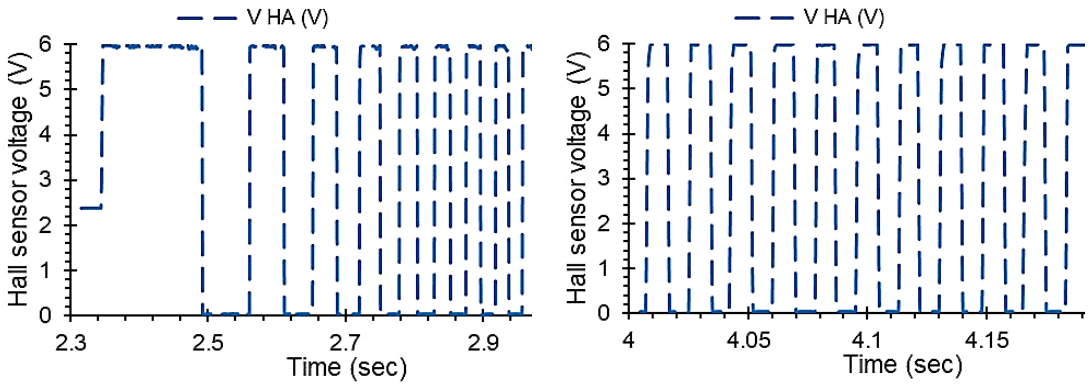

a- Hall A

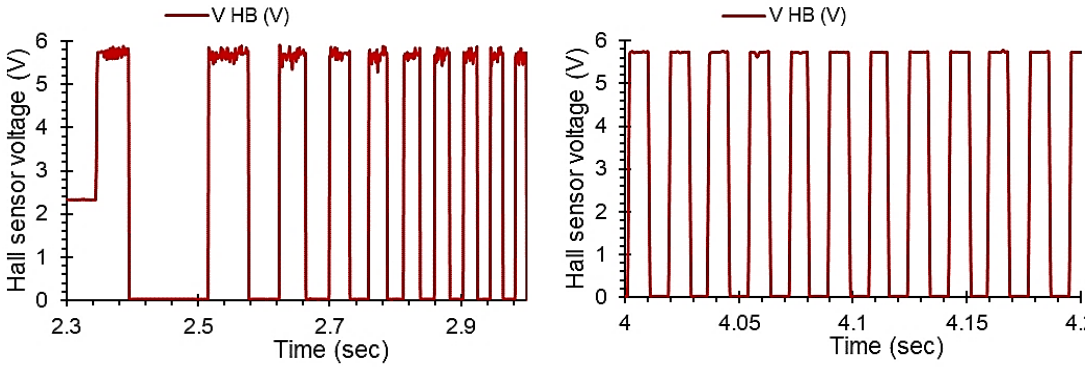

b- Hall B

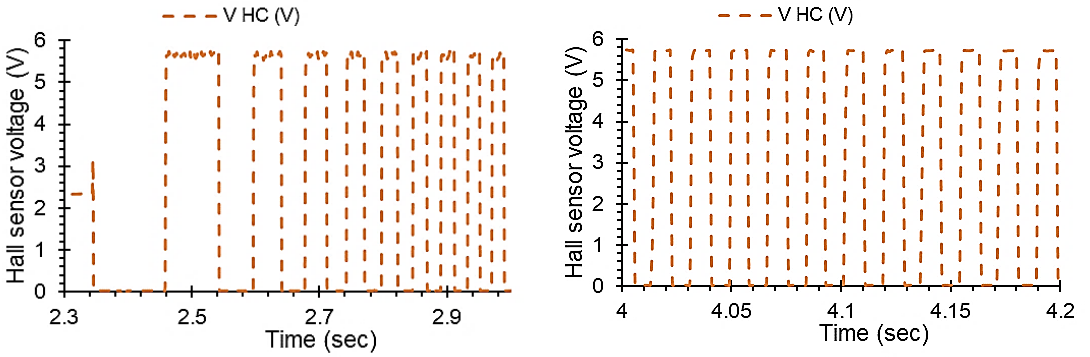

c- Hall C

Figure 3. 17: Individual practical Hall signals used in the test rig

3.4.2.3 The essential terms and definition

Understanding the fundamental terms used in the analysis and control of a PMBLDC motor was vital, and it can be defined as:

- The electrical time constant (t_e): Which represents the ratio of armature inductance to the armature resistance as $t_e = L_a/R_a$.
- The mechanical time constant (t_m): Which defined as the time when the unloaded motor achieves 63.2% of its final speed after applying a DC voltage.
- The fall time (t_f): Which represents the decline of the amplitude of system response to 37% of its study state value after removing the forcing signal.
- The total load current: It represents the armature current of the motor that operates at full load torque, and speed with the nominal voltage applied.
- Full load speed: It represents a motor speed run with maximum load torque and nominal voltage.
- The form factor of a harmonic signal: It was the ratio of RMS value to the average value in a half-cycle.
- Efficiency: It has represented the ratio of output power (p_o) to input power (p_{in}) as $\eta = p_o/p_{in}$.
- Incremental motion system: It was a control system that changes the loading position in separate steps quickly and repeatedly.
- Inertial match: It was a match of inertia J between the motor and the load. It was obtained by selecting the coupling ratio like the load moment of inertia indicated on the motor shaft is equal to the moment of inertia of the motor.
- Linearity for a speed system control: It was the maximum deviation between the actual speed and set speed defined as a percentage of the set speed.
- No-load speed: It was the motor speed with no external load.
- Speed regulation constant: It was the incline of the motor speed-torque characteristic.

3.4.2.4 Load characteristic

In practical applications, different types of loads exist with various torque-speed curves. For instance, conveyors, screw compressors, and feeders represent a constant torque variable speed load (Figure 3.18a). The fan and pump represent variable torque variable speed load (Figure 3.18b). Also, the constant power load can be seen in the traction motors (Figure 3.18c), while the constant power constant torque load represented by the winder motor (Figure 3.18d). Furthermore, the high starting/breakaway torque followed by constant torque load carried by extruders, and screw pumps (Figure 3.18e). The motor load system was designed stable when the developed torque was equal to the load torque requirements. The motor will run in a steady state at a fixed speed. Also, the motor response to any disturbance has given an idea of the stability of the motor loading system. This concept helps in the rapid assessment of the choice of a motor to drive the load. Figure (3.18) shows a comparison of different types of characteristics curves (Parekh 2003).

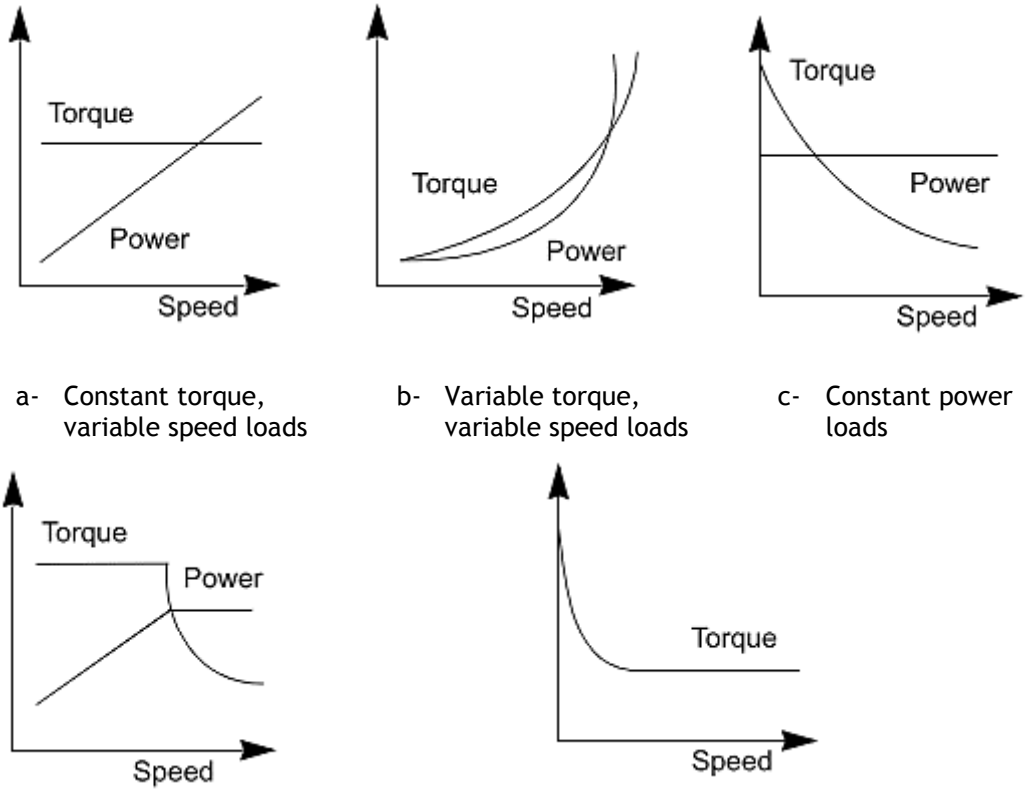

a- Constant torque, variable speed loads

b- Variable torque, variable speed loads

c- Constant power loads

d- Constant power, constant torque loads

e- High starting /breakaway torque followed by a constant torque

Figure 3. 18: Load characteristic curves (adapted from (Parekh 2003))

3.4.3 Mathematical model of the PMBLDC

This section presents the differential equation model for a three-phase PMBLDC motor. The stator has a Y-connected coil, and the internal rotor has PM structure. Three symmetrical hall sensors were arranged in 120° intervals. The system's input was the power source (Vs), measured in (V), applied to the motor, while the output was the shaft position (θ) measured in (rad).

3.4.3.1 Equivalent circuit and electromagnetic torque

The equivalent electric circuit of the PMBLDC motor can be represented, as shown in Figure (3.19).

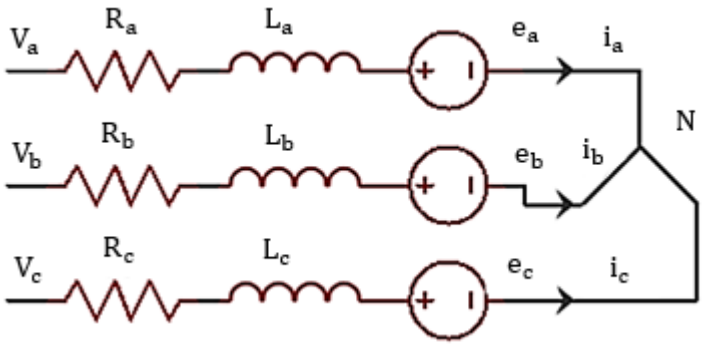

Figure 3. 19: PMBLDC motor circuit diagram

In PMBLDC motor, the input was electrical energy while the output was the mechanical energy with the air gap torque T_{em} at a rotational speed ω_m (Krishan R 2001). Assuming the three phases are similar, therefore the phase resistance $R_{a,b,c}$ and the self and mutual inductance $L_{a,b,c}$ in Figure (3.19) was equal to $R, \text{and } (L-M)$ measured in $(\Omega) \text{ and } (H)$, respectively. By applying Kirchhoff's Voltage Law (KVL) for each closed-loop of phase voltage, as shown in Figure (3.20).

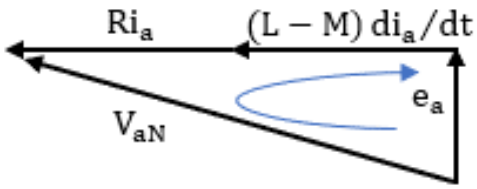

Figure 3. 20: KVL of phase A

Let $V_{aN} = V_a$, the following matrix equation is given:

$$\begin{bmatrix} V_a \\ V_b \\ V_c \end{bmatrix} = \begin{bmatrix} R & 0 & 0 \\ 0 & R & 0 \\ 0 & 0 & R \end{bmatrix} \begin{bmatrix} i_a \\ i_b \\ i_c \end{bmatrix} + \frac{d}{dt} \begin{bmatrix} L-M & 0 & 0 \\ 0 & L-M & 0 \\ 0 & 0 & L-M \end{bmatrix} \begin{bmatrix} i_a \\ i_b \\ i_c \end{bmatrix} + \begin{bmatrix} e_a \\ e_b \\ e_c \end{bmatrix} \quad (3.1)$$

Also, applying Kirchhoff's Current Law (KCL) at node N in Figure (3.19), then:

$$i_a + i_b + i_c = 0 \quad (3.2)$$

Under driving conditions, the internally developed motional emf (referred to back emf) necessary to the supplied voltage (Vs). The back emf produced (E_{back}) measured in (V) is proportional to the angular velocity $(\dot{\theta})$, $(\dot{\theta} = \omega_m)$ measured in (rad/sec), of the axis of rotation by a coefficient factor K_b.

$$e_a = e_b = e_c = E_{back} = K_b\dot{\theta} \quad (3.3)$$

Where, $K_b = K\varphi_f$ measured in V/(rad/sec), and φ_f, is the field flux (weber).

For phase a, to force the current on the motor, V_{aN} must be larger than the $E_{back}\left(K_b\dot{\theta}\right)$, giving the voltage equation of the motor as:

$$L_a\frac{di_a}{dt} + Ri_a = V_{aN} - K_b\dot{\theta} \quad (3.4)$$

At steady-state, the rate of change of armature current i_a is equal to zero because it is constant. Hence, equation (3.4) becomes:

$$V_{aN} = Ri_a + K_b\dot{\theta} \quad (3.5)$$

And, the total input power is obtained as:

$$V_{aN}i_a = Ria^2 + K_b\dot{\theta}i_a \quad (3.6)$$

Where $V_{aN}i_a$, is the total input power measured in watt, Ria^2, is the armature copper losses. While $K_b\dot{\theta}i_a$, is the active power that can be transformed from electrical to mechanical form as an air gap power P_a expressed as electromagnetic torque and rotational speed as:

$$P_a = \omega_m T_{em} = e_a i_a + e_b i_b + e_c i_c \quad (3.7)$$

The total electromagnetic torque (T_{em}) measured in (Nm) defined as:

$$T_{em} = [e_a i_a + e_b i_b + e_c i_c]/\omega_m \quad (3.8)$$

At the 120º conduction mode operation, when the motor in the Y-connection, current with the same magnitude and reverse direction will flow through any two-phases. T_{em} generated by the PMBLDC motor at constant flux, which was directly proportional to the armature current i, by the torque coefficient K_t, measured in Nm/A. Assume that $i_a = -i_b = i$, then:

$$T_{em} = K_t\, i \tag{3.9}$$

Under a consistent unit system such as SI units, the motor torque constant and the back emf constant could be the same as $K_t = K_b = K$ ((Kenjo and Nagamor 1985; Hughes 2006; Krishnan 2010)).

Since the PMBLDC motors stator windings were Y-connected, the line voltage is approximately equal to the DC bus voltage (Vs), when the relevant transistors were activated (Xia 2012). Thus, the bus voltage was a more suitable mathematical model for the active mode, for example ($V_{ab} = V_a - V_b = V_s$). Applying KVL for the closed-loop of the two active phases, as shown in Figure (3.21).

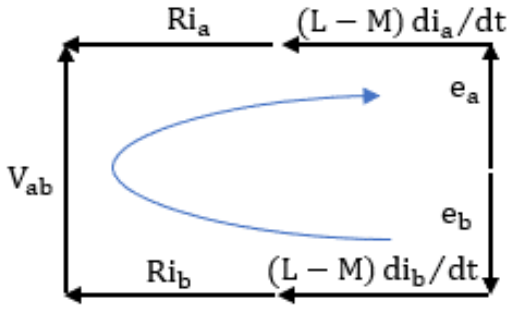

Figure 3. 21: KVL of two phases (A and B)

The following matrix equation is given:

$$\begin{bmatrix} V_{ab} \\ V_{bc} \\ V_{ca} \end{bmatrix} = \begin{bmatrix} R & -R & 0 \\ 0 & R & -R \\ -R & 0 & R \end{bmatrix} \begin{bmatrix} i_a \\ i_b \\ i_c \end{bmatrix} + \frac{d}{dt} \begin{bmatrix} L-M & -(L-M) & 0 \\ 0 & L-M & -(L-M) \\ -(L-M) & 0 & L-M \end{bmatrix} \begin{bmatrix} i_a \\ i_b \\ i_c \end{bmatrix} + \begin{bmatrix} e_a - e_b \\ e_b - e_c \\ e_c - e_a \end{bmatrix} \tag{3.10}$$

Furthermore, the bus voltage V_{ab}, for instance, in equation (3.10) can be expressed as:

$$V_{ab} = V_s = 2Ri + 2(L - M)\frac{di}{dt} + 2e_a = r_e i + L_e \frac{di}{dt} + K_e \dot{\theta} \qquad (3.11)$$

In equation (3.11), e_a, and e_b steadies value was equal in magnitude and reversed in direction when both phases A and B are activated. Also, r_e $(= 2R$), L_e $(= 2(L - M))$, were the total resistance and total inductance between any two phases respectively, and K_e, is the coefficient of bus back emf. Figure (3.22) show the two-phase activation equivalent circuit diagram.

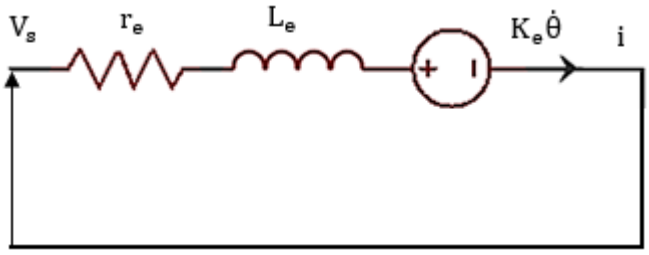

Figure 3. 22: Two-phase PMBLDC motor equivalent circuit diagram

3.4.3.2 Electromechanical modelling

The load was modelled as a moment of inertia (J), measured in (kgm^2/sec^2), with a viscous friction coefficient (b_v), measured in Nm/(rad/sec). The derivative of governing equations based on Newton's 2nd law and Kirchhoff's voltage law stated as:

$$J\ddot{\theta} + b_v\dot{\theta} = T_{em} - T_l = K_t i - T_l = T_a \qquad (3.12)$$

Where, T_a is the acceleration torque, T_l is the load torque measured in Nm.

At no-load operation equation (3.12) can be simplified as:

$$\left.\begin{aligned} J\ddot{\theta} + b_v\dot{\theta} &= K_t i \\ i &= \left(\frac{J}{K_t}\ddot{\theta} + \frac{b_v}{K_t}\dot{\theta}\right) \end{aligned}\right\} \qquad (3.13)$$

3.4.3.3 The transfer function of PMBLDC motor

The PMBLDC motor transfer function is essential for performance analysis and control design. Mathematical models based on transfer function were widely used in the fields of automatic control. Applying the Laplace transform, the

above modelling equations (3.11, 3.13) can be expressed regarding the Laplace variable (s) as:

$$\left.\begin{aligned}(L_e s + r_e)I(s) &= V_s(s) - K_e s\theta(s)\\ s(Js + b_v)\theta(s) &= K_t I(s)\end{aligned}\right\} \quad (3.14)$$

From equation (3.14), the following open-loop transfer function is given:

$$G_v(s) = \frac{\dot{\theta}(s)}{V_s(s)} = \frac{K_t}{(Js + b_v)(L_e s + r_e) + K_e K_t} \quad (3.15)$$

Where $G_v(s)$, is measured in (rad. sec)/volt.

However, the position can be obtained by integrating the speed, therefore:

$$G(s) = \frac{\theta(s)}{V_s(s)} = \frac{1}{s}\left[\frac{K_t}{(Js + b_v)(L_e s + r_e) + K_e K_t}\right] \quad (3.16)$$

Where $G(s)$, is measured in (rad)/volt.

Also, The speed response due to load torque disturbance can be given as:

$$G_l(s) = \frac{\dot{\theta}(s)}{T_l(s)} = \frac{-(L_e s + r_e)}{(Js + b_v)(L_e s + r_e) + K_e K_t} \quad (3.17)$$

Then, the speed response due to load torque disturbance and simultaneous input voltage can be implemented as the summation of their responses as the superposition principle holds:

$$\left.\begin{aligned}\dot{\theta}(s) &= G_v(s)V(s) + G_l(s)T_l(s)\\ \dot{\theta}(s) &= \frac{K_t V(s)}{(Js + b_v)(L_e s + r_e) + K_e K_t} - \frac{(L_e s + r_e)T_l(s)}{(Js + b_v)(L_e s + r_e) + K_e K_t}\end{aligned}\right\} \quad (3.18)$$

The time response of the speed can be implemented by taking the inverse Laplace of equation (3.18) for the change in input voltage and load torque. The structure of the PMPLDC motor control system with load can be built, as shown in Figure (3.23).

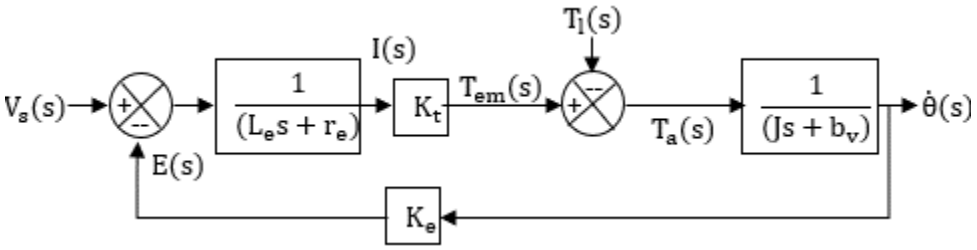

Figure 3. 23: Block diagram of the PMBLDC motor

Furthermore, equation (3.15) indicates that the PMBLDC motor can be implemented as a second-order system so that it can be re-represented as:

$$G_v(s) = \frac{\dot{\theta}(s)}{V(s)} = \frac{K_t}{r_e b_v + K_e K_t} \frac{{\omega_n}^2}{(s^2 + 2\xi\omega_n s + {\omega_n}^2)} \tag{3.19}$$

Where the natural frequency, ω_n, and damping ratio, ξ, of the second-order system is given as:

$$\omega_n = \sqrt{\frac{r_e b_v + K_e K_t}{L_e J}}, \qquad \xi = \frac{1}{2} \frac{r_e J + b_v L_e}{\sqrt{L_e J}\sqrt{(r_e b_v + K_e K_t)}} \tag{3.20}$$

From equation (3.20), the two roots of the characteristic equation of the PMBLDC motor are:

$$s_{1,2} = -\xi\omega_n \mp \omega_n\sqrt{\xi^2 - 1} \tag{3.21}$$

The system response time depends on both ω_n, and ξ. In which the convergence speed of the response curve depends on ω_n and the shape of the response curve determined by ξ.

To consider the mechanical time constant as t_m, which was equal to $(r_e J + b_v L_e)/(r_e b_v + K_e K_t)$, and the electromagnetic time constant t_e, which was equivalent to $(L_e J/(r_e J + b_v L_e))$, so, equation (3.15) can be represented as:

$$G_v(s) = \frac{\dot{\theta}(s)}{V_s(s)} = \frac{K_t}{r_e b_v + K_e K_t} \frac{1}{(s^2 t_m t_e + s t_m + 1)} \tag{3.22}$$

Equation (3.22) can be more simplified as,

$$G_v(s) = \frac{\dot{\theta}(s)}{V_s(s)} = \frac{K_t}{r_e b_v + K_e K_t} \frac{1}{(s t_m + 1)(s t_e + 1)} \tag{3.23}$$

Since, t_e is extremely small compared with t_m, then it is sensible to put, $t_e = 0$ (Kenjo and Nagamor 1985; Xia 2012).

Equation (3.23) can be clarified to be a first-order model as:

$$G_v(s) = \frac{\dot{\theta}(s)}{V_s(s)} = \frac{K_t}{r_e b_v + K_e K_t} \frac{1}{(st_m + 1)} \tag{3.24}$$

And the step response of equation (3.24) can be implemented as:

$$\dot{\theta}(t) = \frac{K_t V_s(t)}{r_e b_v + K_e K_t} (1 - e^{-\frac{t}{t_m}}) \tag{3.25}$$

When a step voltage applied to the motor input, the current will first respond to voltage change through the $1/(st_e + 1)$, with a delay of a time constant t_e. Next, the speed will increase react to the current change through the $1/(st_m + 1)$, with a delay of a time constant t_m (Kenjo and Nagamor 1985).

Figure (3.24) shows the correlation between armature current and angular speed process with a step input voltage.

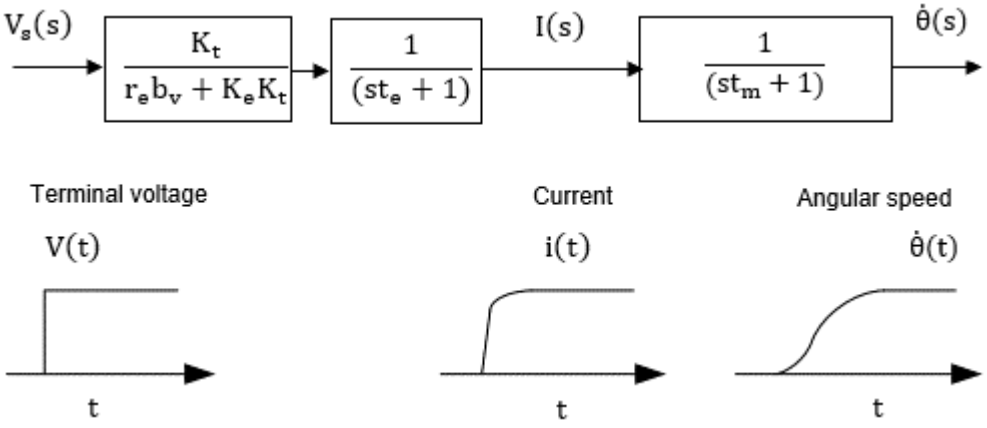

Figure 3. 24: Illustration of equation (3.23)

The mechanical time effect can be preferably achieved with a small value with shorter settling time for quick time response. However, when t_m, was high then a flexible closed control system must be designed and used to increase the response speed. For instance, a voltage or current amplifier with significant gain used in an analogue control system, as well as the more considerable proportional gain of PI controller in the digital control system can increase the open-loop gain of the system. Thus, the rise time of the response speed will be reduced and bring more losses of power switches which

reduce the efficiency of the system. So that response speed should be increased, subject to limits, under the condition of stability.

3.4.3.4 State-space equations of BLDC motor

In modern control theory, the motion condition of the control system was based on the state equation. All independent variables can be executed, and then all motion states of the system can be determined. The standard set of state-space equations can be described as:

$$\begin{aligned} \dot{\mathbf{x}} &= \mathbf{Ax} + \mathbf{Bu} \\ \mathbf{y} &= \mathbf{Cx} + \mathbf{Du} \end{aligned} \tag{3.26}$$

The PMBLDC motor state-space can be driven from the differential equations (3.11, 3.12) depending on the motor speed and armature current form the state variables. Also, armature voltage and load torque can be expressed as input, and rotational speed as output, as:

$$\left.\begin{aligned} \frac{d}{dt}\begin{bmatrix}\dot{\theta}\\ i\end{bmatrix} &= \begin{bmatrix}-\frac{b_v}{J} & \frac{K_t}{J}\\ -\frac{K_e}{L_e} & -\frac{r_e}{L_e}\end{bmatrix}\begin{bmatrix}\dot{\theta}\\ i\end{bmatrix} + \begin{bmatrix}0 & -\frac{1}{J}\\ \frac{1}{L_e} & 0\end{bmatrix}\begin{bmatrix}Vs\\ T_l\end{bmatrix} \\ y &= [1 \quad 0]\begin{bmatrix}\dot{\theta}\\ i\end{bmatrix} \end{aligned}\right\} \tag{3.27}$$

Where, the state variable $\mathbf{x} = [\dot{\theta} \quad i]^t$, the input vector $\mathbf{u} = [Vs \quad T_l]^t$,

$\mathbf{A} = \begin{bmatrix}-\frac{b_v}{J} & \frac{K_t}{J}\\ -\frac{K_e}{L_e} & -\frac{r_e}{L_e}\end{bmatrix}$, $\mathbf{B} = \begin{bmatrix}0 & -\frac{1}{J}\\ \frac{1}{L_e} & 0\end{bmatrix}$, and $\mathbf{C} = [1 \quad 0]$.

The roots of the system are calculated from matrix $\mathbf{A}$ as:

$$\lambda_1, \lambda_2 = \frac{-\left(\frac{r_e}{L_e} + \frac{b_v}{J}\right) \pm \sqrt{\left(\frac{r_e}{L_e} + \frac{b_v}{J}\right)^2 - 4\left(\frac{r_e b_v}{L_e J} + \frac{K_e K_t}{J L_e}\right)}}{2} \tag{3.28}$$

The eigenvalues in equation (3.28) will always have a negative real part, which indicates the motor was stable on the open-loop process (Krishan R 2001).

3.4.4 Performance of electric vehicles (EVs)

The overall driving performance was evaluated by acceleration time, maximum speed and climbing ability. All of these parameters have depended mainly on the features of the speed-power (torque) of the traction motor (Ehsani et al. 2010).

Variable speed drives have represented the characteristics of the traction motor with the motor has two operating zones, as shown in Figure (3.25). At low-speed (less than the nominal (base) speed), the motor has a constant torque. At high-speed (higher than the nominal speed), the torque has constant power. Also, in the low-speed operations, the voltage supply to the motor was increased by increasing the speed through the electronic converter while the flux remains constant. At the nominal speed, the motor voltage has reached the voltage source. After the nominal speed, the motor voltage has remained constant, and weakens the flux, falling hyperbolically with increasing speed. Therefore, the torque also has dropped dramatically with increased speed (Zeraoulia et al. 2010).

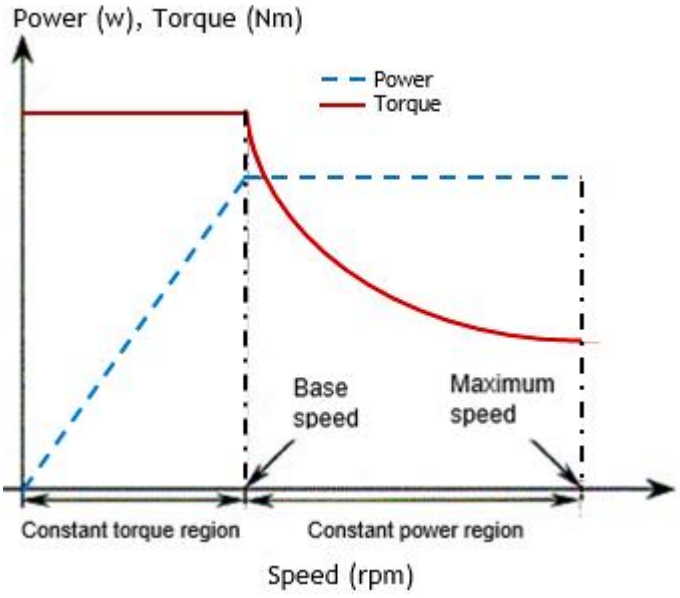

Figure 3. 25: Characteristics of the motor variable-speed

One of the main advantages of the electric motor from its characteristic curve was that it provides maximum torque at the starting speeds, and then controlled by the maximum available power while increasing the motor speed (REN 2010). With an extended constant power region, the most extreme torque of the motor can be significantly expanded, thus improving the vehicle

acceleration and ascending ability performance, and can be simplified the transmission. The maximum motor torque was specified by the motor characteristic curve determined as:

$$T_{max} = \begin{cases} T_N, & \omega_m < \omega_b \\ P_N/\omega_m, & \omega_m \geq \omega_b \end{cases} \quad (3.29)$$

Where T_{max}, is the motor maximum braking torque, T_N, is the motor rated torque, ω_b, is the motor base angular speed, ω_m, is the motor angular speed, and P_N, is the motor rated power. Notwithstanding, each kind of motor inherently has a constrained top speed proportion (Ehsani et al. 2018).

3.5 Drive cycles and Drivetrain

3.5.1 Introduction

A driving cycle was the representative of the road, and it was a set of data points for vehicle speed with time travelling at a specific path. The routes vary depending on countries which have represented driving rates and average driver habits on how to speed up and slow down when moving in a street or highway road (Khajepour et al. 2014). Also, the driving cycle can be considered as a fixed vehicle operating schedule determined by vehicle speed and gear selection based on the time used in the emission test. It was also useful that driving cycles could be used for a variety of purposes other than emission measurements, as an example, for engine durability testing or transmission, and the laboratory kinematic measurements (Gorton et al. 2009).

Furthermore, it was modified to be utilised to compute the amount of energy necessary for a vehicle to complete the journey as well as the regenerative braking (RB) kinetic energy recovery. For engineering studies, some limited situations have been developed that cover in one way or another typical road features and terrain that one might expect to find. Using some of these files, one can create or tune many arbitrary road profiles (Mi et al. 2011). Depending on the nature of the speed and load changes, the cycles can be mainly divided into steady-state (cruising) and transient. The steady-state

process was a series of fixed engine speed and load patterns used to evaluate heavy-duty engine vehicles. While transient driving cycles were at which many changes include representing typical constant speed changes for road driving (Barlow et al. 2009). There were many examples of the transient driving cycle that were tailored to specific requirements. The "New European Driving Cycle" (NEDC), for instance, was used for type approval of vehicle models in the EU. It was a highly stylised cycle, with periods of continuous acceleration, deceleration, and speed, which have little to do with actual driving patterns on the road. A real-world sequence from a trip or segments of data can be compiled from several trips to produce an analogue cycle. However, the drive cycles and drivetrain will be studied in detail for the evaluation and validation of the test platform. Also, it was proposed in the RB process as an alternative to evaluating fuel performance and vehicle emissions, which were added contribution to these research objectives.

3.5.2 The kinematic utility

The International Energy Outlook 2017 (IEO2017) provides information about energy-related carbon dioxide (CO_2) emissions., as shown in Figure (3.26).

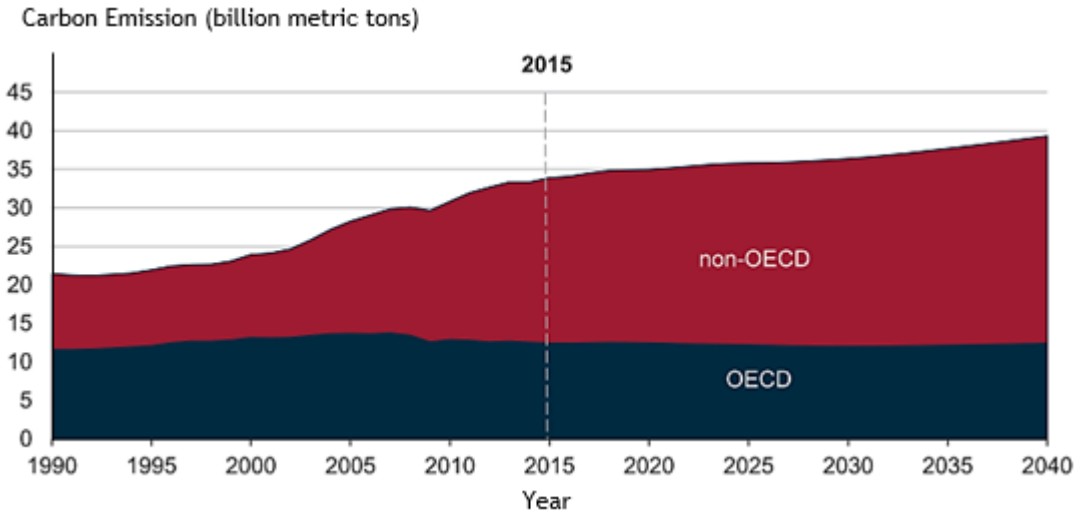

Figure 3. 26: World energy-related CO_2 emissions (adapted from (EIA 2017))

Figure (3.26) indicate that in OECD countries, energy-related CO_2 emissions remain inherently stable until 2040, which was 9% lower than in 2005, even as their economies gradually evolve. While in non-OECD countries, this percentage was increasing at a rate of less than 1% per year from 2015 to

2040. A lower rate than between 1990 and 2015 when emissions have increased by 3% per year. (EIA 2017).

In the transport sector, modelling of emission factors was identified as a discrete function of traffic situations which characterised by a speed profile called the driving pattern. The driving pattern has allowed the calculation of a wide range of kinematic parameters with a quantitative description of any traffic situation. The method of the modelling approach was achieved not only by the speed profile, and the kinematic parameters of the source cycles but also from the testbench measurements (De Haan and Keller 2004). Driving patterns were optimally determined, as the sum of squared differences between the target and the extended mix of sources of kinematic parameters with minimal.

3.5.3 Characteristics of the driving patterns

The kinematic characteristics of the driving modes were used to describe a speed profile comprising n data rows of time measured in seconds, ($t_i: 1 \leq i \leq n$), and speed measured in km/h, $v_i: (1 \leq i \leq n)$. The variable parameter can be computed as shown in Table (3.6) (Barlow et al. 2009);

Table 3. 6: The description of kinematic characteristics of the driving patterns

Distance (m)	
Total driving distance of the driving pattern	$\text{dist} = (t_2 - t_1)\left(\frac{v_1}{3.6}\right) + \sum_{i=2}^{n}(t_i - t_{i-1})\left(\frac{v_i}{3.6}\right)$
Time (sec, or %)	
Drive time spent accelerating	$T_{acc} = \begin{cases} t_2 - t_1 & (a_i > \text{acc\_threshold}) \\ 0 & (\text{else}) \end{cases} + \sum_{i=2}^{n} \begin{cases} t_i - t_{i-1} & (a_i > \text{acc\_threshold}) \\ 0 & (\text{else}) \end{cases}$ With $\text{acc\_threshold} = 0.06\ m/s^2$

	and, $a_i = \begin{cases} \frac{v_2 - v_1}{3.6\,(t_2 - t_1)} & (i = 1) \\ \frac{v_{i+1} - v_{i-1}}{3.6\,(t_{i+1} - t_{i-1})} & (2 \le i \le n-1) \\ \frac{v_n - v_{n-1}}{3.6\,(t_n - t_{n-1})} & (i = n) \end{cases}$
Drive time spent decelerating	$T_{dec} = \begin{cases} t_2 - t_1 & (a_i < -\text{acc\_threshold}) \\ 0 & (\text{else}) \end{cases} + \sum_{i=2}^{n} \begin{cases} t_i - t_{i-1} & (a_i < -\text{acc\_threshold}) \\ 0 & (\text{else}) \end{cases}$
Time spent braking	$T_{brake} = \begin{cases} t_2 - t_1 & (a_i < \text{brake\_threshold}) \\ 0 & (\text{else}) \end{cases} + \sum_{i=2}^{n} \begin{cases} t_i - t_{i-1} & (a_i < \text{brake\_threshold}) \\ 0 & (\text{else}) \end{cases}$
Total time	$T_{total} = t_2 - t_1 + \sum_{i=2}^{n} (t_i - t_{i-1})$
Stopping time	$T_{stop} = \begin{cases} t_2 - t_1 & (v_1 = 0 \wedge a_1 = 0) \\ 0 & (\text{else}) \end{cases} + \sum_{i=2}^{n} \begin{cases} t_i - t_{i-1} & (v_i = 0 \wedge a_i = 0) \\ 0 & (\text{else}) \end{cases}$
Driving time	$T_{drive} = T_{total} - T_{stop}$
Cruise time	$T_{cruise} = T_{drive} - T_{acc} - T_{dec}$
% of time driving	$\%\,drive = T_{drive}/T_{total}$
% of time cruising	$\%\,cruise = T_{cruise}/T_{total}$
% of time accelerating	$\%\,acc = T_{acc}/T_{total}$
% of time decelerating	$\%\,dec = T_{dec}/T_{total}$
% of time braking	$\%\,brake = T_{brake}/T_{total}$
% of the time standing	$\%\,stop = T_{stop}/T_{total}$
Speed (km/h)	
Average speed (trip)	$\bar{v}_{trip} = 3.6\,dist/T_{total}$
Average driving speed	$\bar{v}_{drive} = 3.6\,dist/T_{drive}$

The standard deviation of speed (compatible with $\overline{v}_{trip}$)	$v\_sd = \sigma_v = \sqrt{\frac{1}{n-1}\sum_{i=1}^{n} {v_i}^2}$
Acceleration (m/s^2)	
Average acceleration	$a\_av = \overline{a} = \frac{1}{T_{total}}\sum_{i=1}^{n} a_i$
Average positive acceleration	$a\_pos\_av = \overline{a}_{pos} = \left[\sum_{i=1}^{n} \begin{cases} 1 & (a_i > 0) \\ 0 & (else) \end{cases}\right]^{-1} \sum_{i=1}^{n} \begin{cases} a_i & (a_i > 0) \\ 0 & (else) \end{cases}$
Average negative acceleration	$a\_neg\_av = \overline{a}_{neg} = \left[\sum_{i=1}^{n} \begin{cases} 1 & (a_i < 0) \\ 0 & (else) \end{cases}\right]^{-1} \sum_{i=1}^{n} \begin{cases} a_i & (a_i < 0) \\ 0 & (else) \end{cases}$
The standard deviation of acceleration	$a\_sd = \sigma_a = \sqrt{\frac{1}{n-1}\sum_{i=1}^{n} {a_i}^2}$
The standard deviation of positive acceleration	$a\_pos\_sd = \sigma_{a\_av\_pos} = \sqrt{\frac{1}{n_{a\_poss}-1}\sum_{i=1}^{n} \begin{cases} {a_i}^2 & (a_i > 0) \\ 0 & (else) \end{cases}}$ where, $n_{a\_poss} = \sum_{i=1}^{n} \begin{cases} 1 & (a_i > 0) \\ 0 & (else) \end{cases}$
No. of acceleration (unitless)	$acc\_nr = \sum_{i=1}^{n} \begin{cases} 1 & (a_i > acc\_threshold \wedge a_{i-1} \leq acc\_threshold) \\ 0 & (else) \end{cases}$
Acceleration per km (/km)	$acc\_rate = 1000\frac{acc\_nr}{dist}$
Stop	
Number of stops (unitless) occurring during the driving pattern	$Stop\_nr = \sum_{i=1}^{n} \begin{cases} 1 & (\{v_i = 0 \wedge a_i = 0\} \wedge \{v_{i-1} \neq 0 \vee a_{i-1} \neq 0\}) \\ 0 & (else) \end{cases}$

Stops per km (/km)	$\text{Stop\_rate} = 1000\frac{\text{stop\_nr}}{\text{dist}}$
Average stop duration (m)	$\text{Stop\_T\_av} = \overline{T}_{stop} = \frac{T_{stop}}{\text{stop\_nr}}$
Dynamic oriented	
Relative positive acceleration (m/s^2)	$RPA = \frac{1}{dist}\sum_{i=1}^{n}\begin{cases}\frac{a_i v_i}{3.6} & (a_i > 0)\\ 0 & (\text{else})\end{cases}$
Positive kinetic energy (m/s^2)	$PKE = \frac{1}{dist}\sum_{i=2}^{n}\begin{cases}{v_i}^2 - {v^2}_{i-1} & (v_i > v_{i-1})\\ 0 & \text{else})\end{cases}$
Relative positive speed (RPS), relative real speed (RRS) (unitless)	$RPS, RRS = \frac{\frac{1}{T}\int_0^T (v_i)\,dt}{\overline{v}} = \frac{\int_0^T (v_i)dt}{x}$
Relative square speed (RSS), relative positive square speed (RPSS), and relative real square speed (RRSS) (m/s)	$RSS, RPSS, RRSS = \frac{\frac{1}{T}\int_0^T (v_i)^2\,dt}{\overline{v}} = \frac{\int_0^T (v_i)^2\,dt}{x}$
Relative cubic speed (RCS), relative positive cubic speed (RPCS), and relative real cubic speed (RRCS) (m^2/s^2)	$RCS, RPCS, RRCS = \frac{\frac{1}{T}\int_0^T (v_i)^3 dt}{\overline{v}} = \frac{\int_0^T (v_i)^3\,dt}{x}$
Root mean square of acceleration (m^2/s^2)	$RMSA = \sqrt{\frac{1}{T}\int_0^T (a)^2\,dt}$

3.5.4 Driving cycle examples

The transient driving cycle was designed for requirements. These requirements can be represented as (Barlow et al. 2009);

- Road-side vehicle testing, such as the Environmental Protection Agency (EPA) Inspection and Maintenance (IM240), was represented, as shown in Figure (3.27):

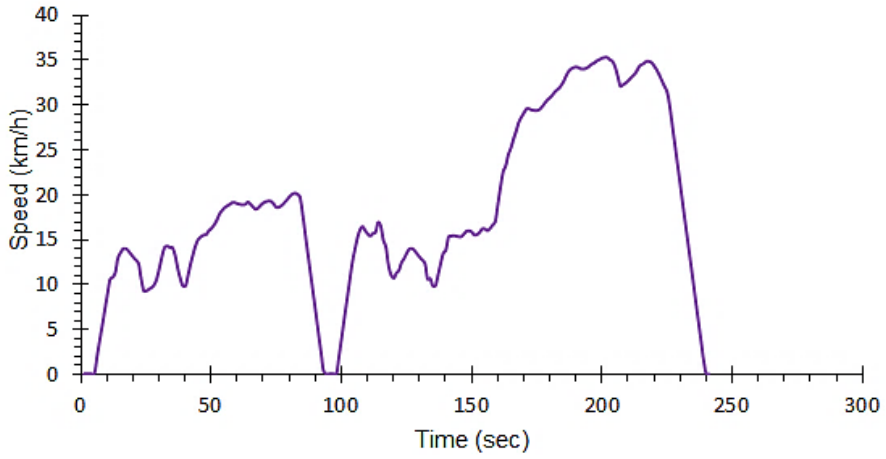

Figure 3. 27: EPA IM240 Inspection & Maintenance Driving Schedule

- The city test "LA4"; used for light-duty vehicle testing, represents city driving conditions such as the US Environment Protection Agency (EPA) designed Urban Dynamometer Driving Schedule (UDDS), was defined, as shown in Figure (3.28):

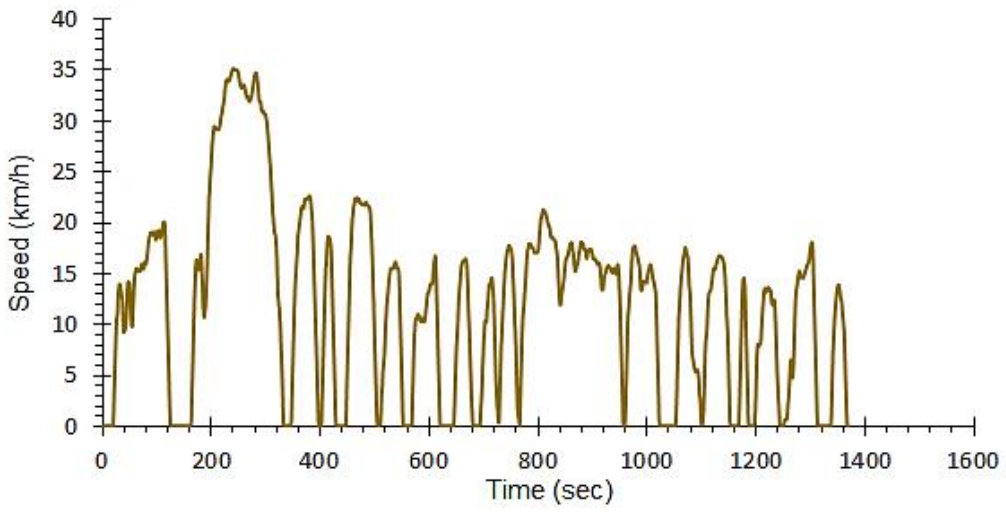

Figure 3. 28: The EPA Urban Dynamometer Driving Schedule (UDDS)

- The UN/ECE Elementary Urban Cycle (Part1); which has included the United Nations, the Economic Commission for Europe (UN/ECE) Agreement WP.29 of 1958 and its addition, as shown in Figure (3.29):

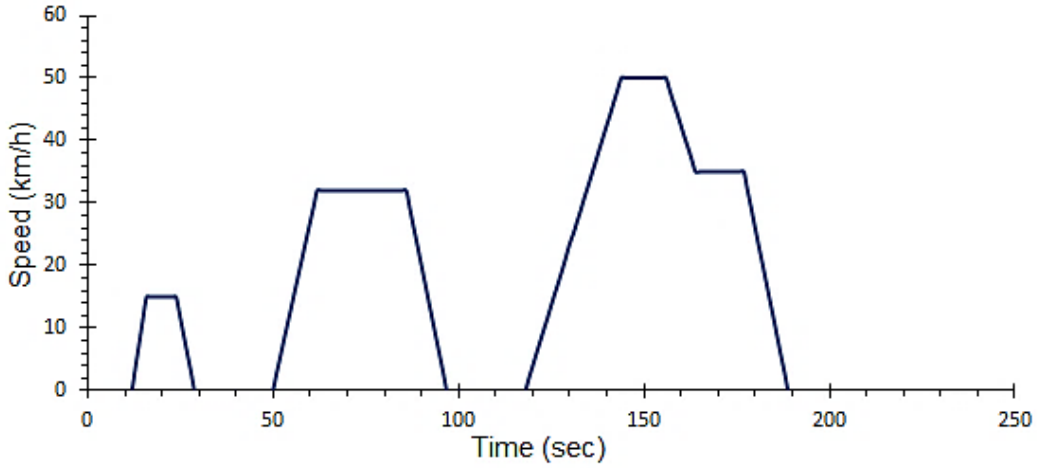

Figure 3. 29: The UN/ECE Elementary Urban Cycle (Part1)

- The UN/ECE Extra-Urban Driving Cycle (Part 2); which was found explicitly in regulation 83 used for Low-Powered Vehicles, as shown in Figure (3.30):

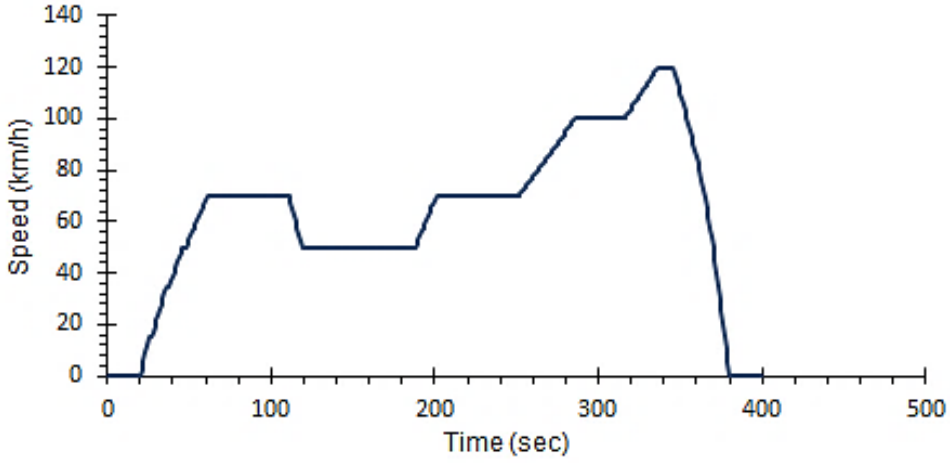

Figure 3. 30: The UN/ECE Extra-Urban Driving Cycle (Part 2)

- Driving specified in the Japanese technical standards (a) (10.15 Mode Driving Schedule): Official guidance was in the technical standards of the Japan Industrial Safety and Health Association (JISHA) for exhaust measurement and fuel economy test, and (b) Japanese 10 Dynamometer Driving Schedule (DDS), as shown in Figure (3.31a, b).

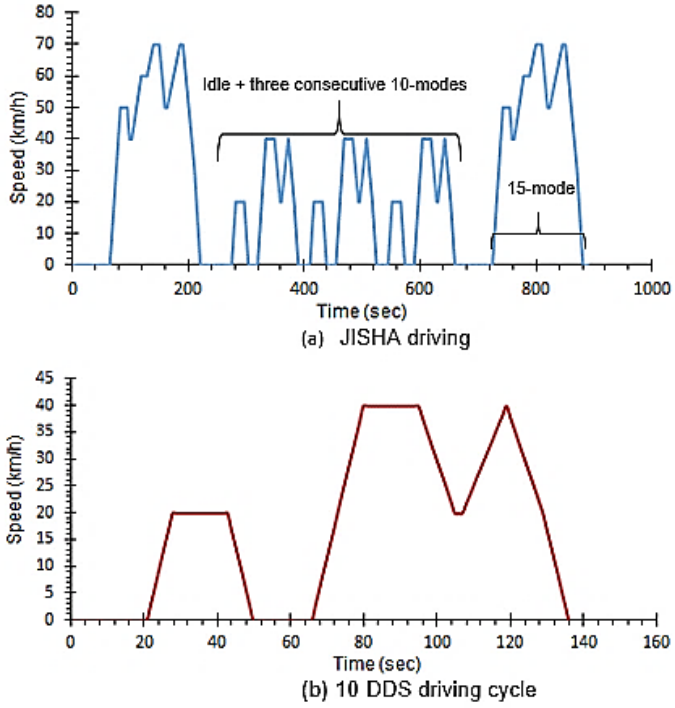

Figure 3. 31: Japanese Driving Schedule

Furthermore, Figure (3.32) shows more driving schedules:

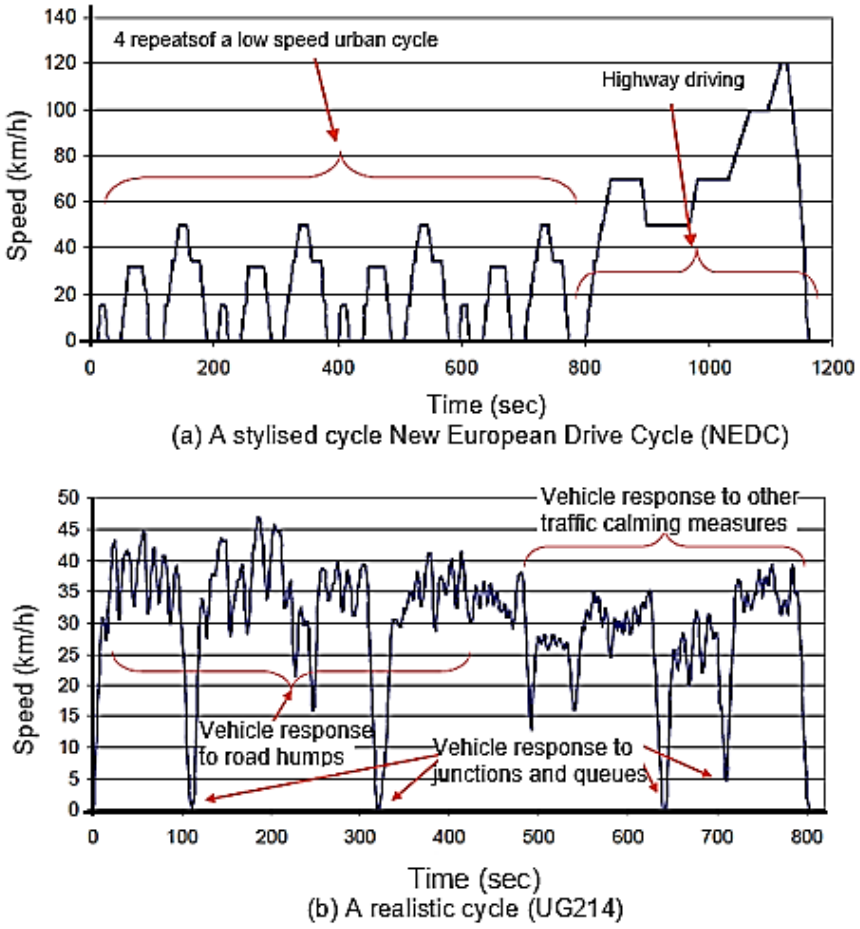

Figure 3. 32: Driving cycle examples (adapted from (Barlow et al. 2009))

3.5.5 Vehicle Road Load and Fuel Economy online calculator

The online tool (available at http://www.virtual-car.org/wheels/wheels-road-load-calculation.html) can be used to calculate the road energy needed to drive a vehicle along with a specific driving cycle. Also, it can be used to estimate the fuel economy the car to achieve the average power train efficiency that specified. It has been implemented in particular examples of drive train analysed for the same input power train to get the traction demand output completed with the velocities contained in a second-by-second driving cycle based on a simple driving motion.

- Driving Cycle: Urban Dynamometer Driving Schedule (UDDS)

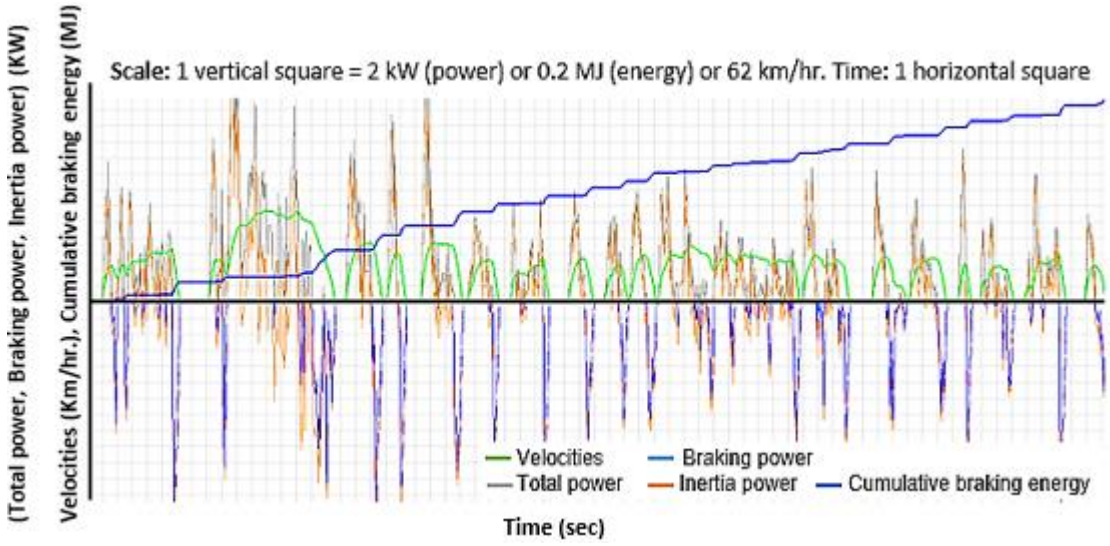

Figure 3. 33: The online UDDS traction demand output

In the analysis of the drive cycle shown in Figure (3.33), with 1369 seconds in the driving cycle, there was 544 sec time in acceleration, 105 sec time in powered deceleration, 109 sec time in a cruise, and 370 sec time in braking. The total distance travelled about 11.99 km. The full power required on wheels was about 5038317.28 J with 49.81% of the energy consumed by the brakes compared with 27% of time braking.

- Driving Cycle: UN/ECE Elementary Urban Driving Cycle (ECE-ELEM)

Figure 3. 34: The online ECE-ELEM traction demand output

In the analysis of drive cycle shown in Figure (3.34), with 195 seconds in the driving cycle, there was 42 sec time in acceleration, 0 sec time in powered deceleration, 57 sec time in a cruise, time in idle 60, 241 sec time in idle, and 36 sec time in braking. The total distance travelled about 0.9978 km. The full power required on wheels is about 361168.70 J with 54.72 % of the energy consumed by the brakes compared with 18.4% of time braking of the total time. The same procedure has been applied to a specific pattern, and the importance of energy recovery in the braking process should be completed to improve system performance and efficiency.

Table (3.7) shows a comparison of three available driving cycle kinematic calculation which can be utilised in RB analysis.

Table 3. 7: Driving kinematic cycle calculation

Cycle name	(a)	(b)	(c)
Total distance (m)	994.60	6955	4165
Total time (sec)	195	400	660
Driving time (sec)	132	359	488
Drive time spent accelerating (sec)	45	110	195
Drive time spent decelerating (sec)	40	49	173
Stopping time (sec)	45	41	172
The standard deviation of speed (km/h)	15.58	26	19.68
Average speed (trip) (km/h)	18.40	62.60	22.70
Average driving speed (km/h)	23.87	69.70	30.73
Maximum speed (km/h)	50	120	70
Average positive acceleration (m/sec^2)	0.35	0.27	0.37
Average negative acceleration (m/sec^2)	-0.39	-0.42	-0.39
Number of accelerations	3	4	13
Number of stops	4	2	8
Stops per km (/km)	4	0.29	1.92
Relative square speed (m/sec)	9.44	21.70	12
Root mean square of acceleration (m/sec^2)	0.18	0.09	0.16
Positive kinetic energy (m/s^2)	3.81	2.42	4.17

Where cycle name (a) represents the UN/ECE Elementary urban cycle (Part1), (b) The UN/ECE extra-urban driving cycle (Part 2), and (c) Japanese 10.15 Mode Driving Schedule (JISHA) respectively.

3.6 DC-DC converters

The DC-DC converters have been designed to provide an efficient energy conversion with a regulated DC power source for a variety of electronic circuit, that was increasingly essential in a wide range of applications (Roberts 2014). Many circuits design has used power at several levels of voltages. Switching power from one source was often more convenient rather than trying to distribute many various supplies, including battery-operated equipment or systems with a spare battery (Krein 1998).

3.6.1 Topologies of DC-DC converters

The DC-DC converters were used in regulated switch mode to convert and to control the DC output voltage in DC motor drive and other applications, such as battery chargers to the desired level. These converters were used in the form of switched-mode DC power supply with an electrical isolation transformer and without isolation in DC motor drive (Cathey 2002). Switching regulators can be categorised into two main types, such as:

- Non-isolated converters

These converters have been recognised as the input and the output share a standard path during the process,

- The isolated converters

These converters' energy has been transmitted through dual magnetic components, where the coupling between input and output has been achieved by an electromagnetic field, which allows isolation between them.

Furthermore, the DC-DC converters should provide a constant DC voltage with low output impedance over a wide range of frequency. These features were known as the output regulation of the inverter. With the non-ideal characteristic of the source, the DC-DC converters must be kept up the trustworthiness of the output power. Unlike linear regulators, which uses a resistive voltage drop with discharge excess energy as heat

to create and regulate the output voltage. While switching regulators have taken advantage of the energy stored in the magnetic field of the inductor or the electric field of the capacitor to transmit power in discrete power groups. The switch controller ensures that the power required by the load was transferred, so this structure is adequate. Figure (3.35) illustrates the simplified system of the switching regulator (Roberts 2014).

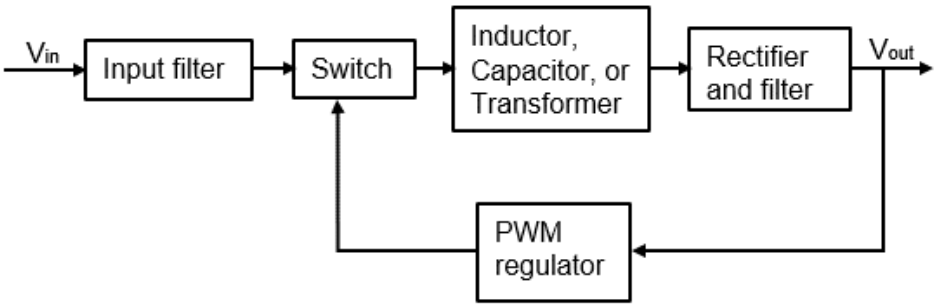

Figure 3. 35: Switch regulator block diagram

Furthermore, in an industrial application, the rapid development of DC-DC conversion techniques have derived from choppers. Choppers or DC-DC converters, which converts DC voltage into various levels of DC voltage, was generally used according to its quadrant operation as a multiple-quadrant chopper (Skvarenina 2002; Luo and Ye 2006). The DC motor was running in the forward or the reverse direction of activities. In the forward motoring (quadrant I) process, its armature voltage $V_{o,\ av}$, and current $I_{o,\ av}$ were both positive. In contrast, in the forward braking regenerating (quadrant II) process, its armature voltage was still positive, and its current was negative. Consequently, during the reverse starting (quadrant III) process, its armature voltage and current were both negative. Although, in the reverse braking regenerating (quadrant IV) process, its armature voltage was still negative, and its current was positive, as shown in Figure (3.36)

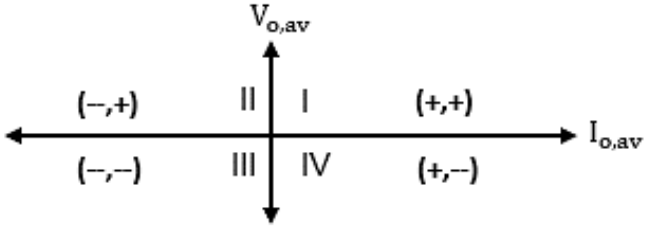

Figure 3. 36: Four quadrant operation chopper

Also, there have been different types of converters used in industrial applications designed to meet the requirements of specific applications. These converters have classified by their functions, characteristics and development sequence to a step down (buck), step-up (boost), and step-down/ step-up (buck/ boost) converters (Johansson 2005), as shown in Figure (3.37).

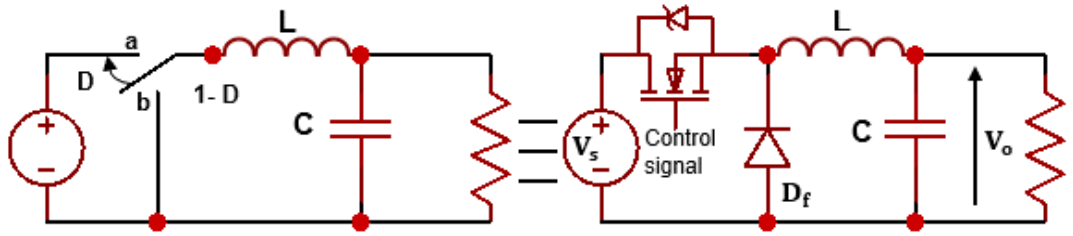

(a) Buck converter

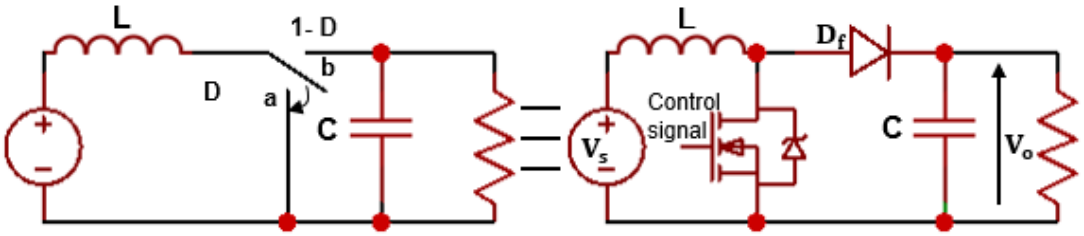

(b) Boost converter

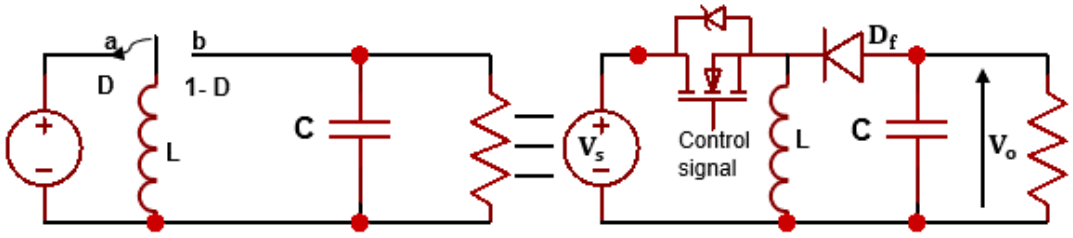

(c) Buck-Boost converter

Figure 3. 37: Basic converter types

The other types have included with a zero-current switching's (ZCS), Cuk, half and full-bridge, and zero voltage switching (ZVS) converters. Figure (3.37) demonstrates the practical realisation of the three essential power converters with non-controlled diode switches and controlled transistors to convert unidirectional power (Roberts 2014). The first and the second types have represented the underlying topology, while all other topologies derived from

these two. The transfer of energy from input to output was achieved in manageable quantities using a regulating technique known as pulse width modulation (PWM) (Kazimierczuk 2008). A variable-width pulse has adjusted the transferred power from the input to the output with a fixed interval. The duty ratio (D), also known as a duty cycle, in PWM was the ratio between the time when energy, was extracted from the source (T_{on}) to the period (T_s) as shown in Figure (3.38). This ratio has represented the inverse of the switching frequency (f_{OSC}) ($T_s = 1/f_{OSC}$) (Roberts 2014).

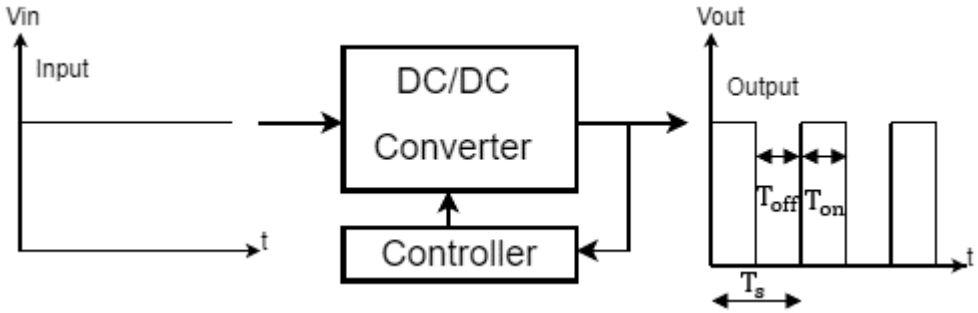

Figure 3. 38: DC-DC converter block diagram

$$D = \frac{T_{on}}{T_s}, T_{on} = DT_s \quad (0 \leq D \leq 1), (0 \leq T_{on} \leq T_s) \tag{3.29}$$

3.6.2 DC-DC converters operating principles

The operating principles of these DC-DC converters as shown in Figure (3.37a, b, c) can be clarified as follows; In buck mode, when the switch was at position (a), the DC source supplies power to the circuit, resulting in an output voltage across the load. When the button changes its status to (b), the stored energy in both inductor and capacitor must be released through the load. Properly controlling the switch position can be kept the output voltage at the desired level underneath the source. In the booster mode, when the switch was at position a, the circuit was partitioned into two sections: on the left, the source charges the inductor. Simultaneously, the capacitor on the right has kept up the output voltage using pre-stored energy. When the switch has changed its position to b, both the DC source and the energy stored in the inductor provide power to the circuit on the right, which expands the output voltage. Also, the output voltage can be kept up at the desired level by

controlling the switching time sequence. Finally, for buck-boost mode, the switch positions a and b has represented the charging and releasing patterns of the inductor. Proper control of the switch succession may have brought about output voltage higher or lower than the DC source. In this case, the output voltage was in the opposite direction of the DC source because of an inductor current direction cannot change.

3.6.2.1 Step down (buck) converter

The reduction buck converter was used to reduce the input voltage level (V_s) at the output V_o, as in the circuit diagram shown in Figure (3.37a). The average output voltage can be calculated as:

$$V_o = \frac{1}{T_s}\int_0^{T_{on}} V_s\,(t)\,dt = \frac{V_s T_{on}}{T_s} = DV_s \qquad (3.30)$$

Hence, the output voltage V_o can be changed from 0 to V_s, the RMS output voltage V_{ORMS} can be evaluated as:

$$V_{ORMS} = \sqrt{\frac{1}{T_s}\int_0^{T_{on}} {V_s}^2\,(t)\,dt} = V_s\sqrt{\frac{T_{on}}{T_s}} = \sqrt{D}V_s \qquad (3.31)$$

When the switch was connected to the terminal a, as shown in Figure (3.39 a)

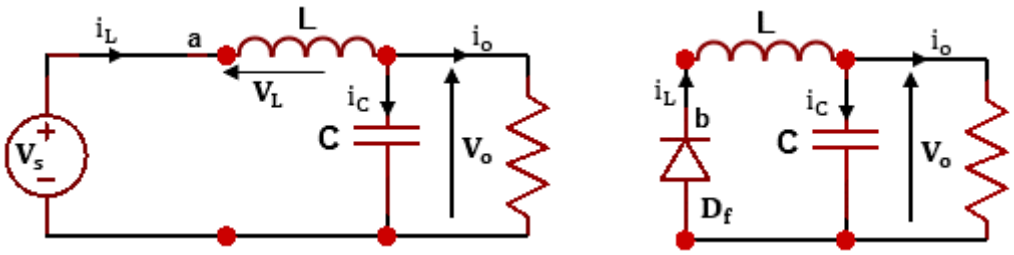

(a) (b)

Figure 3. 39: The circuit of the buck converter during (a) T_{on}, (b) T_{off}

and by applying Kirchhoff's voltage law (KVL) to the closed-loop, then:

$$V_L = V_s - V_o = L\frac{di_L}{dt} = L\frac{\Delta i_L}{T_{on}}, \text{so that } \Delta i_L = \frac{V_s - V_o}{L}DT_s \qquad (3.32)$$

When the switch was connected to the terminal b, the current was discharged in the circuit through the freewheeling diode D_f, as shown in Figure (3.39b). By applying KVL to the closed-loop $(0 = V_L + V_o)$, then:

$$-V_o = L\frac{di_L}{dt} = L\frac{\Delta i_L}{T_{off}}$$

$$\Delta i_L = -\frac{V_o}{L}T_{off} = -\frac{V_o}{L}(1-D)T_s, \text{since } T_{off} = (1-D)T_s \quad (3.33)$$

The net change of the inductor current at any full cycle was zero so that $(\Delta i_L = 0)$. Substituting Δi_L from equation (3.32) in equation (3.33) leads to:

$$\frac{V_s - V_o}{L}DT_s = \frac{V_o}{L}(1-D)T_s$$

$$\frac{V_s - V_o}{V_o} = \frac{(1-D)T_s}{DT_s} = \frac{T_{off}}{T_{on}} \quad (3.34)$$

$$V_o = \frac{T_{on}}{T_s}V_s = DV_s \quad (3.35)$$

$$\Delta i_L = \frac{V_s - V_o}{L}T_{on} = \frac{V_s - DV_s}{L}DT_s,\ F_s = \frac{1}{T_s}$$

$$\Delta i_L = \frac{V_s(1-D)D}{LF_s} \quad (3.36)$$

3.6.2.2 Step-up (boost) Converter

The increased boost converter was used to raise the input voltage level (V_s) to a specified output voltage V_o, as in the circuit diagram shown in Figure (3.37b) with its switching operation was as shown in Figure (3.40);

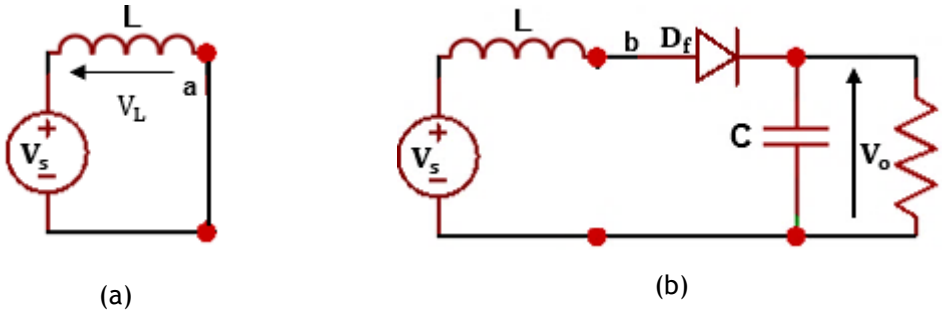

(a) (b)

Figure 3. 40: The circuit of the boost converter during (a) T_{on}, (b) T_{off}

Therefore, the output voltage V_o at T_{on}, was zero. During this period, the inductor has to be charged, and applying KVL leads to $(V_L = V_s)$, then:

$$\left.\begin{aligned} L\frac{di_L}{dt} &= V_s \\ \frac{\Delta i_L}{T_{on}} &= \frac{V_s}{L} \\ \Delta i_L &= \frac{V_s}{L}T_{on} = \frac{V_s}{L}DT_s \end{aligned}\right\} \quad (3.37)$$

When the switch was connected to terminal b then, the current was discharged in the load, as shown in Figure (3.39b). Then,

$$\left.\begin{aligned} V_s &= V_o + L\frac{di_L}{dt} \\ L\frac{\Delta i_L}{T_{off}} &= V_s - V_o \\ \Delta i_L &= \frac{V_s - V_o}{L}T_{off} = \frac{V_s - V_o}{L}(1-D)T_s \end{aligned}\right\} \quad (3.38)$$

Also, the net change of the inductor current at any full cycle was zero so that $(\Delta i_L = 0)$. Substituting Δi_L from equation (3.37) in equation (3.38) gives:

$$\left.\begin{aligned} \frac{V_s - V_o}{L}(1-D)T_s &= -\frac{V_s}{L}DT_s \\ V_o &= \frac{V_s}{1-D}\,, (V_s \le V_o \le \infty) \end{aligned}\right\} \quad (3.39)$$

3.6.2.3 Step up step down (buck-boost) converter

The buck-boost converter has been used to increase the input voltage level or decrease it at the output. The equivalent diagram of the circuit was as shown in Figure (3.37c) with its switching time operation is as shown in Figure (3.41).

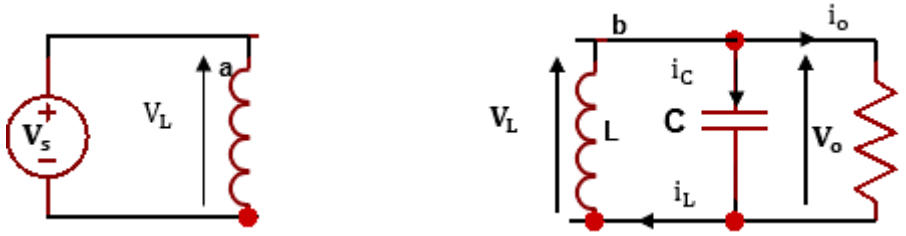

(a) (b)

Figure 3. 41: The circuit of the buck-boost converter during (a) T_{on}, (b) T_{off}

The output voltage V_o at T_{on}, as shown in Figure (3.41a) was zero. And the inductor has to be charged to the supply voltage according to KVL ($V_L = V_s$), then:

$$\left.\begin{aligned} L\frac{di_L}{dt} &= V_s \\ \frac{\Delta i_L}{T_{on}} &= \frac{V_s}{L} \\ \Delta i_L &= \frac{V_s}{L} DT_s \\ \Delta i_L &= \frac{DV_s}{Lf_{OSC}} \end{aligned}\right\} \quad (3.40)$$

When the switch was connected to terminal b, the current was discharged through the load and the diode, and the inductor in the reverse polarity. By applying KVL ($V_o = V_L$), as shown in Figure (3.41b), then:

$$\left.\begin{aligned} L\frac{di_L}{dt} &= V_o \\ L\frac{\Delta i_L}{T_{off}} &= V_o \\ \Delta i_L &= \frac{V_o}{L} T_{off} = \frac{V_o}{L}(1-D)T_s \end{aligned}\right\} \quad (3.41)$$

The net change of the inductor current at any full cycle was zero so that ($\Delta i_L = 0$). Compensating for equation (3.40) in equation (3.41) gives:

$$\left.\begin{aligned} \frac{V_s}{L} DT_s + \frac{V_o}{L}(1-D)T_s &= 0 \\ V_o &= \frac{-D}{1-D} V_s \end{aligned}\right\} \quad (3.42)$$

So, from equation (3.42), the output voltage $|V_o|$ depending on the value of D in the form that:

$$
\begin{aligned}
&D = 0 \Rightarrow |V_o| = 0 \\
&D = 1 \Rightarrow |V_o| = \infty \\
&D = 0.5 \Rightarrow |V_o| = V_s \\
&0 \le D \le 0.5 \Rightarrow 0 \le |V_o| \le V_s, \text{ Buck converter} \\
&0.5 \le D \le 1 \Rightarrow V_s \le |V_o| \le \infty, \text{ Boost converter}
\end{aligned}
\qquad (3.43)
$$

For more investigation and analysis of the DC-DC converter, several PhDs were carried out as a part of the energy management system (Ortúzar 2005; Zhou 2009; Grbovic 2011; Gee 2012; Solano Martínez 2012; Kusakana 2014; Shen 2016). However, in this research, the design and synthesis of DC-DC converters have not been considered. Meanwhile, the available traditional one was used, even with the limitation clarified by the designer manufacturer. This limitation was accepted in the desired application. Also, this goal was developed as an energy enhancement requirement, and as a recommendation for future works.

3.7 Summary

This chapter provides a review and background theory behind the mathematical backgrounds of the RB analysis, and a numerical representation of many components of the RB circuit design, which can be chosen in the test apparatuses have been implemented. Also, it has introduced a revision of different kinds of DC motor used in the RB process. An introduction of varying drive cycle available with the kinematic equation used to evaluate the other variables required has studied in the system analysis.

The next chapter (Chapter 4) presents the design and construction of test devices used in the RB process. Also, it gives a general description of the experimental characteristic equations for the RB analysis with practical implementation to provide the desired system reasonability and activity.

Chapter 4

Test rig Designing and Building

According to the main topic of this research; it has been further reported that there was a significant motivation to build a test platform to take advantage of energy recovery. This test platform should be efficient to represent an entire system. Also, the test platform must be capable and ready to meet all research requirements and be as realistic as possible for laboratory testing. During the development of the elements, despite these preferences in the designing test rig stage, efforts need to be synthesised to ensure that these requirements were valid. Sometimes, the chosen component cannot take full advantage of the characteristics of the illustration in the simulation, leads to reorganising invalidity, which was time-consuming. Furthermore, at the design process, the request for flexibility with cost-effectiveness, and performance has to be considered.

This chapter describes a workflow for building a test rig to represent the regenerative process that can be satisfied with the design requirements. Simulating and testing each component and then gathering the whole system for further simulation and testing. The main contributions gained was that the designed platform could be implemented to represent the real environments that include the underpinning necessity for the design objective. The component and how it can withstand recovered energy from the braking process was considered. However, the implemented test apparatus can be used as demonstrating tools/rig for researchers working on dynamics for different topics in mechanical, electrical, and control engineering.

4.1 Test rig employment

Development of the test rig involved several aspects in being taken into consideration to develop a well-functioning test rig for testing of proposed braking, EMS and RB processes. It has been shown from the previous chapters the fundamental components of the RBs and its essential operation can be accomplished through mathematical analysis and simulation modelling. In this chapter, test rig components were selected, such as the controller and the motor coupled to a designed flywheel that serves as a prime mover considering ease of use and operating requirements.

Furthermore, extensive calculations were done in the designed flywheel element with all parts worked and reacted when they were being subjected to forces. Properties of the test apparatus were developed and fitted with experiments to find its static equation. At the same time, the dynamic modelling is achieved by using system identification tools and throughout simulations completed through utilisation of the "LabVIEW" environment.

4.2 System components selection

This system has comprised entirely of characterising unique elements, as shown in Figure (4.1). For example; the rechargeable ESS batteries and the UCs, flywheel, a most common type of PMBLDC motor with a three-phase inverter and the driver has been determined. The PC with "LabVIEW" simulation platform, current and voltage sensors, and lastly an optical speed sensor has been clarified.

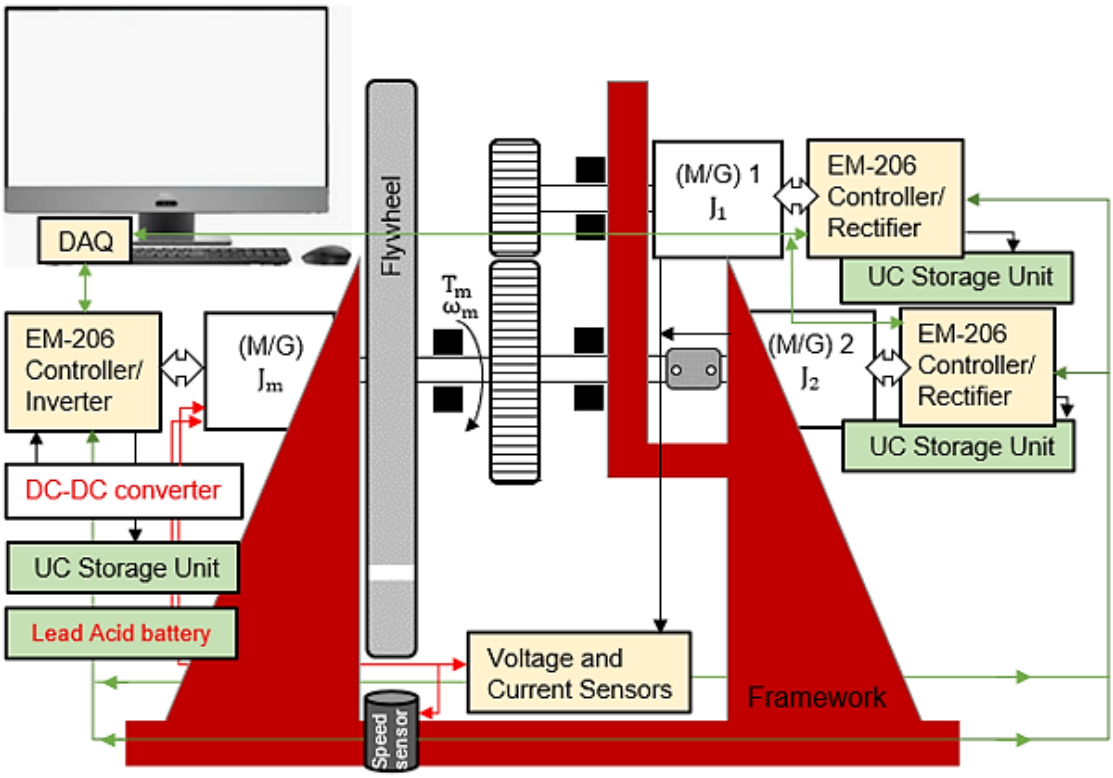

Figure 4. 1: Schematic diagram of the designed test rig

A cage has been intended to shield from breaking rotating equipment, as shown in Figure (4.2). Moreover, the components used in the test rig have been appropriately seized and tested to satisfy the design requirements.

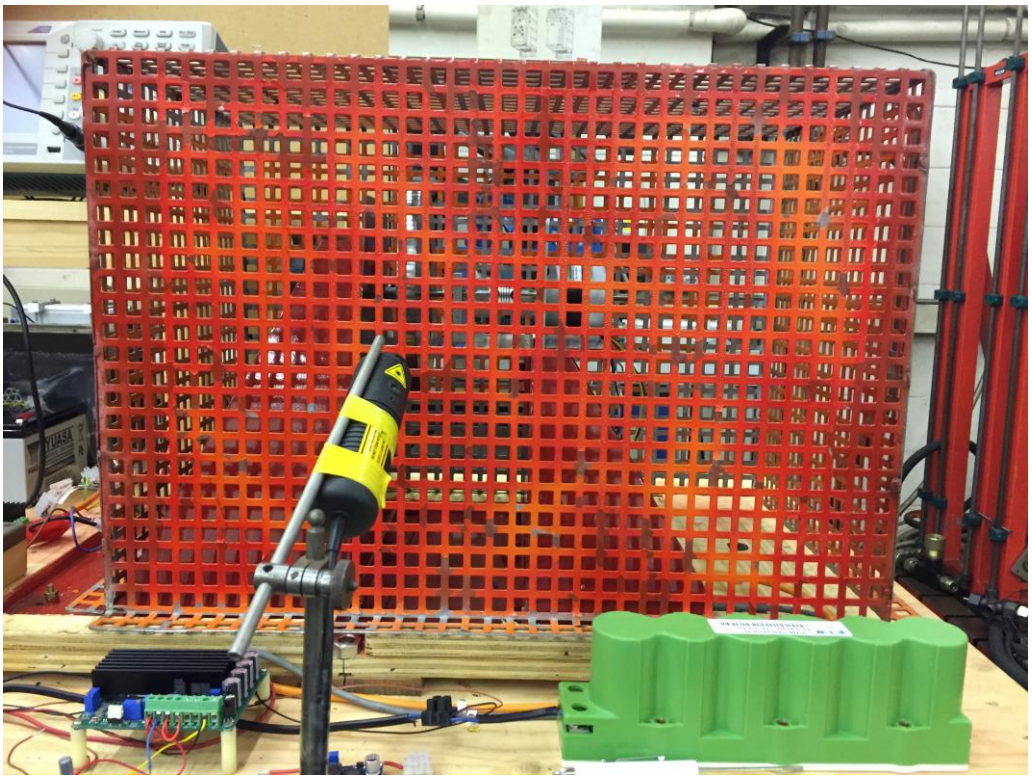

Figure 4. 2: Photo of the test rig protection guard

On the other hand, in the completed designed test rig, the PMBLDC motor has used as a generator as a means of converting rotating inertia into electrical energy.

Furthermore, the UCs ESS has been utilised as a means of storing recovered electrical energy. This arrangement was gathered to simulate the motor in the test rig. In the EVs and HEVs, a compatible electric motor was used as closely as possible. The armature current was supplied from a DC voltage source with a boosted voltage DC-DC converter the regulated voltage was kept constant thereafter. The speed and current controller models for the electric drive were based on a proportional-integral (PI) regulator.

Moreover, the motor output power was fed to the flywheel block as an input, the means of converting electrical energy into inertia, and a rotating object that can store energy as rotational inertia. Figure (4.3) has illustrated the PMBLDC motor used in the designed test rig. Accordingly, the design principle of the PMBLDC motor was to replace the mechanical commutator with the electrical switch circuit. The rotor Hall position sensor, control circuit, and power inverter should be included in the designed system to control motor speed and direction.

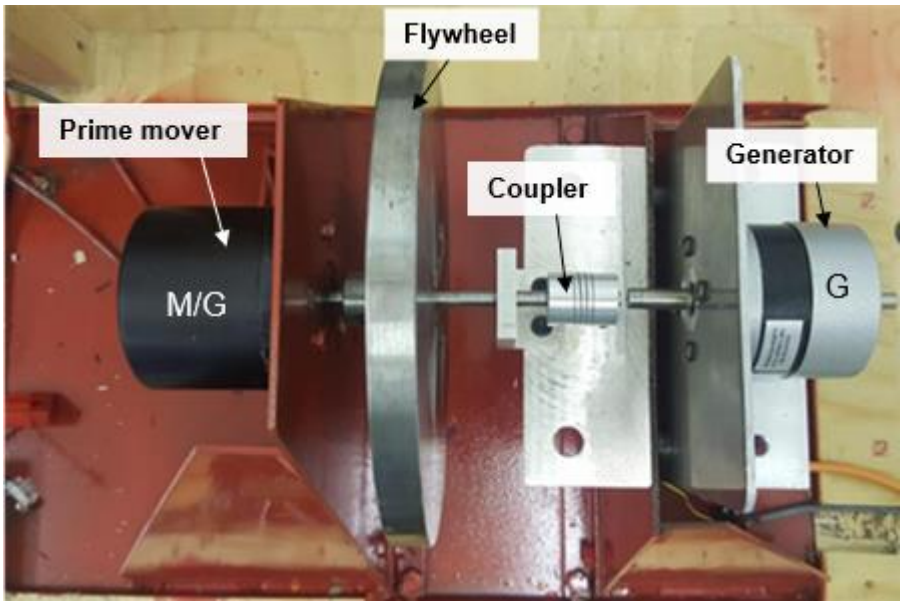

Figure 4. 3: Photo of the PMBLDC motors used in the designed test rig

4.2.1 PMBLDC motors

In the designed testing platform, PMBLDC motor was selected from all the existing types according to its benefits mentioned in the previous chapter. Three different kinds of PMBLDC motors have been used and tested in the application of regenerative braking. The "BL58EE BLDC70W" was considered on the test platform as the prime mover. In the following chapter, the other two motors "RS Pro BLDC 892-8779", and "RS Pro BLDC 536-6030" were used as a generator that could be applied in different scenarios (BL58 EE-70 Watt. 2001; *RS Pro Brushless DC Motor, 536-6030 data sheet* [no date]; *RS Pro Brushless DC Motor, 892-8779 data sheet* [no date]). These different scenarios were used to optimise reused energy to the greatest extent possible to improve system efficiency and decide on the best communication strategies to recover wasted energy. The general information of each motor was represented, as shown in Table (4.1).

Table 4. 1: BLDC motor parameters specification

Motor type	Parameter	Magnitude and Unit of measurement	
BL58EE BLDC 70 W with laminated nine coil stator and 12 poles rotor used as a prime mover and as a generator	Nominal voltage	24	V
	Nominal torque	0.20	Nm
	Nominal speed	3300	rpm
	No-load speeds	4400	rpm
	Torque constant (K_t)	0.06	Nm/A
	B.E.M.F at nominal speed	11.90	V
	Stator resistance between two phases	0.47	ohm
	Stator inductance between two phases	0.60	mH
	Rotor moment of inertia (J)	120 E-6	kgm^2
	Viscous friction constant (b)	3.51 E-6	Nm s
	Electromotive force constant (K_b)	0.03	V/rad/sec
	Hall effect sensor	120°	Electric angle
	Coil configuration	3-phase	Y
RS Pro BLDC motor 892-8779 with four poles rotor used as a generator	Nominal voltage	36	V
	Nominal speed	4000	rpm
	Nominal torque	0.11	Nm
	Current rating	5.50	A
	Hall effect sensor	120°	Electric angle
	Coil configuration	3 phases	Y
	Torque constant (K_t)	0.06	Nm/A
	The line-to-line resistance	1.50	ohm
	Line to line inductance	4.50 E-3	mH
	Rotor moment of inertia (J)	7.50	kgm^2
	Maximum peak torque	0.35	Nm
	Nominal voltage	24	V
	Nominal speed	4000	rpm
	Nominal torque	0.25	Nm

	Hall effect sensor	120º	Electric angle
RS Pro BLDC motor 536-6030 with eight poles rotor used as a generator	Maximum peal torque	0.75	Nm
	Torque constant (K_t)	0.04	Nm/A
	Stator resistance	0.28	ohm
	Stator inductance between two phases	0.54 E-3	mH
	B.E.M.F at nominal speed	15.20 RMS	V
	Maximum peak current	20	A
	Rotor moment of inertia (J)	96 E-6	kgm^2
	Coil configuration	3-phase	Δ

4.2.2 Structure of the drive system

As described in the previous chapter, the controller unit has been selected to coordinate a wide range of the chosen motor to improve system performance. The controller was served to govern timed power distribution by utilising a solid-state circuit commutator system. The "EM-206 DC-motor" controller used in the test rig, as shown in Figure (4.4), was planned for brushless DC motors with Hall sensor feedback control associated by using 60º or 120º commutation signal (Em-206 Brushless Motor Controller. 2010).

Figure 4. 4: Photo of EM- 206 brushless DC-motor controller

The unit has a MOSFET type high-efficiency power stage outfitted with standard controls functions, for example, forwarding, reversing, braking, stopping, and overload protection, as shown in Figure (4.5). Also, the control options have defined as two structures, including the direct (open-loop) control, and the closed-loop frequency control uses Hall sensor feedback for the tuned speed next to the commutation set. Also, the four quadrants-

controlled operations can be used for acceleration and braking in both directions. The input in this system was the measurement of the rotational speed outputs. Consequently, it could be detected when the motor current exceeds the set value to avoid motor overpressure or to overheat. The "EM-206" permits using it as the complete control unit has utilised in the diverse modern application, for instance, in the automotive industry (Em-206 Brushless Motor Controller. 2010).

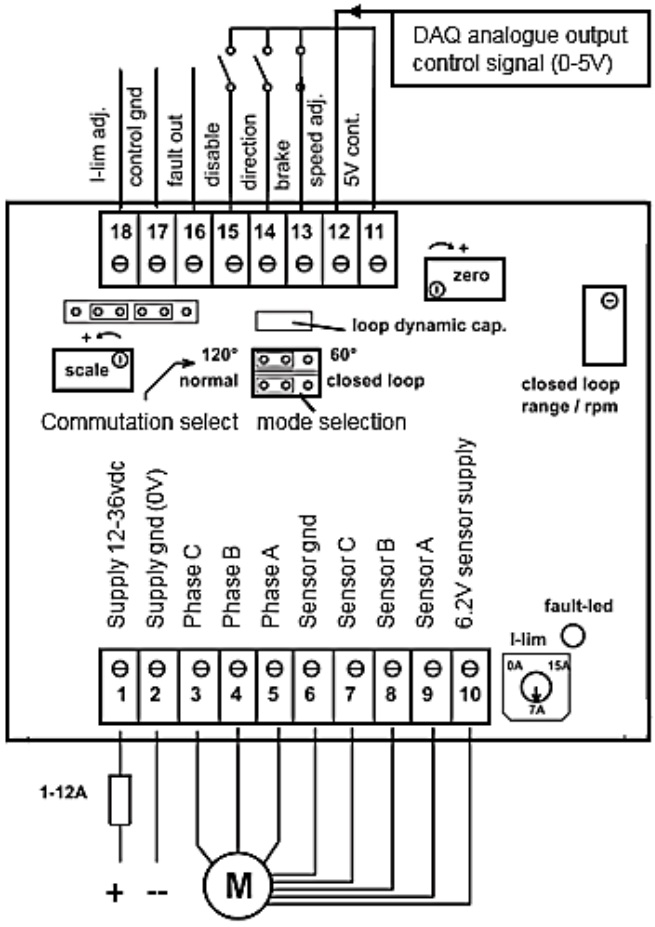

Figure 4. 5: PMBLDC motor and controller pin connection diagram

Figure (4.5) shows the connection diagram of all pins used to establish the desired operation of the motor to operate in a defined direction and speed. The speed can be adjusted using the potentiometer or controlled with the DAQ assistant during the speed setting input using "LabVIEW" software programming. This connection can also be used when the motor was operating as a generator as the excess current can be used to charge the UCs energy storage unit. Therefore, this unit can be used as an inverter and converter in RB applications, reducing the total system cost.

4.2.3 Drivetrain strategies

The possible connection diagram for the experimental investigation was as shown in Figure (4.6).

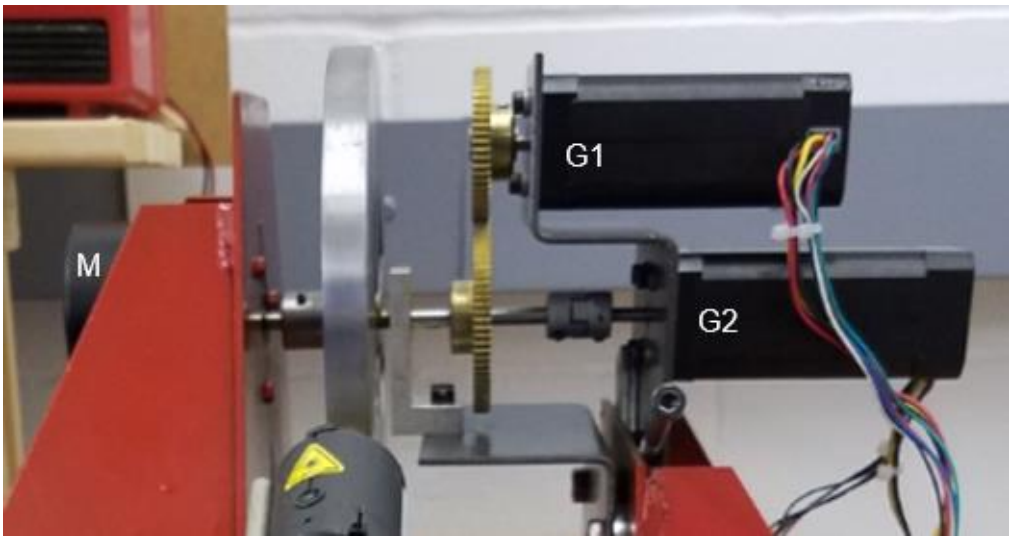

Figure 4. 6: Photo of two identical generators connected with motor diagram

Furthermore, Figure (4.7) shows the photo of gear used in the test apparatus with gear ratio1/2 to increase the speed of operation of the first generator for energy enhancement (waste energy retrieve) study. Few things need to be considered to reduce the friction between these two elements. However, there was an urgent need for precision fitting and care must be taken into consideration when doing a test.

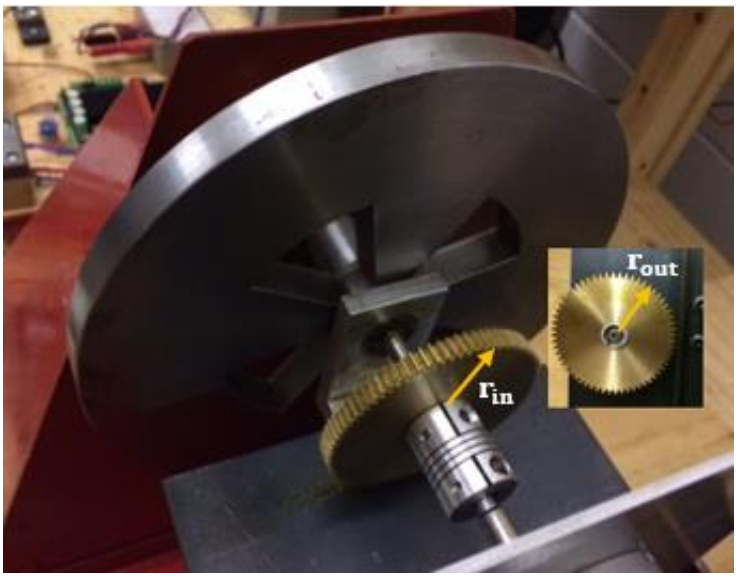

Figure 4. 7: photo of gear used in the test apparatus

The tangent velocity (v_{tan}) at the contact point of the gear teeth were the same as for the two-gear cylinder with different diameters, as it was shown in Figure (4.7), and as it is given in equation (4.1).

$$r_{in}\omega_{in} = v_{tan} = r_{out}\omega_{out} \tag{4.1}$$

$$\omega_{out} = \frac{r_{in}}{r_{out}}\omega_{in}$$

In the designed gear, since $r_{in} = 2\, r_{out}$, $\omega_{out} = 2\omega_{in}$

The transmission ratio (gear ratio, GR), as defined in terms of rate conversion ratio between the input and the output shaft.

$$GR = \frac{\omega_{in}}{\omega_{out}} = \frac{r_{out}}{r_{in}} \tag{4.2}$$

Assuming lossless gear train, such that, $p_{out} = p_{in}$, then, $T_{out}\,\omega_{out} = T_{in}\,\omega_{in}$

The transmission ratio in terms of torque on the two axles is given as:

$$GR = \frac{\omega_{in}}{\omega_{out}} = \frac{T_{out}}{T_{in}} \tag{4.3}$$

Figure (4.8) depicts the connection diagram between "BL58EE" motor, used as a prime mover, and the "EM-206" controller. The designed flywheel has been connected with the motor shaft, which explained in section (4.3.7).

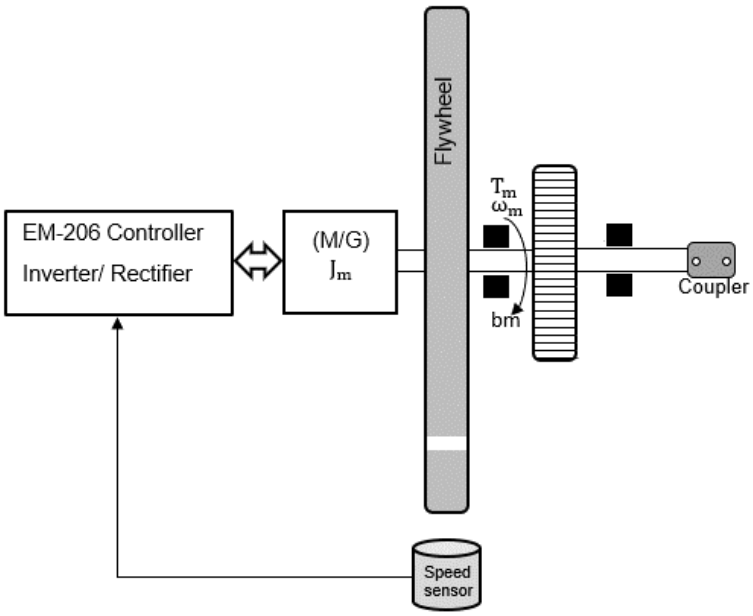

Figure 4. 8: Schematic diagram of the controller and PMBLDC motor with flywheel

A standard test was carriedout in this procedure, as the same motor used as a generator in the RB mechanism. The controller was worked as an inverter in motoring operation and as a rectifier in the regeneration mode. In the other scenario, there was another motor "RS Pro BLDC motor 892-8779" connected to the same shaft to work as a generator instead. The connection can be implemented as shown in Figure (4.9) by using two controllers, one of them as an inverter and the second one as a rectifier for motor and generator operations, respectively.

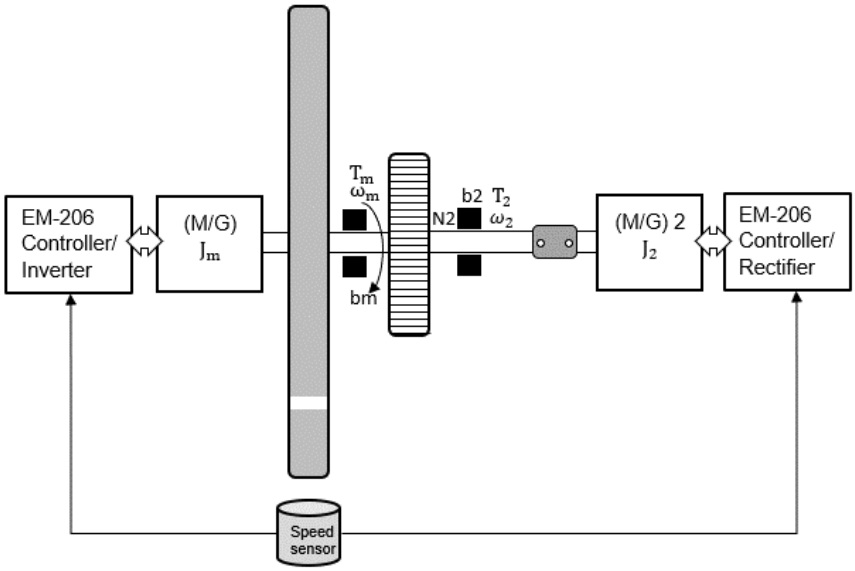

Figure 4. 9: Schematic diagram of the two PMBLDC motors coupled to the flywheel

Furthermore, with the advantage of designed gear, mechanical power transmission equipment has been used to acquire an edge by expanding torque or decreasing speed (Husain 2003). The automated process has used the law of energy conservation. The energy flow remains constant in the ideal transmission. The connection was implemented to get higher speed at the generation side for energy enhancement purposes, as shown in Figure (4.10), which represent another scheme of connecting diagram.

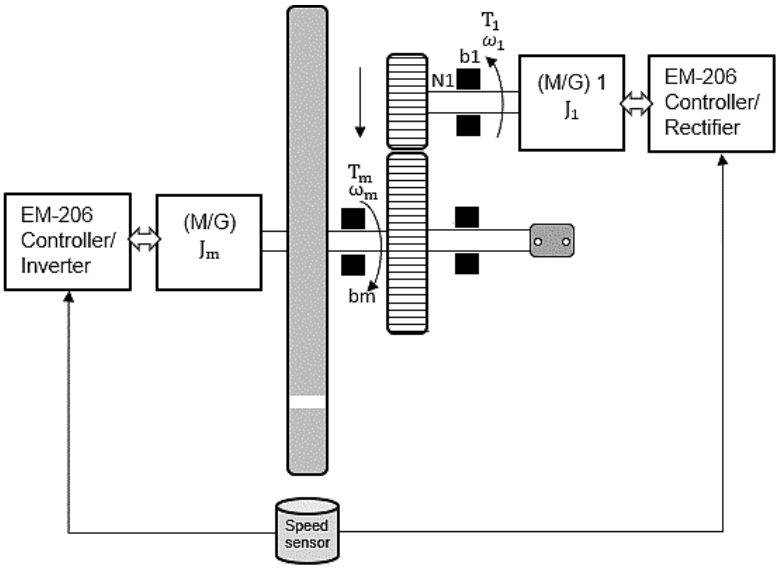

Figure 4. 10: Schematic of the one gear coupling PMBLDC motors

To get adequate information about the third scenario that has been tested with two identical motors, one of them has connected directly with the original motor shaft and the other throughout designed gear equipment to increase the generator speed, as shown in the schematic diagram, Figure (4.11). An experimental study has been used to investigate the efficiency enhancement throughout this design.

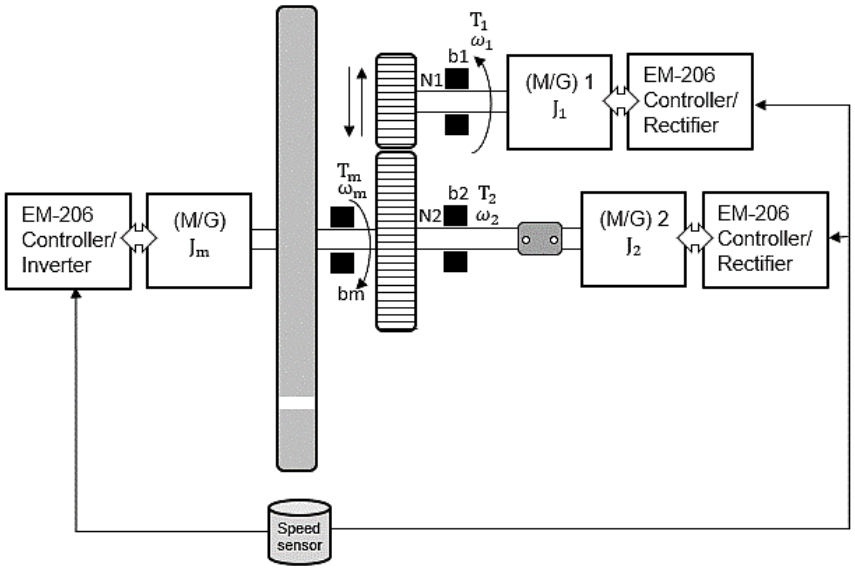

Figure 4. 11: Schematic of the two-gear coupling PMBLDC motors

Regarding the electrical connection, the scheme has been represented in Figure (4.12). This figure shows the link of the six-pole toggle switches pin descriptions. In the energy harvesting process, the output of the boost converter (designed for both motors M1, and M2 output voltage) was

connected to the controller and the UCs inputs for energy recapturing purposes.

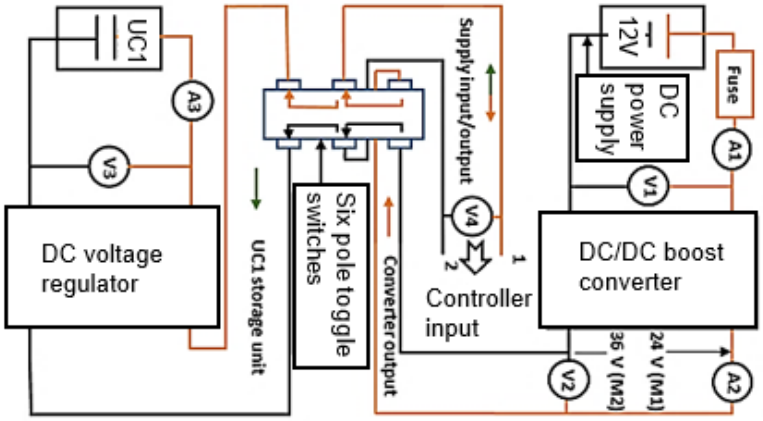

Figure 4. 12: Connection diagram of the six-pole toggle switches in the RB system

4.2.4 The National Instruments NI USB-6008

The NI USB-6008 has provided connectivity to eight single-ended analogue input (AI) with maximum sample rate 10kS/s single and multiple channels, and two analogue output (AO) channels. It also has had a twelve-digital input/output (DIO) channels and an available 32-bit counter with a full-speed USB interface (USER GUIDE NI USB-6008/6009 Bus-Powered Multifunction DAQ USB Device. [no date]). Figure (4.13) show the photo of the NI 6008 DAQ.

Figure 4. 13: NI USB-6008 photo

Also, Figure (4.14) shows the DAQ digital and analogue pins diagram with its descriptions.

Pin diagram	Terminal	Signal
	17	PO.0
	18	PO.1
	19	PO.2
	20	PO.3
	21	PO.4
	22	PO.5
	23	PO.6
	24	PO.7
	25	PI.0
	26	PI.1
	27	PI.2
	28	PI.3
	29	PFI 0
	30	+2.5 V
	31	+5 V
	32	GND

(a) Digital pins

Pin diagram	Terminal	Signal Single ended mode	Signal Differential mode
	1	GND	GND
	2	AI 0	AI 0 +
	3	AI 4	AI 0 -
	4	GND	GND
	5	AI 1	AI 1 +
	6	AI 5	AI 1 +
	7	GND	GND
	8	AI 2	AI 2 +
	9	AI 6	AI 2 +
	10	GND	GND
	11	AI 3	AI 3 +
	12	AI 7	AI 3 +
	13	GND	GND
	14	AO 0	AO 0
	15	AO 1	AO 0
	16	GND	GND

(b) Analogue pins

Figure 4. 14: NI USB-6008 pin description

In the designed test rig, for experiment investigations, the pin connection was chosen, as shown in Figure (4.15, 4.16), which represents the DAQ 6008 instrument connection diagrams.

DAQ Pins	Terminal	Signal	Signal description
	17	PO.0	Switch 1 AA
	18	PO.1	Switch 2 BB
	19	PO.2	Switch 3 CC
	20	PO.3	Switch 4 DD
	21	PO.4	Switch 5 EE
	22	PO.5	Switch 6 FF
	23	PO.6	Switch 7 GG
	24	PO.7	Switch 8 HH
	25	PI.0	
	26	PI.1	
	27	PI.2	
	28	PI.3	
	29	PFI 0	
	30	+2.5 V	
	31	+5 V	
	32	GND	

Figure 4. 15: NI USB-6008/USB Digital pin diagram with signal description

DAQ Pins	Terminal	Signal Single ended mode	Signal Differential mode	Sensor input /output
	1	GND	GND	
	2	AI 0	AI 0 +	Speed
	3	AI 4	AI 0 -	V_{batt}
	4	GND	GND	
	5	AI 1	AI 1 +	I_{batt}
	6	AI 5	AI 1 +	V_{UC1}
	7	GND	GND	
	8	AI 2	AI 2 +	I_{UC1}
	9	AI 6	AI 2 +	V_{UC2}
	10	GND	GND	
	11	AI 3	AI 3 +	i_{UC2}
	12	AI 7	AI 3 +	V_{boost}
	13	GND	GND	
	14	AO 0	AO 0	Speed adj
	15	AO 1	AO 0	
	16	GND	GND	

Figure 4. 16: NI USB-6008 Analog pin diagram with signal description

The sampling process was the selection of a subset of selected data to estimate characteristics of the whole data. It was not usually possible, in a practical case, to measure and to include every available data in our sample. Two advantages of sampling were lower cost and faster data collection than measuring the real data. Each observation was measured by one or more properties of observable data distinguished as independent data. As an example, weights can be applied to the data to adjust for the sample design to meet the design specifications.

The DAQ assistant front panel, in the LabVIEW programming, had been adjusted with all pin configuration with sampling rate, and acquisitions mode, as shown in Figure (4.17). A continuous mode with ten samples read of entire pieces with a rate of 100 Hz had been chosen for data to be observed.

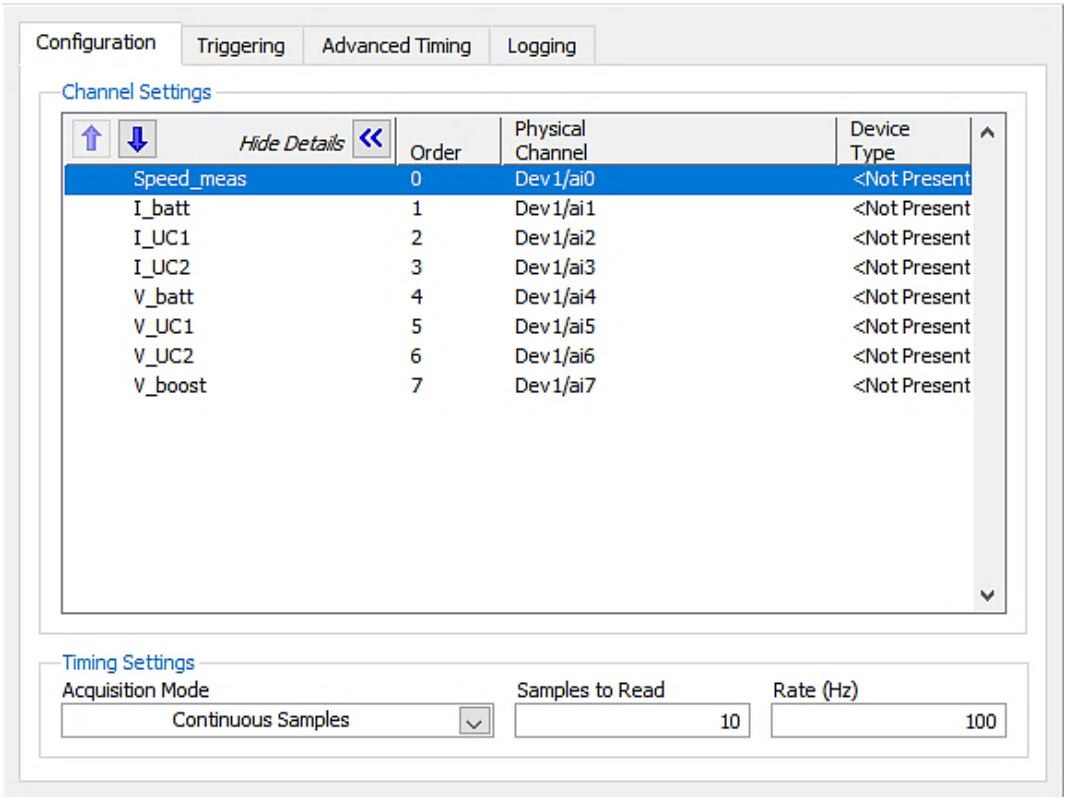

Figure 4. 17: DAQ Assistant for input signal pin configurations

A statistical power indicates the probability of a hypothesis test that, when present, can find a significant effect. Also, the sample size can be used in statistical software to figure out how much data needs to be collected (a reasonable size of data), to be confident in finding results and building an

accurate model. The sample sizes have been chosen in a way that utilises experience with small samples, although this is sometimes unavoidable. Therefore, in the designed test apparatus, many iterative tests were performed to run an experiment to obtain at least 75% detection of the variables that significantly affect the output.

The output control generation model from the DAQ assistant can be represented, as shown in Figure (4.18).

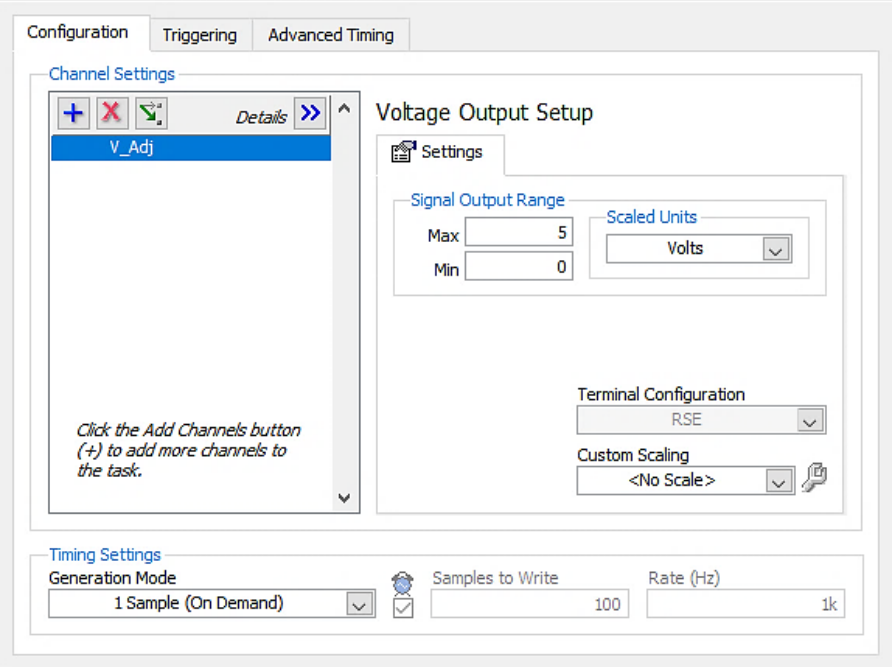

Figure 4. 18: DAQ Assistant for the speed control pin configuration

4.2.5 Speed, current, and voltage Sensoring

A sensor was a device which can be used to convert the physical measurement to an electrical signal in the form of voltage or current. Also, the computation can be represented as a change in resistance or evolution of capacitive and inductive impedance (Ziemann 2018).

4.2.5.1 Current sensor

The current sensor was a device that detects the charge flow and generates a signal proportional to that flow. The type of the signal generated could be an analogy or digital output, and it may be in the form of current or voltage output signal (Current Transducer. [no date]). These signals can be displayed or may be stored in the data acquisition system for further investigation or used in the final control destination. As determined by the datasheet, different current sensors have been used according to its specification and operation. The "ACS712" design was revolved around a completely integrated, direct or alternate current sensing in an industrial system including motor control, switch-mode power supplies and other applications (ACS712. [no date]). One of the advantages of using this type of current sensor was that compatibility with the input voltage limits of the DAQ assistant used. Also, this sensor has been calibrated against a different kind of current sensor (LEM current transducer), and with a digital current meter for more precise measurements (Current Transducer. [no date]). The sensor has comprised an accurate, low-offset, linear Hall-effect sensor circuit with a copper conduction terminal. The use of current coursing through these terminals had created a magnetic field which is detected by the integrated Hall-effect sensor and changed over into a corresponding voltage. The output of the sensor had gotten a positive incline (higher than V_{out}) when the current course through the primary copper conduction terminals from pins (1+2) to pins (3+4) which was used for current sampling. Meanwhile, it has gotten a negative incline (less than V_{out}) when the current pass from pins (3+4) to pins (1+2), which was the way utilised for current detecting, as shown in Figure (4.19).

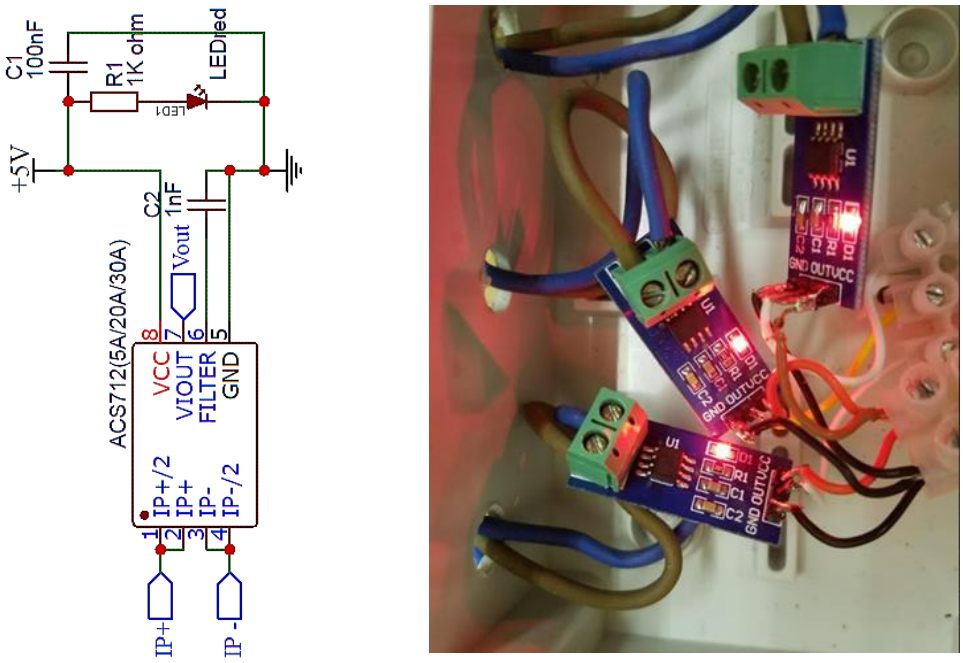

(a) Connection diagram (b) Photo for current measurement

Figure 4. 19: The ACS712 Current sensor

The analogue signal (V_{out}) was varied linearly with the unidirectional or bidirectional (AC or DC) primary sampled current (IP). The capacitor C1 was used for noise management. There were three types of ACS712 sensor dependent on the scope of the current sensing. The essential parameters of any sensor were linearity, offset (for dc sensors) and sensitivity (Halit and Eren 2014). Table (1) gives the individual output sensitivity, (the change in the output in response to a change of 1 A through the primary conductor), for different current measurement ranges which can be programmed through an application.

Table 1: The ACS712 sensitivity for current measurement

IC	Optimised Range, IP (A)	Sensitivity, (mV/A)
ACS712	+/- 05A	185
	+/- 20A	100
	+/- 30A	66

4.2.5.2 Voltage sensor

Several operating principles were applied to achieve the required measurement by processing the input signal using electronic semiconductor devices to measure the voltage. Electronic voltmeters can be divided into analogue and digital electronic voltmeters (Halit and Eren 2014). Also, the voltage sensor used in the test rig was a module that can be used with DAQ6008 with input tolerance of 5V to measure external voltages that are greater than its maximum acceptable value. As with the current sensor, the voltage sensor was calibrated with a digital voltmeter for more accurate measurements. Its schematic was a voltage divider applicable for a series circuit, from which the output voltage was a fraction of the input voltage, as shown in Figure (4.20).

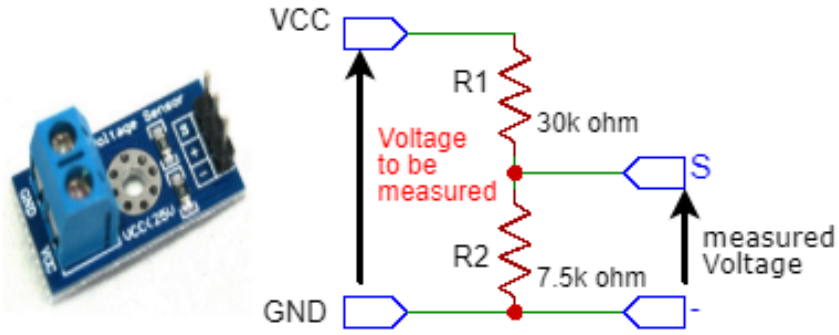

Figure 4. 20: Voltage sensor circuit diagram

The voltage divider rule for two resistors in series can be stated as in equation (4.4) as:

$$\text{Vout (measured voltage)} = \frac{\text{R2}}{\text{R1} + \text{R2}} \text{Vin (voltage to be measured)} \tag{4.4}$$

The voltage sensor was constructed with two resistors with resistances of 30 kΩ and 7.5 kΩ, so that, the output voltage was fifth of the input voltage. Applying these two values on the equation (4.4) with 24 V supply input yields, ((7.5 kΩ /(7.5+30) kΩ)x24 V=4.8 V). The reason for choosing these two values of resistors was due to the limitation of the DAQ used in the circuit which cannot carry a voltage more than 5 V. Also, the sum of each of the resistors should not be too small, as this will generate a higher current drawn from a

voltage source of 0-5 volts, which can affect the measured values according to the internal resistance of the source (Ziemann 2018). The two input terminals were the voltage to be measured (VCC), and the ground (GND).

In comparison, the three output terminals were the sense (S) terminal was connected to the analogue input of the DAQ, the positive terminal was not compared to anything, and the negative must be connected to ground (GND). Figure (4.20) shows the schematic of the voltage sensor with an input voltage not exceed of 25V, so that, the maximum output voltage was 5 V as specified. Also, the combination of this resistance can be used as a voltage regulator in which the desired output voltage can be controlled, as shown in Figure (4.21).

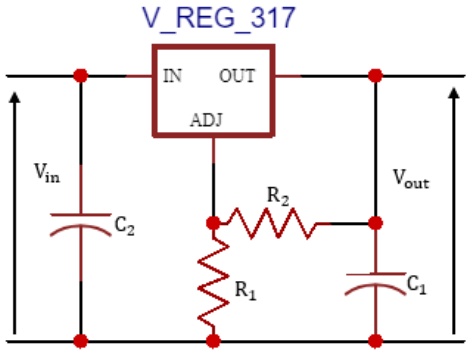

Figure 4. 21: Voltage regulator circuit diagram

For LIM317, the output voltage can be evaluated as:

$$v_{out} = 1.25\left(1 + \frac{R_2}{R_1}\right) \tag{4.5}$$

4.2.5.3 Rotational speed measurement

The VLS series sensors have provided with a pulsed NPN output for each rotating cycle available with a light sensor or laser light for optical range for better response with maximum rotation speed up to 250,000 rpm. This device was typical for data logging applications and where speed monitoring and recording is required. Also, the reflective tape can be used to enhance accuracy. It was useful for control and recording speed data with high rotational speed measurements performed on the test platform using an optical speed sensor with an analogue output VLS/DA1/LSR, as shown in Figure (4.22). The linear voltage to speed measurement was the key features of this

model. Also, for speed ranged from (50-6000 rpm), the analogue output ranged from (0–6 V dc). Also, the high-speed update time was made it ideal for monitoring fast speed changes (Optical Speed Sensor with Analogue Output Speed Sensors VLS / DA1. [no date]).

Figure 4. 22: Photo of laser model VLS/DA1/LSR optical speed sensor

The optical speed sensor has sensed the number of interruptions caused by aperture placed in the rotating object, indicating the number of cycles for a given time. However, the optical speed sensor was a simple data collection tool and can be connected to a DAQ that transmits voltage signals to a computer.

4.2.6 Programmable electronic load (PEL) 300W 8500

In the designing test rig, for system analysis and modelling, the 8500 PEL was utilised to test and to evaluate the DC power supplies, batteries, UCs, and power components. In contrast, voltage/current or resistance/power values were implemented and viewed in real-time measurements, as shown in Figure (4.23).

Figure 4. 23: Photo of the 8500 PLE

Furthermore, all parameters can be adjusted quickly and accurately from the front panel or can be programmed through the USB interface.

The 8500 PEL, wide operating ranges of up to 500 V and 240 A, has made it suitable for describing DC power supplies, DC-DC converters, batteries, fuel cells and solar cells. It can be worked and drew from the DC power supply in different modes such as:

- Constant voltage (CV); It was appropriate for testing battery chargers where the load will try to absorb enough current to control the voltage source to the programmed value.
- Constant current (CC); It can be linked for load regulation tests for DC power supplies or for representing the discharge form of the battery.
- Constant power (CP); It was useful for testing batteries and simulating a pragmatic discharge curve.
- Provide constant resistance (CR); This behaviour mimics an ideal resistance that has not changed depending on the current or the voltage measured. The load has sunk a current proportional to the input voltage in correspondence with the programmed resistance and will stay constant regardless of the level of power (B&K Precision Corp. 2009).

4.2.7 Electrochemical energy storage systems (ESS)

ESS was defined according to the type of fuel used or form of the energy stored. The liquid fossil fuels have used as raw material for the engine include gasoline, oil and natural gas. While the mechanical storage has had flywheel to save energy in forms of kinetic energy, and the electrochemical storage consists of a chemical reaction and charge transfer within the storage units, that can be designed as:

4.2.7.1 Lead-acid battery

The specification of the rechargeable lead-acid battery (10 Ah, 12 V) as remarkable recovery from deep discharge, superior energy density and remarkably has a low self-discharge rate made it useful in the designed SoC

monitoring. Figure (4.24) shows the "YUASA" lead-acid valve-regulated battery with internal resistance less than 20 mΩ and maximum discharge current 40 A (REC 10-12. 2008). The technical features of this battery have included sealed construction and low maintenance operation. The operation, in any direction (charge/discharge) without loss of performance, has made it suitable to be used in the test rig.

Figure 4. 24: (10 Ah, 12 V) Lead-acid battery

4.2.7.2 Ultra-capacitors (UCs)

The UCs storage unit was constructed with high reliability, high-performance materials, green solution for pulse or backup power applications used as battery assist engine starting, especially for frequent starts. The "XVM 16V 65 F" series UCs unit, as shown in Figure (4.25), has provided a way to achieve the higher voltage or discharge time through a series/parallel connection of multiple units. It has contained a maximum internal series resistance (ESR) of 22 mΩ and a maximum leakage current of 23 mA (PowerStor XVM Series. 2014).

Figure 4. 25: Photo of the 65 F, 16V PowerStor XVM Series UCs

4.2.7.2.1 UCs wiring configuration examples

The wiring diagram was achieved by series, parallel, and series/parallel connections for operating with the desired voltage, capacitance and current is as shown in Figure (4.26).

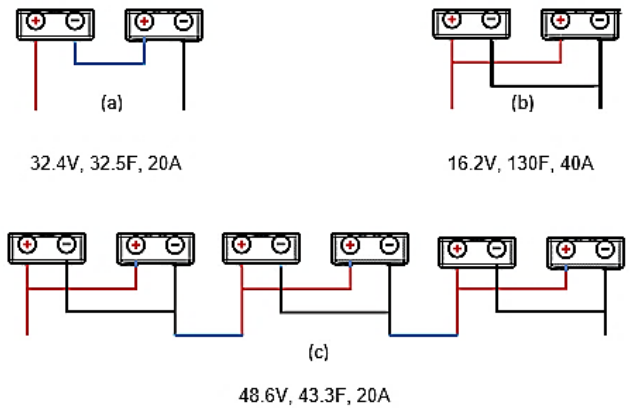

Figure 4. 26: UCs equivalent connection diagrams; (a) Series, (b) Parallel, and (d) Series/ parallel

Further information and more details analysis of the electrochemical storage units have been discussed in the next chapter.

4.2.8 Flywheel electromechanical storage units

In the experimental work, the flywheel energy storage system (FESS) principle of operation was that it could be used as a mechanical energy storage unit, where kinetic energy was stored as rotational energy. Therefore, the flywheel was necessary for two reasons:

a. Vibration-reduction: used to achieve smooth operations of the machine in which it can be worked as a condenser in the electrical circuit to filter output voltage ripples, and to reduce the impact of mechanical shock.
b. Energy storage: It can be utilised to store energy for later use in a rotating mass. Depending on the inertia and rotational speed of the rotating mass, a certain measure of kinetic energy was stored as rotational energy (Bolund et al. 2007; Alamili et al. 2020). In the RB, for instance, when the electrical supply was interrupted, the flywheel continues to supply power during that interruption.

4.2.8.1 FESS principle of operation

The transit results in dynamic loads typically have increased the required engine power. Besides, intermittent duties have caused additional engine design issues. In industry, flywheels were used to influence a variable load (Sebastián and Peña-Alzola 2015). The principle of a flywheel drive was based on the idea that peak load (i.e., shock load) only affects useful work, while it is unimportant in the free-running mode. The advantage of the flywheel was that stagnant energy accumulates on the inertial mass, which was then consumed in the working part of the cycle (Vodovozov 2012).

Furthermore, the shape of the flywheel was essential, and it must be designed so that the materials carry the same stress all the time. When it has used to store energy, part of its power was continuously dissipated as friction and aerodynamic losses. The estimated energy density was significantly affected by the additional weight of the bearings, motor/generator, and the shaft (CLEGG 1996). In the designed test rig, the flywheel was a mass with high inertia rotating about an axis of the motor, directly coupled to the rotor shaft of the "BL58EE70W" PMBLDC motor to increase rotational inertia and to reduce the effects of initial acceleration (i.e., mechanical shock), as shown in Figure (4.27). Again, all these components were placed inside a steel cage, which protects the operator from the danger of the flywheel braking at high speed.

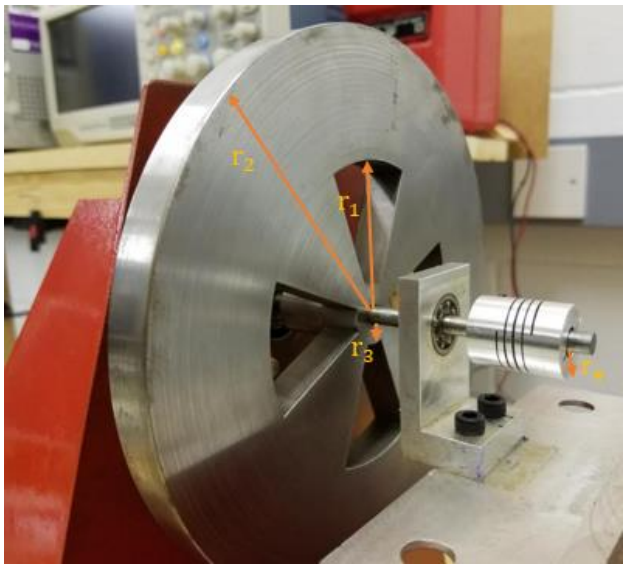

Figure 4. 27: FESS photo used in the designed test rig

4.2.8.2 Mathematical representation of spinning flywheel

When the flywheel accelerated up to speed, its kinetic energy has converted to electricity which then returned to the system by using the motor as a generator or using another generator connected to a coupler. The flywheel was characterised by a significant moment of inertia about the axis of rotation J_{fly}, measured in (kgm^2), and resists changes in rotational speed. The amount of energy transferred to the wheel depended on the moment of mass inertia J_{fly} for accelerating/decelerating, and the square of its rotational speed of the rotating disc, ω (rad/s) as:

$$E_{K_{fly}} = \frac{1}{2} J_{fly}\, \omega^2 \tag{4.6}$$

The moment of inertia of an object as a function of its form and mass (Bolund et al. 2007). For a solid cylindrical disc of mass m in (kg) and radius of inertia r in (m), J_{fly} can be implemented as:

$$J_{fly} = \int r^2\, dm = \frac{1}{2} m r^2 \tag{4.7}$$

Equation (4.7) indicates that a flywheel mass can be modelled as an active load connected to the rotor shaft of an electric machine. In particular, the J_{fly} moment of inertia was given to a solid cylinder of a radius r in m, thickness l in m, and density ρ (kg/m^3) of the concrete cylinder as:

$$J_{fly} = \frac{1}{2} \pi\, r^4 l \rho \tag{4.8}$$

Also, the moment of inertia of a hollow cylinder (composite or steel rim) associated with the axis, (of an outer radius r_2 and inner radius r_1), shown in Figure (4.27), can be carried out as follows:

$$J_{fly} = \int_{r_1}^{r_2} r^2\, dm = \frac{1}{2} \pi l \rho \left({r_2}^4 - \frac{1}{2} {r_1}^4 \right) \tag{4.9}$$

Furthermore, the total torque applied to the flywheel was the electromotive torque of the motor T_{em}, since it was directly attached to the rotor of the motor. In that case, its torque characteristic, according to Newton's law of rotational, has been expressed as follows:

$$T_{fly} = J_{fly}\,\alpha = J_{fly}\frac{d\omega}{dt} = T_{em} \tag{4.10}$$

Where, α (rad/s^2), was the spinning wheel angular acceleration. The amount of energy transferred in and out of the flywheel can also be managed By controlling the torque generated by the PMBLDC motor. Hence, charging and discharging of energy in the wheel was performed by dictating a positive and (or) negative torque command the PMBLDC controller.

The energy storage capability of the FESS relies heavily on the analysis of equation (4.6). Maximum stored energy in the flywheel was accomplished by increasing the rotating speed. Also, inertia J_{fly} , can be increased by placing as much mass as possible on the outside of the disc, but attention must be paid to mechanical constraints at high speeds. However, the rotational speed of the flywheel has limited the stored kinetic energy. Hence, the effectively saved energy of a flywheel (E_{eff}) has used within a speed range from minimum angular velocity (ω_{min}) to the maximum angular velocity (ω_{max}) is given by (Thoolen 1993; Vodovozov 2012);

$$E_{eff} = \frac{1}{2}J_{fly}\,\Delta\omega^2 = \frac{1}{2}J_{fly}({\omega_{max}}^2 - {\omega_{min}}^2) \tag{4.11}$$

Equation (4.11) can be rearranged as, $= \frac{1}{2}J_{fly}\,{\omega_{max}}^2\left(1 - \frac{{\omega_{min}}^2}{{\omega_{max}}^2}\right)$, where the ratio $\left(1 - \frac{{\omega_{min}}^2}{{\omega_{max}}^2}\right)$, was determined by the used transmission type. Also, it represents a depth of discharge factor, which was the ratio between the usable energy to the total stored energy (Genta 1985). It was pointless to downgrade the value of ω_{min} under a certain point. As an insignificant ratio of $(\omega_{min}/\omega_{max})$, puts rigorous requests on the transmission, while the increase of sufficient energy was relatively small. The reasonable settlement is that ω_{min} is one half ω_{max}. For this ratio, (as described in equation (4.11)), three-quarters of the stored energy can be released from the flywheel (Genta 1985; Thoolen 1993).

The energy stored can be expressed regarding tangential speed v (m/s), which was known as a product of orthogonal distance with the spindle axis r (m) and angular or rotational speed ω (rad/sec) as $v = r\omega$, as:

$$E_k = \frac{1}{2}mv^2 = \frac{1}{2}mr^2\omega^2 \tag{4.12}$$

Meanwhile, the energy density (E_d) (J/kg), often, only useful or usable energy was measured, while the inaccessible energy (such as remaining cluster energy) was ignored. For a flywheel, this can be defined as the ratio of energy stored to its mass as:

$$E_d = \frac{1}{2}r^2\omega^2 \tag{4.13}$$

Equation (4.13) indicates that the flywheel mass can be modelled as an active load connected to the rotating shaft of the motor.

Moreover, to evaluate the rotational power, it was essential to convert the angular velocity ($\acute{\omega}$) measured in rpm to units of rad/sec such that:

$$\omega(\text{rad/sec}) = \frac{\acute{\omega}\ (\text{rpm})2\pi}{60} \tag{4.14}$$

Furthermore, the time required for a flywheel to reach its nominal speed can be defined as:

$$t = \frac{\omega}{(d\omega/dt)} = \frac{2\pi\acute{\omega}}{60\ (d\omega/dt)} \tag{4.15}$$

4.2.8.3 Flywheel in practical design

The acceleration of the combined system (flywheel and the PMBLDC motor) from equation (4.10) can be implemented as:

$$\alpha = \frac{d\omega}{dt} = \frac{T_{em}}{J_{fly}} \tag{4.16}$$

Also, from BL58 EE-70-Watt motor datasheet, the speed-torque characteristics curve with the current applied could be given, as shown in Figure (4.28) as:

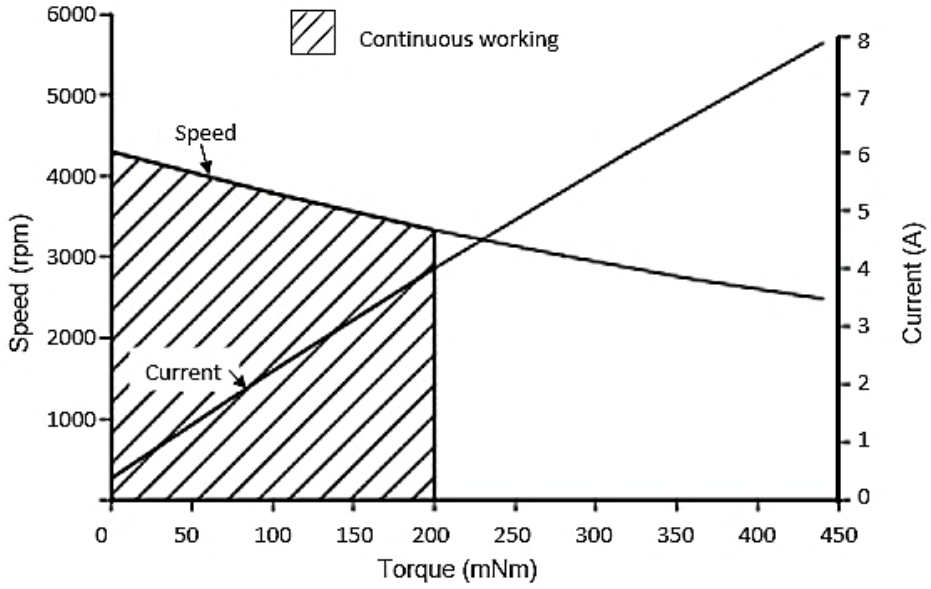

Figure 4. 28: Motor characteristics curve (adapted from (BL58 EE-70 Watt. 2001)**)**

From Figure (4.28), at rated speed (3300 rpm), $T_{em} = 200$ mNm and motor rotor inertia is 120x10^{-6} kg m^2.

The flywheel in the designed test rig was made from mild steel with $\rho = 7859\ \mathrm{kg/m^3}$, and manufactured with an outer diameter of 17.8 cm and an inner of 7.4 cm, a thickness of 1.3 cm, and a mass of 2.3 kg measured by the weight scale, attached to a turning wheel, as illustrated in Figure (4.27).

The following procedure was applied throughout mathematical modelling to clarify flywheel measured parameter for system verification as:

- Since the wheel constructed as a solid cylinder with four symmetrical holes, the moment of inertia can be calculated as a rigid body subtracted from this hollow parts contained as:

$$J_{tot} = J_{fly/r_1} + J_{fly/r_2} + J_{fly/r_3} + J_{coup/r_4} + J_{mot} \qquad (4.17)$$

Where, J_{tot} represents the total moment of inertia. While J_{fly/r_1}, J_{fly/r_2}, J_{fly/r_3} describes the flywheel moment of inertia at the radius mentioned in Figure (4.27). J_{coup/r_4} the coupler moment of inertia with $\rho = 2800\ \mathrm{kg/m^3}$ for aluminium alloy and coupler thickness $h = 0.025$ m. While J_{mot}, was the motor rotor moment of inertia taken from the datasheet.

From equation (4.9), the total moment of inertia can be calculated as:

$J_{tot} = \frac{1}{2}\pi l\rho\{(r_2{}^4 - \frac{1}{2}r_1{}^4) + \frac{1}{2}(r_3{}^4)\} + \frac{1}{2}\pi\rho_{coup}h(R_{out} - R_{in})^4 + J_{mot} = \frac{1}{2}\pi *$
$7850 \times 0.013 \times \{(0.089^4 - \frac{1}{2}0.037^4) + \frac{1}{2}0.013^4\} + \frac{1}{2}\pi \times 280 \times 0.025(0.01 -$
$0.007)^4 + 120 * 10^{-6} = 0.0099 + 989.6 * 10^{-6} + 120 * 10^{-6} = 0.011 \text{kgm}^2$

Then by applying equation (4.7) to find the equivalent mass of the flywheel system as: $m = 2\frac{J_{tot}}{r_2{}^2} = 2 * \frac{0.011}{0.089^2} = 2.78$ kg

Assuming a rigid cylindrical body with mass 2.78 kg, and from equation (4.7):

$J_{tot(theoretical)} = \frac{1}{2}2.78\ (0.089^2) = 0.011$ kgm^2

And, then from equation (4.10, 4.15),

$$\frac{d\omega}{dt} = \frac{T_{em}}{J_{tot(theoretical)}} = \frac{0.2}{0.011} = 18.165 = \frac{\acute{\omega} * 2\pi}{60t} = \frac{3300 * 2\pi}{60\ t}$$

$t = \frac{6600\pi}{60*18.165} = 18.165$ sec.

However, from the experimental data measured, using the datasheet of the PMBLDC motor at the nominal speed of 3300 rpm, torque 0.2 Nm, the time required for the motor to start up from the rest to reach its nominal speed can be calculated as:

From equation (4.7); the time to reach this speed is as follows:

$J_{tot/experiment} = \frac{1}{2}2.3\ (0.089^2) = 0.009$ kg m^2

And, from equation (4.10, 4.15), the change in angular speed at the nominal speed of 3300 rpm can be calculated as:

$$\frac{d\omega}{dt} = \frac{T_{em}}{J_{tot/experiment}} = \frac{0.2}{0.009} = 21.955 = \frac{\acute{\omega} * 2\pi}{60t} = \frac{3300 * 2\pi}{60\ t}$$

$t = \frac{6600\pi}{60*21.955} = 15.74$ sec

The evident that from these analyses, the system under consideration has to be redesigned to consider the time variable. Since the time was too large for the motor to reach the speed at which steady-state occurs, further control was needed to enhance system operation. By controlling the torque generated by the PMBLDC motor, the amount of energy transferred inside the flywheel can also be managed. Hence, charging and discharging of energy in the flywheel was performed by dictating a positive and (or) negative torque command the PMBLDC controller.

4.2.9 PMBLDC speed control

Proportional-integral-derivative (PID) control was the most widespread control algorithm applied in industrial control (Özbay 2016). The prominence of PID controllers can be assigned to their robust performance in enormous operating conditions and their feasibility in a simplified manner. The PID algorithm consists of three primary coefficients; proportional, integral and derivative, which were assorted to acquire an optimal response. The effects of tuning the PI closed-loop control system for PMBLDC speed control are examined in this section.

4.2.9.1 Closed-Loop System control

The closed-loop control system was the process of reading the sensor's output to provide constant feedback and evaluating the desired actuator output repeatedly, as illustrated in Figure (4.29).

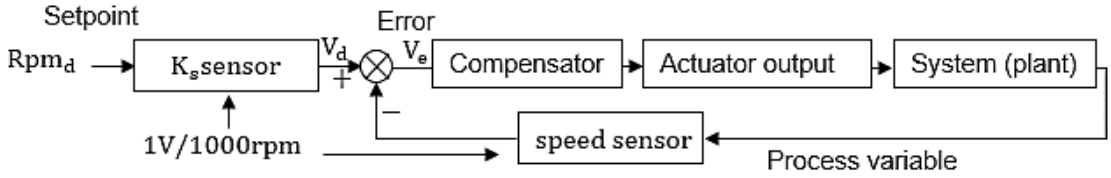

Figure 4. 29: PMBLDC closed-loop speed control strategy

The PMBLDC speed (rpm) was the process variable that must be controlled, and a sensor was used to measure this variable, which has provided feedback to the control system. Furthermore, a setpoint can be defined as the desired value for the process variable in the speed-control system. At any given time, the control system has used the difference between the process variable and the setpoint to determine the required actuator output to control the system.

4.2.9.1.1 Modelling and control design

Since the complexity of the controller was promptly related to the complexity of the model, it was imperative to have low order models. The parameters of PID controllers can be evaluated by modelling process dynamics and providing a method for control design. The driving torque (T_d) was directly proportional to the driving voltage (V_d) from the driver. The analysis was implemented

from the open-loop experiment test with rotational speed changed from 500 rpm to 1000 rpm, to determine the required control variables, as shown in Figure (4.30).

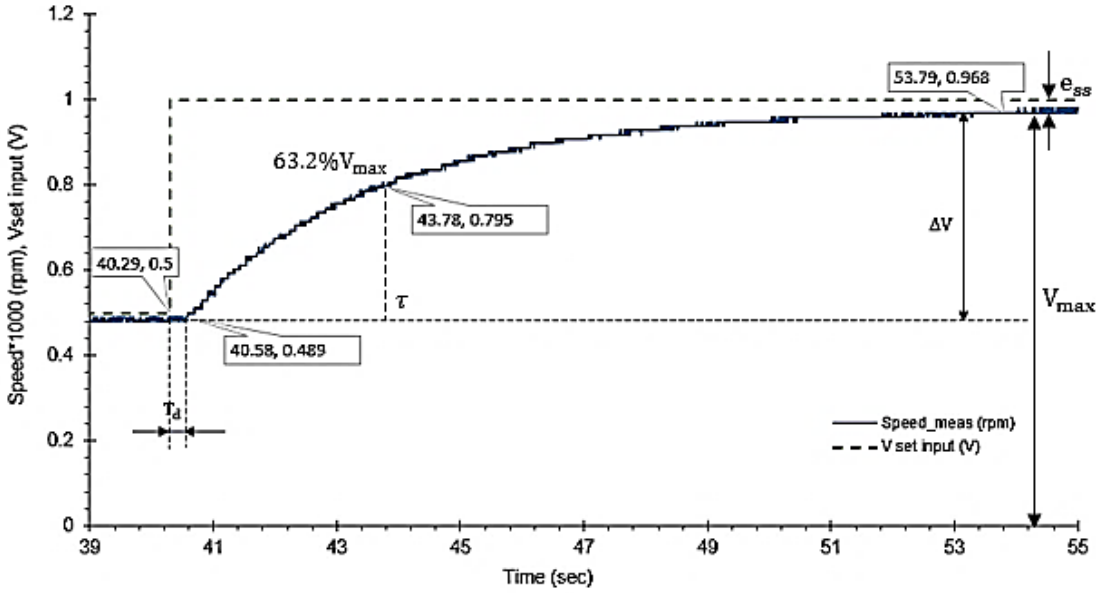

Figure 4. 30: Open-loop motor speed experimental test

4.2.9.1.2 Modelling process dynamics

This procedure of control was utilised to enhance system operation. Figure (4.30) show the speed curve of the PMBLDC motor used in the designed test rig. The driving time delay (T_d) from the open-loop test was equal to the time at what the system response after excitation, which was equivalent to ($T_d = 40.58 - 40.29 = 0.29$ sec). Accordingly, the time-delay of the motor T_d can be ignored in the applications of the RB process because it represents the starting motor operation that does not affect the generation operation in the braking process. Also, the change in the voltage (ΔV) corresponding to the change in the speed can be calculated as; ($\Delta V = 0.968 - 0.489 = 0.479V$), and the steady-state error (e_{ss}) is equal to ($e_{ss} = 1 - 0.968 = 0.032$ V). The voltage at which the speed reaches 63.2% of its final steady-state (V_{max}) can be implemented as ($\Delta V x 63.2\% + 0.489 = 0.305 + 0.489 = 0.795$ V).

The approximation was feasible for systems in which mass, momentum and energy can be stored using a single state variable, as an example, the rotating speed control. From the open-loop speed diagram Figure (4.30), the time (τ)

at which the speed reaches this value can be evaluated as ($\tau = 43.78 - 40.29 = 3.49$ sec).

Then when it was compared to a first-order transfer function gives:

$0.5\mathrm{K} = \Delta\mathrm{V} = 0.479$ V, which gives $\mathrm{K} = 0.958\mathrm{V}$, then the process dynamics were approximated by a first-order transfer function as:

$$\mathrm{G}_{(\mathrm{s})} = \frac{\mathrm{K}}{1 + \tau\mathrm{s}} = \frac{0.958}{1 + 3.94\mathrm{s}} \tag{4.18}$$

Then, for closed-loop control, the designed PI controller is as shown in Figure (4.31):

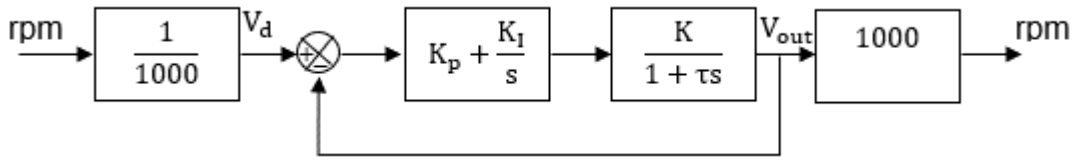

Figure 4. 31: Closed-loop system design and control representation

From Figure (4.31), the PI controller has the transfer function $\mathrm{C(s)} = \mathrm{K_p} + \frac{\mathrm{K_I}}{\mathrm{s}}$, and the overall transfer function can be evaluated as:

$$\begin{aligned} \frac{\mathrm{V_{out}}}{\mathrm{V_d}} &= \frac{\left(\mathrm{K_p s} + \mathrm{K_I}\right)\mathrm{K}}{\mathrm{s}\left(1 + \tau\mathrm{s}\right) + \mathrm{K}\left(\mathrm{K_p s} + \mathrm{K_I}\right)} \\ &= \frac{\left(\mathrm{K_p s} + \mathrm{K_I}\right)\mathrm{K}}{\tau\mathrm{s}^2 + \left(1 + \mathrm{KK_p}\right)\mathrm{s} + \mathrm{KK_I}} \\ &= \frac{\left(\mathrm{K_p s} + \mathrm{K_I}\right)\mathrm{K}/\tau}{\mathrm{s}^2 + \left(\frac{1 + \mathrm{KK_p}}{\tau}\right)\mathrm{s} + \frac{\mathrm{KK_I}}{\tau}} \end{aligned} \tag{4.19}$$

The above controller can be designed by the pole placement method, considering a reference characteristic equation $(1 + \tau_r\mathrm{s})^2 = 0$, which can be described as:

$$(1 + \tau_r\mathrm{s})^2 = 0 \;\Rightarrow \mathrm{s}^2 + \frac{2}{\tau_r}\mathrm{s} + \frac{1}{{\tau_r}^2} = 0 \tag{4.20}$$

Then, by equating the characteristic polynomial of equations (4.19) and (4.20) which leads to:

$$s^2 + \left(\frac{1 + KK_p}{\tau}\right)s + \frac{KK_I}{\tau} = s^2 + \frac{2}{\tau_r}s + \frac{1}{{\tau_r}^2} \tag{4.21}$$

then the controller parameters are represented by:

$$\frac{1 + KK_p}{\tau} = \frac{2}{\tau_r}, \qquad K_p = \frac{1}{K}\left[\frac{2\tau}{\tau_r} - 1\right] \tag{4.22}$$

so that,

$$\frac{2\tau}{\tau_r} - 1 > 0, \qquad \tau_r < 2\tau \tag{4.23}$$

And,

$$\frac{KK_I}{\tau} = \frac{1}{{\tau_r}^2}, \qquad K_I = \frac{\tau}{K{\tau_r}^2} \tag{4.24}$$

The parameter $\frac{1}{\tau_r}$, determines the response speed.

Since $\tau = 3.49\ \text{sec}$, and $K = 0.958\ \text{V}$, assuming the required time $\tau_r = 2\ \text{sec}$, then, from equation (4.23), $K_I = 3.49/(0.958 * 4) = 0.9102$.

Also, from equation (4.22), $K_p = \left(\frac{1}{0.958558}\right)(3.49 - 1) = 2.597$.

- To determine the integral time T_I measured in (min) used in the test rig such as, $K_p + \frac{K_I}{s} = K_p\left(1 + \frac{1}{T_I s}\right)$.

Since $K_I = \frac{K_p}{T_I}$, then $T_I = \frac{K_p}{K_I} = \frac{2.59765189}{0.9102214} = 2.853$ sec= 0.047 min.

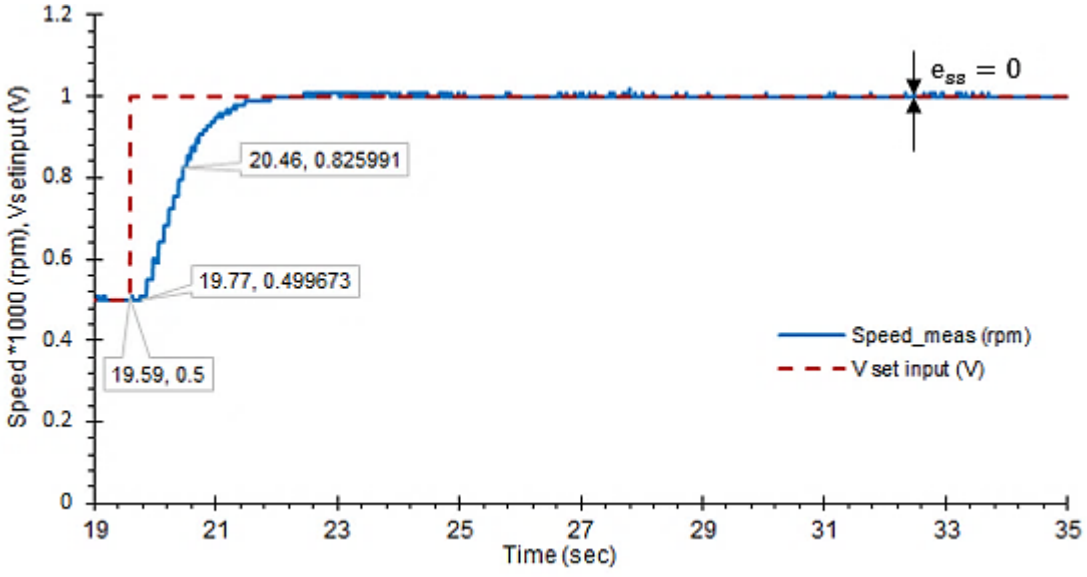

Figure 4. 32: Closed-loop designed controller for speed control

Figure (4.32) shows the PMBLDC motor with the designed controller. The driving time delay (T_d) from the closed-loop test was equal to ($T_d = 19.77 - 19.59 = 0.18\,\text{sec}$) which improve the response time of the motor speed control. Also, the e_{ss} was equal to zero. The τ time at which the speed approaches 63.2% of its final steady-state (V_{max}) is equal to (τ = 20.46 -19.77 = 0.69 sec) compared to 3.49 sec in open-loop test shown in Figure (4.30).

4.3 Experimental calculation of moments of inertia

The moment of inertia J_L of the PMBLDC motor can be calculated experimentally based on the free-running equation (4.10), $J_L \frac{d\omega}{dt} = T_{L,}$ as:

a) The motor runs at a defined speed ω_L, and then the power P_L was measured, in which the torque also can be calculated as $T_L = \frac{P_L}{\omega_L}$,

b) After that, when disconnecting the motor, the free-run stop was achieved. At t = 0, the tangent curve in the speed track was defined as, $d\omega_L / dt = \Delta \omega_L / \Delta t$,

c) Process (a), and (b) is repeated at a different value of ω_L, and then J_L was evaluated as an average value for all measured inertia.

In the next section, a laboratory examination of the effect of rotational inertia on energy recovery in RB was studied, and further investigations were conducted.

4.3.1 Studying the effect of rotational inertia on RB process

Dynamic energy recovery in EVs and HEVs can assist in restoring kinetic energy during descending and braking operations. The FES was used in a variety of modern applications; for instance, it has tended to be associated with the motor shaft to assist in starting the EVs from rest. Several components have been utilised to execute the motoring and braking mechanism in a structured test rig. However, there was an urgent need to represent this application within the limits of the laboratory facilities while being able to simulate the natural system. The mathematical model of regenerating energy from braking can be determined by analysing the charging and discharging characteristics of the battery and the DC motor throughout energy stored in the rotating mass

object considering the motor braking torque required and braking torque limit.

Consequently, this section has been examined the effect of rotating inertia at a different rotating speed in the drive system on propelled energy. Moreover, it has been demonstrated the experimental probing and mathematical modelling of the motor/flywheel (lumped into an equivalent inertial mass), which was used in different drive cycle schemes to simulate real system behaviour. The analysis was accomplished with an experimental verification highlighted the advantage of the new approach to evaluating storage capacity, and it gives the static and dynamic (time dependency) equations. This analysis shows an accurate system representation as a ready-made model (black box), which can be used to determine the overall system performance.

4.3.2 Review of proposed system modelling

In the RB, at the instant of braking, the electric motor connected to the flywheel has worked as a generator to convert rotational mechanical energy into electrical energy. The variable characteristic of the generated voltage from the generator/flywheel at braking was used to charge the storage unit (Bolund et al. 2007; Kim et al. 2014a). This variable produced voltage has depended on the flywheel's rotating inertia and on the capacity of both the generator and the storage units, which can be identified experimentally (Alamili et al. 2019).

Furthermore, mathematical models of dynamic systems were necessary for most fields of scientific research, and they can take many structures, such as differential equations, state-space equations, and transfer functions, as discussed in the previous chapter. The most widely used method for numerical demonstrations involves the development of mathematical equations based on the known physical laws that govern the system's attitude (Thoolen 1993; Hanselman 2006). The drawbacks of this technique were that the resulting models often complex. The available data did not readily estimate them due to identifiability problems which make it challenging to use this approach in system design applications. If there was enough empirical or operational data, then the "identification system" can be used as an alternative to physical-

based physical modelling. Also, this system was based on data that can be applied to virtually any system and generally provides relatively simple models that can well-describe system demeanour within specific operating conditions. These models can be used in a “black box”, which only represents the behaviour of the input and output or other descriptive interiors such as state-space equations, which can explain physically meaningful judgments (Bohlin 2006; Garnier and Wang 2008).

In the designed test bench, a model was developed based on observed data measurement and the dynamic analysis of the system to represent the overall system response. The PMBLDC motor response (static and dynamic) for both open-loop and closed-loop speed control can be implemented experimentally. Numerous results of experiments and simulations have allowed controlling the parameters of the RB process. The essential operation of the electric motor was that, when it continues to turn in one direction, it transforms the electrical energy into mechanical energy. And at braking, while it continues to turn, a properly structured motor has become an electric generator changing the mechanical energy into electrical energy. These methods have attempted to link the braking process to the ESU, which perform two main functions; recover and save braking energy and absorb excess energy during a light load operation. Such that resulting model faithfully has simulated the real system behaviours to show the valuable benefits. The analysis was accomplished with experimental verification, and the statics and dynamics equations of the lumped component represented as a ready-made (black box) models, used in determining overall system performance.

4.3.3 The process of building models from data analysis

The following steps were utilised to extract the best adequate of the data-based on experiments with enough information with disturbance, allowing to represent a system model and then validate the results as follows:

- Gathering input/output data (experiment data collection).
- Estimate the model from collected data by choosing the structure and finding the best model fits.

- Validating the model with a new dataset.

So, it can be observed that to evaluate the process; the sampling interval must be adjusted according to the dynamics of the process. Besides, it may be necessary to manage trends and offsets and to use filters to reduce disturbances for incorrect measurements. The quality of the product model depends primarily on the chosen structure that the intended application may represent. Additionally, the result was evaluated for the final model structure that includes the model size (order and delay) to validate the experiment data-driven.

4.3.4 System under considerations

In this section, a short mathematical model and simulation were used to assess energy harvesting through braking to improve overall system efficiency and performance. Different strategies have been implemented to extend the driving range to achieve the desired performance.

4.3.4.1 Power and torque analysis

The practical solution available to convert kinetic energy and subsequent return to electrical energy from the braking process has been described and explained throughout the speed and torque diagram, as shown in Figure (4.33).

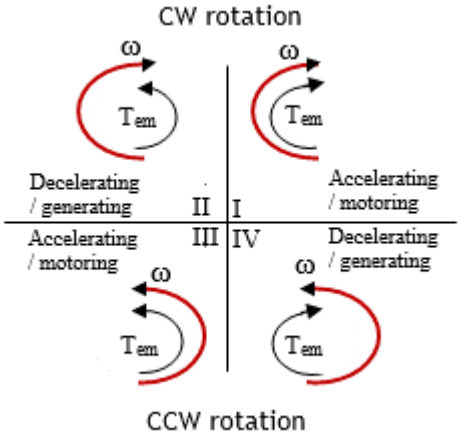

Figure 4. 33: Drive mapping applications according to angular speed and rotational torque

The quadratic control operation (driving, reversing, and braking motors) can be described as follows:

i. A first quadrant (I): where the angular speed (ω) and torque (T_{em}) have the same direction (accelerating) in CW rotation, in which the power ($P = \omega * T_{em}$) flows from the inverter to the rotating object. For instance, this range of applications can be found with variable or constant torque in the extruder or conveyors applications.

ii. The second quadrant (II): the direction of torque can change while the direction of rotation remains unchanged (decelerating). The II process may be needed in many industries, for example, as in the emergency stop of machinery and regenerative braking.

iii. The third and fourth quadrant (III and IV): the speed was in CCW rotation, and torque direction can be changed. It can be used as accelerating (III) or decelerating (IV) drive depending on torque direction. These applications were usually used in many motor operations that require frequent movement and torque changes, such as in elevators and the automotive industry.

When the drive was running in I or III, the motor operates as a driving force: I represent the front rotation, and III the reverse rotation. When the drive was running in II or IV, the torque was reversed in direction with motor rotation providing a controlled brake or deceleration force called regeneration or regenerative braking. Meanwhile, the overall system power flow in motoring and braking can be represented as in Figure (4.34).

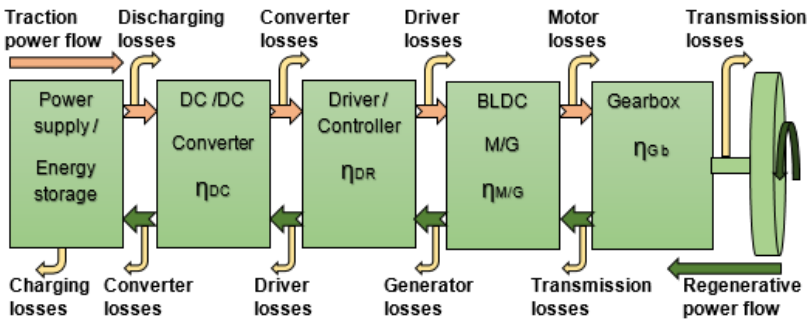

Figure 4. 34: Power flow diagram

The electrical power (P_e) supplied to the PMBLDC motor was converted into mechanical power (P_m) with addition to frictional power losses (P_{loss}), as, $P_{e=} P_m + P_{loss.}$ In the case of rotational mechanical motion, such as in EVs, the mechanical power represents the rotational power (P_{rot}), which was the product of torque T_{em} (Nm) multiplied by angular velocity ω (rad /sec).

$$P_{rot} = T_{em}\,\omega = E_{back}\,I_a \tag{4.25}$$

Equation (4.25) neglecting the losses in power, and assuming that $P_{e,}$ which equal the back (or counter) electromotive force E_{back} has produced in PMBLDC motor, as an example, multiplied by armature current (I_a), was equal to the P_{rot}. Where E_{back} , was the generated, induced back electromotive force (emf) measured in (V), and I_a was measured in (A).

Also, E_{back} can be calculated from motor geometry as:

$$E_{back} = \frac{p\phi ZN}{60A} \tag{4.26}$$

Where, p is the number of the motor poles, ϕ flux per pole in (web), (Z/A) is the armature winding number of parallel paths, N speed of rotation (rpm), and Z is the total number of armature conductors. The induced emf is a fundamental phenomenon when the DC machine is acting as a generator, then E_{back} represents the generated voltage E_{gen}.

The rotational energy E_{rot}, can be calculated as:

$$E_{rot} = \int P_{rot}\,dt \tag{4.27}$$

Moreover, to evaluate the rotational power P_{rot}, it was essential to convert the angular velocity measured in rpm to units of rad/sec with the help of equation (4.14). Typically, loads are arranged as constant torque ($T_{load} = C$), which was directly proportional with speed, and the power can be resolved from equation (4.18), which can be rearranged as:

$$P_{load} = T_{load}\,\omega = C\omega \tag{4.28}$$

Moreover, in some cases, loads have arranged as the quadratic torque (proportional to the square of the speed) (*Technical guide No. 8 - Electrical Braking* 2018), in which the torque and power can be measured as:

$$T_{load} = C\omega^2$$
$$P_{load} = T_{load}\,\omega = C\omega^3 \quad (4.29)$$

From the above equations, it was evident that braking torque and power requirements vary significantly concerning the time of these two types of loads.

4.3.4.2 Construction of the characteristic equation

In the designed test rig, the overall system response of PMBLDC motor (static and dynamic behaviours), which was connected directly with the flywheel, for both open-loop and closed-loop speed controls can be represented in the flowchart as shown in Figure (4.35, a and b) respectively.

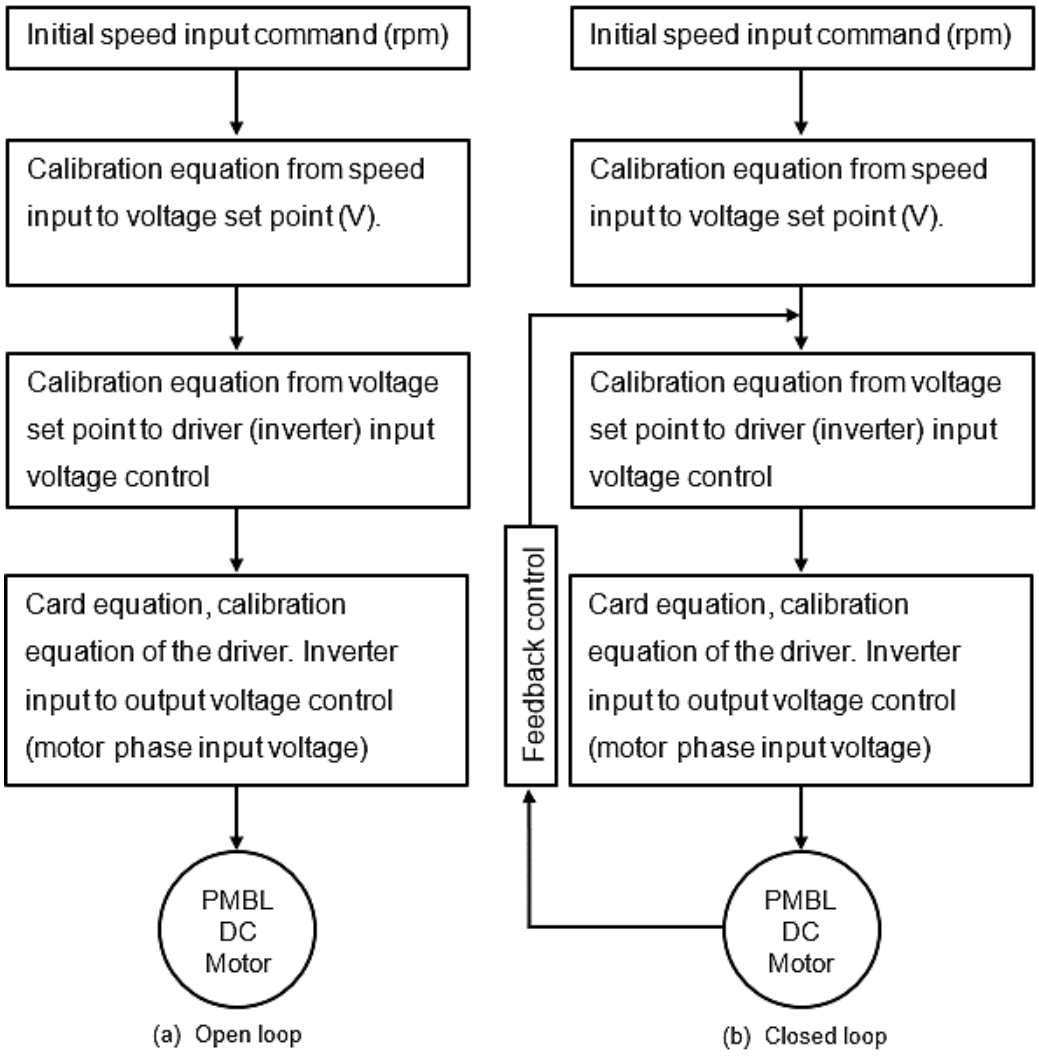

Figure 4. 35: PMBLDC motor, representation and speed control

4.3.4.2.1 System static equations determination

The experimental data extraction has been taken from the open-loop test to estimate the system's behaviour. Figure (4.36) shows the LabVIEW block diagram for speed control, voltage and current measurements.

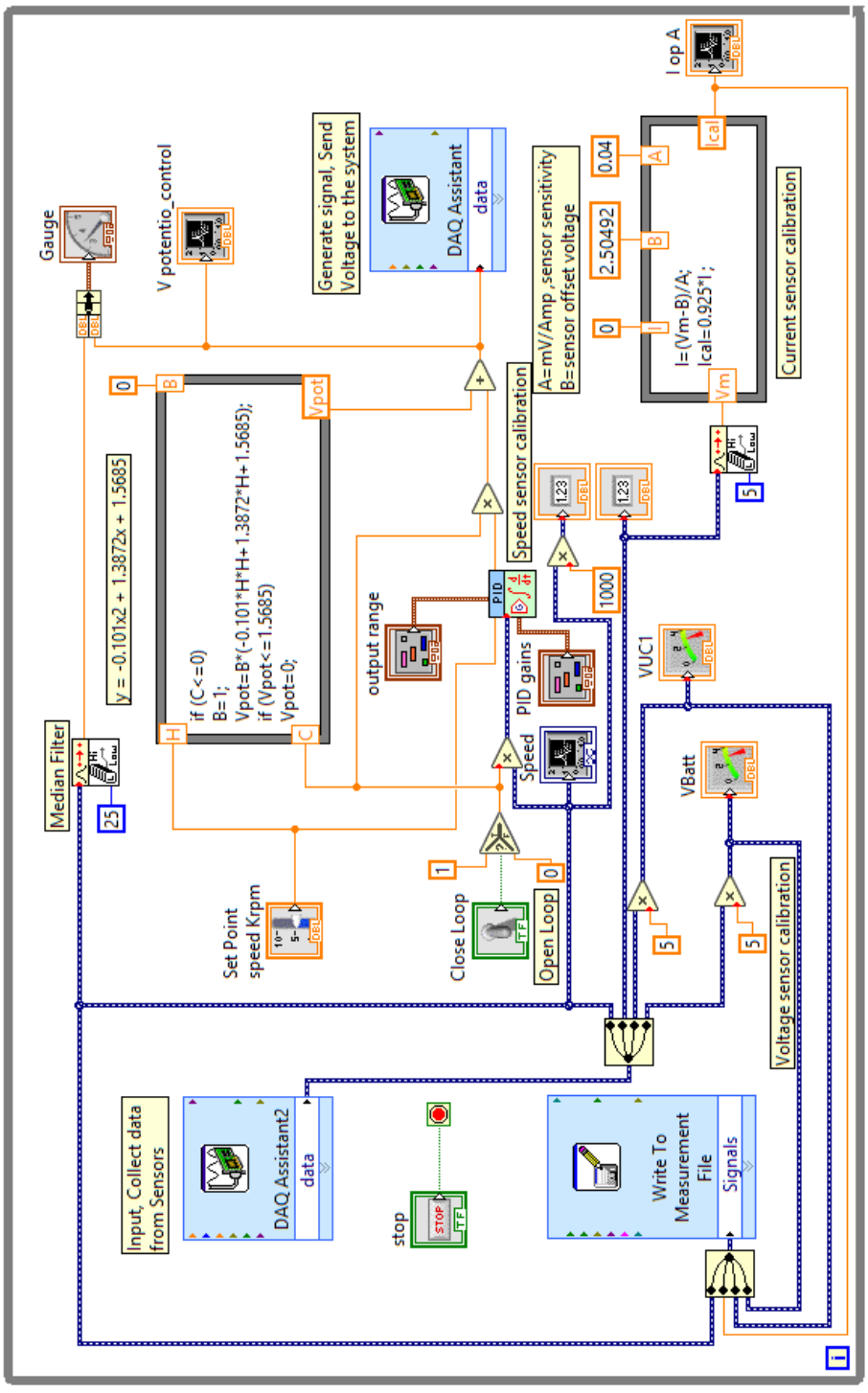

Figure 4. 36: LabVIEW Control and measurements for PMBLDC motor

Also, the data measured were represented in Table (4.2).

Table 4. 2: Experimental data for PMBLDC motor characteristic equations

Set voltage (V)	Drive voltage control (V) (inverter input)	Phase to ground voltage AC (V) (inverter output)	Motor speed (rpm)
0.20	1.83	3.60	0117
0.30	1.96	4.05	0229
0.40	2.10	4.30	0331
0.50	2.23	4.60	0413
0.60	2.36	5.35	0504
0.70	2.49	5.60	0606
0.80	2.61	5.82	0698
0.90	2.74	5.98	0800
1.00	2.85	6.10	0902
1.20	3.08	6.62	1106
1.40	3.31	7.04	1310
1.60	3.52	7.45	1524
1.8	3.74	7.80	1730
2.00	3.93	8.10	1942
2.40	4.35	8.58	2371
2.8	4.66	8.90	2778
3.00	4.82	9.00	2982
3.20	4.98	9.05	3186

Table (4.2) has been implemented from the open-loop experiment test to represent motor behaviour and the characteristics' equation. Also, Excel software has been used to evaluate the trend lines of unknown data fitting, and the accuracy has been determined by a sum of squared residuals (R^2) to measure the overall error for the best fit to the actual data. The following equations that have been extracted from each figure described as:

- The voltage setting as an indication of the required motor speed: Provides calibration of the speed sensor used in the test rig, which was a linear function associated with compensation, can be represented as shown in Figure (4.37).

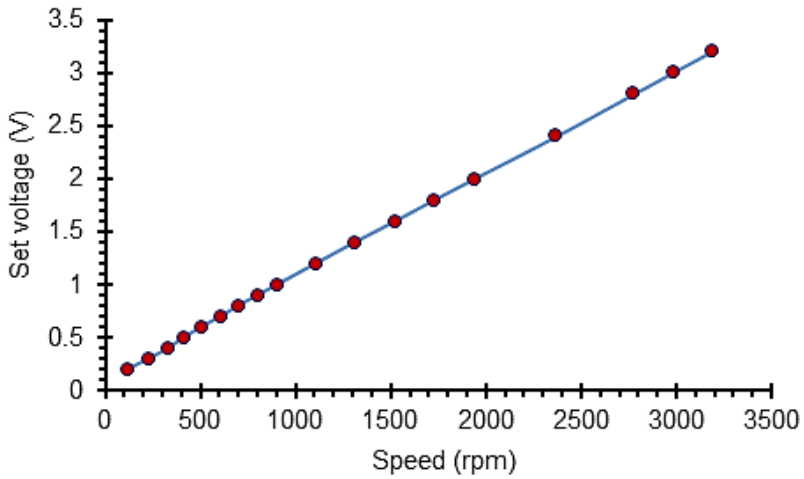

Figure 4. 37: Set voltage as a function of the desired Speed

With trends can be represented as:

$$y = 0.001x + 0.1047,\ R^2 = 0.9997 \qquad (4.30)$$

- Drive input control voltage (potentiometer voltage) concerning set voltage can be represented, as shown in Figure (4.38):

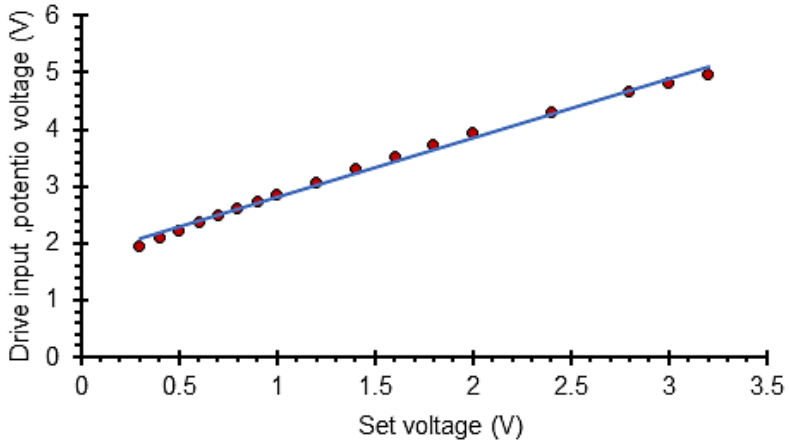

Figure 4. 38: Drive input voltage as a function of the set voltage

With trends can be represented as:

$$y = 1.044x + 1.7651, R^2 = 0.9945 \qquad (4.31)$$

- Card characteristic equation: the output AC phase to ground voltage as a function of the input control voltage (inverter calibration equation), can be represented, as shown in Figure (4.39):

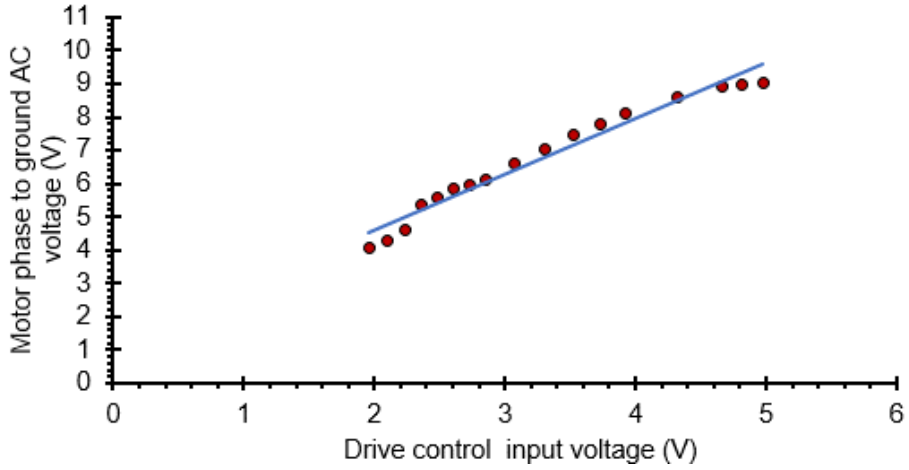

Figure 4. 39: Motor phase to ground AC voltage concerning driving input voltage (card equation)

With trends can be represented as:

$$y = 1.6676x + 1.2631, R^2 = 0.9665 \quad (4.32)$$

- Motor static equation: the speed as a function of its terminal AC voltage taken, can be represented, as shown in Figure (4.40):

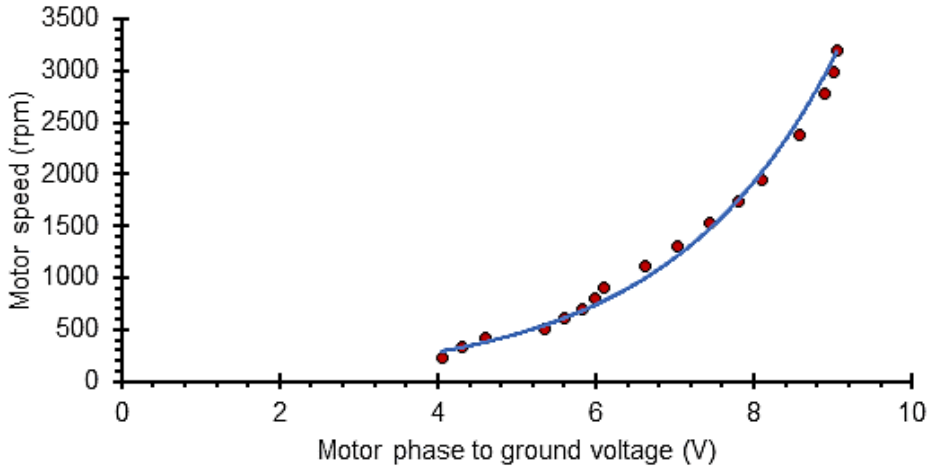

Figure 4. 40: Motor speed regarding its phase voltage

With trends can be represented as:

$$y = 56.319e^{0.4421x}, R^2 = 0.997 \quad (4.33)$$

- Motor dynamic equation

Furthermore, to complete the overall motor modelling, the dynamic response was derived from motor speed-time graph, as in Figure (4.41).

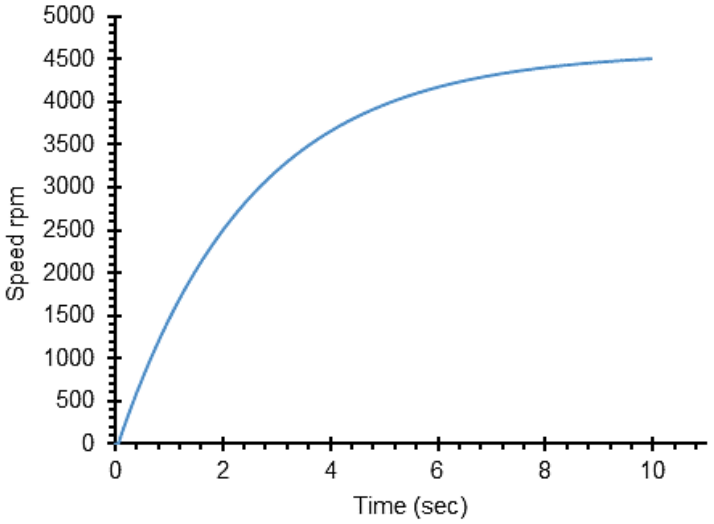

Figure 4. 41: Experimental no-load response

From this curve, a third-order difference equation can fit it.

$$y = 8.5646x^3 - 195.74x^2 + 1556.7x + 56.725,\ R^2 = 0.999 \qquad (4.34)$$

However, this research proposed a linearization method, that the graph is compared with a simulated first-order transfer function $(tf = 1/(5s + 1))$, as shown Figure (4.42), which gives the compatibility and by using system identification tool for comparison to get the best curve fitting.

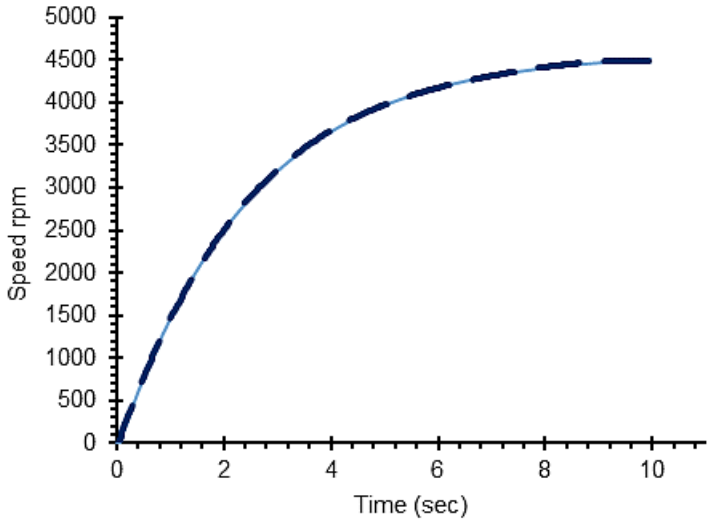

Figure 4. 42: Simulated transfer function curve fitting

4.3.4.3 LabVIEW simulation

The overall system equations extracted from the experimental test (4.30-4.33) can be represented in the LabVIEW program. The complete simulation of the closed-loop control for the motor can be seen in Figure (4.43):

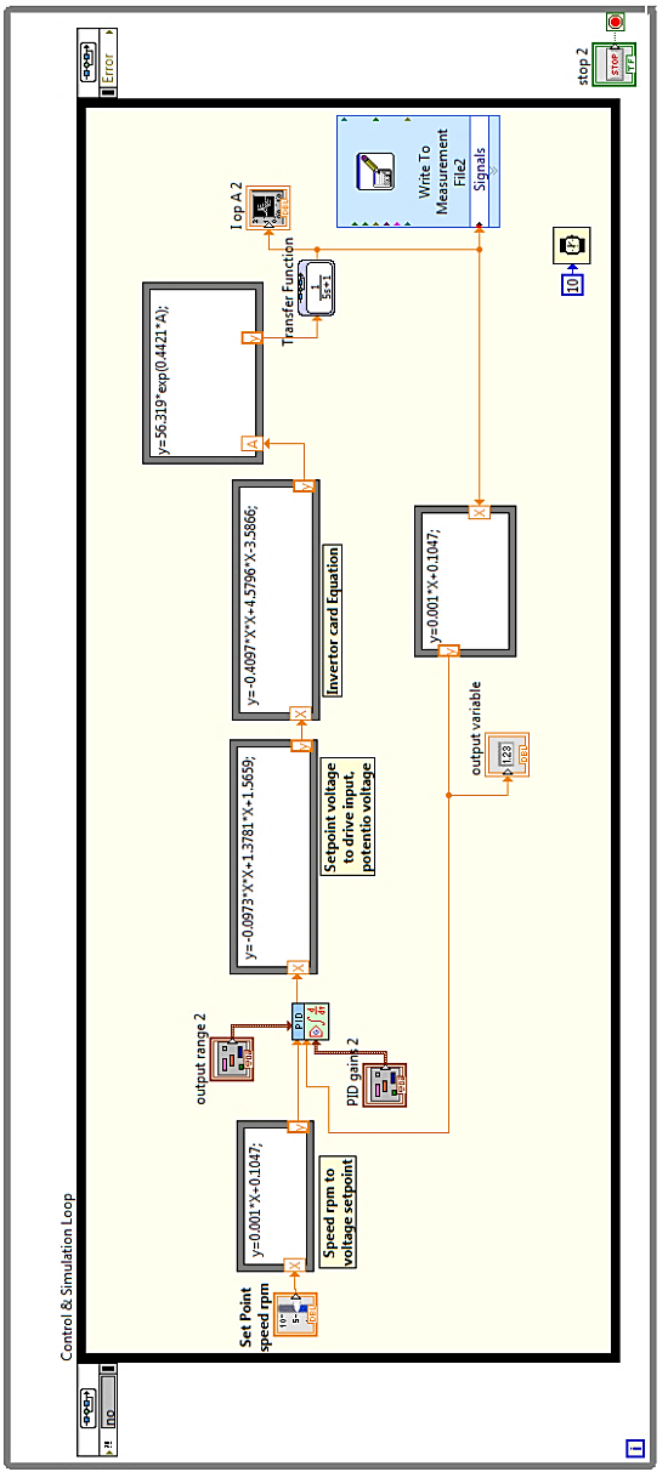

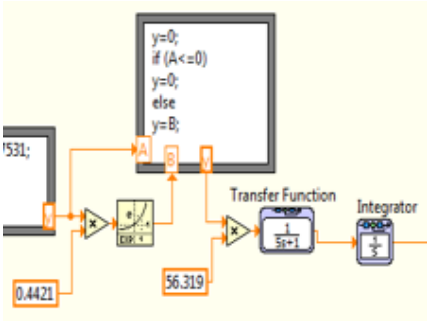

Equation (4.33)

Figure 4. 43: LabVIEW control and simulation loop

As shown in Figure (4.43), the conventional PI controller was used to determine the speed in the designed system. Furthermore, equations (4.30-4.34) were used to create a closed-loop simulation in the LabVIEW environment to study system behaviour with the effect of rotational inertia on energy recovery, which can then be widely applied to any system being tested using the same procedure.

4.3.4.4 Generating voltage operation

There are many strategies used for braking, the best achieved with a renewed approach since some dissipated power has returned to the system and stored in the storage units. The essential operation comes from electricity generated when the motor works as a generator during descending and braking of the EVs due to rotational energy stored in the flywheel. The experimental data extraction has been made to find the relation between generated voltage with different rotation speeds to estimate the generator's behaviour as represented in Table (4.3).

Table 4. 3: Experimental data for PMBLDC generator static equation

Speed (rpm)	Motor voltage phase to ground (V)	Generated voltage (V)
0280	0.69	0.57
0373	0.89	0.96
0464	1.10	1.38
0627	1.49	2.15
0851	2.02	3.27
1106	2.63	4.60
1341	3.20	5.78
1677	4.01	7.51
2136	5.09	9.84
2238	5.34	10.39
2666	6.39	13.14
2850	6.83	14.06
3268	7.82	16.18

The generated voltage as an indication of the speed provides the calibration equation of the generator used in the test rig, which was a linear function associated with compensation, as shown in Figure (4.44).

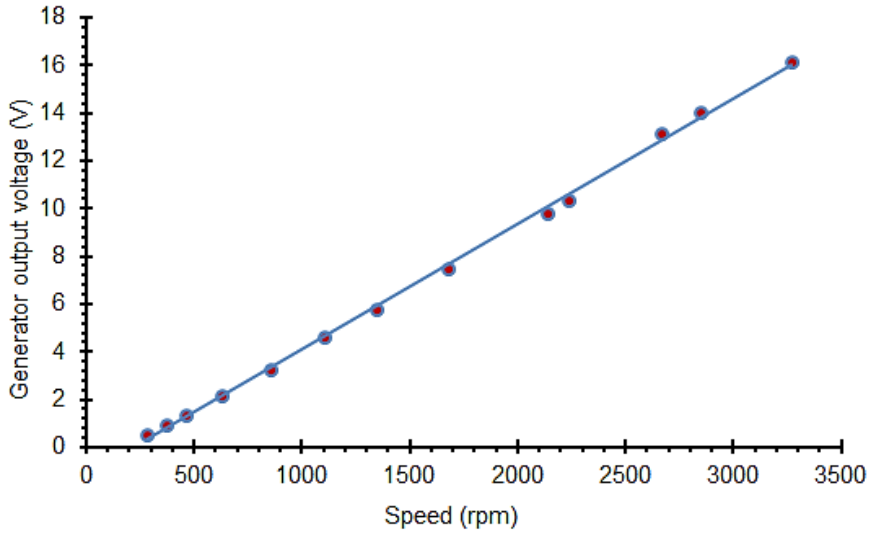

Figure 4. 44: Generator output voltage at various speed

With trends can be represented as:

$$y = 0.0053x\text{-}1.1345,\ R^2 = 0.999 \qquad (4.35)$$

Figure (4.45) represents PMBLDC generator (lumped with the flywheel) dynamic response. This figure was used to test the generator stopping time due to the moment of inertia alone at a speed of 3000 rpm with no load attached to its terminals.

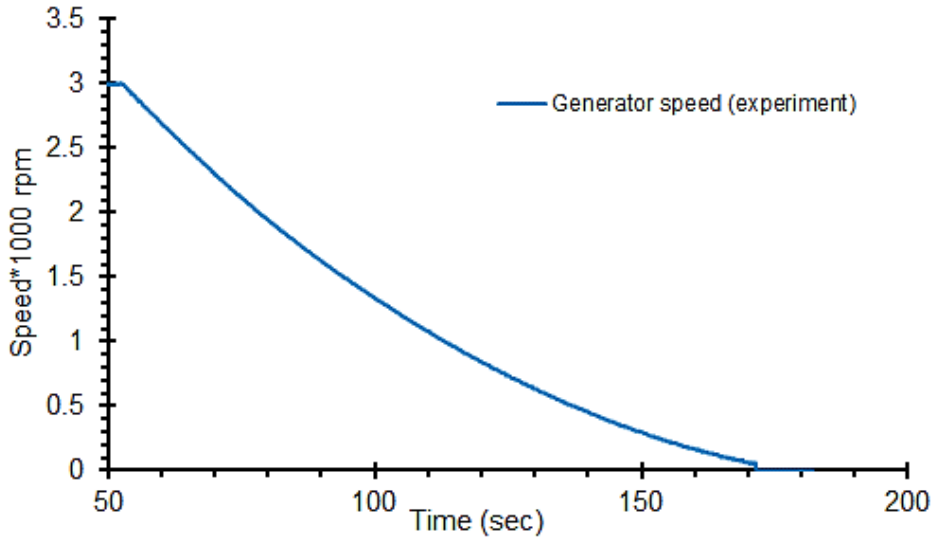

Figure 4. 45: No-load generator speed descending

From this curve, the dynamic equation of the generator can be extracted, and the system was represented as:

$$y = 0.00008x^2 - 0.0299x + 2.9294, R^2 = 0.9995 \quad (4.36)$$

The no-load speed graph is compared to the second-order simulated transfer function to complete the general modelling of the generator, $(tf = 1/(0.9s^2 + 0.6s + 1))$, which gave the symmetry and compared with system identification tool to get the best curve fitting, as shown in Figure (4.46) with the simulation in Figure (4.47).

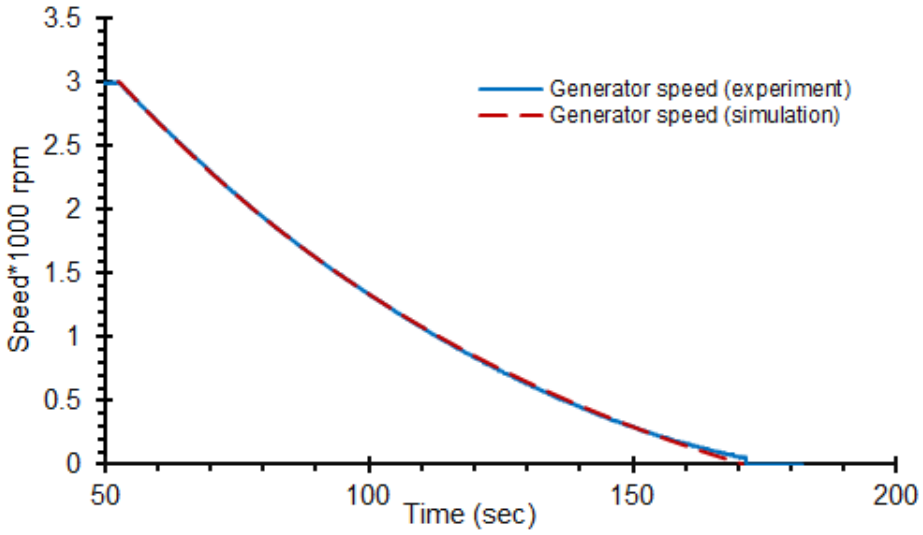

Figure 4. 46: Simulated generator speed curve fitting

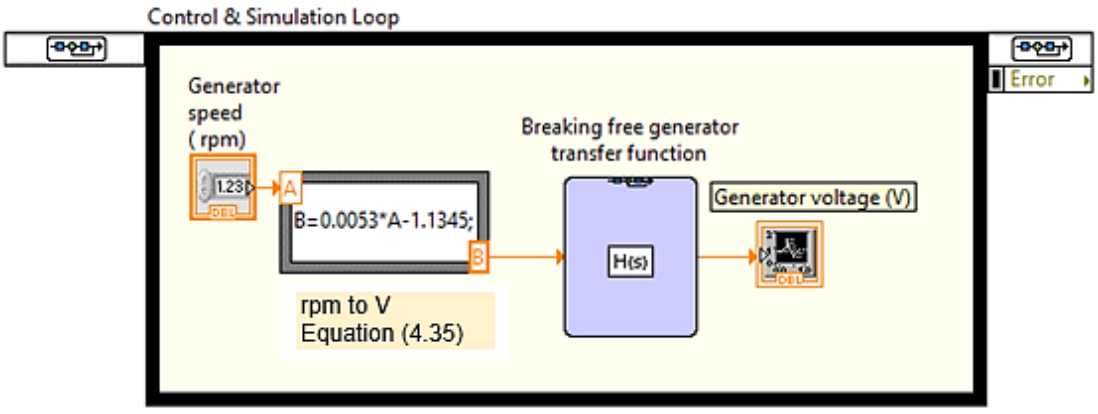

Figure 4. 47: Simulation generated voltage of the generator

The VV generated by the generator at braking operation can be used to charge the UCs for energy recovery mechanism in the control simulation loop, as shown in Figure (4.48).

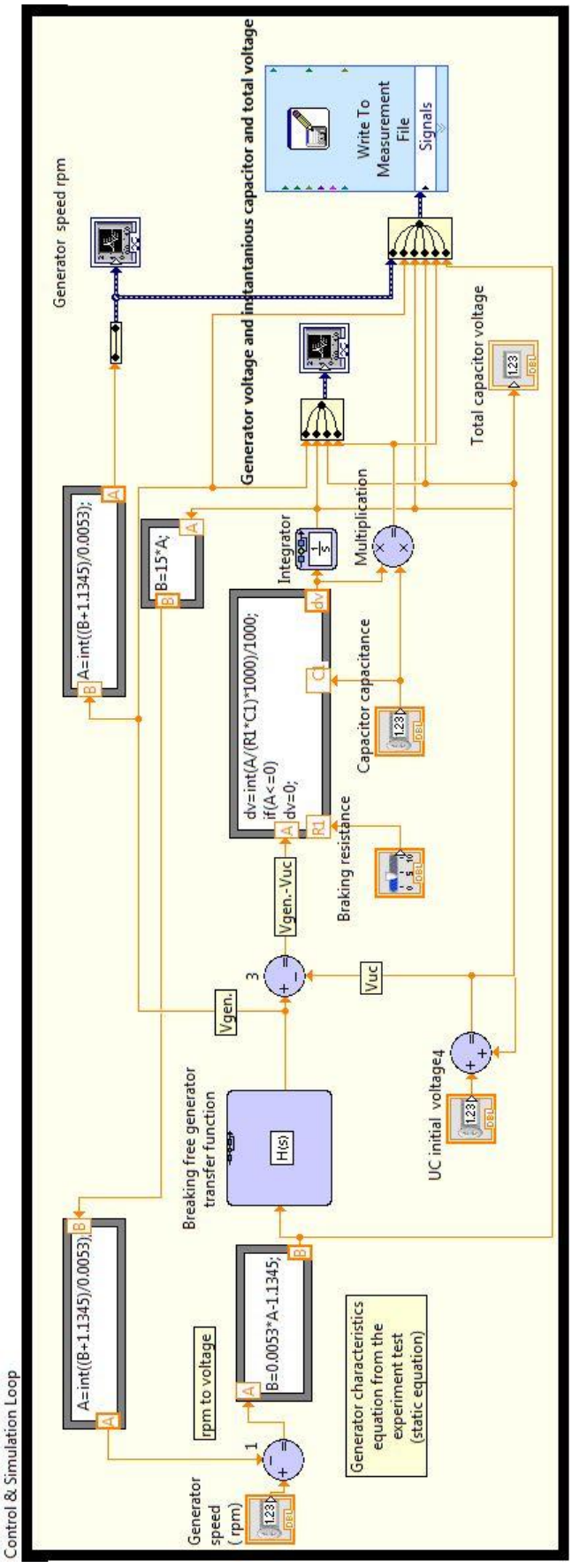

Figure 4. 48: Simulation of RB energy recovery

Meanwhile, the overall system representation for motoring and generating operation can be implemented as a flowchart as in Figure (4.49), which represent the motoring and generating operation with the energy stored in the UCs storage unit, which has been determined in the next chapter.

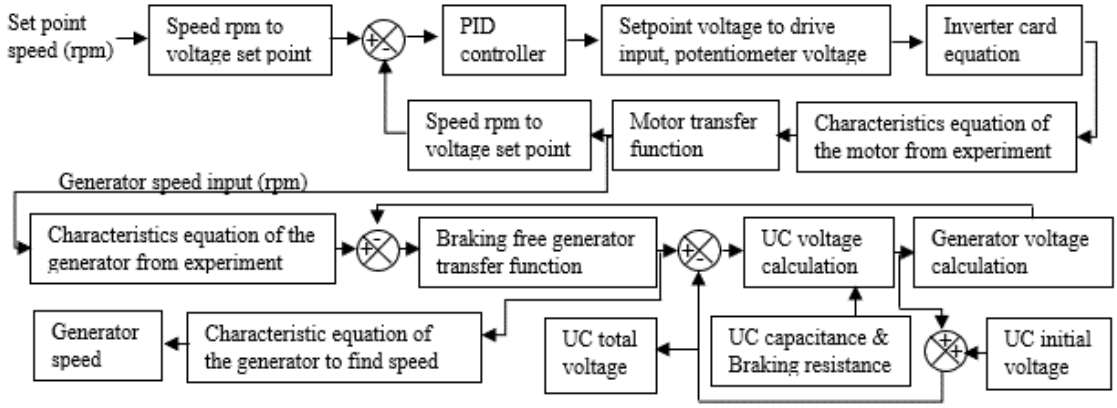

Figure 4. 49: Simulation flow chart

4.4 Summary

The contribution to this chapter was determined by developing a representation of designed test equipment to represent the RB process. The model was developed based on the experimental data measurement and dynamic system analysis as a "black box". Also, the designing of the flywheel to represent the kinetic energy recovery. Besides, the pole placement method, considering a reference characteristic equation, has been chosen to reduce the complexity of the controller design.

The next chapter (Chapter 5) presents the derivation of dynamic models of the rechargeable storage unit must be more convenient in the RB process. Also, the element and how it can withstand to recover energy from the braking technique will be considered with a new design for the UCs and the generator as a leading part in the RB process.

Chapter 5
Studying Energy Storage Units, and Energy Management System

In today's world, clean energy innovations, including storage and conversion, has played the most crucial role in the sustainable development of human society and turn into the most critical components in defeating reliance on fossil fuel and worldwide contamination. Among the potential clean energy solutions, the electrochemical energy was the most viable, sustainable and flexible energy. However, these technologies and the materials used to develop them continue to face high cost and performance challenges (Shen et al. 2016). This chapter has addressed the need for understanding a more realistic model for these storage units and how to use this model in different applications such as in RB process and the energy management system (EMS). The significant contribution of this chapter can be summarised as follows:

- Implementing a modelling enhancement of electrochemical battery. Making the designed circuit compatible with the experimentally observed parameter,
- Proposing a new insight into modelling and validating the UCs storage units,
- Finding the state of charge (SoC) of ESS, which was a benchmark of the fuel tank in customary vehicles and was an essential parameter that indicates the remaining electric charge in the battery, used to measures the distance that it can cover and monitoring track performance, and,
- Finally, proposing an energy management system (EMS) for charge transferred and energy augmented.

In the following section, a review of electrochemical storage systems has been presented. Also, an introduction to the modelling of a battery storage unit followed by the detailed analysis and study of the UCs storage unit, as two types of commonly used electrochemical energy storage units has been examined. Lastly, the implementation of energy management procedure and the overall contribution of the chapter has been presented.

5.1 Review of electrochemical storage systems

The master (rechargeable) energy storage system (ESS) of the vehicles were the electrochemical batteries and the UCs. These energy storage units have become increasingly important in the current applications. However, a detailed analysis of this element requires an understanding of its basic construction and operation. There was a resurgent interest in the combination of power-dense UCs with dense energy batteries at both the physical and package levels (Miller 2011). The outlines of classes of the electrochemical energy storage units are as shown in Figure (5.1).

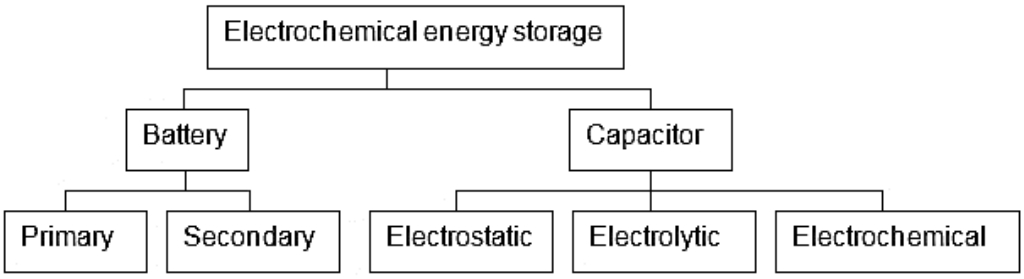

Figure 5. 1: Classification of electrochemical energy storage

The difference between the primary and the secondary batteries was that the former could not be recharged, while the latter can be recharged or reused, and also it can be used as a primary battery. Shen et al. (2016) concluded that several primary battery batteries used in different cathode-anode combinations. However, relatively few applications have been successfully used in practical applications (Shen et al. 2016).

On the other hand, electrostatic capacitors have contained a metal electrode and dielectrics such as mica or vacuum as separate units. Whereas electrolytic capacitors have included an electrical dielectric, as an oxide layer film was deposited or formed on a single electrode. The second electrode was the electrolyte which can be liquid or solid. Meanwhile, an electrochemical capacitor was a mixture of a reducing and oxidising agent, which were physically separated from each other by a salt bridge and were in chemical contact with each other. The UCs rechargeable ESS has used in different industrial applications. It has been used to transmit high current on acceleration and to deliver RB energy on descending and braking in electric vehicles (EVs), and hybrid electric vehicle (HEVs) power applications (Ahmad

Hamidi et al. 2015; Alamili et al. 2019). The UCs has been used to assist the battery in achieving the energy density of cells, offering almost an extended lifespan, and no environmental issues (Ren et al. 2015; Itani et al. 2017). Moreover, UCs have been utilised to store energy that has additionally made a fundamental advantage in the electric power system (Sangdehi 2015). Most importantly, these technologies have vigorously relied on upon battery packs as the primary storage unit. Also, the battery in the ESS should be used within the safe temperature and voltage ranges to operate safely and efficiently. The practical implementation was required to provide a continuous SoC monitoring system to ensure that the ESS was kept sufficiently charged and discharged with a given level using indicators from the automatic control systems. In this next section, different approaches have been presented for designing and modelling of battery ESS.

5.2 Electrochemical battery ESS overview

The Baghdad battery (BB) sometimes referred to as the Parthian Battery, was a clay pot surrounded by a copper cylinder. In the middle of this cylinder was an iron rod that does not touch it. Both the copper cylinder and the iron rod are installed in an asphalt socket, as shown in Figure (5.2). These artefacts were discovered during prospecting in the ancient village of Khujut Rabu near Baghdad in 1936. The village is about 2,000 years old and was built during the Parthian period (250 BC to 224 AD) (Franz and Feldhaus 1869). This precious historical and scientific effect, carefully made of materials with precise chemical properties, was one of the most extraordinary mysteries in history. It was an achievement of the ancient civilisation, which surprised modern man, like the most impressive monuments, unique architecture, and timeless drawings.

Figure 5. 2: BB graph (adapted from (Clark [no date]))

However, today, in industrial applications, the request for batteries to meet progressively stringent performance prerequisites has been a challenge for achieving the application's desired services. Accelerated attention to EVs, and HEVs, and energy storage systems for utilities have accelerated the development of larger rechargeable batteries (Linden and Reddy 2002). The electrochemical rechargeable batteries are of extraordinary significance in power systems since they give the electric energy in a way that can be promptly accessible (Shen et al. 2016; Group [no date]). The battery was designed to convert chemical to electrical energy during acceleration (discharging process) or to converts electrical to chemical energy during deceleration (charging) process (Linden and Reddy 2002). Lead-acid batteries have been used since the 20th century.

Interestingly, the system has not changed significantly since then. The system consists of the lead current collector, spongy lead as active negative material, lead oxide as an active, positive material and sulphuric acid diluted as an electrolyte. During discharge, the active substance on the positive and negative plate was converted to lead sulphate (Lukic et al. 2008). Various dynamic models include all the essential factors that affect execution, which can be used to evaluate the performance of the battery.

In EVs and HEVs, as the battery was the primary energy source, the motor will not only operate as a generator to retrieve energy from braking instead of dissipating it as heat as in the conventional braking but will also act as a starting engine (Ehsani et al. 2010). One of the essential features of utilising the DC motor as a propulsion engine was that it has low noise, with low maintenance and CO_2 emissions (LAU and LIVINA 2015).

However, battery behaviour and its response during operation have played an essential role in energy transfer and energy management system (EMS). A simple, useful equivalent circuit for lead-acid batteries have been implemented to simplify the battery part of the system model. The circuit model and an estimation of the battery parameters from laboratory data have described in detail in which it can deliver an accurate representation and simulation results.

5.2.1 Battery Model

In the design method, numerous battery models with various levels of accuracy and complexity have been developed. These models can be primarily categorised as the battery-electric, battery thermal and combination of them (Liu et al. 2019). Battery models were used to estimate the performance and operating constraints required to analyse and simulate its behaviours used in the RB system design and process, with different kinds of control approach, transducers, and auxiliary components.

Most importantly, these technologies have vigorously relied on battery packs as the central storage unit. It is in this way critical to creating accurate cell models that can advantageously be utilised with a simulation of EMS (Ostadi and Kazerani 2015; Xu and Cao 2015). The battery model can be extracted in different ways. It can be modelled through experimental and electrochemical models suitable for representing cell dynamics for the aim of state estimates for battery, and researchers suggested that the best modelling technique was in the electric circuit-based system (Lee et al. 2008; Roscher and Sauer 2011; Kim et al. 2014b). González-Longatt (2006), in his study, gave a review of several circuit-based batteries, including simple, modified and dynamic models (González-Longatt 2006). In electric circuit-based models, the

selection of all parameters depends on a sophisticated technology established to demonstrate the electrochemical behaviour of the battery. However, for monitoring the state of charge (SoC), the electric circuit-based models can be valuable to represent the electrical properties of cells as a state variable capable of providing accurate simulation results (Hausmann and Depcik 2013; Chen et al. 2017).

5.2.1.1 Battery equivalent circuit model

The equivalent circuit models of the electrical battery behaviours were adopted by a combination of passive circuit components, including resistors, capacitor, and variable voltage source. This model has been extensively used due to its simple structure in different applications. On the other hand, the discharging and charging models, for instance, were developed using a different technique which relies directly on experimental data and the manufacturer's datasheet. The equivalent circuit model virtually has connected a controllable voltage source and a series resistor to form the internal circuit of the battery. A simplified model was selected to represent and to monitor battery packs accurately and to determine the number of physical tests needed to choose the component. The circuit has had an ideal voltage source, indicating an open-circuit voltage (V_{oc}) connected in series with an ohmic resistance (R_o), and the R_pC_p parallel combination describing the polarisation phenomenon to fit the electrical battery behaviours and its performance, as shown in Figure (5.3).

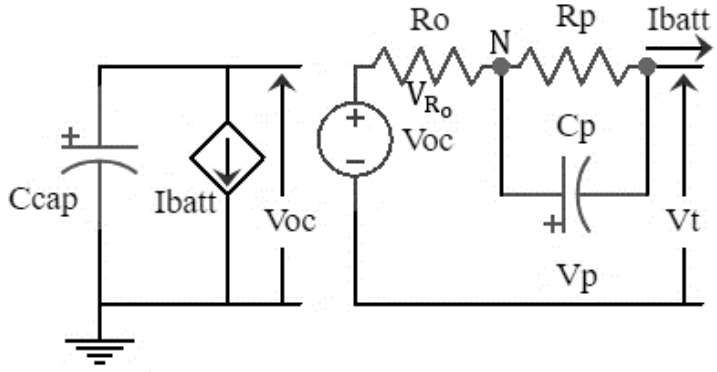

Figure 5. 3: Battery equivalent circuit

Capacity calibration was performed by the constant current-constant voltage (CCCV) test (Zou et al. 2015). Applying Kirchhoff's current and voltage laws (KCL, and KVL), as in Figure (5.4), and ohms law to the battery equivalent circuit, can be represented as shown in Figure (5.3:

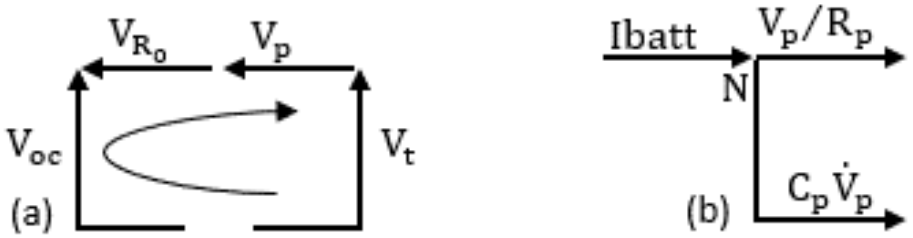

Figure 5. 4: (a) KVL, (b) KCL phasor diagram

$$\dot{V}_p = \frac{1}{C_p}\,\mathrm{Ibatt} - \frac{V_p}{R_p C_p} \tag{5.1}$$

$$V_t = V_{oc} - V_{R_o} - V_p \tag{5.2}$$

$$V_{R_o} = R_o\,\mathrm{Ibatt} \tag{5.3}$$

Where V_t represents the variable output terminal voltage (R_p, C_p) represents the parameters that describe the battery's dynamic responses, and the Ibatt means the charging and discharging current-controlled current source. V_p represents the voltage across the parallel branch, and V_{oc}, represents the controlled voltage source referred to the voltage of the open-circuit voltage (OCV). The solution of the first-order differential equation (5.1), is given as:

$$V_p(t) = V_p(0)\, e^{\frac{-t}{RpCp}} + R_p\,\mathrm{Ibatt}\left(1 - e^{\frac{-t}{RpCp}}\right) \tag{5.4}$$

Substitution of equations (5.4) and (5.3) into equation (5.2) yields,

$$V_t = V_{oc} - \mathrm{Ibatt}\left(R_o + R_p\right) + \left(\mathrm{Ibatt}\,R_p - V_p(0)\right) e^{\frac{-t}{RpCp}} \tag{5.5}$$

Equation (5.5) used to perform experimental parameter estimation regarding input-output voltage measurement as in Table (5.1).

Table 5. 1: Terminal voltage measurement

Conditions	Output measurement
$(t \to \infty)$, $Ibatt = 0$	$V_t\,(t \to \infty) = V_{oc}, V_p\,(t \to \infty) = 0$
$(t \neq \infty)$, $Ibatt = 0$	$V_t(t) = V_{oc} - V_p(0)\, e^{\frac{-t}{RpCp}}$
$(t \neq \infty)$, $Ibatt \neq 0$, $V_p\,(0) = 0$	$V_t = V_{oc} - Ibatt\,(R_o + R_p) + (Ibatt\, R_p)\, e^{\frac{-t}{RpCp}}$
$(t \neq \infty)$, $Ibatt \neq 0$, $V_p\,(0) \neq 0$	$V_t = V_{oc} - Ibatt\,(R_o + R_p) + (Ibatt\, R_p - V_p(0))\, e^{\frac{-t}{RpCp}}$

Moreover, the battery ESS, stores energy in many cells which can be connected in a series-parallel configuration to acquire the desired capacity and voltage range (Alexander and Sadiku 2001; Theraja and Theraja 2005).

Unlike the conventional equivalent circuit, the model filters the actual current for the filtered current i^*, and then multiply it with the polarisation resistor, which set to the state of charge (SoC) of the battery to obtain the polarisation voltage of the cell. Furthermore, from the discharge curve, the dynamic voltage has represented by the polarisation voltage when the current changes, takes into consideration open-circuit voltage (V_{oc}), as a function of SoC, and the ohmic voltage drop. In the model, the non-linearity of the voltage with the SoC was designed by the polarisation voltage term $(k\frac{Q}{Q-it}it)$.

The battery voltage can be obtained from Shepherd model, which describes battery behaviour in terms of voltage and current (R.C. et al. 2008; Jiang and Zhang 2015), as:

$$V_{oc} = E_0 - k\frac{Q}{Q-it}it - Ri + Ae^{-Bit} - k\frac{Q}{Q-it}i^* \qquad (5.6)$$

Where E_0 is the battery internal voltage (V), k is the polarisation constant (V/ Ah). Also, Q represents battery capacity in (Ah), A is an exponential zone voltage (V), B exponential zone inverse time constant $(Ah)^{-1}$, R is the internal resistance (Ω), i, is the battery current (A), and i^*, is the filtered current flowing through the polarisation resistance (A). Figure (5.5) gives the design circuit corresponding to equation (5.6).

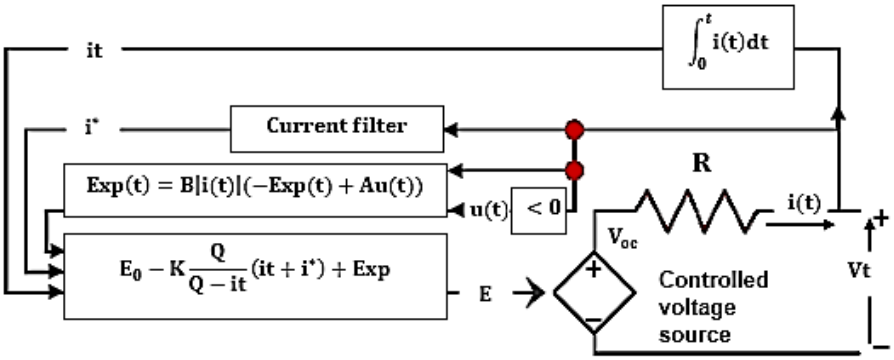

Figure 5. 5: Battery circuit diagram

In the designed test rig, the proposed modified generic battery model, consists of power electronic converters describe the electrochemical behavioural of the cell, as in Figure (5.6) was chosen (Tremblay et al. 2007).

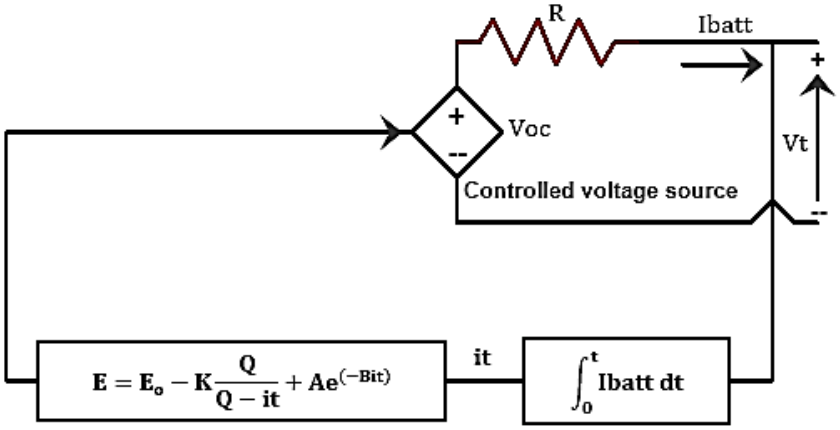

Figure 5. 6: Battery modified circuit diagram

Where $\int Ibatt\, dt$, was battery charge (Ah).

Also, the discharging characteristic was accomplished when it utilised to power a PMBLDC motor (BL58EE70W). In this process, the battery voltage was an indication of the prompt motor state as follows:

- In accelerating (motoring) mode, the battery voltage has gone below maximum, which was an indication for the controller to take energy from the UCs to support the source,

- In descending (generating) mode, the battery voltage has escalated due to regenerative braking in which the controller activates the UCs to store the kinetic energy that changed to electricity.

5.2.1.2 Experiments setup for battery discharging analysis

The test had been done to evaluate the performance and to design an accurate model of the battery storage unit by charging/discharging the battery with a specified current profile to determine its behaviour and to use extracted data to initiate boundary conditions on EMS.

In the experimental test, the primary storage lead-acid battery which has a capacity of 10Ah with 12V nominal voltage connected with a programmable electronic load (PEL) “300W 8500”. Figure (5.7) can be used to perform experimental parameter estimation regarding input-output voltage measurement to investigate the discharging characteristic curve. In this analysis, the PEL has operated in CCCV operating modes, where current and voltage values were assessed and instantly monitored as in Figures (5.8, 5.9). The characteristics curve from the datasheet, as in Figure (5.10) has demonstrated the battery terminal voltage during the discharging process.

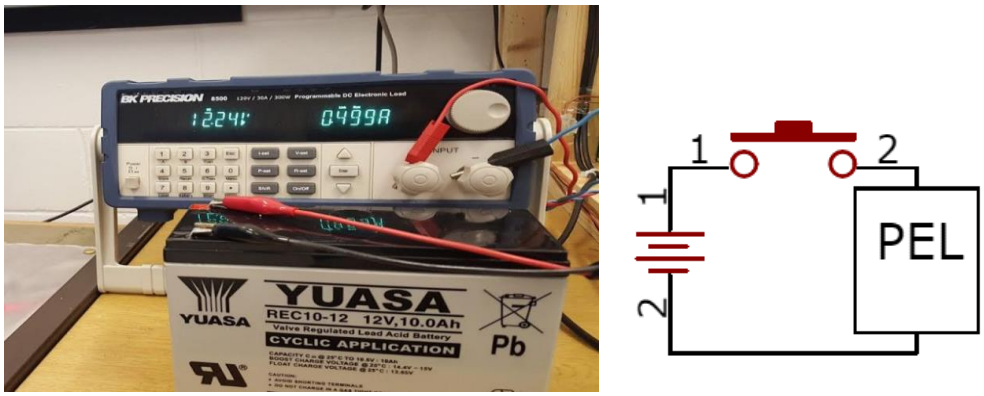

(a) (b)

Figure 5. 7: Discharging battery experimentally (a) photo (b) circuit diagram

The voltage drops were linearly within the nominal zone, while massive breakdown happened after that.

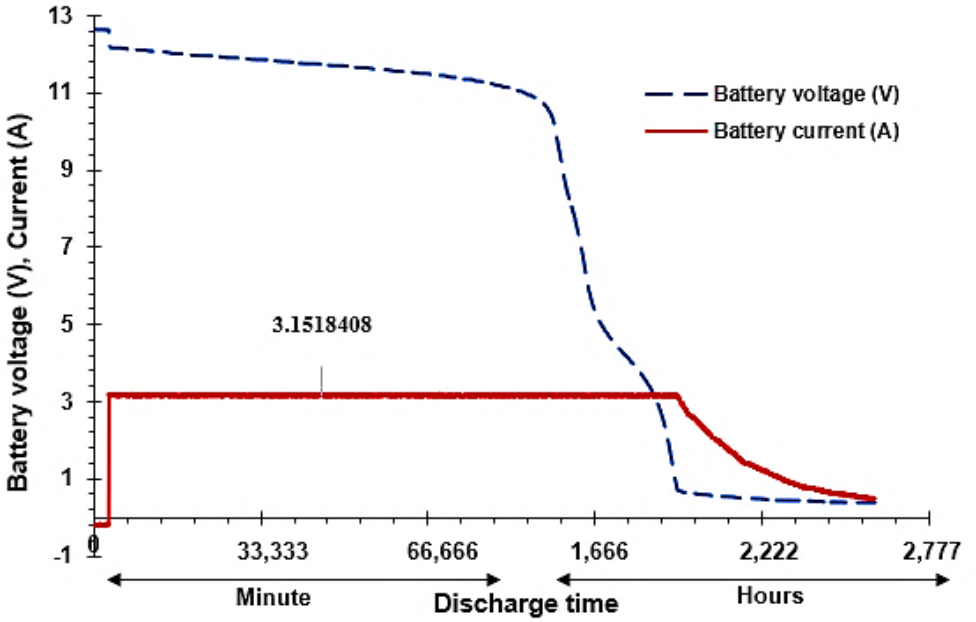

Figure 5. 8: Battery discharge characteristics (at 3.15A) curves at room temperature

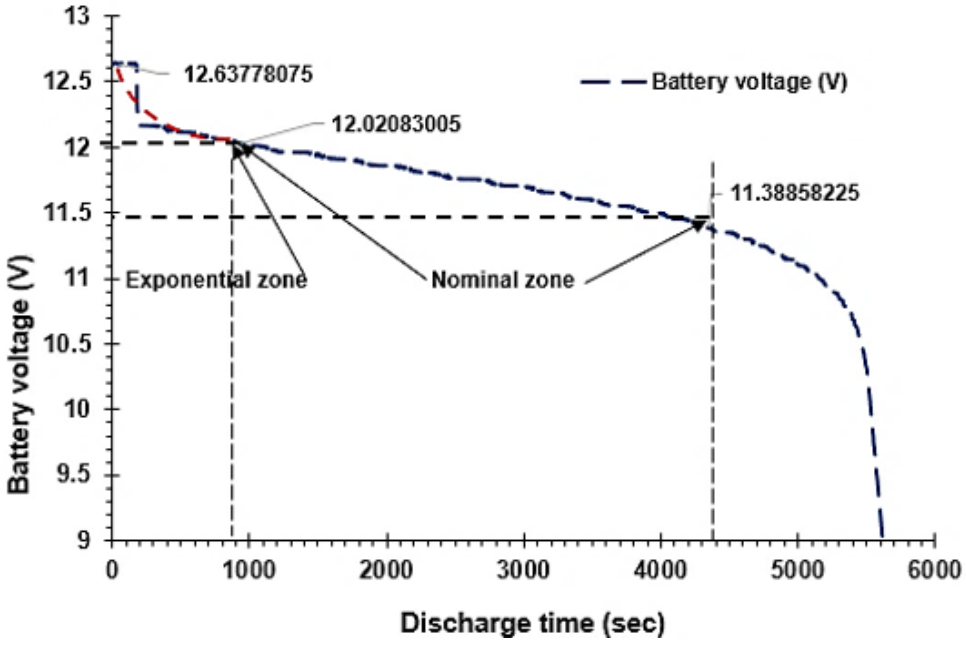

Figure 5. 9: Battery operation region

Figure (5.9) has been taken from Figure (5.8) to enlarge the battery region of operation, and to understand each zone precisely.

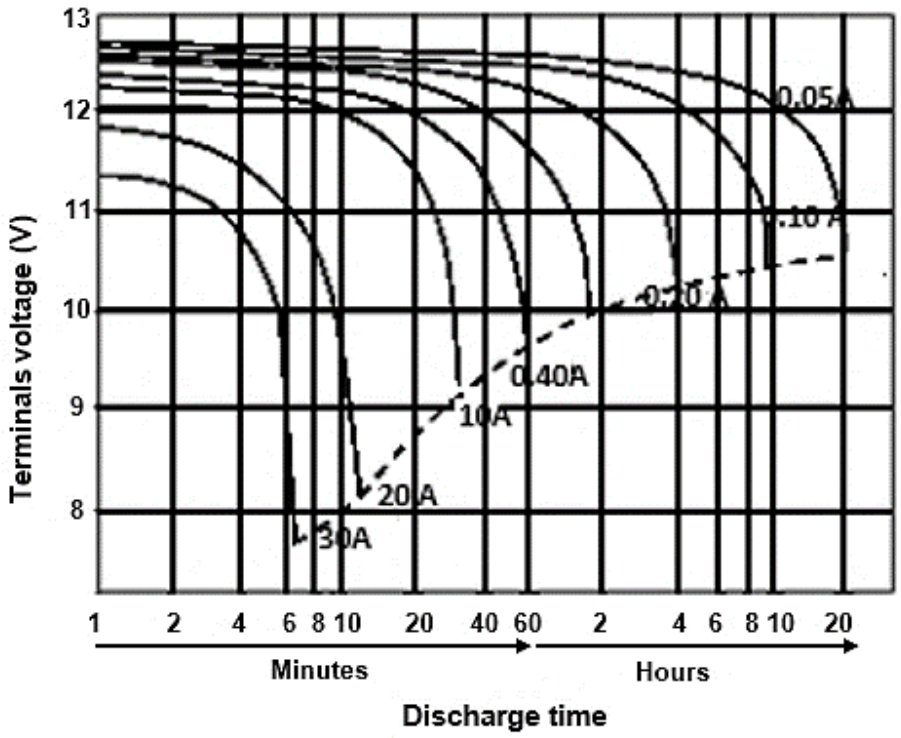

Figure 5. 10: Datasheet discharge characteristics curves (adapted from (REC 10-12. 2008)**)**

Battery manufacturer and its user expressed the value of the current used to charge and discharge cells and batteries as multiples of the capacity, C-rate, can be calculated as, (R.C. et al. 2008):

$$I_t = C_n/M \qquad (5.7)$$

Where I_t is measured in amperes (A), C_n is the rated capacity demonstrated by the manufacturer in ampere-hours (Ah), and the time base M is in hours (h) at rated capacity.

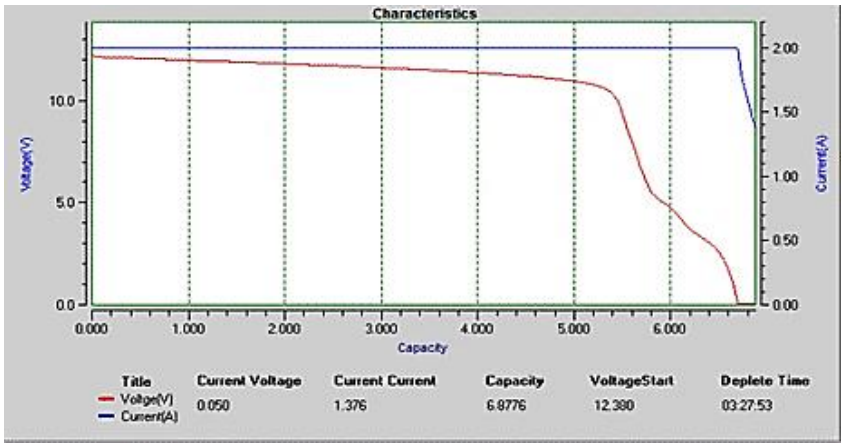

Figure 5. 11: PEL discharging characteristic curve

Figure (5.11) has represented an experimental test used to investigate the battery discharging curve with the PEL front panel. It was used to show battery discharging voltage at a constant discharging current CC (2A) starting from 12.39V steady-state voltage until it reaches about the minimum value 0.05V. The depletion time has represented the time at which the battery depleted from energy (discharge operation). This test has been done for an experimental investigation to show the various operating region with the battery capacity and voltage states used for determining voltage constraints in the system control and optimisation analysis. In practice, there was over-discharge protection to maintain the battery voltage at a specified level as it can be seen from the discharge curve.

5.2.1.3 Theoretical and experimental SoC Measurement

In the previous section, an approach has been examined for designing and modelling of battery ESS. However, to operate safely and efficiently, batteries ESS should be used within the safe temperature and voltage ranges. In this case, the battery state of charge (SoC) status monitoring and observation have become a crucial point in these applications. If the SoC was not controlled, bringing about conditions, it could degrade the ability of the battery-pack to future power transients (Dussarrat and Balondrade 2013).

There were many techniques provided to evaluate the SoC as; the discharge technique, current integration technique used to count the amount of current pass the battery in two directions and the open-circuit voltage (OCV).

5.2.1.3.1 Coulomb counting method

A direct onboard theoretical measurement widely used to determine the SoC of the cell, which was equal to the integration of overtime the discharging current (Ng et al. 2009; Liu et al. 2019). Therefore, the remaining capacity (charge) can be determined using the calculated current passing through this storage unit. The internal discharge current also affects the overall measurement, and for simplicity, it was assumed to equal to zero in this analysis. The battery capacity used in the test rig from the datasheet was equal to 10Ah. Moreover, for simulation and circuit design of the modelled cell, the conventional assumption of current follow have been taken as a negative sign when it was discharged, and a positive sign when it was charged.

$$\mathrm{SoC(t)} = \mathrm{SoC(0)} - \frac{\eta}{\mathrm{C_n}} \int_0^{\mathrm{t}} \mathrm{Ibatt(t)}\ \mathrm{dt} \tag{5.8}$$

Where $\mathrm{SoC(0)}$ is the initial value of SoC (Ah), η is the coulomb efficiency (range (1-0.98)), $\mathrm{C_n}$, is the nominal battery capacity, which is the health indicator of the battery. The charge counting performance is analysed experimentally and theoretically.

5.2.1.3.2 Hydrometer

On the other hand, the hydrometer was an alternative experimental measurement used to measure SoC of flooded lead-acid batteries. When charging the battery, the sulfuric acid has gotten heavier, increasing the specific gravity (SG). The SoC has decreased during discharge, making electrolyte density lighter and more hydrated and reducing SG. Table (5.2) contains the battery council international (BCI) values of starting batteries (BU-903. [no date]).

Table 5. 2: BCI of lead acid-battery

Approximate SoC	100%	75%	50%	25%	0%
OCV (V)	12.65	12.45	12.24	12.06	11.89
Average specific gravity	1.27	1.23	1.19	1.16	1.120

The Measurements have been taken at 26 °C after 24 hours of rest. Figure (5.12) shows **SoC** as a function of **OCV** with four segments; segment (A) represents over-discharging. In contrast, segment (D) has described the overcharging area where the battery was separated to protect it. The space between the other two layers was the certainty and health operation area. The **SoC** trends can be assessed as:

$$\mathrm{SoC\%} = 130.65\,(\mathrm{OCV}) - 1551.5 \tag{5.9}$$

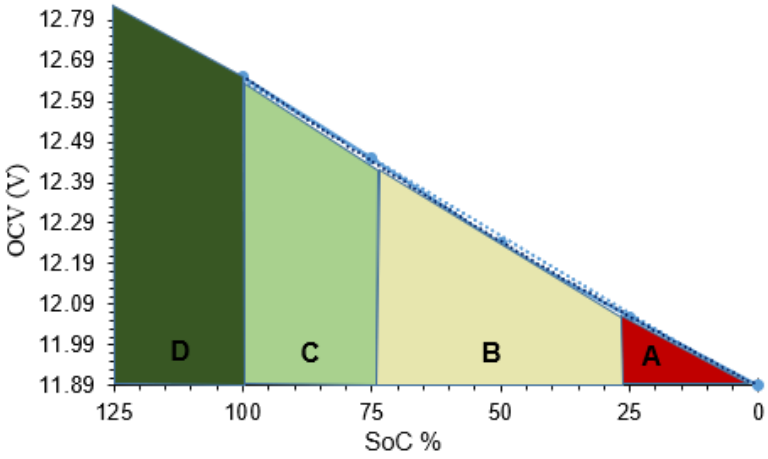

Figure 5. 12: BCI (OCV- SoC) segments of operation

5.2.2 Monitoring of the state of charge (SoC)

For SoC monitoring, the electric circuit-based models can be valuable to represent the electrical properties of cells as a state variable capable of providing accurate simulation results necessary for component selection; a simplified model was selected to serve and to monitor battery packs accurately. In the battery storage unit protection, RB must drive the battery to a high SoC; conversely, excessive acceleration drained the battery to a low SoC. The monitoring system utilised to sense the SoC of the cell and to adjust it when it was getting too close to the specified limit. Round trip energy (charged and released) efficiency would fluctuate mainly with the design and cell electrochemistry. It has been chosen between 25% to 75%; however, they quickly degrade for any overloaded or released cell. The technique used for the SoC prognostic must determine not only to what extent the battery will perpetuate, yet additionally how the vehicle's distance was covered. The

power discharge limit ensures that no additional power was extracted from the battery amid powerful acceleration while charging power constraints force the controller to actuate mechanical brake early to absorb the untapped power portion that cannot be used to charge the battery.

5.3 Ultracapacitors (UCs) ESS overview

Electrochemical capacitors were discovered in the 19th century. The storage of energy in a double-layer electric capacitor (DLEC), which determines the interface between a conductive solid and an electrolyte, has been known for more than a century, but not until 1957 that H.I. Becker of General Electric (GE) patented a primitive carbon device based on this phenomenon (Miller 2011; Rachel Carnegie et al. 2013). The UCs (designed by Robert A. Raymond, how was improved carbon-carbon electrochemical in 1962), was electrochemical capacitors that have a high energy density compared to conventional capacitors. Usually, the capacitor was developed with a dielectric set between restricted electrodes, working as capacitors by collecting charges in the dielectric material which can be then harnessed in an external circuit. The aggregate energy stored in this design was a blend of the number of charges stored and the terminal voltage between the plates. The former was a component of size and the material properties, while the dielectric breakdown between the plates constrains the latter. However, the UCs does not have any dielectrics in general but instead use the phenomena conventionally assessed as the electric double layer in which the adequate thickness of the dielectric is excessively thin, and as a result of the nature of the carbon, the surface area was to a significantly high degree, which means a high capacitance (Miller 2011; Singh 2015; Group [no date]). Figure (5.13) shows UCs construction during the different process.

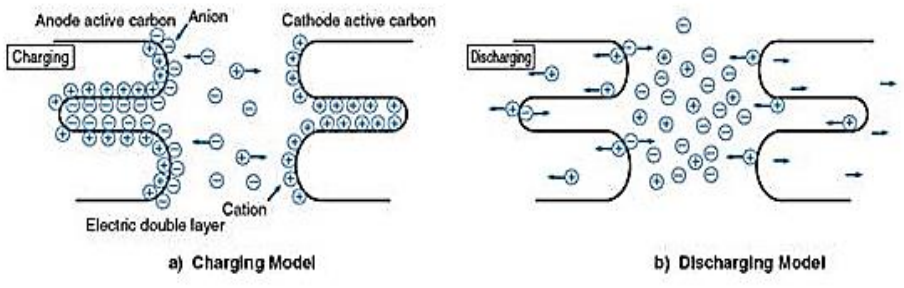

Figure 5. 13: UCs Charge Separation, (adapted from (Group [no date]))

5.3.1 Internal cell construction of the UCs

Although the UCs was a type of electrochemical device, no chemical reactions were involved in storing its electrical energy which means that the UCs effectively remains an electrostatic device that holds its electrical energy in the construction of an electric field between two conducting electrodes, as shown in Figure (5.14).

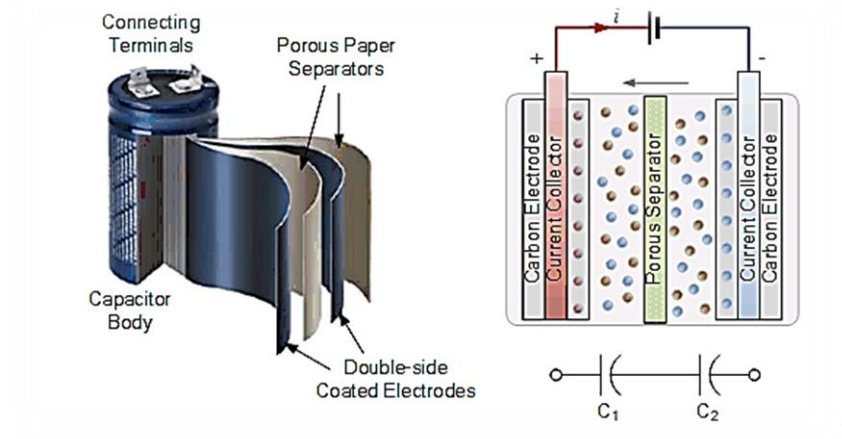

Figure 5. 14: UCs internal construction (adapted from (Ultra-capacitors. 2019))

The double-sided coated electrodes were being produced from graphite carbon as enacted conductive carbon, carbon nanotubes or carbon gels (Shan et al. 2015). A porous paper layer called a separator has kept the electrodes separated; however, it enables the positive ion to go through while hindering the more prominent electrons (Rachel Carnegie et al. 2013). Both the carbon electrodes and paper separator were being impregnated with the fluid electrolyte with an aluminium foil utilised in the middle of the two to act as the current collector making electrical connection with the UCs welded terminals.

To expand the capacitance C of the UCs, plainly by increasing the contact area (A) as $C = \varepsilon A/d$, where (ε) represents absolute permittivity of the dielectric material being used measured in F/m or utilise a different sort of electrolyte to broaden the available, positive ions to raise conductivity. The UCs has made great vitality storage devices because of their high capacitance value, due to the little separation (d) or partition of their plates and the electrodes high surface area to form on the surface of a layer of electrolytic ions form a double layer. This development productively has created two capacitors, one in every carbon terminal, giving the UCs arrangement of two capacitors in series. Indeed, the UCs are accessible with capacitance at a higher range, and it tends to be utilised as batteries. However, the UCs could be conveyed up to 10-20 times more power than batteries (Khaligh and Li 2010; Maher [no date]). For instance, because they were being capable of charging and discharging millions of times, so that, they need not be disposed of and repaired over life. Accordingly, this process has made them an exceedingly green type of energy storage.

Table 5. 3: Comparison of different storage units (adapted from (Maher [no date]))

Available performance	Lead Acid Battery	Ultra-capacitors (UCs)	Conventional Capacitor
Charge time	1 to 5 hrs	0.3 to 30 sec	10^{-3} to 10^{-6} sec
Discharge time	0.3 to 3 hrs	0.3 to 30 sec	10^{-3} to 10^{-6} sec
Energy (Wh/kg)	10 to 100	1 to 10	< 0.1
Cycle life	1000	> 500000	> 500000
Specific power (W/kg)	< 1000	< 10000	< 100000
Charge/ discharge efficiency	70% to 85%	85% to 98%	> 95%

From Table (5.3), the UCs cycle life was 500 times longer than the battery cycle life. The energy density (Wh/kg) of the battery was ten times greater than that of UCs. In contrast, the power density (W/kg) of UCs was higher than that of the battery with approximately at the same percentage. The most critical parameter was that the charging time of the UCs is faster than that of the battery, which has played a vital role in braking analysis, So, the UCs can be utilised not only to supply energy for acceleration but also to deliver RB power.

5.3.2 Internal cell connection

The UCs has been manufactured with their low terminal voltage characterises. However, to store charge at a sensible voltage, UCs must be connected in series to increase their nominal terminal voltage to a higher voltage, and the total system equivalent series resistance (ESR) has also relied upon the number of cells arranged in series (Zhao 2016). Besides, cells must be connected in parallel to accomplish higher capacitance values which reduce the ESR of the overall system in proportion to the number of parallel cells. In contrast, the leakage current for the series connection must be the same as the single-cell and has increased when cells connected in parallel (Saichand and John 2017). The total voltage $\mathrm{V_{tot}}$, total capacitance $\mathrm{C_{tot}}$, total equivalent series resistance $\mathrm{ESR_{tot}}$ and the leakage current (LC) of the UCs bank can be defined as:

$$\left.\begin{aligned} \mathrm{V_{tot}} &= \mathrm{V_{cell}\ x\ N} \\ \mathrm{ESR_{tot}} &= \mathrm{ESR_{cell}\ x\ \frac{N}{M}} \\ \mathrm{C_{tot}} &= \mathrm{C_{cell} x\ \frac{M}{N}} \\ \mathrm{LC_{tot}} &= \mathrm{LC_{cell}\ x\ M} \end{aligned}\right\} \quad (5.10)$$

Where: M is the number of UCs connected in parallel, and N is the number UCs connected in series, as shown in Figure (5.15).

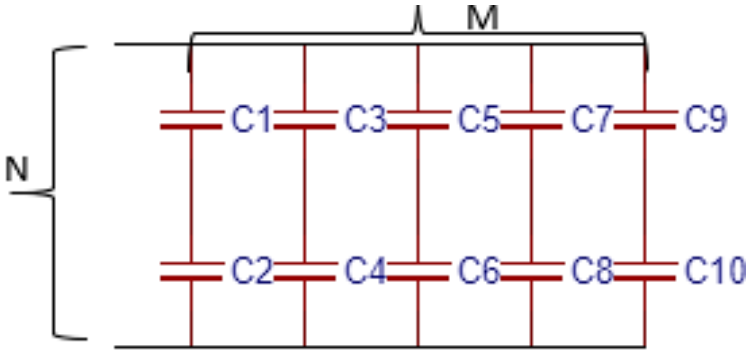

Figure 5. 15: NxM (3x5) UCs connection diagram

5.3.3 UCs application

In industrial applications, the UCs were used from a range of small to large-sized cells applied to hold up power for various electronic forms. Furthermore, it can be provided reliable tentative power, regardless of whether the primary source fluctuates or falls to operate. UCs has delivered maximum power to the load while drawing standard power from the primary source and with advantage to storing energy from low power sources, empowering support for high power loads. Furthermore, the UCs that passes charge and discharge cycles frequently in high current and short duration has been used to assist the battery and to store energy that has additionally made fundamental advances into electric power system (Karden et al. 2007; Sangdehi 2015). Similarly, this feature has been expanded to support renewable power generation due to a variable current generation to reduce the sudden surge peak absorption. The UCs application can be summarised, as shown in Figure (5.16) (Miller 2011).

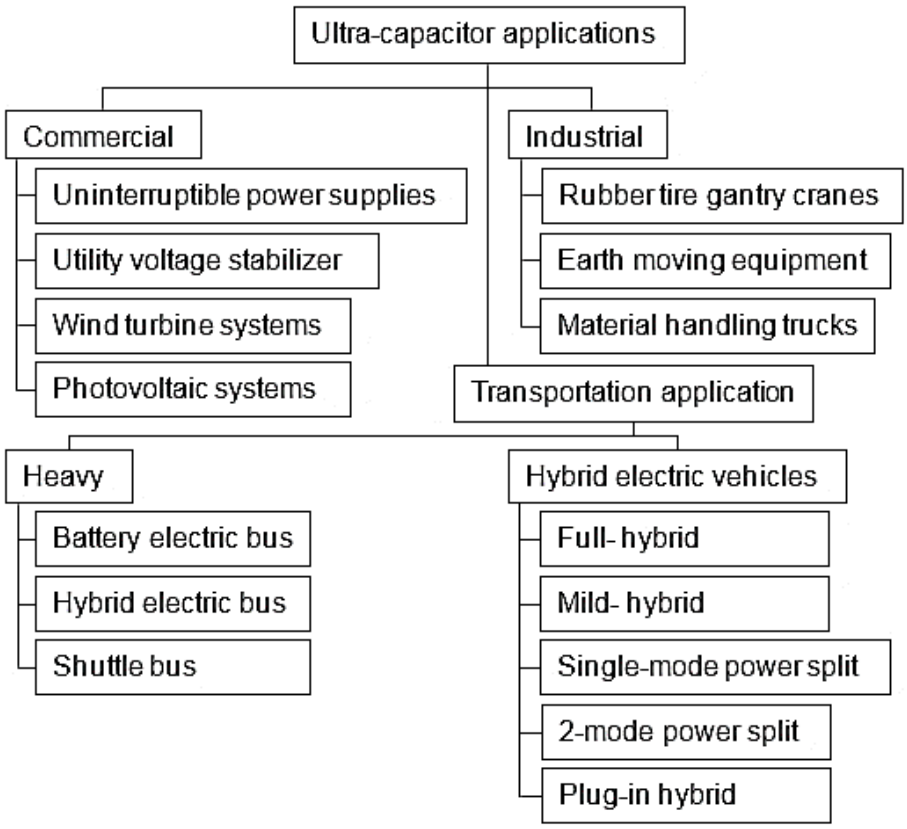

Figure 5. 16: UCs applications in different sectors

5.3.4 UCs modelling

Providing UCs circuit models for use in circuit analysis and simulation was an essential component of system design. This representation has been made, according to the level of behaviour, based on the experimental characterisation of the cells. This pattern has designed of three parts (Saichand and John 2017) as:

- Cell parasitic components,
- Electrode dynamic depiction of equivalent series resistance (ESR dc) and (ESR ac): which was contributed significantly to energy loss during the charging and discharging capacitor, and
- Fundamental branching, and parallel resistance EPR of UCs: These two parameters have been represented as leakage components of the model (which affects self-discharge). The self-discharge has occurred when the voltage in a charged cell decreases after a specified time without loading.

The mathematical modelling representation of UCs can be implemented in different approaches which can be represented as:

5.3.4.1 The electronic equivalent circuit model

The compatible circuit model should be capable of accurately capturing the time and frequency behaviours of the UCs. The model advancement has begun with the identification of parasitic components as:

- First-order equivalent circuit

Figure (5.17) shows an equivalent circuit of the UCs, which contains resistor, inductor and capacitor elements to define its properties (Yang et al. 2013). The slow charging procedure was used for measuring the equivalent parallel resistance (EPR) of the UCs until the UCs reaches its nominal voltage then allows a long time before measuring the voltage at the UCs terminals again. The EPR can be calculated as (Sharma and Bhatti 2010);

$$\mathrm{EPR} = -\mathrm{t}/((\ln(\mathrm{V}_2/\mathrm{V}_1)\,\mathrm{C}) \qquad (5.11)$$

Where t, is the measured time measured in a sec, V_1, and V_2, is the initial and final voltages measured in V, and C is the equivalent circuit capacitance of UCs. The time constant $(C \text{ x } EPR)$ is significant so that EPR can be neglected. Furthermore, the equivalent series resistance (ESR) can be measured from the change in voltage, ΔV, to the change in the current, ΔI, during the charging process as:

$$ESR = \Delta V/\Delta I \tag{5.12}$$

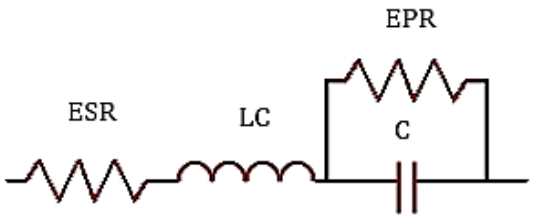

Figure 5. 17: First order equivalent circuit diagram

The capacitance C can be evaluated by a change in the stored charge process, which is given by (Spyker 2000);

$$C = \frac{\Delta Q}{\Delta V} = \frac{\int_{t_1}^{t_2} i(t)\, dt}{(V_2 - V_1)} \tag{5.13}$$

Where time t_1 , t_2, is the start and the end of the current flow, respectively.

Also, C can be determined by the energy change during the charging/discharging approach, which is given by:

$$\left.\begin{aligned} \Delta E &= \frac{1}{2} C \left(V_2{}^2 - V_1{}^2\right) = \int_{t_1}^{t_2} v(t)\, i(t)\, dt \\ C &= \frac{2 \int_{t_1}^{t_2} v(t)\, i(t)\, dt}{\left(V_2{}^2 - V_1{}^2\right)} \end{aligned}\right\} \tag{5.14}$$

5.3.4.2 The experimental equivalent circuit model

- **Introduction**

In the experiment, the UCs were charged at different scenarios to get the desired level of response in the practical implementation. At first, a constant current (CC), in which the voltage applied was varied to maintain an immutable current flowing used to charge the UCs. And then this voltage was cut-off when the voltage reaches its full charging level. Moreover, the UCs was charged at a constant terminal voltage (CV), (regulated DC power supply), to determine its behaviour at this state. In contrast, in studying the effect of variable voltage (VV) on charging the UCs, has been used to represent the RB strategies. The basic knowledge of fluid mechanics has been taken from the flow rate between two tanks connected at different voltage levels was utilised to simulate this response. The contribution of this chapter towards the objectives of this research was accomplished by focusing on a modification process with a new model proposed for charge transfer had been made. The representation of the generator and the UCs as two storage units with varying charging flow rate at various voltage levels have been considered.

However, in the proposed model, the variable pumping charge of the generated voltage (VV) when the DC motor works as a generator during braking and descending process have been investigated and implemented with experimental setups at a low power level in the designed test rig. Based on the results, conclusions have been given for the variable charging capability of the generator and the UCs charging response at different stages in the RB system UCs charging test.

- **Experimental setup**

Charging of the UCs regularly has incorporated some utilisation of consumption of energy by the charging supply. This energy was saved in the electrostatic field set up in the dielectric medium. On releasing the UCs, the field breakdown, and the stored energy were discharged. The energy (E)

measured in (J) consumed on charging the UCs having a capacitance C to a voltage V was given as:

$$E = \int_0^V CV dv = \frac{1}{2}CV^2 \quad (5.15)$$

Equation (5.15) represents the energy stored in the UCs.

Because the UCs, such as the lead-acid battery, can store the charge, it can theoretically be used as an electrical battery. It was possible to calculate the capacity of the lead-acid battery (12-volt, 10Ah), used in the test rig as:

$$Q = It = 10x3600 = 36000 \text{ A sec (columb)} \quad (5.16)$$

Where Q Indicates the charge enclosed, and the energy $= QV$ =36000x12 = 432000 J, indicates the energy stored in a battery. From equation (5.15) the capacitance of the cell, C was equal to $2E/V^2 = 2x432000/12\text{^}2$ = 6000 F, which was 92.3 more times than the UCs capacitance (65 F) used in the test bench.

A test was done to evaluate the performance of the UCs storage unit to determine its behaviour and to use data extracted from this analysis to initiate boundary conditions on designing and on the simulation process. In an experiment, "Eaton 16.2V 65 F" UCs storage unit was connected in series with "300 W 8500" PEL powered by a DC power supply, as shown in Figure (5.18).

(a) (b)

Figure 5. 18: Discharging UCs (a) photo (b) circuit diagram

The circuit also contains a DC-DC converter has utilised for voltage regulation. The PEL operates in various operation mode as a CC and CV, with voltage and current values, were evaluated and presented in real-time. In an experimental test, charging UCs was carried out with a CC, and a CV source

to assess its performance used to perform an accurate model for the UCs, as shown in Figure (5.19).

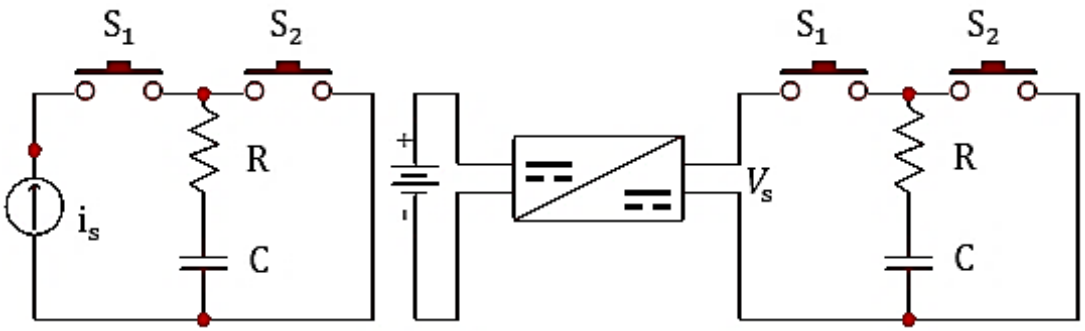

(a) Constant current (CC) (b) Constant voltage (CV)

Figure 5. 19: Charging and discharging UCs with different sources

❖ The UCs Charging with a CC source.

The circuit of Figure (5.19a), shows an arrangement when the UCs charged through resistance R from a CC (i_s= constant) source. The UCs voltage can be calculated at switches state as the switch closed at time =0, as:

- With S_1 closed and S_2 opened (charging process):

$$v_{UC(t)} = \frac{i_s}{C}\int_0^t dt = \frac{i_s}{C}t \qquad (5.17)$$

Therefore, the voltage across its terminal was a linear function and formed a ramp with a gradient equal to $\frac{i_s}{C}$, as shown in Figure (5.20):

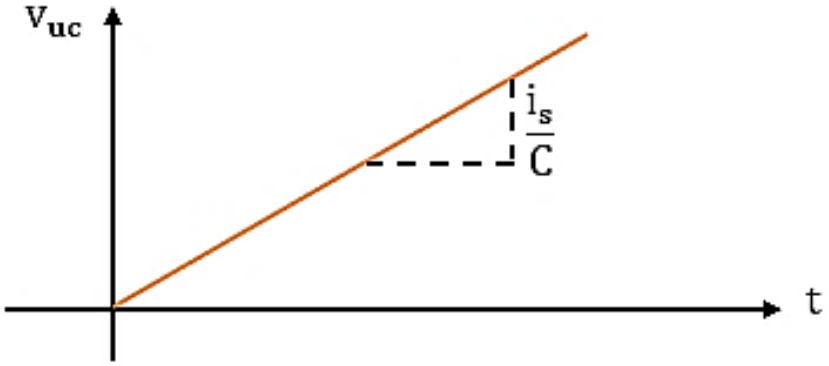

Figure 5. 20: UCs voltage at a CC source

- With $\mathbf{S_2}$ closed and $\mathbf{S_1}$ opened (discharging process):

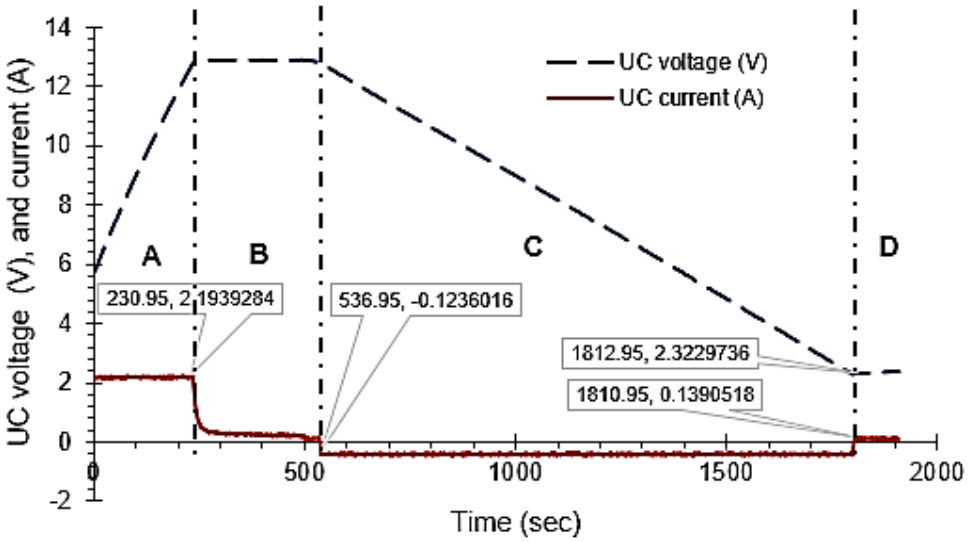

Figure 5. 21: UCs charging and discharging curve at CC mode

Figure (5.21) has demonstrated the voltage and current characteristics curve of the charging and releasing of the UCs ESS. In CC mode, the load has been sink a current as indicated by the programmed current value oblivious to the input voltage. The inclination of the charging process has differed from that of the discharging process because the sinking current in charging and discharging process was selected at 2A, and at 0.5A, respectively. Furthermore, the above figure has shown that on charging process (region A), the voltage was raised linearly during a CC charge, and then, the current was fallen as expected without the need of a full-charge detection circuit and merely stops flowing when the UCs was fully charged as in the region (B). On the other hand, on the discharging process (region C) (this carried out when the switch S_1 was opened, and the switch S_2 was closed in the circuit diagram), in the same way, the voltage was decayed linearly across the resistance R (represented by the PEL). However, the UCs discharging time was ended when the load requirements can no longer be met the prerequisites. The UCs voltage has approached to a minimum boundary constraint in the discharging process, released through the resistance R at a time (t), which has given the same behaviour as a linear ramp function with $(-i_s/C)$ gradient, with the current cut-off used with the intention of the over-discharging protection (region D).

Moreover, to preserve a steady wattage level as the voltage drops; a DC-DC boost converter could be connected across UCs output terminal to starts drawing increasingly current with falling voltage (this case not shown in the above figure).

- ❖ Nonlinear behaviour of the UCs

The UCs nonlinear case occurs where $q(t) = f(v_t)$, exhibits a capacitance that could be decreased as the voltage increased. At the same time, for some experiment, the UCs during the discharge process has shown the unusual relationship in its $q(v)$ behaviour in which the capacitance has increased nonlinearly with voltage due to the onset of pseudo-capacitance, as shown in Figure (5.22) (Miller 2011).

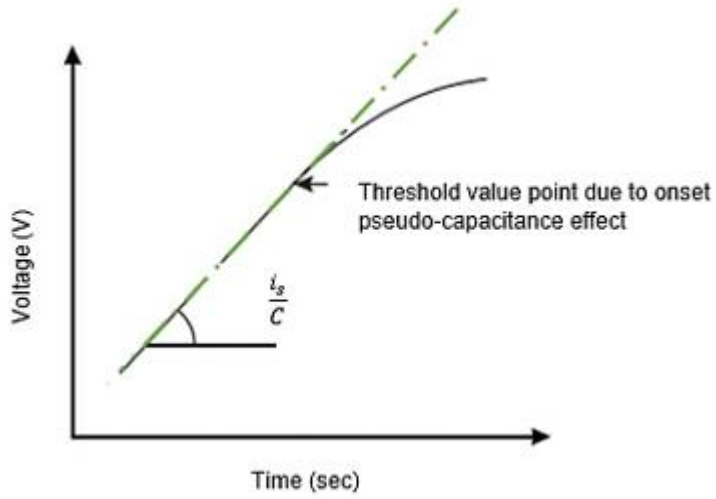

Figure 5. 22: UCs nonlinear charging process

The charging current becomes nonlinear due to the onset of pseudo-capacitance, which has the exponential terms represented by Tafel relation as:

$$I = C\,dv/dt + I_o e^{kv} \tag{5.18}$$

Where ($e^{kv} = 1 + kv + \cdots$), in which the dv/dt can be evaluated as:

$$dv/dt = (I - I_o)/C - kI_o v/C \tag{5.19}$$

The nonlinear behaviour of capacitance has occurred when an incremental voltage rise leads to the charge accumulated more than that in a linear dielectric capacitor (Conway 1999; Miller 2011).

Finally, it can be concluded that the charging characteristic of the UCs was the same as an electrochemical battery, and the handling capability restricts the charging current. The underlying charge can be made quickly, and the topping charge will take additional time. An arrangement must be prepared to restrain the inrush current while charging a fully discharged UCs as it will suck up everything it can. The UCs was not subject to overcharge and has not required full-charge detection; the current stops are merely flowing when it was full.

❖ Charging the UCs with a CV source

The time-varying currents and voltages were resulting from the sudden application of sources, usually due to switching. In the RC circuit, this had happened when the capacitor charged or discharged through resistance at a time t. The circuit of Figure (5.19b) had shown when the UCs charged with a CV source. The constant voltage was achieved by using a DC-DC voltage regulator. As the switch closed at time =0, the UCs voltage can be calculated at switches state as:

- Charging process: With S_1 closed and S_2 opened; The RC series circuit switched ON to a CV source of voltage V_s at t =0, results into a voltage across the UCs, $v_{UC(t)}$, was builds up exponentially. The current $i_{UC(t)}$ was maximum at the starting time then decreases dramatically and finally stops when the potential difference across UCs terminal was equal to and counter to supplied voltage V_s . With initial conditions at the beginning of the charging process at t = 0, $v_{UC(t)} = 0$ is given by:

$$\left.\begin{aligned} v_{UC(t)} &= V_s\left(1 - e^{-t/\tau}\right) \\ i_{UC(t)/char} &= (V_s/R)(e^{-t/\tau}) \end{aligned}\right\} \quad (5.20)$$

Where $\tau = RC$, is a time constant (sec), is defined as the time constant of the circuit, as the time when the UCs voltage reached the maximum value of V_s if they maintained at the initial rate of ascending.

Under steady-state conditions, the circuit has shown as a capacitor with open-circuit, and the voltage across R was significantly reduced exponentially from the initial maximum value (V_s) to zero, as indicated in the relationship:

$$v_R = V_s\, e^{-t/\tau} \tag{5.21}$$

The simulation result of the current and the voltage time-changes across the UCs is shown in Figure (5.23):

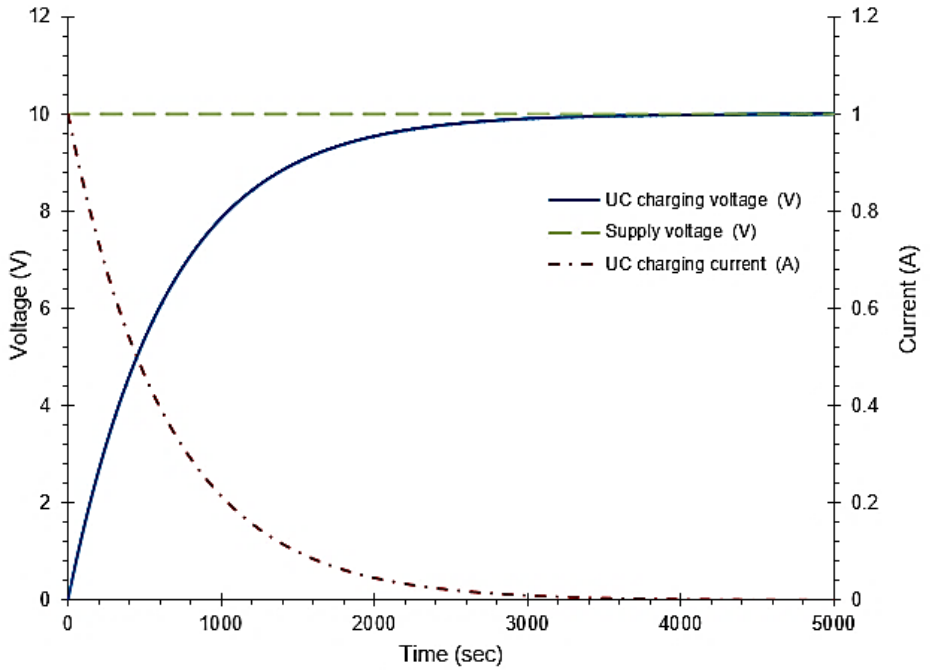

Figure 5. 23: Voltage and current CV of the UCs charging characteristic curve

From Figure (5.23), the UCs current $i_{UC(t)/char}$ was maximum at the beginning because the voltage across its terminal is zero, so that, no counteract to the applied electrical voltage. The time constant (τ) can be varying as:

a) When the $v_{UC(t)}$, at the starting of the charging activity was zero; the initial rate of UCs voltage increased $dv_{UC(t)}/dt$ measured in V/sec can be determined as follows:

$$\left[\frac{dv_{UC(t)}}{dt}\right]_{t=0} = \frac{V_s}{RC} = \frac{V_s}{\tau} \tag{5.22}$$

And the initial change of v_R and $i_{UC(t)/char}$ are given by:

$$\left.\begin{aligned}\left[\frac{d_{v_R}}{dt}\right]_{t=0} &= -\frac{V}{\tau}\\ \left[\frac{d\, i_{UC(t)/char}}{dt}\right]_{t=0} &= \frac{I_o}{\tau},\quad I_o = \frac{V_s}{R}\end{aligned}\right\} \tag{5.23}$$

While the rate of change during the charging transient at any time are as follows:

$$\left[\frac{d\, v_{UC(t)}}{dt}\right]_{t=0} = \frac{V_s}{\tau} e^{-t/\tau}$$

$$\left[\frac{d_{v_R}}{dt}\right]_{t=0} = -\frac{V}{\tau} e^{-t/\tau}$$

$$\left[\frac{d\, i_{UC(t)/char}}{dt}\right]_{t=0} = -\frac{I_o}{\tau} e^{-t/\tau} \qquad (5.24)$$

When the switch S_1, was closed (S_2 was opened); the current flows through R, and hence, transient voltages in the R and C were developed until they reach their final steady values. The period in which current and voltage changes occur was the transition state. Any R and C circuit starting from a fixed initial state has been passed through a transient state in a short period when it goes into its final state.

b) By replacement of the time t in equation (5.20) with the time constant τ, it becomes:

$$v_{UC(t)} = V_s\left(1 - e^{-\tau/\tau}\right) = V_s(1 - e^{-1}) = 0.632V_s$$

$$i_{UC(t)/char} = \frac{V_s}{R}\left(e^{-\frac{\tau}{\tau}}\right) = 0.368\frac{V_s}{R} \qquad (5.25)$$

Thus, when the 65 F UCs was connected in series with a 10-Ω resistor the time constant can be defined as the time when the voltage raised to 0.632 from its final steady value or the time when the charging current dropped to 0.368 of its initial maximum value in the transient region.

Table (5.4), represents the charging voltage and current at different time constant (τ) (RC =10x65= 650 (sec)):

Table 5. 4: RC charging time constant table

The time constant (RC) (τ) (sec)	Percentage of maximum	
	Voltage (V)	Current (A)
0.5 RC = 325	39.34%	60.70%
0.7 RC = 455	50.34%	49.70%
1RC = 650	63.21%	36.80%
2RC = 1300	86.47%	13.50%
3RC = 1950	95.02%	5%
4RC = 2600	98.17%	1.80%
5RC = 3250	99.33%	0.70%

Figure (5.24) shows the transient and study state periods in different regions (in charging and discharging process).

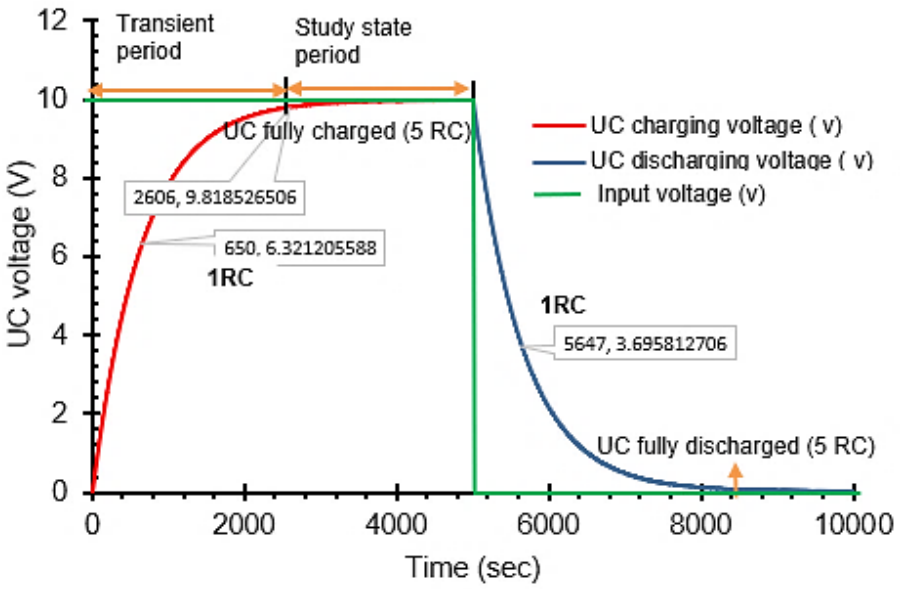

Figure 5. 24: Simulation of UCs at charging and discharging states

The energy dissipating as heat at time Δt is given as; $\Delta w_R = i^2 R \Delta t$

$$w_R = R\int_0^{\infty} i^2\,dt = \frac{E^2}{R}\int_0^{\infty} (e^{-t/\tau})^2 dt = \frac{1}{2}CV^2 \qquad (5.26)$$

Equation (5.26) illustrates energy stored on the UCs at the end of the charging process, which was the same as energy as in equation (5.15). The trends of energy stored in the 65 F UCs can be represented as:

$$E = 32.5\, v_{UC(t)}{}^2 \qquad (5.27)$$

- Discharging process: With S_1 opened and S_2 closed; the RC series circuit switched ON with the short circuit at t =0, results into that the UCs discharged through the resistance R. The discharging current was circulated in the direction opposite to that of the charging current. The voltage across the UCs $v_{UC(t)}$ has been decayed exponentially to zero, and it was equal to 36.8% of initial value at one-time constant (τ). The current $i_{UC(t)}$, was maximum at the starting time, but in the negative direction, then descent dramatically and finally stopped when the potential difference across UCs terminal was equal to zero (until it ceased when the UCs was fully discharged). With initial conditions at the beginning of the discharging process at t = 0, $v_{UC(t)} = V_s$ is given by:

$$\left.\begin{aligned} v_{UC(t)} &= V_s\,(e^{-t/\tau}) \\ i_{UC(t)/disch} &= -V_s/R\left(e^{-t/\tau}\right) \end{aligned}\right\} \quad (5.28)$$

The voltage across R was significantly reduced exponentially in the opposite direction from the initial maximum negative value $(-V_s)$ to zero, as indicated in the relationship:

$$v_R = -V_s e^{-t/\tau} \quad (5.29)$$

When the switch S_2, was closed (S_1, was opened), the UCs undergoes to the discharging cycle. Before the starting of the transient state, the UCs current and resistance voltage was equal to zero, while the UCs voltage was at its maximum steady state. After that, when the transient was at the beginning, the current has flown through R, and hence, transient voltages in the R and UCs current have maximum values and decreases exponentially to zero at the end of the transient periods. However, all rates of change in the discharging process, have opposite polarity to that during the charging process. The different rates of change during the discharge transients at any time has been specified as:

$$\left.\begin{aligned} \frac{d\,v_{UC(t)}}{dt} &= -\frac{V_s}{\tau}e^{-t/\tau}, \text{and } \frac{d_{v_R}}{dt} = \frac{V}{\tau}e^{-t/\tau} \\ \frac{di_{UC(t)/disch}}{dt} &= \frac{I_o}{\tau}e^{-t/\tau} \end{aligned}\right\} \quad (5.30)$$

Figure (5.25) shows the simulation result of the current and the voltage across the UCs.

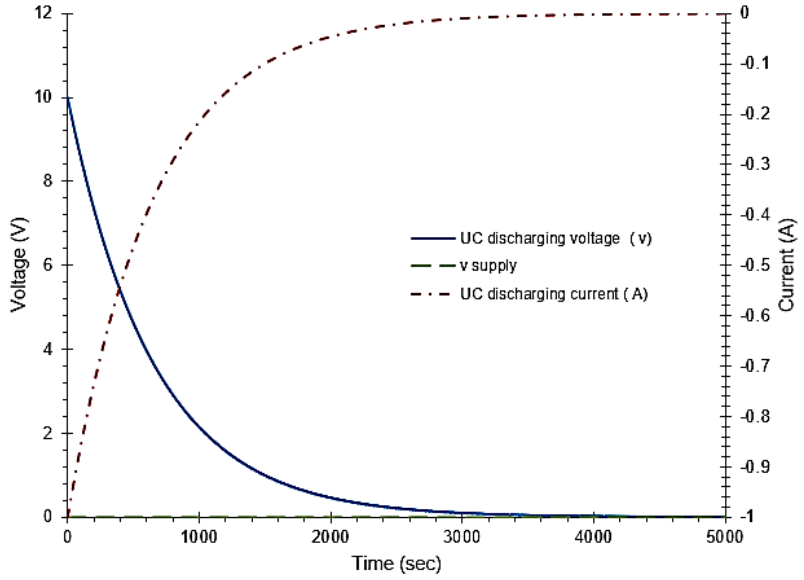

Figure 5. 25: Voltage and current of the UCs discharging characteristic curve

Table (5.5) shows all the possible values for the different timing approach for the voltage and the current calculations in the discharging process.

Table 5. 5: RC discharging time constant table

The time constant (RC) (τ) (sec)	Percentage of maximum	
	Voltage (V)	Current (A)
$0.5\ RC = 325$	60.70%	39.35%
$0.7\ RC = 455$	49.70%	50.34%
$1RC = 650$	36.80%	63.21%
$2RC = 1300$	13.50%	86.47%
$3RC = 1950$	5%	95.02%
$4RC = 2600$	1.80%	98.17%
$5RC = 3250$	0.70%	99.33%

- Charging and discharging of the UCs with an initial voltage state

If UCs has an initial charge stored ($V_{UC/ini}$) less than V_s and opposed it, as in the simulation shown in Figure (5.26), then the initial rate of ascending of V_{UC} was slightly lower than that when the UCs was uncharged initially.

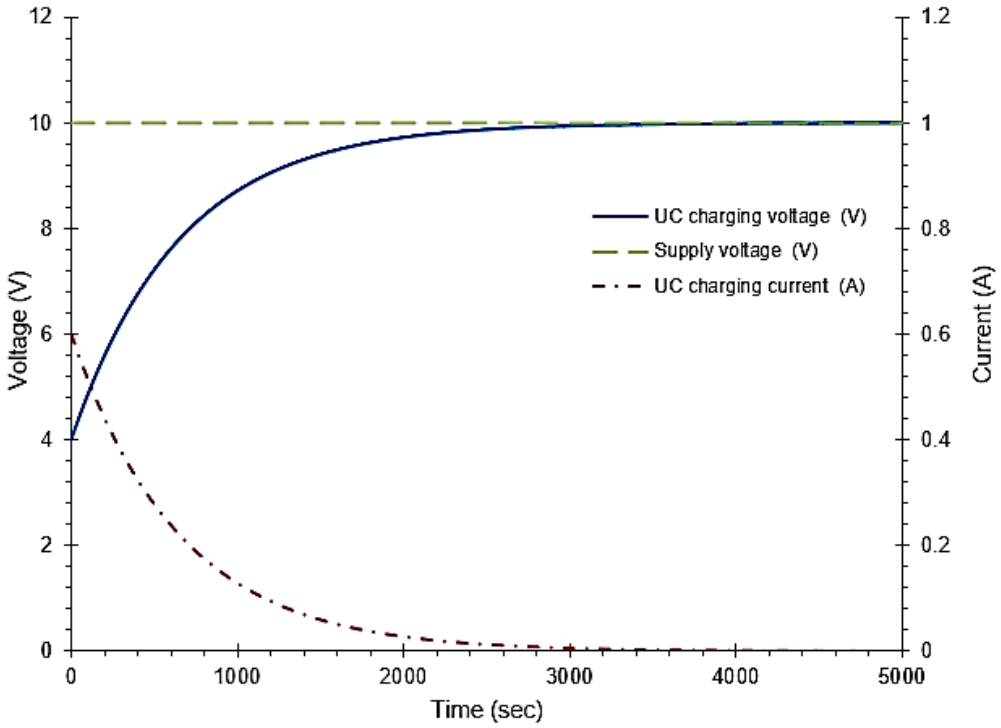

Figure 5. 26: Voltage and current of the UCs (UCs initial voltage =4v)

Since the UCs voltage has increased in a single time constant from an initial value of (V_{UC-ini}) to the final value of V_s, its initial increment rate is given by:

$$\left[\frac{d\, v_{UC(t)}}{dt}\right]_{t=0} = \frac{V_s - V_{UC/ini}}{RC} = \frac{V_s - V_{UC/ini}}{\tau} \tag{5.31}$$

During the charging cycle, the UCs voltage at any given time is specified as:

$$v_{UC(t)} = (V_s - V_{UC/ini})(1 - e^{-\frac{t}{\tau}}) + V_{UC/ini} \tag{5.32}$$

From equation (5.32) the required time for the UCs voltage, during the charging cycle, to get any value of $v_{UC(t)}$ is calculated as:

$$t = \tau \ln\left[\frac{V_s - V_{UC/ini}}{V_s - V_{UC}}\right] \tag{5.33}$$

❖ Remarks in the UCs I/ V relationships

The exchange rate for a stored charge on the UCs can be represented as:

$$i(t) = \frac{dQ}{dt} = C\frac{dV}{dt}, \text{ since } Q = CV \tag{5.34}$$

The basic facts can be inferred from equation (5.34):

1) Since $Q = CV$, this implies the voltage at the UCs was corresponding to charge not on current.
2) The UCs can store charge, and it can deliver energy.
3) The UCs could have voltage on its terminal even if the current was not flowing.
4) From $i(t)$, it tends to be seen that the current in the UCs exists just when the voltage on it changes over time. If $\frac{d\,v_{UC(t)}}{dt} = 0$, (at a steady voltage or constant voltage), then the current $i_{UC(t)} = 0$; thus, the UCs was acting as an open circuit.
5) From $i(t)$, the change in the applied voltage, $\frac{d\,v_{UC(t)}}{dt} = \frac{i_{UC(t)}}{C}$ for a given amount of (charging/discharging) current $i(t)$, the voltage change rate was contrarily corresponding to the capacitance C. Expanding the capacitance of the UCs prompt a slower pace of capacitive voltage change, which cannot be changed promptly.
6) The principle of superposition was applied to find UCs voltage when it charged at different time intervals.
7) In transient case, the UCs acts like a short circuit, while in the steady-state conditions, it acts as an open circuit.
8) The data has extracted from this analysis with the voltage and current relationship of the charging and releasing of the UCs ESS in CC mode, and in CV mode has been used to initiate boundary conditions on simulation and on designing of the UCs for full-charge detection and over-discharge protection when has been used in energy recovery and energy management system (EMS).
9) Although, from Figure (5.26), the effect of resistance (R) was on system behaviour and stopping time response. In EVs and HEVs, for example,

the impact of varying pedal pressure on braking can be represented as a variable resistance. Hence, the expended time for the engine to stop was depended on R-value (neglecting the ESR of the UCs) as compared with braking resistance. The simulation of the effect of resistance on charging/discharging time is as shown in Figure (5.27).

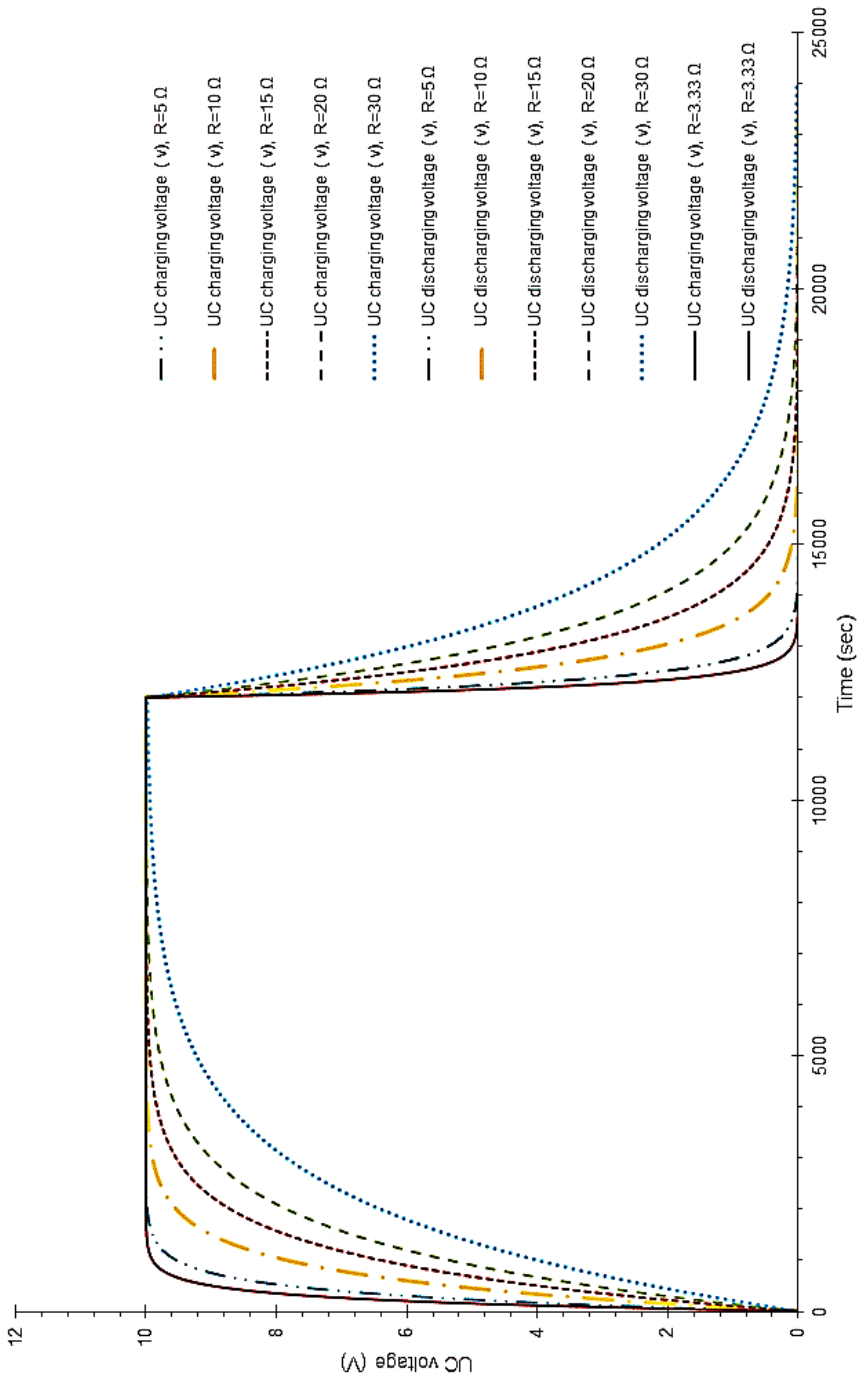

Figure 5. 27: Effect of braking resistance on charging/discharging time

5.4 Practical application of the UCs in the RB system

According to works of literature, in a vehicular point of view considering available computer software packages, different software used to simulate the ESS and the powertrain like “SIMPLORER” and “ADVISOR” software (Melnyk and Trokhanyak 2004; Lee 2005; Gao et al. 2007; Moselle et al. 2010; Zhang et al. 2018). Among them, it has been used limited data and has not integrated all the features of ESS. So, modelling UCs might be considered as an electric circuit as discussed in section (5.3.4.1) (Shi and Crow 2008; He et al. 2010). The propulsion engine such as PMBLDC motor can be represented using differential equations for all three-phase voltages (Khaligh and Onar 2010; Krishnan 2010). In comparison, this section has accomplished with a case study of an experimental investigation to get the advantage of an accurate representation of system behaviour of the UCs ESS. Starting from designing circuit and system representation as a ready-made (black box) models and the lumped component, including the PMBLDC motor connected with a hollow cylinder flywheel, have been determined in the characteristics and dynamics equations to represent overall system performance.

5.4.1 Charging UCs with variable voltage (VV) source

The VV has resulted from the sudden application of supply sources, usually, due to switching. On the other hand, the braking of EVs and HEVs has driven by electric motors in regenerative braking (RB) was achieved when the motor was temporarily working as a generator converting mechanical energy to electrical energy. Pumping charge by the generator to the UCs at braking, due to the voltage difference, neither as in a regulated constant voltage source nor as in a steady current source and even it cannot be represented simply like discharging of a capacitor to another one. In the experimental test, the UCs has been shown a variety of behaviours, the response which has given a spotlight of this research to measure and to handle the effect of the generated voltage and the response of the UCs storage unit. Hence, the time-varying generating voltage (VV) has been actualised by using the “BL58EE70W” PMBLDC motor connected with the designed flywheel on the test rig.

5.4.1.1 The proposed model

In this section, experiments were performed and verified by simulation, considering the variable characteristic of the voltage generated from braking utilised to charge the UCs in ESS. The newly proposed mechanism for the RB system evaluation considering that two interacting tanks placed in series with the interconnection streamflow rate q, as shown in Figure (5.28). So, the exit flow from the large tank, having a height h_2 and a cross-sectional area A_2, represents the generator (lumped with a connected flywheel) with a terminal voltage V_2 and a capacity C_2, in the equivalent electric circuit, respectively. Also, the flow into the small tank, having a height h_1 and a cross-sectional area A_1, represents the UCs with a terminal voltage V_1 and a capacity C_1, respectively. The flow rate q between the two tanks and the flow input q_i represents the current i and i_i, in the equivalent electric circuit, respectively. While q_g, and q_C describes the leakage flow of the of tank$_2$ and tank$_1$ flow as i_g and i_c respectively. Also, R, R_C and R_g represents the valve resistance which represents braking, generator, and UCs resistance, respectively, as shown in Figure (5.28):

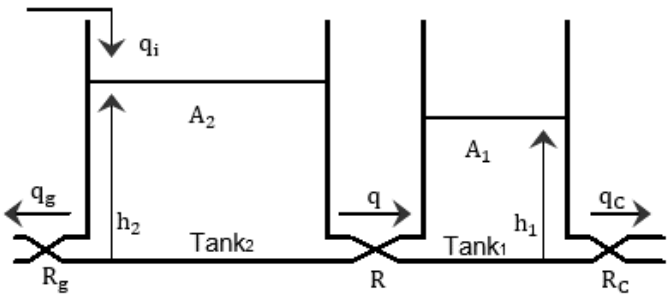

Figure 5. 28: Schematic of two tanks in series whose liquid level interact

The proposed equivalent circuit diagram for the two tanks system can be represented as an electrical component, as in Figure (5.29):

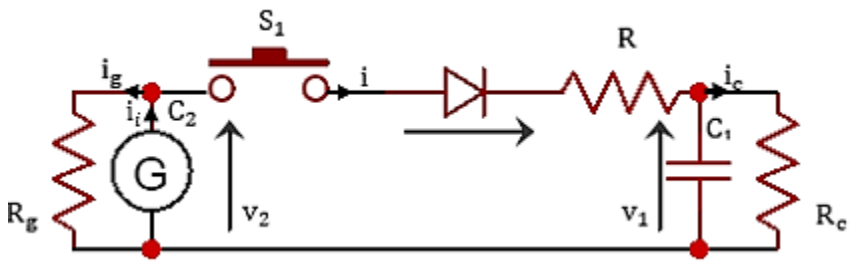

Figure 5. 29: Equivalent electrical circuit of two storage tanks system

At the time when the height of both tanks was at the same level, q valve was closed. Where q_g and q_C has exemplified the generator i_g and the UCs leakage current i_c in the equivalent circuit diagram, in such a way that the generator output voltage diminished at the stopping period due to friction resistance R_g. And the UCs voltage reduced due to internal discharge resistance R_C.

From Figure (5.28), different scenarios have been implemented as:

a) In a typical operation, when the valve between the two tanks was closed ($R \sim \infty$), and there was no flow between the two tanks ($q = 0$). In which it was equivalent to open switch in the electric circuit, and the lumped components (generator connected with the flywheel) represents the motoring operation.

For tank$_2$: the amount of accumulated fluid in the tank can be formulated as:

$$A_2 \frac{dh_2}{dt} = q_i - q_g \tag{5.35}$$

And,

$$q_g = \frac{h_2}{R_g} \tag{5.36}$$

Substitution of equation (5.36) in equation (5.35) and simplifying yields:

$$A_2 R_g \frac{dh_2}{dt} = R_g q_i - h_2 \tag{5.37}$$

By taking the derivative and Laplace transform of equations (5.36, 5.37) gives:

$$\left.\begin{aligned} &Q_g(s) = \frac{1}{R_g} H_2(s) \\ &A_2 R_g \, s H_2(s) + H_2(s) = R_g Q_i(s) \\ &\frac{H_2(s)}{Q_i(s)} = \frac{R_g}{A_2 R_g s + 1} \\ &\frac{Q_g(s)}{Q_i(s)} = \frac{1}{A_2 R_g s + 1} = \frac{1}{\tau_2 s + 1}, \; \tau_2 = A_2 R_g \end{aligned}\right\} \tag{5.38}$$

By replacing the variable of the two tanks from equation (5.38) with its equivalent circuit variable, the following equations can be taken as:

$$
\begin{aligned}
&I_g(s) = \frac{1}{R_g} V_2(s) \\
&C_2 R_g \, s V_2(s) + V_2(s) = R_g I_i(s) \\
&\frac{V_2(s)}{I_i(s)} = \frac{R_g}{C_2 R_g s + 1} = \frac{R_g}{\tau_{2e} s + 1}, \tau_{2e} = C_2 R_g \\
&\frac{I_g(s)}{I_i(s)} = \frac{1}{C_2 R_g s + 1} = \frac{1}{\tau_{2e} s + 1}
\end{aligned}
\qquad (5.39)
$$

Equation (5.39) represents the voltage generated by the generator as a function of the motor input current.

The following analysis was performed in the system under study shown in figure (5.29), which was used to verify the validity of the above procedure, which can be represented as a circuit diagram as shown in figure (5.30), as:

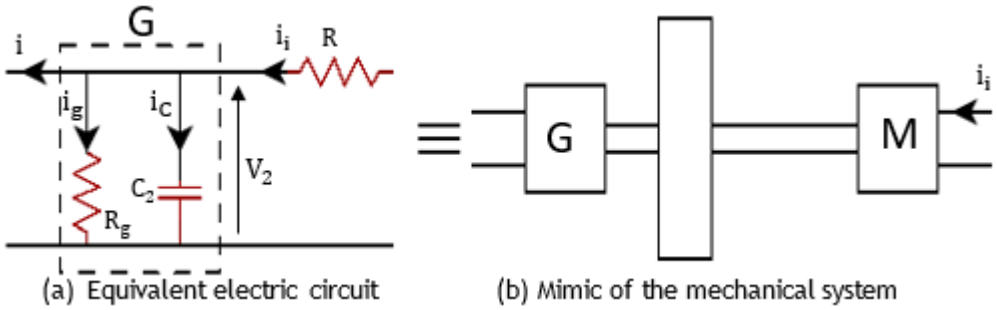

Figure 5. 30: Simplified equivalent electrical circuit

Where i_i represents the motor input current, i_C charging the generator $(V_2(0) = 0)$ assumed as a capacitor with parallel resistance to represent the leakage current. Applying KCL, the following equations can be given as:

$$
\begin{aligned}
&i_i = i_g + i_C \\
&i_i = \frac{V_2}{R_g} + C_2 \frac{dV_2}{dt} \\
&i_i R_g = V_2 + R_g \, C_2 \frac{dV_2}{dt} \\
&R_g I_i(s) = V_2(s) + C_2 R_g \, s V_2(s)
\end{aligned}
\qquad (5.39a)
$$

By comparison, equation (5.39a) was the same as equation (5.39) derived from two tanks of analysis, which verify the proposed study.

b) When the valve of tank$_1$ was closed ($R_C \sim \infty$), $q_C = 0$. The differential equation when the valve inadvertently opened ($0 < R < \infty$) and when $h_1 > h_2$, is given as:

$$\left.\begin{aligned} A_1 \frac{dh_1}{dt} &= -q \\ q &= \frac{h_1 - h_2}{R} \\ A_2 \frac{dh_2}{dt} &= q_i + q - q_g \end{aligned}\right\} \quad (5.40)$$

This condition was not considered when the RB process was executed. If the voltage of the UCs was higher than the generated voltage, then its voltage was transferred through a booster instead of supplying energy to the motor directly, to achieve the objectives of maximum conserved energy. In the electrical circuit, the existence of the diode, which in this case was in the reverse biasing operation, functions as an open circuit has prevented the current from passing through.

c) When the valve of tank$_2$ was closed ($R_g \sim \infty$), $q_g = 0$ and the valve between the two tanks were partially open ($0 < R < \infty$) with $h_2 > h_1$.

The equation for flow from tank$_2$ to tank$_1$ to reflect that physical feature of generating electricity from the generator rotates at a constant speed, and the UCs has a leakage current, which can be given as:

For tank$_1$: the amount of accumulated fluid in the tank can be formulated as:

$$A_1 \frac{dh_1}{dt} = q - q_C \quad (5.41)$$

Assuming linear resistance to flow, the rate of change of fluid transfer q and q_c can be calculated as:

$$\left.\begin{aligned} q &= \frac{h_2 - h_1}{R} \\ q_C &= \frac{h_1}{R_C} \end{aligned}\right\} \quad (5.42)$$

Substitution of equation (5.42) in the equation (5.41) yields:

$$A_1 \frac{dh_1}{dt} = \frac{1}{R}(h_2 - h_1) - \frac{h_1}{R_C} \quad (5.43)$$

From which the height h_2 can be calculated:

$$h_2 = RA_1 \frac{dh_1}{dt} + \frac{Rh_1}{R_C} + h_1 \tag{5.44}$$

By taking the derivative of the equation (5.44) which gives:

$$\frac{dh_2}{dt} = RA_1 \frac{d^2h_1}{dt^2} + \left(\frac{R}{R_C} + 1\right) \frac{dh_1}{dt} \tag{5.45}$$

For tank2: the amount of fluid charged from the tank can be formulated as:

$$A_2 \frac{dh_2}{dt} = q_i - q \tag{5.46}$$

Substitution of equation (5.45) in equation (5.46) and rearranged as:

$$A_2 RA_1 \frac{d^2h_1}{dt^2} + \left(\frac{R}{R_C} + 1\right) \frac{dh_1}{dt} + \frac{h_1}{R_C} = q_i \tag{5.47}$$

So, by taking the Laplace transform of equations (5.44, 5.47), the level transfer function can be implemented as:

$$\left.\begin{aligned} &\frac{H_1(s)}{H_2(s)} = \frac{R_C/R}{\tau_1 s + (R_C/R + 1)} \\ &\tau_1 = R_C A_1, \tau_3 = RA_2 \\ &\frac{H_1(s)}{Q_i(s)} = \frac{R_C}{\tau_1 \tau_3 s^2 + \tau_3(2 + R_C/R)s + (1 + R_C/R)} \end{aligned}\right\} \tag{5.48}$$

By replacing the variable of the two tanks from equation (5.48) with its equivalent circuit variable, the following equations can be taken as:

$$\left.\begin{aligned} &\frac{V_1(s)}{V_2(s)} = \frac{R_C/R}{\tau_{1e} s + (R_C/R + 1)} \\ &\tau_{1e} = R_C C_1, \tau_{3e} = RC_2 \\ &\frac{V_1(s)}{I_i(s)} = \frac{R_C}{\tau_{1e}\tau_{3e} s^2 + \tau_{3e}(2 + R_C/R)s + (1 + R_C/R)} \end{aligned}\right\} \tag{5.49}$$

Equation (5.49) gives an indication of the UC charging voltage with respect to the induced voltage and motor input current, respectively.

d) Assuming the flow input $q_i = 0$, and there was no leakage at tank$_2$ ($R_g \sim \infty$) $q_g = 0$ and tank$_1$ ($R_C \sim \infty$) $q_C = 0$. Also, the valve between the two tanks was partially open ($0 < R < \infty$) with $h_2 > h_1$.

The equation of flow from tank$_2$ to tank$_1$ can be driven to reflect that physical feature of generating electricity at braking when the same motor works as a generator. The amount of the accumulated fluid at tank$_1$ and the amount of charged fluid from tank$_2$ can be formulated as:

$$\left.\begin{aligned} A_1 \frac{dh_1}{dt} &= q \\ A_2 \frac{dh_2}{dt} &= -q \end{aligned}\right\} \quad (5.50)$$

Rearrange equation (5.50) which gives:

$$\left.\begin{aligned} A_1 \frac{dh_1}{dt} &= -A_2 \frac{dh_2}{dt} \\ \text{So,} & \\ \frac{dh_1}{dh_2} &= -\frac{A_2}{A_1} \end{aligned}\right\} \quad (5.51)$$

So, by taking the Laplace transform of equations (5.51), the level transfer function can be implemented as:

$$\frac{H_1(s)}{H_2(s)} = -\frac{C_2}{C_1} \quad (5.51a)$$

The equivalent electric circuit, as shown in Figure (5.29) with this case, can be simplified, as shown in Figure (5.31):

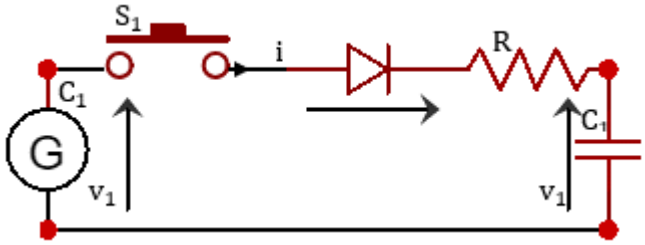

Figure 5. 31: The VV simplified electrical circuit

Figure (5.31) represents the charging UCs with variable voltage (VV) generated by the motor when it was working as a generator in the braking system. Where the charge flow per unit time t (i) represents the current $i_{uc(t)}$, passing from

the generator to the UCs storage unit in the charging process. The diode has been used to ensure that one direction current flow.

By replacing the variable of the two tanks from equation (5.51) with its equivalent circuit variable, the following equations can be taken as:

$$\left.\begin{aligned} C_1 \frac{dv_1}{dt} = -C_2 \frac{dv_2}{dt} = i_{uc(t)} = \frac{dQ}{dt} = q \\ \frac{dV_1}{dV_2} = -\frac{C_2}{C_1} \end{aligned}\right\} \quad (5.52)$$

Equation (5.52) can be rearranged to calculate the unknown generator capacitance C_2 as:

$$C_2 = -C_1 \frac{dv_1}{dv_2} \quad (5.53)$$

It cleared from equation (5.53) that the internal resistance of the generator and the UCs have not considered, and it can be added with the effect of the braking resistance. At any given speed, the voltage recovered by the UCs storage unit (initially at zero energy for precise measurement) to the maximum generated voltage by the generator at the instant of switching (represent the maximum induced voltage) multiplied by UCs capacitance C_1, which was known, represents the generator capacitance C_2. So, equation (5.53) can be simplified as $C_2 = -KC_1$. Where K can be evaluated from the experimental measurement, which can be described as:

$$K = \frac{dv_1}{dv_2} \quad (5.54)$$

So that K can be implemented as a maximum stored voltage in the UCs initially fully discharged to the maximum back electromotive force (emf) (E_{back}) generated from the PMBLDC motor at the braking process. Table (5.6) represents the experimental investigation to define the generator capacitance according to equation (5.53), with 65 F UCs load.

Table 5. 6: Experimental data extraction for generator capacitance calculation

Speed (rpm)	dv_2 generator (V)	dv_1 UCs(V)	K	C_2 generator (F)
1000	- 4.098	0.308	- 0.075	4.885
1500	- 6.698	0.518	- 0.077	5.027
2000	- 9.398	0.781	- 0.083	5.401
2500	- 12.198	1.044	- 0.085	5.563
3000	- 15.098	1.307	- 0.086	5.627

The change in the generator capacitance C_2 at a lower generated voltage (back emf) corresponding to the different speed of operation, because of internal friction of all moving component, have been constructed the test platform. Then, to precisely determine C_2, a recommended test must be evaluated at the nominal speed to get maximum induced voltage with the minimum effect of friction force. Figure (5.32) shows the variation of the generator capacitance measured from equation (5.53).

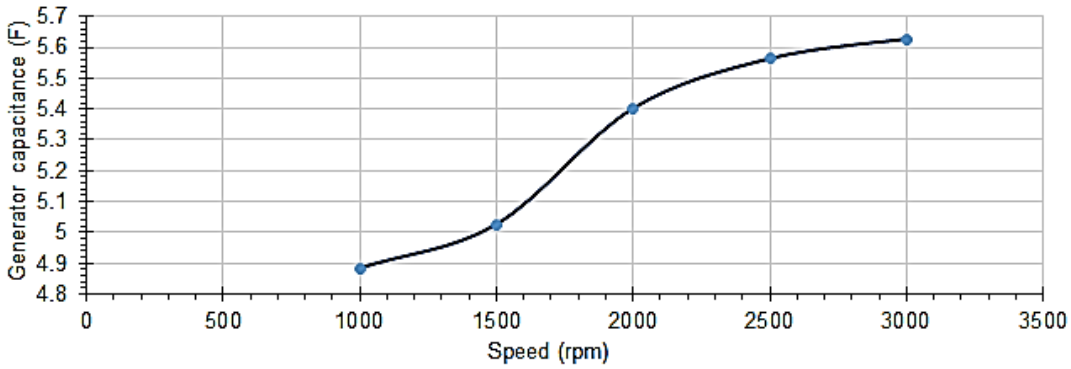

Figure 5. 32: Proposed measurement of the generator capacitance

Furthermore, from the circuit of Figure (5.30), the rate of change in v_1, which represents the UCs voltage rise when the charge accumulated on it, by applying Kirchhoff's voltage law can be determined as:

$$\left.\begin{aligned} \frac{dv_1}{dt} &= \frac{(v_2 - v_1)}{RC_1} \\ v_1 &= \frac{1}{RC_1}\int (v_2 - v_1)\, dt \end{aligned}\right\} \quad (5.55)$$

While the rate of change in v_2, which represents the generator voltage decrease when the charge transferred to the UCs storage unit, can be determined from equation (5.53) as:

$$dv_2 = -\frac{C_1}{C_2}\, dv1 \quad (5.56)$$

Where $dv_2 = 0 - v_2 = -v_2$, represents the change of the generated voltage starting from a maximum value E_{back}, until it reaches zero when the generator has been stopped. While the voltage difference in the UCs storage unit initially at zero states which conserves energy from the system until it reaches the steady-state value, can be calculated as $dv_1 = v_1 - 0 = v_1$, so that:

$$v_2 = \frac{C_1}{C_2}\, v_1 \quad (5.57)$$

5.4.1.2 Simulation and experimental results

The designed and built test rig that presented in chapter three has been used for energy management and regenerative braking process. The mechanical energy stored in the flywheel can be implemented as a variable charging voltage since it depends on the motor rotational speed.

The overall system simulation can be implemented as in Figure (5.32), which depict the system beginning from the PMBLDC motor when acting as a generator in the braking process. The generating voltage has been used to charge the UCs storage unit considering its state and voltage level. The generated voltage and the UCs voltage has been implied and continuously monitored to get the overall system performance.

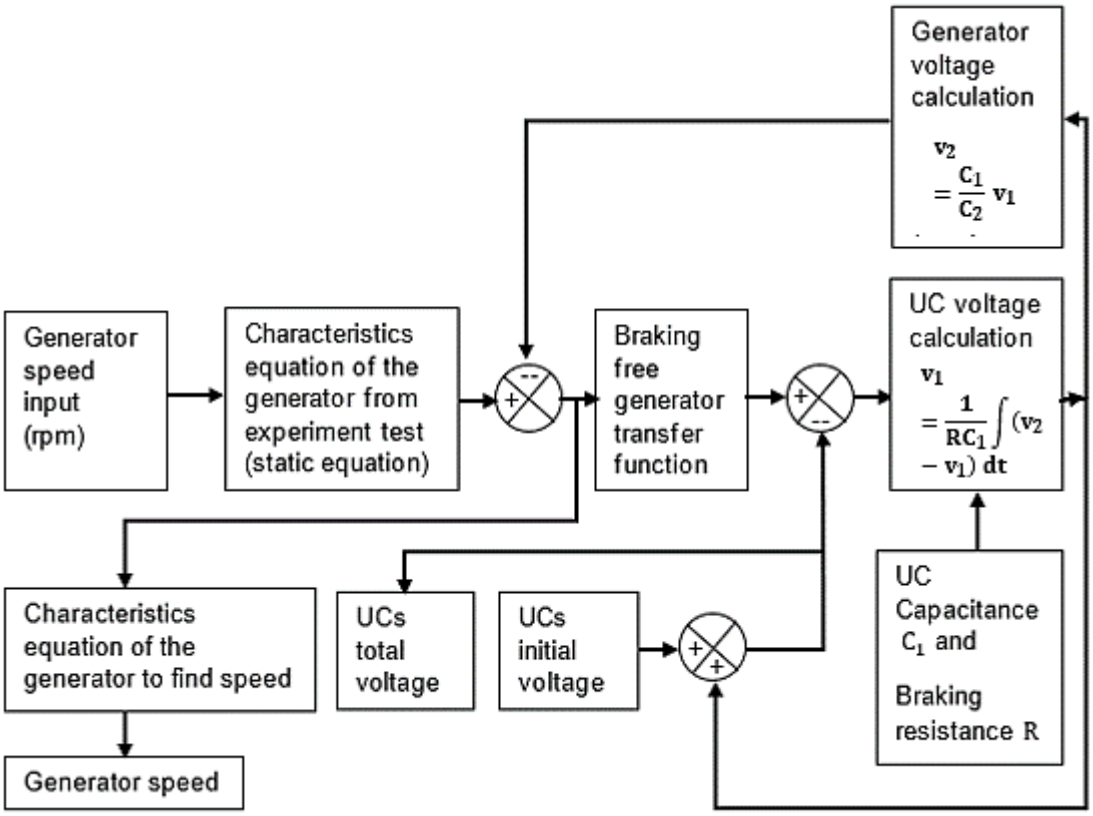

Figure 5. 33: Simulation flowchart

Figure (5.33) demonstrates the steps used to extract the best fit of data retrieved from experiments. The characteristics' equation of the generator from the experimental test has been implemented as $y = 0.0053x\text{-}1.1345$ from the previous chapter. The calibration equation has been used at different stages, starting from speed input ending with the inverter output voltage to each phase of the PMBLDC motor for simulation of the designed test rig.

Furthermore, the dynamic equation has been performed using the system identification tool available in the" LabVIEW" program and checked by the tuning process as described in the previous chapter. The RB and energy recovery have been achieved in the proposed modelling analysis of the generator and UCs storage unit to verify conservative energy during the braking process.

e) When the valve was closed between the two tanks ($R \sim \infty$), and there was no flow between the two tanks ($q = 0$). The amount of discharged fluid from tank$_1$ (q_C partially opened) to represent the UCs internal discharging process can be formulated as:

$$q_c = \frac{h_1}{R_c} \tag{5.58}$$

And, by taking the Laplace transform of equation (5.58) gives:

$$Q_c(s) = \frac{1}{R_c} H_1(s) \tag{5.59}$$

By replacing the variable of $tank_1$ from equation (5.59) with its equivalent circuit variable, the following equation can be taken as:

$$I_C(s) = \frac{1}{R_c} V_1(s) \tag{5.60}$$

Equation (5.60) represents the discharged current of the UCs due to its internal resistance.

5.5 Studying RB analysis

5.5.1 Studying the impact of external load

The study of the effect of the external load was achieved by examining the UCs effect in measuring the stopping time at braking. The PMBLDC motor rotates at a constant speed of 3000 rpm, and then the same motor was used as a generator to charge the external load (UCs in this process). Initially, the motor was used without a connecting load, and the speed was reduced because of friction until stop, as shown in Figure (5.34).

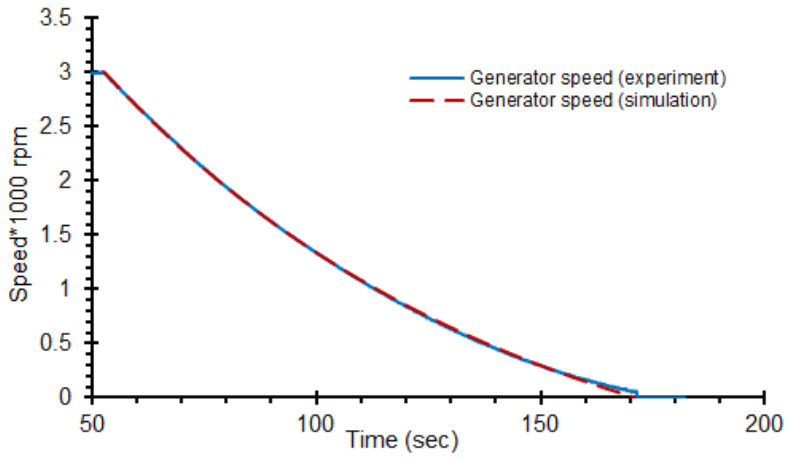

Figure 5. 34: No-load stopping time with simulated generator speed curve fitting

Meanwhile, the stopping time was affected by the external load connected to the generator terminals, studying the different region of operation has been indicated the parameter of that load.

The 65 F UCs was connected to the generator terminals, and the braking process was applied, then the generator speed is as shown in Figure (5.35).

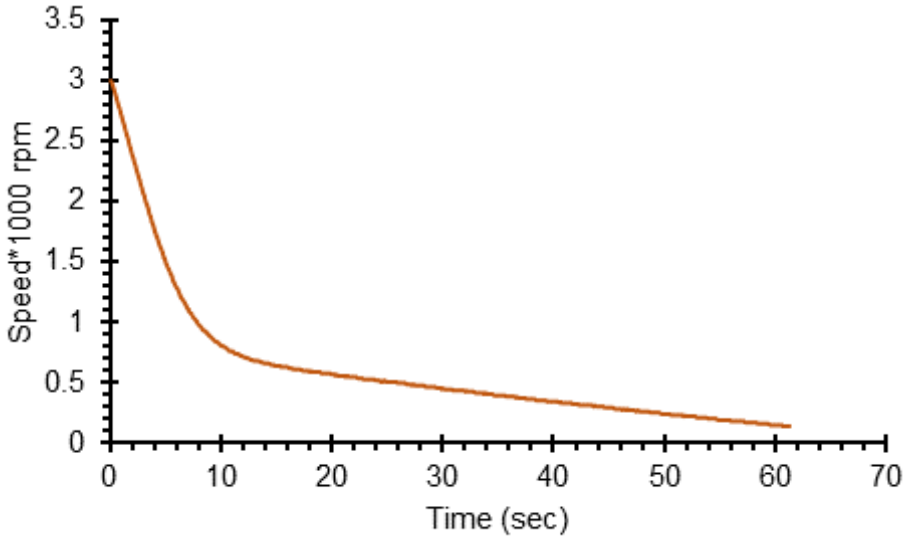

Figure 5. 35: Generator speed at 65 F UCs load

When the no-load stopping time (Figure 5.34) compared to the demeanour time (figure 5.35), the output can be performed, as shown in Figure (5.36).

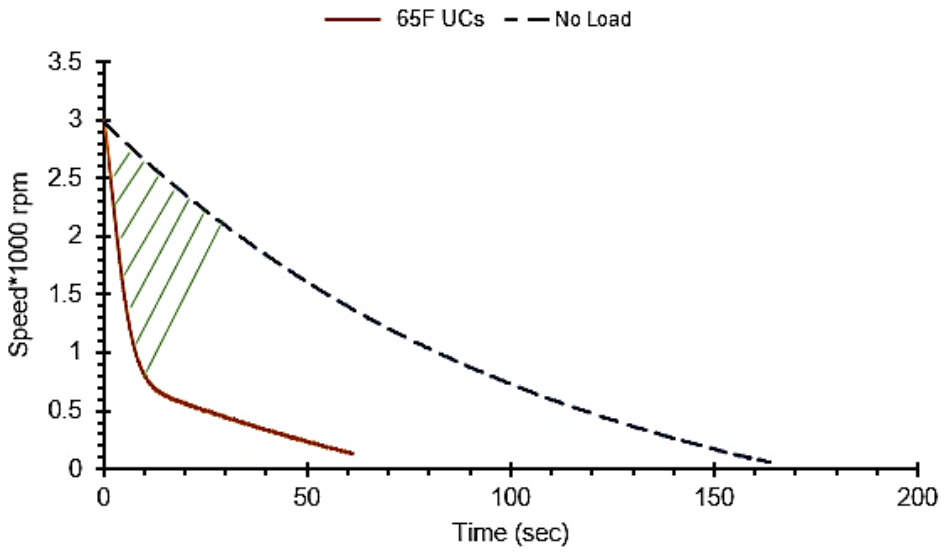

Figure 5. 36: No-load, and loaded generator stopping time response

From Figure (5.36), when the load curve approaches the y-axis, it follows that the area between these two curves (dashed lines) has been increased,

resulting in more energy recovery; therefore, it affects the stop time that to be reduced. For the same rotation speed, it can be concluded that when the curve has been approached the no-load stop curve, then the UCs storage unit was fully charged and vice-versa. Also, it can be seen from Figure (5.37), when these two curves have been compared, there was non-recoverable energy in the region when these two curves coincide with each other, and the loaded generator behaves like the open-circuit generator.

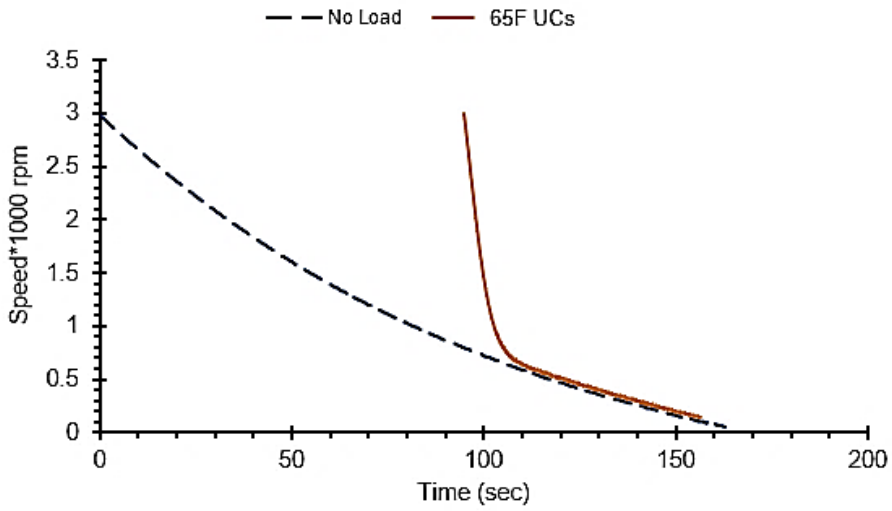

Figure 5. 37: Region of unrecovered energy

5.5.2 Examine the effect of UCs capacitance on stopping time

When the motor rotates at 4000 rpm, the free-running and the loaded generator speed at a different value of the UCs capacitance corresponding to the stopping time has been shown in Figure (5.38-5.41).

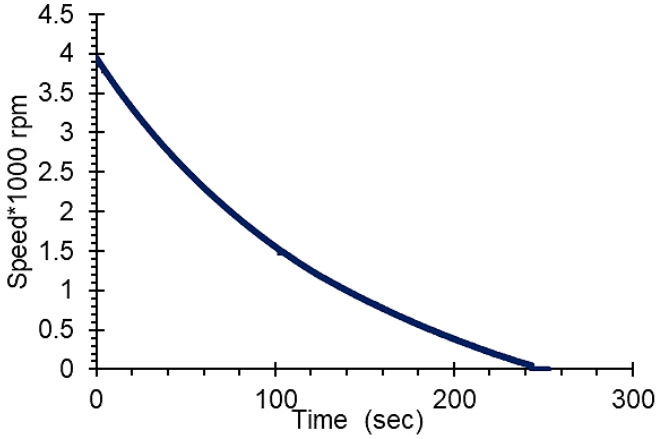

Figure 5. 38: Generator speed at 4000 rpm No-load

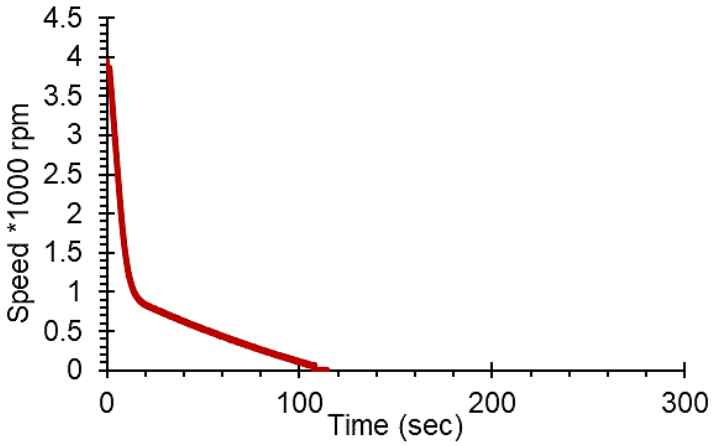

Figure 5. 39: Generator speed at 65 F UCs - load

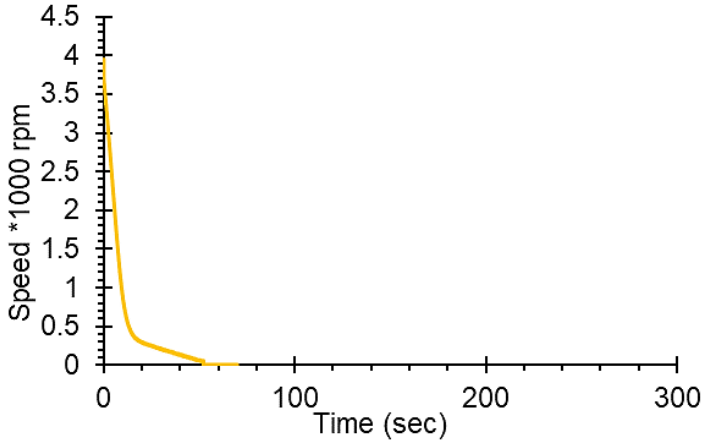

Figure 5. 40: Generator speed at 2000F UCs - load

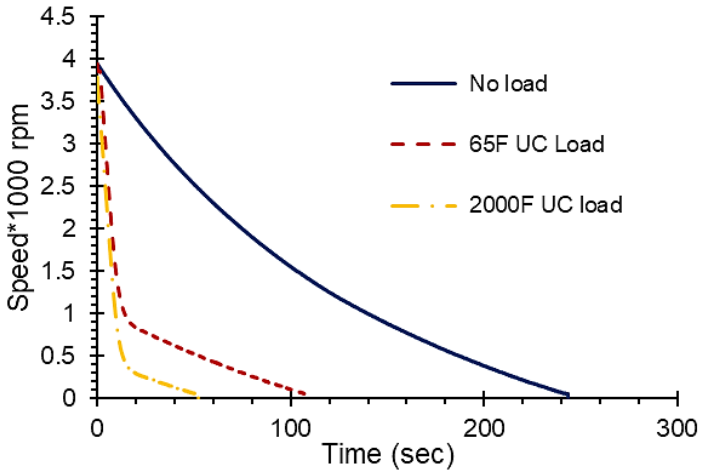

Figure 5. 41: Generator speed at; No-load, 65 F and 2000F UCs for comparison

According to Figure (5.41), the stopping time has been reduced due to the externally connected load. The 2000F UCs was eliciting the lowest stopping time, which can be used if the hard braking was required.

5.5.3 Examine the UCs voltage level effect on stopping (braking) time measurement

To study the impact of UCs voltage level on the stopping time, the UCs has been charged at a different voltage state and then connected to the generator terminals at the instant of braking to absorb the excess of the generated energy by the generator. The stopping time has been measured in each UCs charging state. Figure (5.42) shows the generator stopping time corresponding to different value of the UCs voltage levels at 3000 rpm generator starting speed.

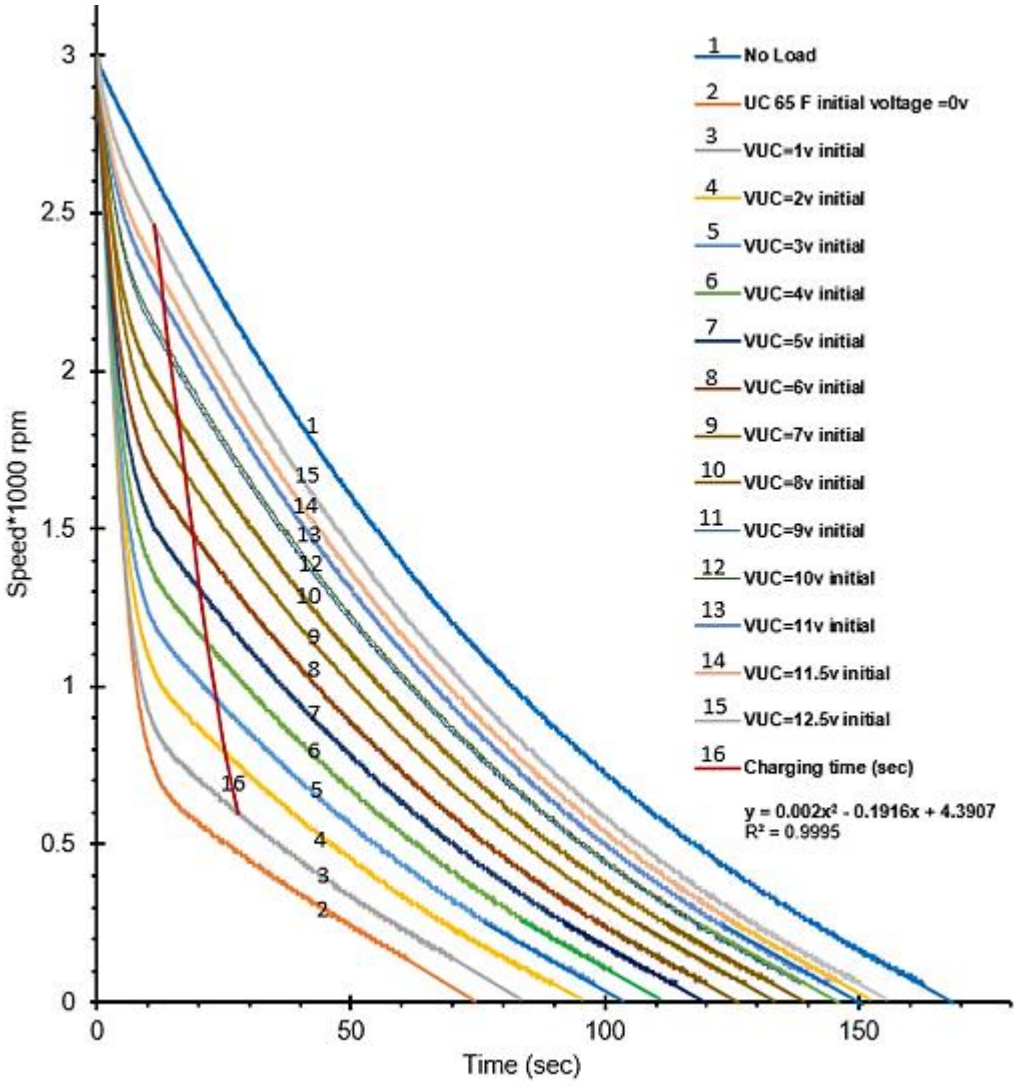

Figure 5. 42: Stopping time at different UCs voltage states

From Figure (5.42), each curve can be subdivided into three distinct sectors with other trends, as shown in Figure (5.43).

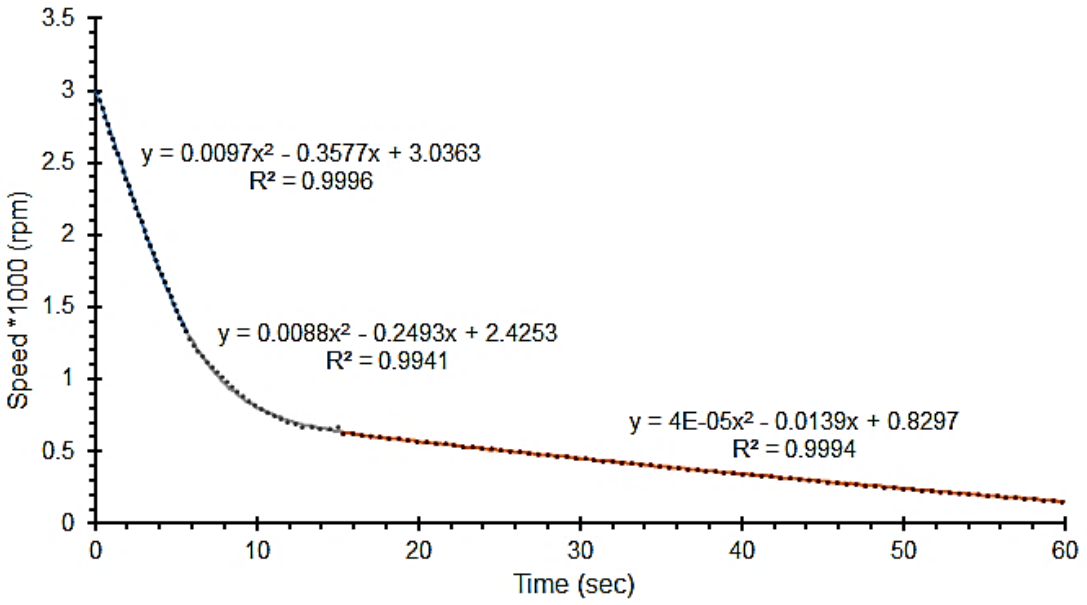

Figure 5. 43: Generator speed region of operation

Initially, at the start-up speed, the descending generator was in the sector in which an enormous amount of energy was recovered by the UCs. In contrast, the second part has represented a transition sector in which the UCs voltage fluctuates until it reaches a stable state, and no energy was conserved. Finally, the third part has been served as a part where there was no energy recovered and trends behave like no-load generator speed of operation. This sector was the principal focus of solutions for energy recovery improvement. However, the remaining generated electricity can be lost as heat internally or by applying a frictional force as in an emergency case. So, in charging mode, the UCs can absorb more energy when it was in a low voltage state, and the stopping time highly depends on the UCs voltage levels. The average braking time was increased significantly at the highest UCs voltage level, compared to the voltage at the lowest value, where more energy can be stored in the UCs. Therefore, it was essential to meet the UCs voltage with a specific amount when used in different operating conditions.

On the test platform, to determine the charging analysis of the storage unit in RB, the 65 F UCs was charged by the variable generated voltage (VV) in the braking process, as represented in Figures (5.44a-5.44l).

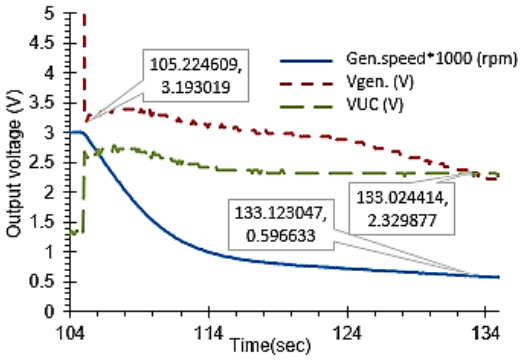

(a) V_{UC} initial=1.31V

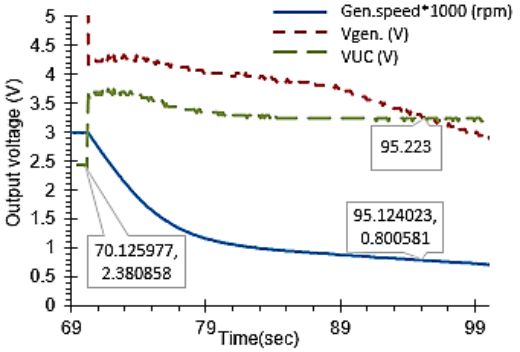

(b) V_{UC} initial =2.38V

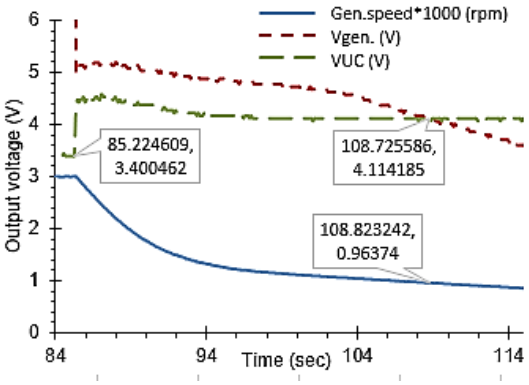

(c) V_{UC} initial =3.4V

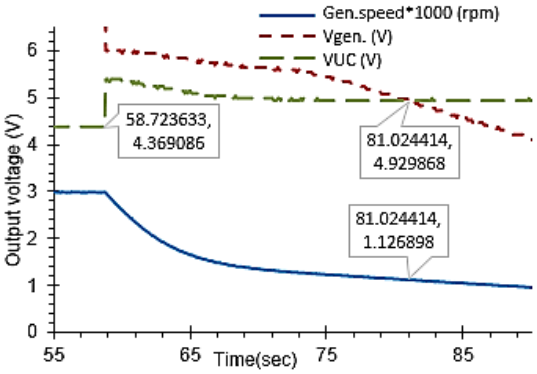

(d) V_{UC} initial=4.37V

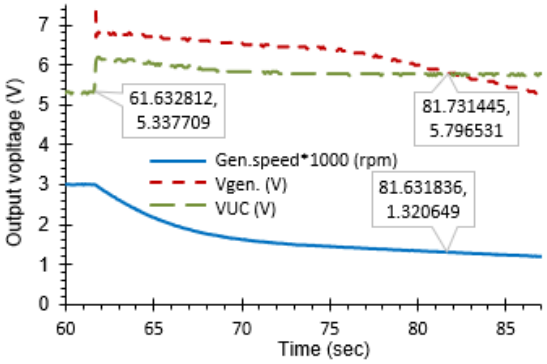

(e) V_{UC} initial=5.337V

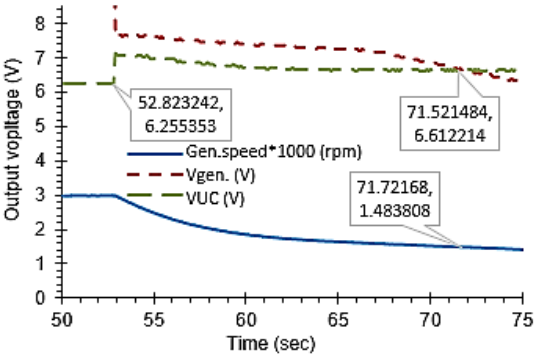

(f) V_{UC} initial=6.255V

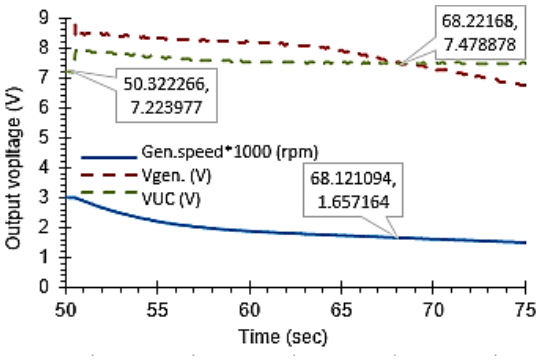

(g) V_{UC} initial=7.2245V

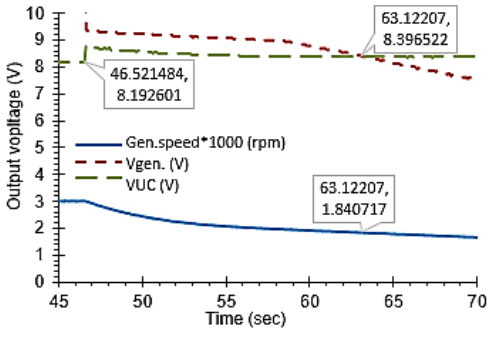

(h) V_{UC} initial=8.192V

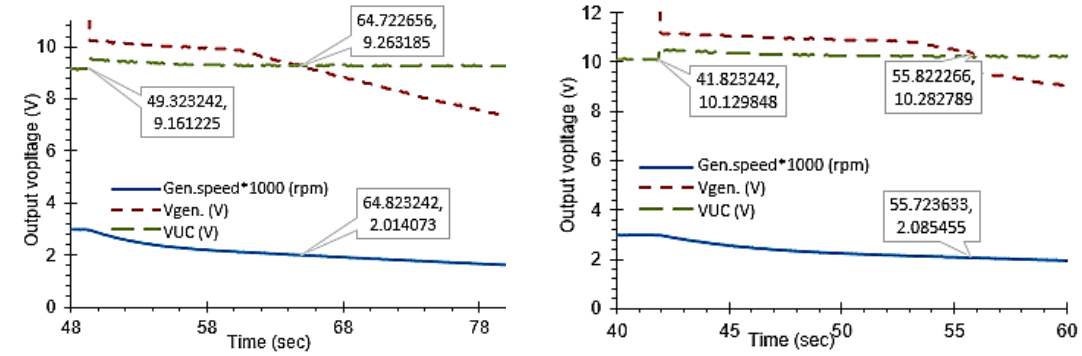

(i) V_{UC} initial=9.161V (j) V_{UC} initial=10.123V

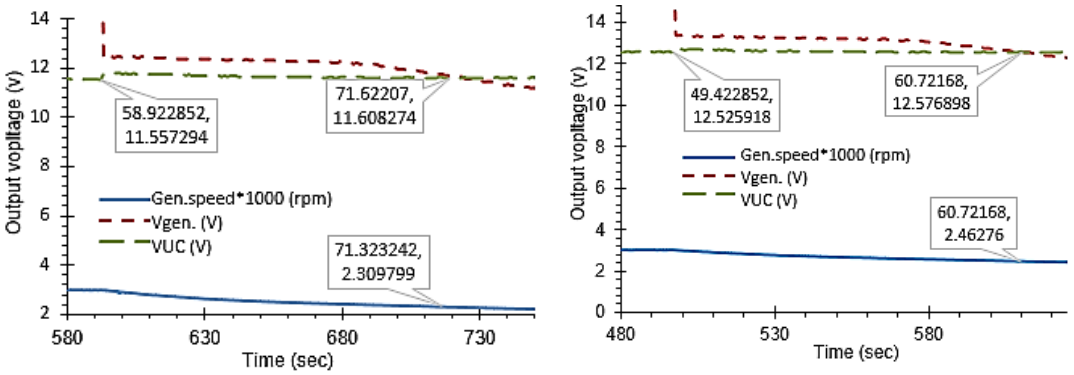

(k) V_{UC} initial=11.5573V (l) V_{UC} initial=12.526V

Figure 5. 44: Charging UCs from VV RB process

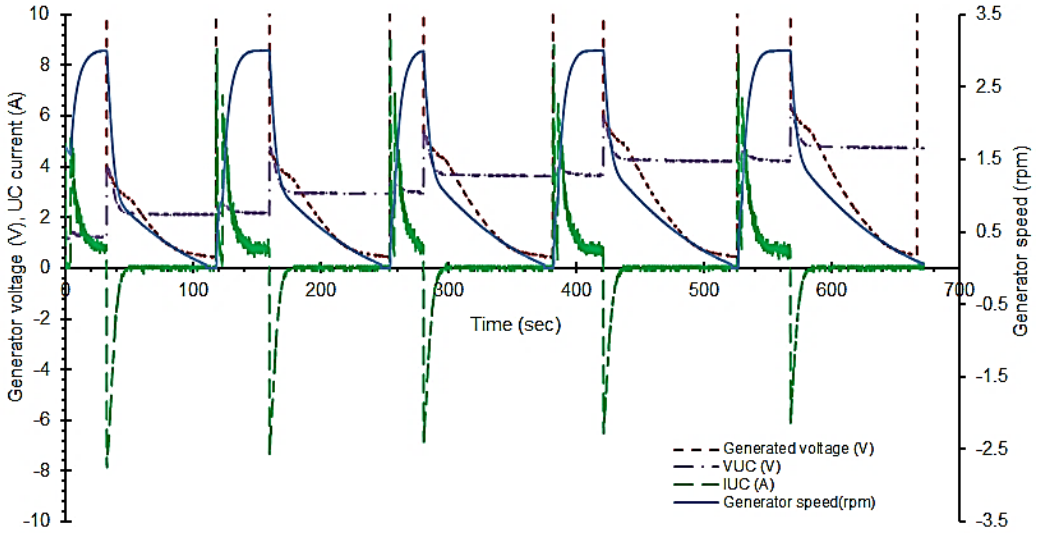

Figure 5. 45: UCs charging process

Figure (5.45) shows the voltage and the current waveforms of the charging 65 F UCs connected in series with 20 Ω resistive load at RB process. The electric charge has been accumulated in the UCs at each time when braking happened. The extracted data for this figure has been attached in Appendix Table 2.

From Figures (5.44a-5.44l), the following table has been extracted to assess the total energy stored in each state and the level at which the UCs shuts down.

Table 5. 7: Extracted data from RG process shown in Figure (5.44)

Sample	S_1 (rpm)	T_{Charge} (s)	V_{UC-ini} (V)	V_{UC-fin} (V)	ΔV (V)	E_{UCs} (J)	T_{total} (s)	$\%T_{charge}$
1	450	29.40	0.10	1.28	1.18	52.92	85	34.60
2	597	27.60	1.31	2.33	1.02	120.67	96	28.75
3	800	25.12	2.38	3.25	0.87	159.19	104	24.15
4	963	23.48	3.40	4.11	0.71	173.29	112	20.96
5	1127	21.80	4.37	4.93	0.56	169.26	120	18.17
6	1320	20.10	5.34	5.80	0.46	166.54	127	15.83
7	1483	18.90	6.26	6.63	0.37	155.00	134	14.10
8	1600	17.90	7.22	7.48	0.26	124.22	139	12.88
9	1770	16.60	8.19	8.40	0.21	113.23	144	11.53
10	2085	14.00	9.16	9.26	0.10	59.87	152	09.21
11	2309	12.50	11.50	11.52	0.02	14.96	159	7.86
12	2462	11.30	12.50	12.51	0.01	8.13	170	6.65

Where, S_1 = The speed at which the UCs stope charging (rpm),

T_{charge} = Charging time (s),

V_{UC-ini}= UCs initial voltage (V),

V_{UC-fin} = UCs final voltage (V),

ΔV = UCs net voltage = $V_{UC-fin} - V_{UC-ini}$ (V),

E_{UCs} = Stored energy in the UCs= 0.5 * C*($V_{UC-fin}^2 - V_{UC-ini}^2$) (J),

T_{total} = Total stopping time (s),

$\%T_{charge}$ = % Charging time= % T_{charge}/T_{total}

Also, Table (5.7) has been included the whole stopping time and the entire time spent during braking, which was determined in the RB process.

The charging time at which UCs stop charging has been represented with a dozen samples, as shown in Figure (5.46).

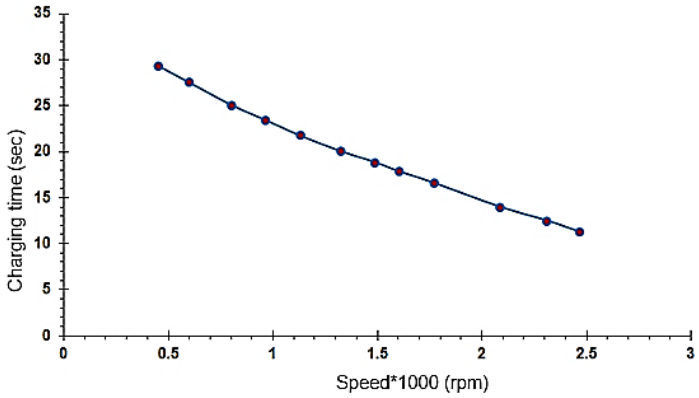

Figure 5. 46: Charging time vs speed relationship

The speed axis has represented the speed at which the generator falls from its initial value (3000rpm) to the measured value when the UCs stop charging. So, the trends can be represented by an equation as:

$$y = -8.788\,x + 32.312 \tag{5.61}$$

Also, the initial and final value of the UCs voltage level has been given an indication of how efficient the system was evaluating performance regarding energy recovery, as shown in Figure (5.47).

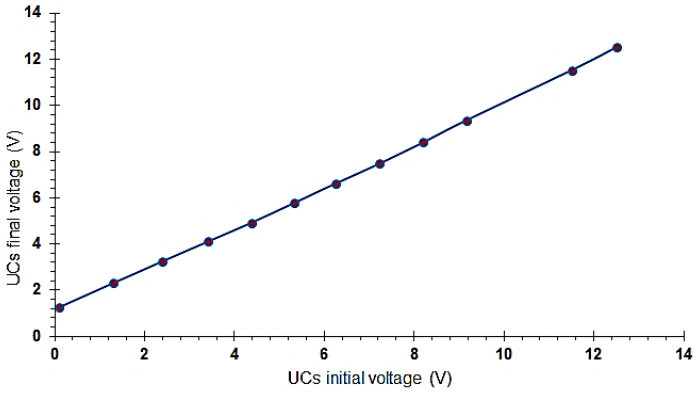

Figure 5. 47: UCs initial and final voltages charging state during RB process

Figure (5.48) shows the trends that can be represented by an equation as:

$$y = 0.9042x + 1.0604 \tag{5.62}$$

The relationship was a straight line with an offset represents the initial value of the UCs voltage state used in UCs over-discharging protection purposes. Figure (5.48) shows the most apparent shape of the percentage of charging time for each sample. It can be concluded that the UCs at lower voltage state absorbs high energy with about 35% of overall stopping time.

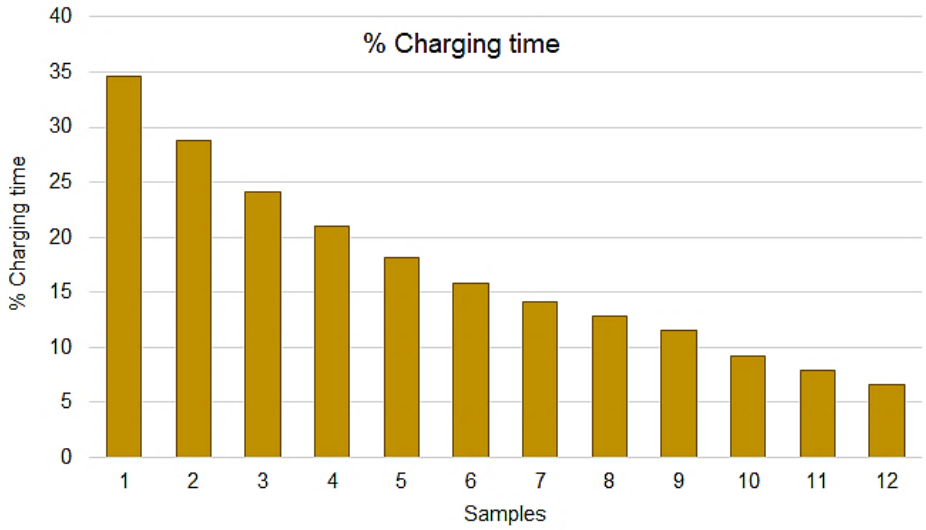

Figure 5. 48: Percentage of the UCs charging time

The changes in the UCs stored energy in each sample affected by its initial storage charged has been implemented, as shown in Figure (5.49).

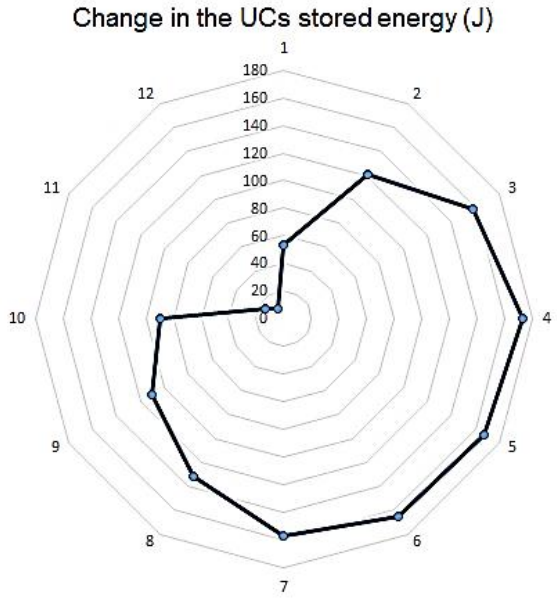

Figure 5. 49: UCs energy at different voltage states

5.5.4 Experiment and the simulation validation

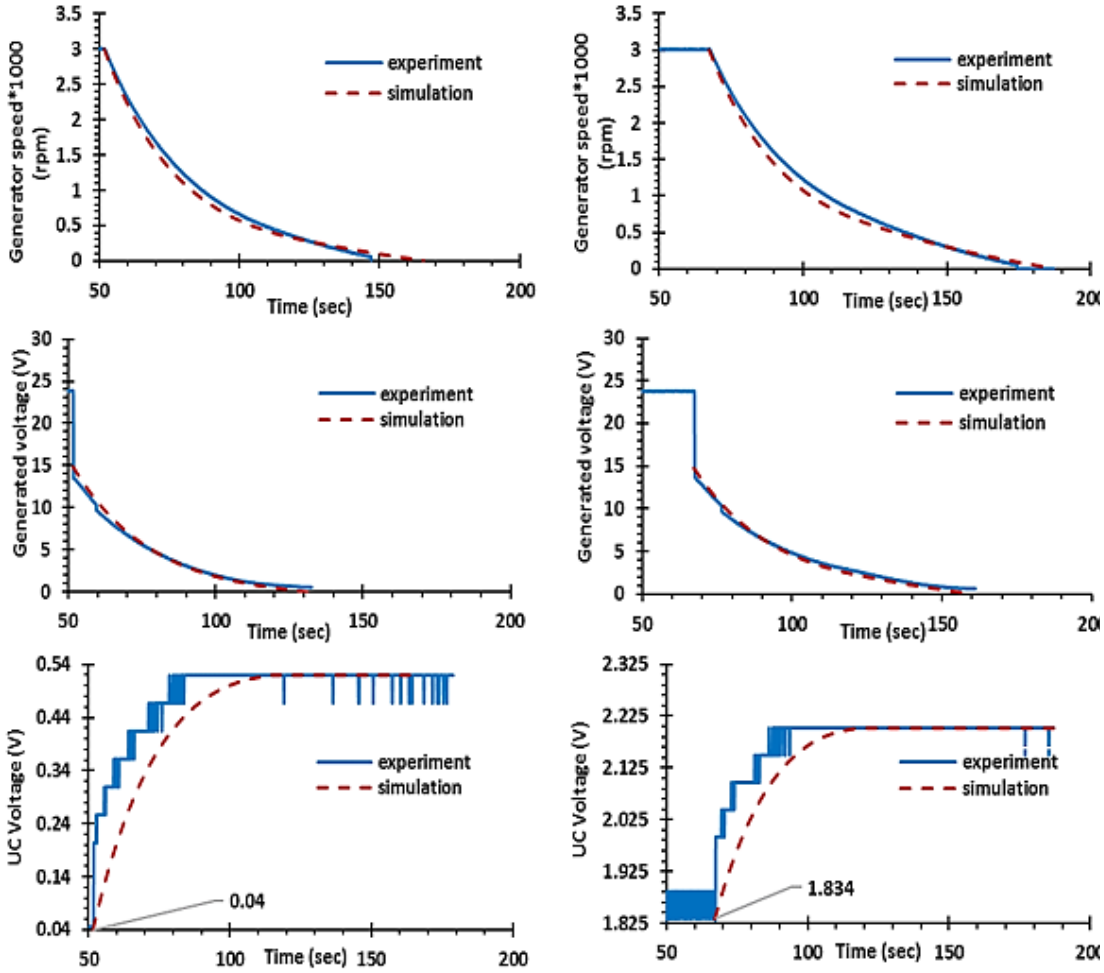

(a) At 0.04v UCs initial value (b) At 1.834v UCs initial value

Figure 5. 50: Verification at two UCs voltage states

Figure (5.50) shows the experiment and the simulation validation of the RB analysis concerning the generator speed, generator voltage and the UCs charging process at two voltage levels. The extracted data for this figure has been attached in Appendix Table 2.

5.5.5 Model findings

The newly proposed modelling, and the algorithm, which has been taken the essential information of the system from the flow rate associated with the two connected tanks to represent the charge flow rate in RB. The capacity of the tank which can be defined by the mass in kg of water required to raise its height by one meter, equivalently, the capacitance of a capacitor was characterised by the necessary amount of charge to make a unit of the potential difference between its plates. The impact of variation in UCs voltage state and charging value to the driving characteristics (deceleration and speeding) has been highly relied on its features and its behaviours. The main finding has been achieved by defining and representing generator capacitance which is an essential term in the simulation. Also, studying the UCs effect on energy recovery enhancement which reflect the braking time for safety requirements.

5.5.6 Energy Management System (EMS)

EMS has been referred to the system designed to achieve efficient transfer of energy between the different rechargeable ESS concerning bus voltage. There was a vast extent of arrangements for consolidating hybrid ESS, for instance, battery and UCs (Rajashekara, Ashoka K. S. Bhat 2000; Alamili et al. 2019). Based on the proposed developing of hybrid energy unit, improvement of properties can be taken advantage of the combination of batteries (higher energy density) with UCs (higher power density) (Ren et al. 2015; Itani et al. 2017). The UCs was being assisted in achieving the energy density of cells, offering almost unlimited lifespans, widen temperature run and no environmental issues. Moreover, it has been used to disconnect the electric motor from the battery through electronic control, utilising UCs to transmit of high current on acceleration and to accept regenerative braking energy on descending makes it ideal as energy storage for EVs and HEVs power applications.

5.5.6.1 Types of EMS

According to work on literature, there was a wide range of arrangements to standardise hybrid ESS in EMS, for instance, battery and the UCs. The passive and active hybrid ESS approaches have been followed by various researchers (Ehsani et al. 2010; Michalczuk et al. 2012; Zhang and Deng 2016) as defined in the literature. Zhang et al. (2015), show an example of the classification of different technologies for the hybrid ESS system design, as shown in Figure (5.51) (Zhang et al. 2015).

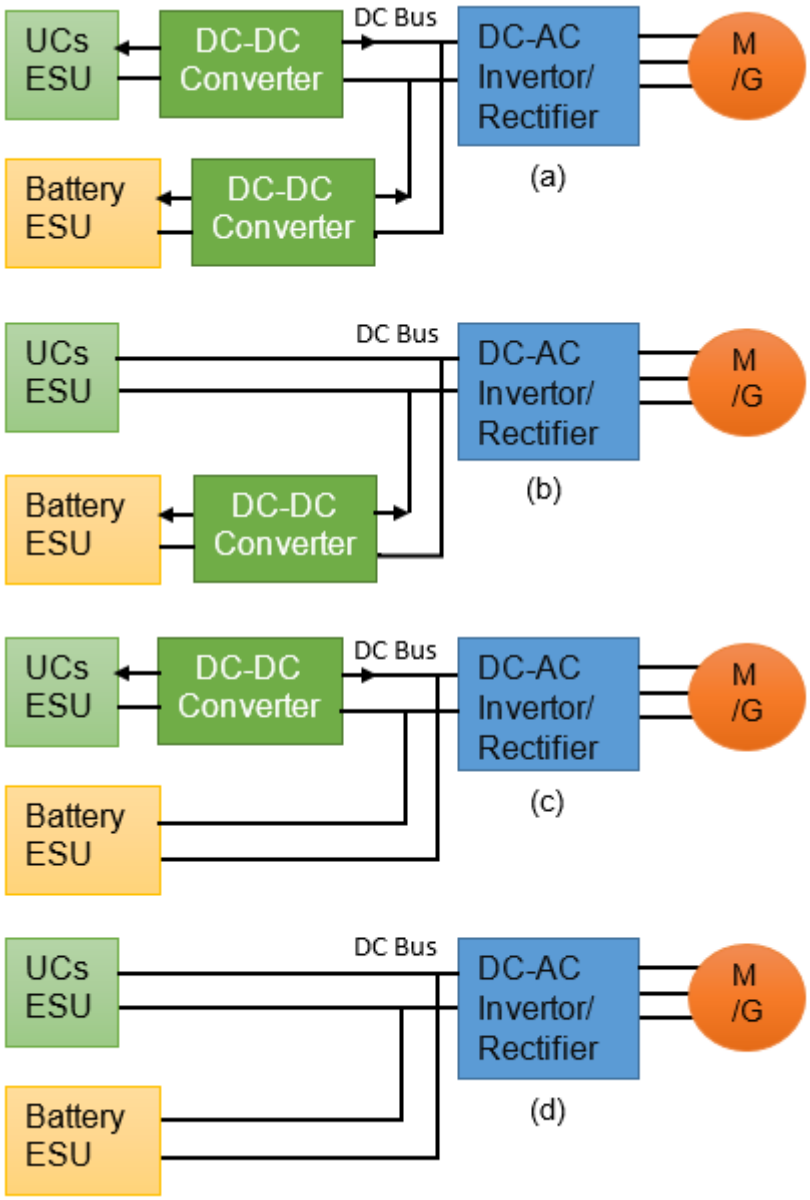

Figure 5. 51: Hybrid energy topologies (a) UCs and battery with DC-DC converter, (b) Battery with DC-DC converter, (c) UCs with DC-DC converter, (d) UCs and battery without a DC-DC converter

Figure (5. 51) illustrates the hybrid energy storage used to provide energy for propulsion (driving) and absorb energy in RB (generating). Also, the converter was allowed for bidirectional electricity flow and the concept of a hybrid power train with the battery as the central storage unit and the UCs as an auxiliary unit with the possibility of different power flow paths.

In the structure shown in Figure (5.52a), which represents an active hybrid, the energy efficiency of the system has been decreased, and the system cost has been increased due to the use of two bidirectional DC-DC converters. While, in the designed system, as in Figure (5.52b), a model was developed to evaluate a semi-active configuration with a boost DC-DC converter to enhance system performance and cost and to control energy transfer between battery ESS and the central voltage of the DC bus. The UCs was connected directly to the bus to allow a direct exchange of energy between the UCs and the bus without the use of a converter, which was useful for restoring excess power in the braking process. The battery power flow was controlled by a DC-DC converter, which enables boosting battery voltage in motoring operation. Moreover, the system restricts the UCs voltage to be less than the back electromotive force (E_{back}) of the driving motor when working as a generator in the braking process. Although the structure, shown in Figure (5.52c), enable the control strategy of the DC-DC converter connected with the UCs to provide the power during peak operation at motoring acceleration.

Figure (5.52d) was represented the passive hybrid connection in which the DC bus act as a voltage of the driveline. In this design topology, the UCs can release about 75% of energy E_{UCs} as the voltage of the system has been reduced from maximum (V_{max}) to its halve value ($V_{min} = 0.5V_{max}$), as in equation (5.63) (Omar et al. 2012).

$$E_{UCs} = 0.5\, C_{UCs}(V^2{}_{max} - V^2{}_{min}) \tag{5.63}$$

There were many operating conditions available with two storage units to meet operating requirements as:

1. The battery alone had provided its power to the motor when the UCs was wholly discharged, as in Figure (5.52a).
2. The UCs alone offered its power to the motor used when the battery was almost empty, as in figure (5. 52b).
3. The battery and the UCs have provided their power to the motor simultaneously. (Used on demand for high energy, such as during acceleration or when climbing slopes), as in Figure (5. 52c).
4. The UCs was getting power from the kinetic energy of the vehicle recovered by the electric motor when acting as a generator, as in Figure (5. 52d). The UCs has been transferred the recovered energy to the battery for later use, as in Figure (5. 52dd).
5. The battery charges the UCs while the vehicle was parked or in a downward motion, in which no power goes into or comes from the motor, as in Figure (5. 52e).
6. The UCs has accepted power from the battery and the generator simultaneously, in which both RB energy and the battery charge the UCs simultaneously, as in Figure (5. 52f).
7. The battery has provided its power to the motor and the UCs simultaneously. This mode was achieved when the battery propels the vehicle and charges the UCs simultaneously, as in Figure (5. 52g).
8. The battery charges the UCs, as in Figure (5.52h), and then the UCs has provided its power to the motor, as in Figure (5. 52hh).
9. The battery has offered its energy to the motor, as in Figure (5. 52i), and then the generator has provided its energy to the UCs, as in Figure (5. 52ii).
10. In case of both storage units are full, the generated electricity has been dissipated through a braking resistance, which converts the excess of energy in the system to the form of heat.

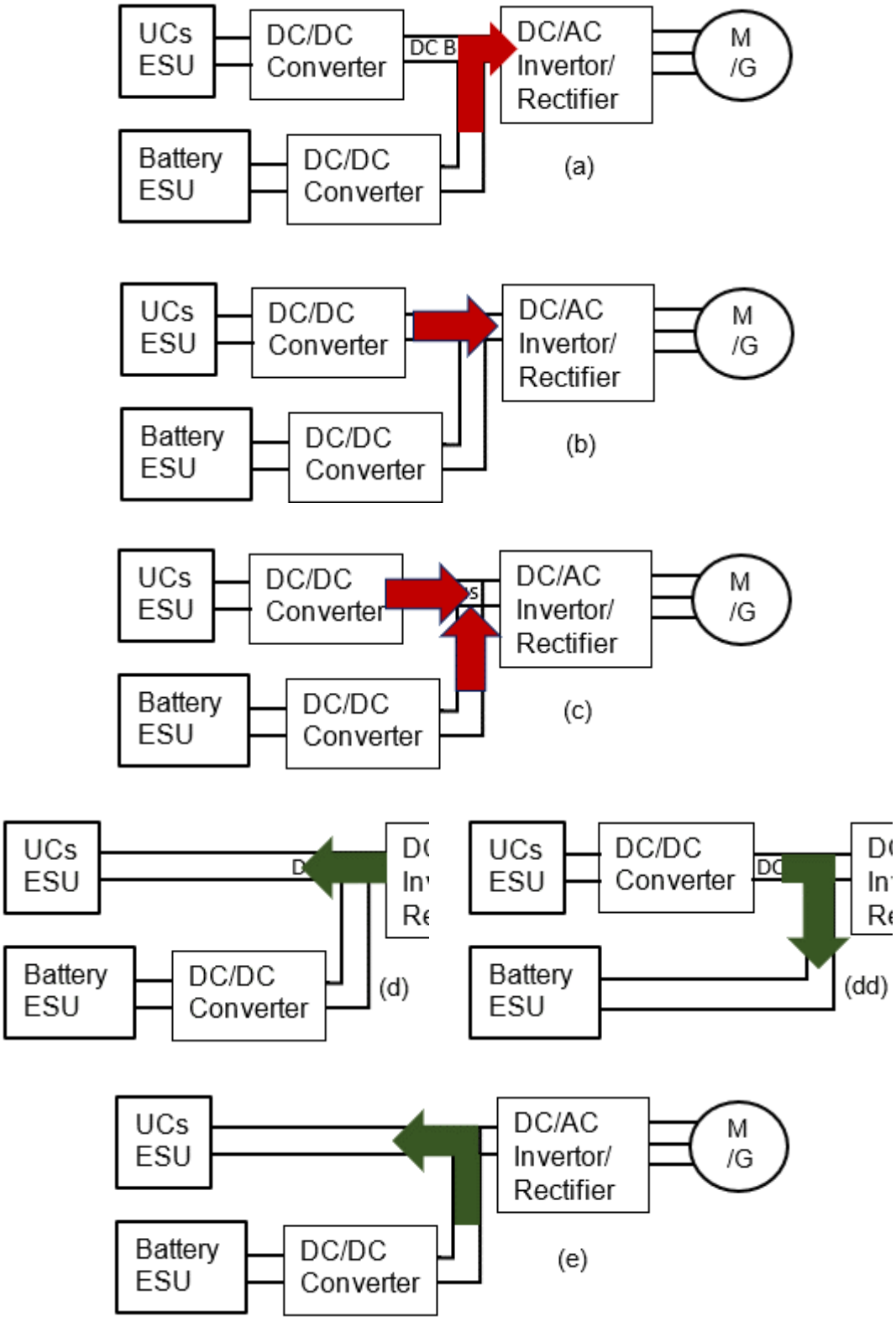
UCs
ESU
DC/DC
Converter
DC B
DC/AC
Invertor/
Rectifier
M
/G
Battery
ESU
DC/DC
Converter
(a)
UCs
ESU
DC/DC
Converter
DC/AC
Invertor/
Rectifier
M
/G
Battery
ESU
DC/DC
Converter
(b)
UCs
ESU
DC/DC
Converter
DC/AC
Invertor/
Rectifier
M
/G
Battery
ESU
DC/DC
Converter
(c)
UCs
ESU
Battery
ESU
DC/DC
Converter
(d)
UCs
ESU
DC/DC
Converter
Battery
ESU
(dd)
UCs
ESU
DC/AC
Invertor/
Rectifier
M
/G
Battery
ESU
DC/DC
Converter
(e)

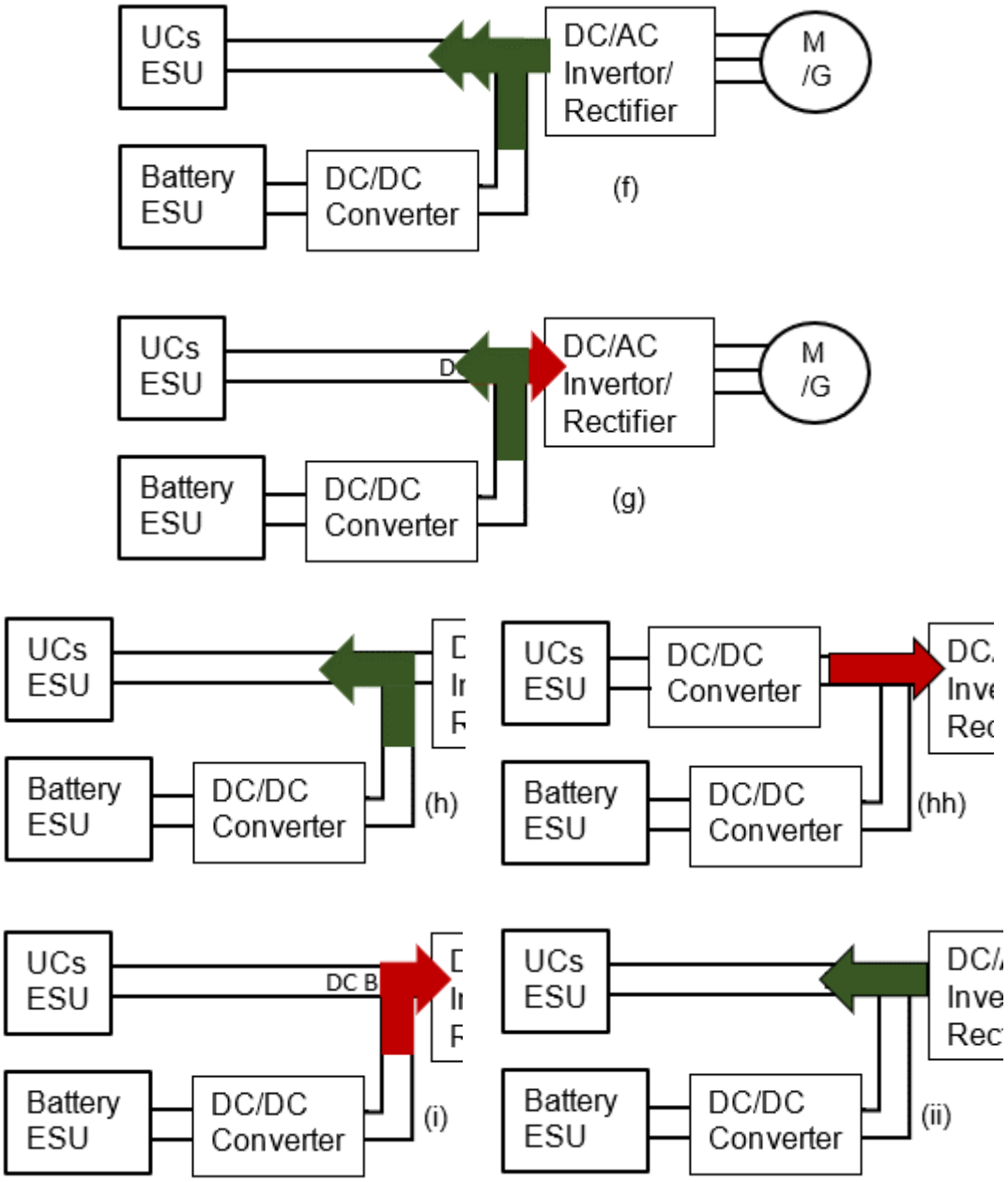

Figure 5. 52: Hybrid energy storage units operating conditions

In all cases, an arrow pointing towards the storage units' input has been used to represent the charging process and an arrow pointing towards the inverter used to describe motoring operation. Also, a direct connection between the UCs storage unit and the generator was proposed for maximum power transfer and to reduce the power loss in the converter. Meanwhile, charging the UCs was performed by the battery and the generator in case of need for maximum acceleration.

5.5.6.2 EMS design implementation

In EMS design implementation, the SoC of ESS, counterpart the fuel tank in conventional vehicles have been used to measure the distance that it can cover, have been evaluated to measure the terminal voltage and then compared concerning bus voltage, which can be used to avoid overcharging and discharging of storage units. Moreover, monitoring SoC of each group and by optimising unique processes designed for the automatic control procedures can show significant energy not only available in motoring but also in capturing energy throughout the RBS as well as it was suitable to use the power generated by descending vehicles (Ostadi and Kazerani 2015).

Furthermore, the best battery performance can be accomplished with additional UCs in EMS. In the structured system, the UCs was connected to the bus as in Figure (5.52d) to allow the immediate exchange of energy between them without the utilisation of a converter, which was beneficial for excessive recapture energy in the braking process. The energy progression from the battery was constrained by a DC-DC converter, which empowers boosting battery voltage in motoring activity. Moreover, the system has imposed constraints that the UCs voltage must be less than the back electromotive force ($\mathrm{E_{back}}$) of the driving motor when functioning as a generator in the braking process. The high power with the RB current (charging) was generally volatile and pursued the driver's brake behaviour. However, the discharge process has been taken longer because it represents acceleration and ascent in the duty cycle. Also, as in equation (5.64), the energy efficiency was determined back and forth, which represent the deviations of the battery voltage from the voltage when the battery was actuated in either direction.

$$\text{Round} - \text{trip energy efficiency} = \frac{\text{Q discharge}}{\text{Q charge}} \tag{5.64}$$

In EMS, several points must be considered at SoC observing, in which the arrangement must be made to restrict the inrush current while charging a fully discharged capacitor. The UCs was not liable to overcharge and does not require full-charge detection; the current mostly ceased when the capacitor was fully charged. The UCs has also been made critical inroads into electric powertrains. To avoid voltage sag during acceleration of the motor and to

diminish peak power usage, the UCs was being tested in a laboratory. The virtue of UCs has made it ideal as a peak-load enhancer for EVs and HEVs.

In energy harvesting from the braking process, the control procedure for the UCs voltage constraints was as follows; when the motor runs at high speeds, the UCs was kept at the lower level of energy (approximately 25% of maximum stored energy for over-discharge protection) to prepare the UCs to receive energy during braking. If the motor was at a standstill, the UCs was charged at extreme permissible energy (for overcharge protection) to set up the UCs to supply the required energy during acceleration. At medium motor drive speeds, the UCs energy was preserved at a medium level of energy to allow upcoming accelerations (motoring) or deceleration (generating) process. However, the battery SoC was used as a reference signal to control the voltage level of the UCs at predefined limited values as follows: When the battery was eventually charged, the voltage level of the UCs was kept at 25% of its maximum voltage. When the battery was ultimately discharged, the voltage level of the UCs was preserved at a maximum specified voltage. With the DC-DC voltage regulator was used at the output of the battery storage unit. A steady-state level of the voltage drops was accomplished when the DC-DC converter starts drawing progressively current in which the end of release was achieved when the load necessities never can again be met. Furthermore, in the charging process, the initial charge can be made rapidly, and the topping charge will take extra time. Figure (5.53) has delineated the structure of the circuit component designed at the test apparatus to validate the proposed ESS energy management technique as an element of SoC monitoring. Different switches connected to the digital output signal from the DAQ 6800, as discussed in chapter three. For the limited output range of the DAQ, as in the datasheet, any input has special keys to meet its working requirements (USER GUIDE NI USB-6008/6009 Bus-Powered Multifunction DAQ USB Device. [no date]).

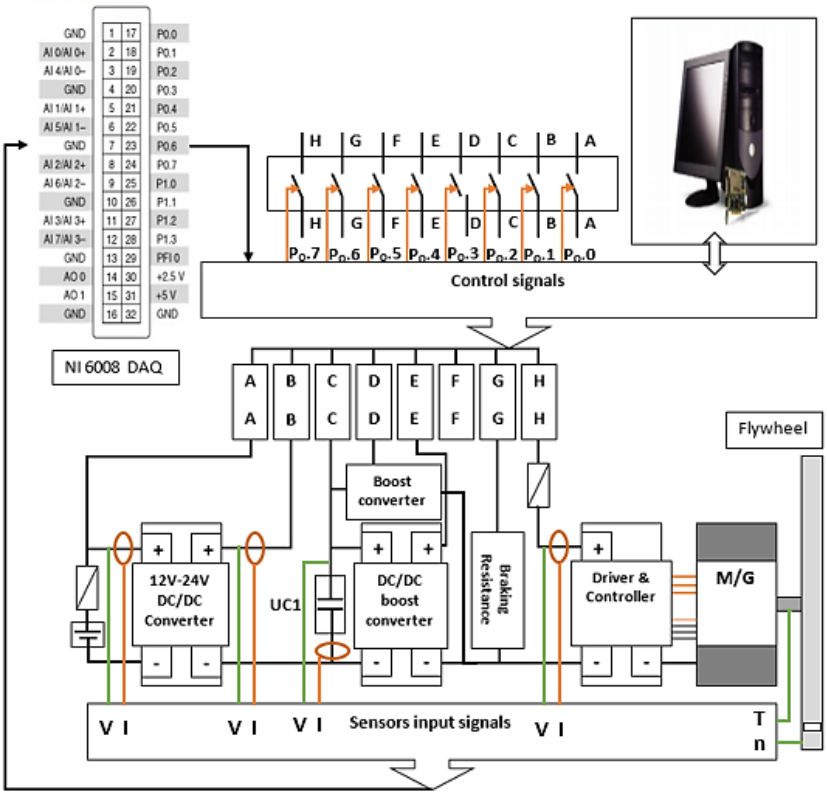

Figure 5. 53: **Proposed EMS control and monitoring strategy**

One of the primary advantages of the designed circuit shown in Figure (5.53) was that all the hybrid energy topologies were shown in Figure (5.52) can be used individually, which can be proposed as a central contribution of EMS. Table (5.8) gives the connection diagram of all switches in the designed circuit.

Table 5. 8: EMS switches connection diagram

EMS Topology	Closed switches
Figure (5.51a)	BB, and HH
Figure (5.51b)	EE, and HH
Figure (5.51c)	BB, EE, and HH
Figure (5.51d, and dd)	HH, and CC; EE, and AA
Figure (5.51e)	BB, and CC
Figure (5.51f)	BB, HH, and CC
Figure (5.51g)	BB, CC, and HH
Figure (5.51h, and hh)	BB, and CC; EE, and HH
Figure (5.51i, and ii)	BB, and HH; HH, and AA

The advantage of using the UCs as a secondary storage unit was that it could be charged and discharged many times without degradation of performance. Moreover, despite batteries that can store exceeding energy than UCs energy, UCs presents a better performance in specific power than any battery performs. It was also used to avoid transient performance during acceleration and descending speed which increases the useful life of the cells.

Furthermore, the correct setting of the voltage limit was critical and reached from 11.89V to 12.65V on the battery terminal. Setting the voltage limit was a compromise. The battery needs to be charged entirely to get the most significant capacity, and the current starts to drop as the battery begins to saturate. Finally, this part of the research that includes energy management and designing of the DC-DC converter has been made among the priorities for future work.

5.6 Summary

In this chapter, the newly proposed mechanism for the RB system was considered. Also, the derivation of dynamic models of the rechargeable storage unit was determined. Moreover, the definition of charging of the UCs and how it carries on within sight of various voltage states were found. Furthermore, the description of the voltage and current constraints used in EMS, indicated how the UCs could possess enough energy to challenge batteries used in monitoring and for system protection was covered. Moreover, the advantage of using the hybrid storage unit for supply, and absorbed excess energy generated from braking was also included. Furthermore, an introduction of test rig used to satisfy the designed circuit contains a case of an application where the monitoring of battery and UCs SoC show incorporated into systems validation was utilised as a part of the final simulation of the energy EMS with PMBLDC motor used as a generator in the energy harvesting process. EMS has been studied because there was an expected surplus of brake-generated electricity. When the voltage generated is equal to or less than the voltage of the storage units at the instant of braking, there was wasted energy that must be dealt with. Satisfaction with kinetic energy was determined using mathematical models of the flywheel,

and the SoC levels of the storage units in a specified range reflect the characteristics of the integrated test system design. Thus, the systems subjected to axial loading should have excellent performance regarding energy and power density capabilities during the acceleration and braking process. However, monitoring the status of the SoC of these storage units using mixed analysis has been shown the fundamental valuation parameters for EM and system design tools.

The next chapter (Chapter 6) presents the research contribution in the designing and building test apparatus and system operation. Also, it describes the main finding and gives conclusions and outreach future work.

Chapter 6
Conclusions and Future Work

6.1 Summary of the Tasks Carried Out

The tasks presented in this thesis has examined the collecting energy from lost brakes energy which used to reduce the impact of carbon dioxide emissions and global warming, as well as the oil crisis. The research objectives have been accomplished regarding energy. The first part has been determined as a reliable and practical technique to evaluate the real behaviour of the vehicle in the designed test rig, which lead to offering a model for measuring and monitoring energy storage unit on charging and discharging process. The second part has been used to evaluate energy management, which influences the motor operation during a braking action. In this part, a strategy used to evaluate the energy recovery regarding stopping time. The third part has been implemented to investigate the enhancement of the recovered energy during the braking process. However, the tasks were undertaken for this research based on the main objectives identified in Chapter 1 can be summarised as follows:

- Task 1: An efficient and successful testing platform has been implemented with the limits of the laboratory.
- Task 2: An investigation into the behaviour of the storage units (batteries and the UCs) during the charging and discharging process has been accomplished as a component of the RB system. Also, an approach for measuring the SoC and terminal voltage based on an experiment has been proposed.
- Task 3: An accurately monitoring of the SoC of SUs acting under different operating conditions has been implemented to protect the system from an inaccurate operation environment.
- Task 4: The development of an alternative method has been depicted and recommended determining the generator capacity.
- Task 5: In the completeness of the designed system practically, many factors have been taken to represent a perfect system such as in the designing flywheel and component selection.

The next section has been used to summarise the main contributions of our work in the development of the electronic design of the test equipment to

restore the energy from the braking mechanism. Furthermore, the conclusions reached in this study and the suggestions for future work were also outlined.

6.2 Contributions and limitations

Besides the contribution mentioned at the end of each chapter, this research was an original contribution to the field of the design of an improved testing platform for energy recovery system to simulate the descending and braking representative analogue model vehicle. This research aims to conduct an experimental evaluation of the effect of brakes, the factors that can influence energy generation and which units that can be store this energy. Also, the development of a practical test device capable of representing the system under study has been studied. Proposing a simple model to monitor the SoC of the storage unit at its main propulsion, which represents a study and transient behaviour of the storage units has been included. The theoretical development was based on the underlying differential equation of the discharging curve of a storage unit. This model aims to identify loading conditions on the braking that determine the sign of the slope of the discharging curve to evaluate the internal parameters.

The mechanically stored energy transferred to electricity in the braking process has been represented in the rig, which highly depends on the flywheel moment of inertia. Also, different sensor calibration has been made for the determination of the desired level of accuracy, which highly depends on the sensor measurement for maximum accuracy. Also, the controller has been allocated the duration of the storage units charging process during descent speed and coasting, considering local system constraints. These constraints were obtained through the practical experiment of the elements that comprise the system, which answer research question one.

Furthermore, conducting a new experimental study of a different scenario that proposed to find the best condition on which the overall the system efficiency can be enhanced. The tests were performed on a single motor used as a generator and with a motor connected to a different scheme of connected generators. The DAQ system was utilised to capture three specific output

signals during the braking operations. These outputs were included voltage, current and speed.

During the braking process, the energy management can be divided into three main categories stages: namely capturing stage, transfer stage, including transition stage, and charging stage. In this research, only the capturing stage has been implemented. The knowledge gained can be used to distinguish between the energy stored from braking and the stopping time. Due to the limitation of the existing test platform, EMS has been covered theoretically with the proposed analysis of recovering energy to improve the level of efficiency, which answer research question two.

A study of the impact of a loaded generator has been indicated the time needed to stop as well as the recovered energy. Maximum recovered energy with minimum stopping time has been achieved when the UCs storage units are partially empty, and the generated voltage was high at braking, which answers research question three.

Presumably, the ideal situation was that the linear motion of the motor has been not considered. And it was likewise accepted that the vehicle has one motor connected with the gear and that the proportion can be determined. Additionally, there was no friction brake for the blended braking strategies, which was recommended for future work.

The different powertrain has been implemented to achieve the desired performance and to simulate the actual vehicle's behaviours for recovering energy throughout using a simplified control strategy of RB process, which answer research question four.

6.3 Conclusions

The main conclusions can be drawn based on the research work embedded in chapter 3 to 5 inclusive, were summarised in the areas of:

1- The development of test rig It was generally understood that an AC motor with an inverter could inherently include power flow from the machine to the driver when running as a generator. In the same way, the concept of electromechanical energy conversion, represented by a DC motor was based on knowledge with many basic concepts of the electrical, electronic, and mechanical fields upon which the general process depends and was verified.

2- There was an excellent motivation for the development of the designed test rig to be able to provide reliable data in the long run by considering all the factors that have been overlooked from being outside the scope of the current research. And the commitment to the limits of the amounts that have been spent on the aforementioned platform. It can be confirmed that there was still a room to develop the test platform, considering the need to simulate the system realistically to identify the variables that need to be verified.

3- The development of the designed flywheel coupled with the generator in the test rig has been used to clarify the importance of its operation in the energy recovery process as a lumped element based on the characteristic equation of building a test rig component.

4- It was hard for a motor to generate electricity and convey it to the ESU, because of the shortened back emf E_{back} generated when the motor angular speed ω_m was very slow.

5- EVs and HEVs brakes were achieved using electric brakes to ensure smooth operation in speed-up tracking and allow kinetic energy recovery. In contrast, for safety and emergency brake systems, the mechanical brake has been remained essential to ensure system stability.

6- The best battery performance can be achieved by using additional UCs ESU. The UCs has been used to achieve the energy density of cells,

providing almost unlimited lifespan, extending temperature operation and without environmental problems.

7- During the identification of the regenerative process, SoC monitoring can provide useful information to understand the braking process.

8- The researcher sees the possibility of using different storage units that have been studied in the literature to verify the suitability of the application and to explore the possibility of improving the efficiency of the system by increasing the recovery of the amount of lost energy.

9- The EVs propulsion system has consisted of a motor as a power source. From the point of view of literature, there was no perfect engine, because a controller may have an advantage for an application, but with failure in another way. This difference may be because different controllers have unique properties that make them suitable for applications used in various industrial applications.

10- It was noted that the influence of the voltage level state of the UCs storage unit. However, when the UCs at a high state, the need for a conventional friction brake is necessary.

11- It was concluded that the stopping time and energy recovery, which was the most crucial issue, relies upon the state of charge (SoC) of the storage units. Also, the stopping time was depended on the kinetic energy stored in the rotating inertia flywheels, which affect the system operation.

12- An attempt was also made to get a suitable representation of the control energy transfer between different storage units.

6.4 Recommendation for future work

This study explores the energy recovery in small representations of the designed test platform. The fact that the internal construction has a significant impact on this process. Several areas that would warrant further investigation were discussed as follows:

1- Concerning with the first task, there was still an area that must be covered by building an integrated system that represents the EVs as parts identical to the actual reality and on this basis, the need to design blueprints to accommodate this application as a contribution to reducing the costs was not an easy task.
2- More research investigation of the other types of storage units, as described in chapter two, need to be accomplished as components of the RB system. Also, different approaches for measuring the SoC of the storage units need to be introduced to get more proper system behaviour according to task two and three.
3- Develop and study an approach to EMS technologies that should be considered in various aspects, for example, considering the design and representation of the DC-DC converter to become a practical component in the RB analysis.
4- Applying smart control systems, supported by adequate energy storage systems and energy transmission infrastructure. Besides, the design of hybrid systems proposed to be used to solve the complexity of power supplies to meet load requirements.

References

1- A.Laughton, M. (2003) *Renewable Energy Sources Watt Committee Report Number 22*. Taylor & Francis Books, Inc.

2- Abu-Rub, H., Malinowski, M. and Al-Haddad, K. (2014) *POWER ELECTRONICS FOR RENEWABLE ENERGY SYSTEMS, TRANSPORTATION, AND INDUSTRIAL APPLICATIONS*. John Wiley & Sons Ltd Registered.

3- 'ACS712' (no date) *datasheet*, pp. 1–15.

4- Agency, D. & V. S. (no date a) *Electronic Braking Performance Monitoring System Industry Standard Specification*.

5- Agency, D. & V. S. (no date b) *Guide to Electronic Braking Performance Monitoring System (s)*.

6- Ahmad Hamidi, S., Ionel, D. M. and Nasiri, A. (2015) 'Modelling and Management of Batteries and Ultracapacitors for Renewable Energy Support in Electric Power Systems-An Overview', *Electric Power Components and Systems*, 43(12), pp. 1434–1452. doi: 10.1080/15325008.2015.1038757.

7- Ahn, J. K., Jung, K. H., Kim, D. H., Jin, H. B., Kim, H. S. and Hwang, S. H. (2009) 'ANALYSIS OF A REGENERATIVE BRAKING SYSTEM FOR HYBRID ELECTRIC VEHICLES USING AN ELECTRO-MECHANICAL BRAKE', *International Journal of Automotive Technology*, 10(2), pp. 229–234. doi: 10.1007/s12239-009-0027-z.

8- Al-sharif, L. (2016) 'Overview and Comparison of Electrical and Mechanical Braking in Drive Systems', pp. 1–3. doi: 10.13140/RG.2.2.15476.76163.

9- Alamili, A., Xue, Y. and Anayi, F. (2019) 'An experimental and analytical study of the ultra-capacitor storage unit used in regenerative braking systems', *Energy Procedia*. Elsevier B.V., 159, pp. 376–381. doi: 10.1016/j.egypro.2018.12.073.

10- Alamili, A., Xue, Y. and Anayi, F. (2020) 'Laboratory-based examination of the effect of rotational inertia on energy recuperation in the regenerative braking process', *Energy Reports*. Elsevier Ltd, 6, pp. 43–52. doi: 10.1016/j.egyr.2020.02.026.

11- Alexander, C. K. and Sadiku, M. N. O. (2001) *Fundamentals of Electric Circuits*. Third Edit.

12- Andre, D., Appel, C., Soczka-Guth, T. and Sauer, D. U. (2013) 'Advanced mathematical methods of SOC and SOH estimation for lithium-ion batteries', *Journal of Power Sources*. Elsevier B.V, 224, pp. 20–27. doi: 10.1016/j.jpowsour.2012.10.001.

13- ANDREA, J. J. (1970) 'PHASE LOCKED LOOP WITH DIGITAL CAPACITOR AND VARACTOR TUNED OSCILLATOR'.

14- Association, W. N. (2018) *Nuclear power in the United Kingdom, World Nuclear Association.*

15- B&K Precision Corp. (2009) '8500 Series DC Electronic Loads', *B&K Precision Corp.*, p. 76.

16- Bala, B. K. and Siddique, S. A. (2009) 'Optimal design of a PV-diesel hybrid system for electrification of an isolated island-Sandwip in Bangladesh using genetic algorithm', *Energy for Sustainable Development*. International Energy Initiative,

13(3), pp. 137–142. doi: 10.1016/j.esd.2009.07.002.

17- Bao, R. (2015) 'The architecture of pneumatic regenerative systems for the diesel engine', *Phd thesis*.

18- Barin, A., Canha, L. N., Abaide, A. R., Magnago, K. F., Wottrich, B. and Machado, R. Q. (2011) 'Multiple Criteria Analysis for Energy Storage Selection', *Energy and Power Engineering*, 03(04), pp. 557–564. doi: 10.4236/epe.2011.34069.

19- Barlow, T., Latham, S., Mccrae, I. and Boulter, P. (2009) 'A reference book of driving cycles for use in the measurement of road vehicle emissions', *TRL Published Project Report*, p. 280. Available at: http://www.trl.co.uk/online_store/reports_publications/trl_reports/cat_traffic_and_the_environment/report_a_reference_book_of_driving_cycles_for_use_in_the_measurement_of_road_vehicle_emissions.htm%5Cnhttps://www.gov.uk/government/uploads/system/uploads/a.

20- Basha, S. A., Gopal, K. R. and Jebaraj, S. (2009) 'A review on biodiesel production, combustion, emissions and performance', *Renewable and Sustainable Energy Reviews*, 13(6–7), pp. 1628–1634. doi: 10.1016/j.rser.2008.09.031.

21- Bishop, R. H. (2002) *The Mechatronics Handbook, United States of America: University of Texas*. CRC PRESS. doi: 10.2307/1437898.

22- 'BL58 EE-70 Watt' (2001) *Premotec Datasheet*.

23- Bohlin, T. (2006) *Advances in Industrial Control; Practical Grey-box Process Identification Theory and Application*. Springer-Verlag London Limited.

24- Bolund, B., Bernhoff, H. and Leijon, M. (2007) 'Flywheel energy and power storage systems', *Renewable and Sustainable Energy Reviews*, 11(2), pp. 235–258. doi: 10.1016/j.rser.2005.01.004.

25- Bouiabady, M. M., Aliabad, A. D. and Amiri, E. (2017) 'Switched Reluctance Motor Topologies: A Comprehensive Review', in *Switched Reluctance Motor - Concept, Control and Applications*. InTech.

26- Briand, D., Yeatman, E. and Roundy, S. (2015) *Micro Energy Harvesting*. Germany: Wiley-VCH Verlag GmbH & Co.

27- Brown, W. (2002) 'Brushless DC Motor Control Made Easy', *Microchip Technology Inc*, pp. 1–48. Available at: http://ww1.microchip.com/downloads/cn/AppNotes/cn012037.pdf.

28- BU-903 (no date) *Battery University*. Available at: https://batteryuniversity.com/learn/article/how_to_measure_state_of_charge (Accessed: 27 April 2019).

29- Castaings, A., Lhomme, W., Trigui, R. and Bouscayrol, A. (2016) 'Comparison of energy management strategies of a battery/supercapacitors system for electric vehicle under real-time constraints', *Applied Energy*. Elsevier Ltd, 163, pp. 190–200. doi: 10.1016/j.apenergy.2015.11.020.

30- Cathey, J. J. (2002) *Schaum's outline of theory and problems of electronic devices and circuits, Schaum's outline series*. doi: 10.1016/S0026-2692(98)80022-0.

31- Chan, C. C. and Chau, K. T. (2001) *Modern Electric Vehicle Technology*. Oxford Uni.

32- Chapman, S. J. (2012) *ELECTRIC MACHINERY FUNDAMENTALS*. FIFTH EDIT. McGraw-Hill Companies, Inc.

33- Chapman, S. J. and Ninni, G. (2004) *Instructor's Manual to accompany Electric Machinery Fundamentals*. McGraw-Hill, Inc.

34- Chatzivasileiadi, A., Ampatzi, E. and Knight, I. (2013) 'Characteristics of electrical energy storage technologies and their applications in buildings', *Renewable and Sustainable Energy Reviews*, 25, pp. 814–830. doi: 10.1016/j.rser.2013.05.023.

35- Chen, B. C. B., Gao, Y. G. Y., Ehsani, M. and Miller, J. M. (2009) 'Design and control of a ultracapacitor boosted hybrid fuel cell vehicle', 2009 *IEEE Vehicle Power and Propulsion Conference*, pp. 696–703. doi: 10.1109/VPPC.2009.5289783.

36- Chen, Z., Shu, X., Sun, M., Shen, J. and Xiao, R. (2017) 'Charging strategy design of lithium-ion batteries for energy loss minimization based on minimum principle', 2017 *IEEE Transportation Electrification Conference and Expo, Asia-Pacific, ITEC Asia-Pacific 2017*. doi: 10.1109/ITEC-AP.2017.8080833.

37- Chiara, F. and Canova, M. (2013) 'A review of energy consumption, management, and recovery in automotive systems, with considerations of future trends', *Proceedings of the Institution of Mechanical Engineers, Part D: Journal of Automobile Engineering*, 227(6), pp. 914–936. doi: 10.1177/0954407012471294.

38- Chicurel, R. (1999) 'A compromise solution for energy recovery in vehicle braking', *Energy*, 24(12), pp. 1029–1034. doi: 10.1016/S0360-5442(99)00054-7.

39- Chishty, O. and Melis, W. J. C. (2012) 'Energy regeneration from decelerating vehicle', *World Congress on Sustainable Technologies*, WCST 2012, pp. 12–15. Available at: http://www.scopus.com/inward/record.url?eid=2-s2.0-84875944134&partnerID=tZOtx3y1.

40- Choe, Y. Y., Oh, S. Y., Ham, S. H., Jang, I. S., Cho, S. Y., Lee, J. and Ko, K. C. (2012) 'Comparison of concentrated and distributed winding in an IPMSM for vehicle traction', *Energy Procedia*, 14, pp. 1368–1373. doi: 10.1016/j.egypro.2011.12.1103.

41- Chong, A. (2010) 'The Growth of Automotive Electronics in Apace, the Next Frontier', *Driving Asia - As Automotive Electronics Transforms a Region*, pp. 13–27.

42- Chu, L., Sun, W., Yao, L., Zhang, Y., Ou, Y., Wei, W., Liu, M. and Li, J. (2009) 'Integrative control strategy of regenerative and hydraulic braking for hybrid electric car', *5th IEEE Vehicle Power and Propulsion Conference, VPPC '09*, pp. 1091–1098. doi: 10.1109/VPPC.2009.5289726.

43- Cibulka, J. (2009) 'Kinetic Energy Recovery System by means of flywheel energy storage', *Advanced Engineering*, 3(1), pp. 27–38. Available at: http://edu-point.eu/digitaledition/adveng/AE0301/AE0301_027_038.pdf.

44- Clark, T. (no date) *Magnetism, Electricity, and The Baghdad Battery*.

45- Clarke, P., Muneer, T. and Cullinane, K. (2010) 'Cutting vehicle emissions with regenerative braking', *Transportation Research Part D: Transport and Environment*. Elsevier Ltd, 15(3), pp. 160–167. doi: 10.1016/j.trd.2009.11.002.

46- CLEGG, S. J. (1996) *A review of regenerative braking systems, Institute of Transport Studies, University of Leeds, Working Paper 471*. doi: 10.1016/S1366-5545(02)00012-1.

47- Conway, B. E. (1999) *Electrochemical Supercapacitors: Scientific Fundamentals and Technological Applications*. Kluwer Academic/ Plenum.

48- Corporation, N. (2019) *Claw Pole Type PM Motor, Nidec Corporation*. Available at: https://www.nidec.com/en-NA/technology/motor/basic/00031/?prt=1 (Accessed: 23 July 2019).

49- 'Current Transducer' (no date) *LEM datasheet*.

50- Davis, R. I., Company, F. M. and Reger, P. E. A. (1990) 'United States Patent'.

51- Delsing, J., Gustafsson, J., Svensson, M., Lungqvist, L., Elektronik, S. and Fonjallaz, P. (2016) 'Roadmap for Smarter Electronics Systems'.

52- Denton, T. (2004) *Automobile Electrical & Electronic System*. Third Edit. Elsevier Butterworth-Heinemann.

53- Díaz-González, F., Sumper, A., Gomis-Bellmunt, O. and Villafáfila-Robles, R. (2012) 'A review of energy storage technologies for wind power applications', *Renewable and Sustainable Energy Reviews*. Elsevier Ltd, 16(4), pp. 2154–2171. doi: 10.1016/j.rser.2012.01.029.

54- Dixon, J., Bosch, S., Castillo, C. and Mura, M. (2009) 'Ultracapacitors as unique energy storage for a city-car using five-level converter', *IECON Proceedings (Industrial Electronics Conference)*, pp. 3854–3859. doi: 10.1109/IECON.2009.5415362.

55- Dixon, J. W., Ortúzar, M. and Wiechmann, E. (no date) 'Regenerative Braking for an Electric Vehicle Using Ultracapacitors and a Buck-Boost Converter'.

56- Dubey, G. K. (2002) *Fundamentals of Electrical Drive*. Second Eid. Alpha Science International Ltd.

57- Dufo-López, R. and Bernal-Agustín, J. L. (2005) 'Design and control strategies of PV-diesel systems using genetic algorithms', *Solar Energy*, 79(1), pp. 33–46. doi: 10.1016/j.solener.2004.10.004.

58- Dussarrat, J. and Balondrade, G. (2013) *Design of a test bench for battery management*.

59- Ehsani, M., Gao, Y., Longo, S. and Ebrahimi, K. M. (2018) *Modern Electric, Hybrid Electric, and Fuel Cell Vehicles*. Third Edit. Taylor & Francis Group.

60- Ehsani, M., Gao, Y. and Emadi, A. (2009) *Modern Electric, Hybrid Electric, and Fuel Cell Vehicles*. doi: 10.1017/CBO9781107415324.004.

61- Ehsani, M., Gao, Y. and Emadi, A. (2010) *Modern Electric, Hybrid Electric, and Fuel Cell Vehicles Fundamentals, Theory, and Design*. Second Edi. Edited by L. Taylor and Francis Group. USA: CRC Press.

62- EIA (2017) 'International Energy Outlook 2017 Overview', *U.S. Energy Information Administration*, IEO2017(2017), p. 143. doi: www.eia.gov/forecasts/ieo/pdf/0484(2016).pdf.

63- Ekren, O. and Ekren, B. Y. (2010) 'Size optimization of a PV/wind hybrid energy conversion system with battery storage using simulated annealing', *Applied Energy*. Elsevier Ltd, 87(2), pp. 592–598. doi: 10.1016/j.apenergy.2009.05.022.

64- 'Em-206 Brushless Motor Controller' (2010) *Datasheet*.

65- Emadi, A. and Ehsani, M. (2001) 'Multi-converter power electronic systems: Definition and applications', PESC Record - *IEEE Annual Power Electronics Specialists Conference*, 2, pp. 1230–1236. doi: 10.1109/PESC.2001.954287.

66- *Engineering Insider* (2017). Available at: https://engineeringinsider.org/brakes-types/2/ (Accessed: 17 June 2019).

67- Enterprise, D. G. and Munich, I. (2016) 'Study on the Competitiveness of the Electrical and Electronic Engineering Industry Final Report', (December 2013).

68- Erdinc, O. and Uzunoglu, M. (2012) 'Optimum design of hybrid renewable energy systems: Overview of different approaches', *Renewable and Sustainable Energy Reviews*. Elsevier Ltd, 16(3), pp. 1412–1425. doi: 10.1016/j.rser.2011.11.011.

69- Erno Pentzin (2013) 'Direct torque control of AC drive', (July), pp. 58–62. Available at: http://texample.net/tikz/examples/ac-drive-dtc/.

70- Farahani, K. M. (2012) 'Modeling and Analysis of a Flywheel Energy Storage System for Voltage Regulation'.

71- Fei, W.-Z. (2011) 'Permanent magnet synchronous machines with fractional slot and concentrated winding configurations', (January). Available at: http://dspace.lib.cranfield.ac.uk/handle/1826/6150.

72- Fernando, W., Gupta, N., Kamyab, G. and Suheyl, C. O. (2019) 'Feasibility Study of Small-Scale Battery Storage Systems Integrated with Renewable Generation Technologies for Sri Lankan Domestic Applications', 2019 *54th International Universities Power Engineering Conference (UPEC)*. IEEE, pp. 1–7. doi: 10.1109/upec.2019.8893549.

73- Fleurbaey, K., Omar, N., Baghdadi, M. El and Timmermans, J. (2014) 'Analysis of Hybrid Rechargeable Energy Storage Systems in Series Plug-In Hybrid Electric Vehicles Based on Simulations', *Energy and Power Engineering*, 6(August), pp. 195–211. doi: 10.4236/epe.2014.68018.

74- Fontaras, G., Zacharof, N. G. and Ciuffo, B. (2017) 'Fuel consumption and CO2 emissions from passenger cars in Europe – Laboratory versus real-world emissions', *Progress in Energy and Combustion Science*. Elsevier Ltd, 60, pp. 97–131. doi: 10.1016/j.pecs.2016.12.004.

75- Franz, N. L. and Feldhaus, M. (1869) 'Charles Cros, der später als erster die Idee des Phonographen niederschrieb, veröffentlicht 1869 zu Paris eine Schrift " Solution générale du problème de la photographie des couleurs "', pp. 2–3. Available at: https://www.deutsche-digitale-bibliothek.de/item/DLE3SBKHHYY6LKCAW6X6NXXXNOEG6Q25.

76- Gamazo-Real, J. C., Vázquez-Sánchez, E. and Gómez-Gil, J. (2010) 'Position and speed control of brushless dc motors using sensor-less techniques and application

trends', Sensors, 10(7), pp. 6901–6947. doi: 10.3390/s100706901.

77- Gao, L., Dougal, R. a, Member, S. and Liu, S. (2005) 'Power Enhancement of an Actively Controlled Battery / Ultracapacitor Hybrid Power Enhancement of an Actively Controlled Battery / Ultracapacitor Hybrid', 20(1), pp. 236–243.

78- Gao, Y., Chu, L. and Ehsani, M. (2007) 'Design and control principles of hybrid braking system for EV, HEV and FCV', VPPC 2007 - *Proceedings of the 2007 IEEE Vehicle Power and Propulsion Conference*, (1), pp. 384–391. doi: 10.1109/VPPC.2007.4544157.

79- Garnier, H. and Wang, L. (2008) *Advances in Industrial Control series; Identification of Continuous-time Models from Sampled Data*. Springer-Verlag London Limited.

80- GAY, S. E. (2005) *CONTACTLESS MAGNETIC BRAKE FOR AUTOMOTIVE APPLICATIONS*.

81- Gee, A. M. (2012) *Design and Assesment of a Battery-Supercapacitor Hybrid Energy Storage System for Remote Area Wind Power Systems*.

82- Genta, G. (1985) *Kinetic energy storage, Theory and practice of advanced flywheel systems*. Butterwort. doi: 10.1016/B978-0-408-01396-3.50007-2.

83- 'Geothermal' (2013) in *World Energy Resources: Geothermal, World Energy Council*, pp. 1–62.

84- GIERAS, J. F. (2010) 'Permanent magnet motor technology/design and application', in. CRC Press.

85- Glaize, C. and Genies, S. (2013) *Lithium Batteries and Other Electrochemical Storage Systems*. First. ISTE Ltd and JohnWiley & Sons, Inc. doi: 10.1002/9781118761120.ch9.

86- *Global Power Solutions, Power Supply Technical Guide 2010/11* (2010).

87- González-Gil, A., Palacin, R. and Batty, P. (2013) 'Sustainable urban rail systems: Strategies and technologies for optimal management of regenerative braking energy', *Energy Conversion and Management*, 75, pp. 374–388. doi: 10.1016/j.enconman.2013.06.039.

88- González-Longatt, F. M. (2006) 'Circuit Based Battery Models: A Review', *2Do Congreso Iberoamericano De Estudiantes De Ingenieria Electrica*, pp. 1-5.

89- Gorton, G. E., Hebert, D. A. and Gannotti, M. E. (2009) 'Assessment of the kinematic variability among 12 motion analysis laboratories', *Gait and Posture*, 29(3), pp. 398–402. doi: 10.1016/j.gaitpost.2008.10.060.

90- Grbovic, P. J. (2011) 'Ultra-capacitor based regenerative energy storage and power factor correction device for controlled electric drives Dispositif correcteur de facteur de puissance à base de super-condensateur pour variateur de vitesse'. Available at: https://tel.archives-ouvertes.fr/tel-00585405/.

91- Group, T. (no date) *Ultracapacitor & Supercapacitor Frequently Asked Questions*. Available at: https://www.tecategroup.com/products/ultracapacitors/ultracapacitor-FAQ.php (Accessed: 3 August 2019).

92- 'Grundfos Motor Book/ Single phase motors' (no date) in, pp. 18–29 .

93- Guarnieri, M. (2011a) 'When Cars Went Electric, Part 1', *IEEE Industrial Electronics Magazine,* 5(2), pp. 61–62.

94- Guarnieri, M. (2011b) 'When Cars Went Electric, Part 2', *IEEE Industrial Electronics Magazine*. IEEE, 5(2), pp. 46–53.

95- Guideline, A. (2011) *DC Injection Braking*.

96- Gupta, A., Saini, R. P. and Sharma, M. P. (2008) 'Computerized modelling of hybrid energy system - Part I: Problem formulation and model development', *Proceedings of ICECE 2008 - 5th International Conference on Electrical and Computer Engineering*, (December 2008), pp. 7–12. doi: 10.1109/ICECE.2008.4769164.

97- Gupta, A., Saini, R. P. and Sharma, M. P. (2011) 'Modelling of hybrid energy system-Part III: Case study with simulation results', *Renewable Energy*. Elsevier Ltd, 36(2), pp. 474–481. doi: 10.1016/j.renene.2009.04.036.

98- De Haan, P. and Keller, M. (2004) 'Modelling fuel consumption and pollutant emissions based on real-world driving patterns: The HBEFA approach', *International Journal of Environment and Pollution*, 22(3), pp. 240–258.

99- Halit, J. G. W. and Eren, H. (2014) *Measurement, Instrumentation, and Sensors Handbook Electromagnetic, Optical, Radiation, Chemical, and Biomedical Measurement*. SECOND EDI, Measurement, Instrumentation, and Sensors Handbook. SECOND EDI. CRC Press.

100- Han, J., Park, Y. and Park, Y. S. (2011) 'Adaptive regenerative braking control in severe cornering for guaranteeing the vehicle stability of fuel cell hybrid electric vehicle', *2011 IEEE Vehicle Power and Propulsion Conference, VPPC 2011*. doi: 10.1109/VPPC.2011.6043014.

101- Hanselman, D. C. (2006) *Brushless permanent magnet motor design*.

102- Hausmann, A. and Depcik, C. (2013) 'Expanding the Peukert equation for battery capacity modeling through inclusion of a temperature dependency', *Journal of Power Sources*. Elsevier B.V, 235, pp. 148–158. doi: 10.1016/j.jpowsour.2013.01.174.

103- He, H.-W., Xiong, R. and Chang, Y.-H. (2010) 'Dynamic Modeling and Simulation on a Hybrid Power System for Electric Vehicle Applications', *Energies*, 3(11), pp. 1821–1830. doi: 10.3390/en3111821.

104- He, Y. (2014) *The Assessment of Battery-Ultracapacitor Hybrid Energy Storage Systems*.

105- Hedlund, M., Lundin, J., de Santiago, J., Abrahamsson, J. and Bernhoff, H. (2015) 'Flywheel energy storage for automotive applications', *Energies*, 8(10), pp. 10636–10663. doi: 10.3390/en81010636.

106- Herrera, V., Milo, A., Gaztañaga, H., Etxeberria-Otadui, I., Villarreal, I. and Camblong, H. (2016) 'Adaptive energy management strategy and optimal sizing applied on a battery-supercapacitor based tramway', *Applied Energy*. Elsevier Ltd, 169, pp. 831–845. doi: 10.1016/j.apenergy.2016.02.079.

107- Hoo, G. O. H. K. I. M. (2013) 'Investigation of direct-current brushed motor-based energy regenerative automotive damper'.

108- Hughes, A. (2006) *Electric Motors and Drives Fundamentals, Types and*

Applications. Third edit. Elsevier Ltd.

109- Husain, I. (2003) 'Electric and Hybrid Vehicles: Design Fundamentals', *Crc Press*, p. 388. doi: 10.1109/MCD.2005.1517392.

110- Information Portal-reegle (2012) *Iraq (2012) - Policy and Regulatory Overviews - Clean Energy*.

111- Itani, K., De Bernardinis, A., Khatir, Z. and Jammal, A. (2017) 'Comparative analysis of two hybrid energy storage systems used in a two front wheel driven electric vehicle during extreme start-up and regenerative braking operations', *Energy Conversion and Management*. Elsevier Ltd, 144, pp. 69–87. doi: 10.1016/j.enconman.2017.04.036.

112- Jiang, J. and Zhang, C. (2015) 'Battery State Estimation', in *Fundamentals and Applications of Lithium-ion Batteries in Electric Drive Vehicles*. John Wiley & Sons Singapore Pte Ltd. Published 2015 by John Wiley & Sons Singapore Pte Ltd, pp. 43–99.

113- Joerissen, L. and Frey, H. (2009) 'Energy Storage', *Energy*, (492), pp. 215–231. doi: 10.1016/B978-0-12-382036-5.00046-X.

114- Johansson, B. (2005) *DC-DC Converters - Dynamic Model Design and Department of Industrial Electrical Engineering*.

115- Kapoor, R. and Parveen, C. M. (2013) 'Comparative Study on Various KERS', III, pp. 1–5.

116- Karden, E., Ploumen, S., Fricke, B., Miller, T. and Snyder, K. (2007) 'Energy storage devices for future hybrid electric vehicles', *Journal of Power Sources*, 168(1 SPEC. ISS.), pp. 2–11. doi: 10.1016/j.jpowsour.2006.10.090.

117- Kazimierczuk, M. K. (2008) *Pulse-width Modulated DC - DC Power Converters*. doi: 10.1002/9780470694640.

118- Kefayat, M., Lashkar Ara, A. and Nabavi Niaki, S. A. (2015) 'A hybrid of ant colony optimization and artificial bee colony algorithm for probabilistic optimal placement and sizing of distributed energy resources', *Energy Conversion and Management*. Elsevier Ltd, 92, pp. 149–161. doi: 10.1016/j.enconman.2014.12.037.

119- KELJIK, J. (2013) *ELECTRICITY 4: AC/DC MOTORS, CONTROLS, AND MAINTENANCE. 10TH EDITI*. Delmar, Cengage Learning.

120- Kenjo, T. and Nagamor, S. (1985) *Permanent-Magnet and Brushless DC Motors*. Oxford University Pres.

121- Khajepour, A., Fallah, S. and Goodarzi, A. (2014) *ELECTRIC AND HYBRID VEHICLES TECHNOLOGIES, MODELING AND CONTROL: A MECHATRONIC APPROACH*. First edit. John Wiley & Sons Ltd.

122- Khaligh, A. and Li, Z. (2010) 'Battery, ultracapacitor, fuel cell, and hybrid energy storage systems for electric, hybrid electric, fuel cell, and plug-in hybrid electric vehicles: State of the art', *IEEE Transactions on Vehicular Technology*, 59(6), pp. 2806–2814. doi: 10.1109/TVT.2010.2047877.

123- Khaligh, A. and Onar, O. G. (2010) *ENERGY HARVESTING Solar, Wind, and*

Ocean Energy Conversion Systems. Taylor and Francis Group, LLC. doi: 10.1017/CBO9781107415324.004.

124- Kim, B. H., Kwon, O. J., Song, J. S., Cheon, S. H. and Oh, B. S. (2014) 'The characteristics of regenerative energy for PEMFC hybrid system with additional generator', *International Journal of Hydrogen Energy*. Elsevier Ltd, 39(19), pp. 10208–10215. doi: 10.1016/j.ijhydene.2014.03.200.

125- Kim, J. H., Lee, S. J., Kim, E. S., Kim, S. K., Kim, C. H. and Prikler, L. (2014) 'Modelling of battery for EV using EMTP/ATP Draw', *Journal of Electrical Engineering and Technology*, 9(1), pp. 98–105. doi: 10.5370/JEET.2014.9.1.098.

126- Kitanov, S. and Podol'skii, A. (2008) 'Analysis of Eddy-Current and Magnetic Rail Brakes for High-Speed Trains', *The Open Transportation Journal*, 2, pp. 19–28. doi: 10.2174/1874447800802010019.

127- Ko, J., Ko, S., Son, H., Yoo, B., Cheon, J. and Kim, H. (2014) 'Development of Brake System and Regenerative Braking Co-operative Control Algorithm for Automatic Transmission-based Hybrid Electric Vehicle', *IEEE Transactions on Vehicular Technology*, PP (99), pp. 1–1. doi: 10.1109/TVT.2014.2325056.

128- Krein, P. T. (1998) *Elements of Power Electronics*. OXFORD UNIVERSITY PRESS. doi: 10.1049/sqj.1949.0045.

129- Krishan R (2001) *Electric Motor Drives: Modeling Analysis and Control*. Prentice Hall.

130- Krishnan, R. (2010) *Permanent Magnet Synchronous and Brushless DC Motor Drives*. Taylor and Francis Group, LLC.

131- Kusakana, K. (2014) *Optimal Operation Control of Hybrid Renewable Energy Systems*.

132- LAU, E. and LIVINA, V. (2015) 'Carbon savings of demand side response of a UK energy aggregator', *Npl Report Ms 19*, (September).

133- Lee, C.-Y. (2011) *Computational and experimental study of air hybrid engine concepts*.

134- Lee, J. (2005) *Rotating Inertia Impact on Propulsion and Regenerative Braking for Electric Motor Driven Vehicles By Rotating Inertia Impact on Propulsion and Regenerative Braking for Electric Motor Driven Vehicles*.

135- Lee, S., Kim, J., Lee, J. and Cho, B. H. (2008) 'State-of-charge and capacity estimation of lithium-ion battery using a new open-circuit voltage versus state-of-charge', *Journal of Power Sources*, 185(2), pp. 1367–1373. doi: 10.1016/j.jpowsour.2008.08.103.

136- Li, L., Zhang, Y., Yang, C., Yan, B. and Marina Martinez, C. (2016) 'Model predictive control-based efficient energy recovery control strategy for regenerative braking system of hybrid electric bus', *Energy Conversion and Management*. Elsevier Ltd, 111, pp. 299–314. doi: 10.1016/j.enconman.2015.12.077.

137- Li, R., Pottharst, a, Fröhleke, N. and Böcker, J. (2005) 'Design and Implementation of a Hybrid Energy Supply System for Railway Vehicles', *Applied*

Power Electronics Conference and Exposition, 2005. APEC 2005. Twentieth Annual IEEE, pp. 1–7. doi: 10.1109/APEC.2005.1452979.

138- Linden, D. and Reddy, T. B. (2002) *HANDBOOK OF BATTERIES*. Third Edit. Edited by D. Linden and T. B. Reddy. McGraw-Hil. doi: 10.1016/0378-7753(86)80059-3.

139- Liu, H., He, X., Chu, L. and Tian, J. (2011) 'Study on control strategy of regenerative braking for electric bus based on braking comfort', *Proceedings of 2011 International Conference on Electronic and Mechanical Engineering and Information Technology, EMEIT 2011*, 2, pp. 1037–1040. doi: 10.1109/EMEIT.2011.6023184.

140- Liu, K., Li, K., Peng, Q. and Zhang, C. (2019) 'A brief review on key technologies in the battery management system of electric vehicles', *Frontiers of Mechanical Engineering*, 14(1), pp. 47–64. doi: 10.1007/s11465-018-0516-8.

141- Liudvinavičius, L. and Lingaitis, L. P. (2007) 'Electrodynamic braking in high-speed rail transport', *Transport*, 22(3), pp. 176–186. doi: 10.1080/16484142.2007.9638122.

142- Lodha, C. and Shukla, V. (2016) 'Power Management of a Stand-Alone Photovoltaic / Fuel Cell Hybrid Energy System', *International Journal of Scientific Research Engineering & Technology (IJSRET)*, 5(4), pp. 222–226.

143- Long, B., Lim, S. T., Ryu, J. H. and Chong, K. T. (2014) 'Energy-regenerative braking control of electric vehicles using three-phase brushless direct-current motors', *Energies*, 7(1), pp. 99–114. doi: 10.3390/en7010099.

144- Lukic, S. M., Jian, C., Bansal, R. C., Rodriguez, F. and Emadi, a (2008) 'Energy storage systems for automotive applications', *IEEE Transactions on Industrial Electronics*, 55(6), pp. 2258–2267.

145- Luo, F. L. and Ye, H. (2006) *Essential DC/DC Converters*. Edited by L. Taylor & Francis Group .

146- Lv, C., Zhang, J., Li, Y. and Yuan, Y. (2015) 'Mechanism analysis and evaluation methodology of regenerative braking contribution to energy efficiency improvement of electrified vehicles', *Energy Conversion and Management*. Elsevier Ltd, 92, pp. 469–482. doi: 10.1016/j.enconman.2014.12.092.

147- Ma, D. M. and Shiau, J. K. (2011) 'The design of eddy-current magnet brakes', *Transactions of the Canadian Society for Mechanical Engineering*, 35(1), pp. 19–37.

148- Maher, B. (no date) *Ultracapacitor and the Hybrid Electric Vehicle*.

149- Maleki, A., Ameri, M. and Keynia, F. (2015) 'Scrutiny of multifarious particle swarm optimization for finding the optimal size of a PV/wind/battery hybrid system', *Renewable Energy*. Elsevier Ltd, 80, pp. 552–563. doi: 10.1016/j.renene.2015.02.045.

150- Manzer, D. G., Varghese, M. and Thorp, J. S. (1989) 'Variable reluctance motor characterization', *IEEE Transactions on Industrial Electronics*, 36(1), pp. 56–63. doi: 10.1109/41.20345.

151- Masters, G. M. (2004) *Renewable and Efficient Electric Power Systems*. JOHN WILEY & SONS, INC. doi: 10.1002/0471668826.

152- McComb, M. (2007) 'Introduction to Stepper Motors', *Micro Chip Web Seminars*, pp. 1–49.

153- Melnyk, B. and Trokhanyak, S. (2004) *Modeling the work of electrical circuits elements in SIMPLORER environment*, *International Workshop "Computational Problems of Electrical Engineering"*.

154- Mi, C., Masrur, M. A. and Gao, D. W. (2011) *HYBRID ELECTRIC VEHICLES PRINCIPLES AND APPLICATIONS WITH PRACTICAL PERSPECTIVES*. First Edit. John Wiley & Sons, Ltd.

155- Michalczuk, M., Grzesiak, L. M. and Ufnalski, B. (2012) 'A lithium battery and ultracapacitor hybrid energy source for an urban electric vehicle', *Przeglad Elektrotechniczny (Electrical Review)*, (4), pp. 158–162.

156- Microchip Technology Inc. (2017) *Motor Control and Drive Design Solutions*.

157- Midgley, W. J. B., Cathcart, H. and Cebon, D. (2013) 'Modelling of hydraulic regenerative braking systems for heavy vehicles', *Proceedings of the Institution of Mechanical Engineers, Part D: Journal of Automobile Engineering*, 227(7), pp. 1072–1084. doi: 10.1177/0954407012469168.

158- Midgley, W. J. B. and Cebon, D. (2012) 'Comparison of regenerative braking technologies for heavy goods vehicles in urban environments', *Proceedings of the Institution of Mechanical Engineers, Part D: Journal of Automobile Engineering*, 226(7), pp. 957–970. doi: 10.1177/0954407011433395.

159- Milivojevic, N., Krishnamurthy, M., Gurkaynak, Y., Sathyan, A., Lee, Y. J. and Emadi, A. (2012) 'Stability Analysis of FPGA-Based Control of Brushless DC Motors and Generators Using Digital PWM Technique', *IEEE Transactions on Industrial Electronics*, 59(1), pp. 343–351. doi: 10.1109/TIE.2011.2146220.

160- Miller, J. M. (2011) *Ultracapacitor Applications*. First Edit. London, United Kingdom: The Institution of Engineering and Technology. doi: 10.1049/PBPO059E.

161- Mirabadi, A. and Najafi, M. (2011) 'Energy management system in hybrid trains using fuzzy control: A comparative study', *Proceedings of the Institution of Mechanical Engineers, Part F: Journal of Rail and Rapid Transit*, 225(3), pp. 267–276. doi: 10.1243/09544097JRRT397.

162- Miyamasu, M. and Akatsu, K. (2011) 'Efficiency comparison between Brushless dc motor and Brushless AC motor considering driving method and machine design', *IECON 2011 - 37th Annual Conference of the IEEE Industrial Electronics Society*, pp. 1830–1835. doi: 10.1109/IECON.2011.6119584.

163- Moran, M. J., Shapiro, howard n., BoEttnEr, daiSiE d. and BailEy, M. B. (2018) *Fundamentals of Engineering Thermodynamics*. 9th Edit. Wiley.

164- Moselle, B., Padilla, J. and Schmalensee, R. (2010) *Harnessing Renewable Energy in Electric Power Systems - Theory, Practice, Policy*. Edited by First. RFF Press.

165- Muradov, N. Z. and Veziroglu, T. N. (eds) (2012) *CARBON-NEUTRAL FUELS AND ENERGY CARRIERS*. CRC Press.

166- Murthy, A. S., Magee, D. P. and Taylor, D. G. (2015) 'Vehicle braking strategies based on regenerative braking boundaries of electric machines', *2015 IEEE Transportation Electrification Conference and Expo, ITEC 2015*, (3). doi: 10.1109/ITEC.2015.7165809.

167- Murthy, S. S., Berg, G. J., Jha, C. S. and Tandon, A. K. (1984) 'A Novel Method of Multistage Dynamic Braking of Three-Phase Induction Motors', *IEEE Transactions on Industry Applications*, IA-20(2), pp. 328–334. doi: 10.1109/tia.1984.4504415.

168- Mutoh, N. and Akashi, H. (2011) 'Electric and mechanical brake cooperative control method for FRID EVs under various severe road conditions', *IECON Proceedings (Industrial Electronics Conference)*, pp. 4570–4576. doi: 10.1109/IECON.2011.6120063.

169- Nagata, T., Watanabe, H., Ohno, M. and Sasaki, H. (2002) 'A multi-agent approach to power system restoration', *PowerCon 2000 - 2000 International Conference on Power System Technology, Proceedings*, 17(2), pp. 457–462. doi: 10.1109/ICPST.2000.898202.

170- Naseri, F., Farjah, E. and Ghanbari, T. (2017) 'An efficient regenerative braking system based on battery/supercapacitor for electric, hybrid, and plug-in hybrid electric vehicles with BLDC motor', *IEEE Transactions on Vehicular Technology*, 66(5), pp. 3724–3738. doi: 10.1109/TVT.2016.2611655.

171- Nehrir, M. H., Wang, C., Strunz, K., Aki, H., Ramakumar, R., Bing, J., Miao, Z. and Salameh, Z. (2011) 'A review of hybrid renewable/alternative energy systems for electric power generation: Configurations, control, and applications', *IEEE Transactions on Sustainable Energy*, 2(4), pp. 392–403. doi: 10.1109/TSTE.2011.2157540.

172- Ng, K. S., Moo, C. S., Chen, Y. P. and Hsieh, Y. C. (2009) 'Enhanced coulomb counting method for estimating state-of-charge and state-of-health of lithium-ion batteries', *Applied Energy*. Elsevier Ltd, 86(9), pp. 1506–1511. doi: 10.1016/j.apenergy.2008.11.021.

173- Nian, X., Peng, F. and Zhang, H. (2014) 'Regenerative braking system of electric vehicle driven by brushless DC motor', *IEEE Transactions on Industrial Electronics*, 61(10), pp. 5798–5808. doi: 10.1109/TIE.2014.2300059.

174- Niapour, S. A. K. H. M., Garjan, G. H. S. and Shafiei, M. (2015) 'Review of Permanent-Magnet Brushless DC Motor Basic Drives Based on Analysis and Simulation Study', *International Review of Electrical Engineering (I.R.E.E.)*, 9(5), pp. 930–957. doi: 10.13140/RG.2.1.2949.4883.

175- Nidec Corporation (2019) *What Is A Brushless DC Motor?* Available at: https://www.nidec.com/en-NA/technology/motor/basic/00018/ (Accessed: 3 April 2019).

176- O'Sullivan, D., Murray, D., Hayes, J., Egan, M. G. and Lewis, A. W. (2011) 'The Benefits of Device Level Short Term Energy Storage in Ocean Wave Energy Converters', in Carbone, P. R. (ed.) *Energy Storage in the Emerging Era of Smart*

Grids. InTech.

177- Office for Low Emission Vehicles (2013) 'Driving the Future Today - A strategy for ultra-low emission vehicles in the UK', *EVS28 International Electric Vehicle Symposium and Exhibition*, (September), p. 104. Available at: https://www.gov.uk/government/uploads/system/uploads/attachment_data/file/239317/ultra-low-emission-vehicle-strategy.pdf.

178- Omar, N., Daowd, M., Hegazy, O., Bossche, P. Van den, Coosemans, T. and Mierlo, J. Van (2012) 'Electrical double-layer capacitors in hybrid topologies-assessment and evaluation of their performance', *Energies*, 5(11), pp. 4533–4568. doi: 10.3390/en5114533.

179- 'Optical Speed Sensor with Analogue Output Speed Sensors VLS / DA1' (no date) *datasheet*, 44(0), pp. 532544–532544.

180- Ortúzar, M. E. (2005) *Design , Implementation and Evaluation of an Auxiliary Energy System for Electric Vehicles , Based on Ultracapacitors and Buck-Boost Converter Evaluation of an Auxiliary Energy System for Electric Vehicles , Based on Ultracapacitors and Buck-Boost Convert* .

181- Ostadi, A. and Kazerani, M. (2015) 'A Comparative Analysis of Optimal Sizing of Battery-Only, Ultracapacitor-Only, and Battery-Ultracapacitor Hybrid Energy Storage Systems for a City Bus', *IEEE Transactions on Vehicular Technology*, 64(10), pp. 4449–4460. doi: 10.1109/TVT.2014.2371912.

182- Özbay, H. (2000) *Introduction to Feedback Control using Design Studies* .

183- Ozcira, S. and Bekiroglu, N. (2011) 'Direct Torque Control of Permanent Magnet Synchronous Motors', in Lamchich, M. T. (ed.) *Torque Control*. InTech.

184- Papanikolaou, N., Karatzaferis, J., Loupis, M. and Tatakis, E. (2013) 'Theoretical and Experimental Investigation of Brake Energy Recovery in Industrial Loads', *Energy and Power Engineering*, 2013(September), pp. 459–473.

185- Parekh, R. (2003) 'AC Induction Motor Fundamentals', *Microchip Technology Inc*, pp. 1–24. Available at: http://jimfranklin.co.uk/microchipdatasheets/00887a.pdf.

186- Park, G., Lee, S., Jin, S. and Kwak, S. (2014) 'Integrated modeling and analysis of dynamics for electric vehicle powertrains', *Expert Systems with Applications*. Elsevier Ltd, 41(5), pp. 2595–2607. doi: 10.1016/j.eswa.2013.10.007.

187- Passino, K. M. (2001) 'Intelligent Control: An Overview of Techniques', in Samad, T. (ed.) *Perspectives in Control Engineering Technologies, Applications, and New Directions*. IEEE Press, pp. 1–34. doi: 10.1109/9780470545485.ch5.

188- Pay, S. and Baghzouz, Y. (2003) 'Effectiveness of battery-supercapacitor combination in electric vehicles', *2003 IEEE Bologna PowerTech - Conference Proceedings*, 3, pp. 728–733. doi: 10.1109/PTC.2003.1304472.

189- Pillai, S. K. (1989) *A First Course on Electrical Drives*. Second Edi. Wiley eastren limited.

190- Pochiraju, A. (2014) *Design Principles of a Flywheel Regenerative Braking*

System.

191- 'PowerStor XVM Series' (2014) *EATON Datasheet*, (April).

192- Protogeropoulos, C., Brinkworth, B. J. and Marshal, R. H. (1997) 'SIZING AND TECHNO-ECONOMICAL OPTIMIZATION FOR HYBRID SOLAR PHOTOVOLTAIC/WIND POWER SYSTEMS WITH BATTERY STORAGE', *INTERNATIONAL JOURNAL OF ENERGY RESEARCH*, 21, pp. 465–479.

193- R.C., K., P.T., K., Kroeze, R. C. and Krein, P. T. (2008) 'Electrical battery model for use in dynamic electric vehicle simulations', *Power Electronics Specialists Conference, 2008. PESC 2008. IEEE*, pp. 1336–1342. doi: 10.1109/PESC.2008.4592119.

194- Rachel Carnegie, Gotham, D., Nderitu, D. and Preckel, P. V. (2013) *Utility Scale Energy Storage Systems: Benefits, Applications, and Technologies*.

195- Rajashekara, Ashoka K. S. Bhat, B. K. (2000) 'Power Electronics', in *The Electrical Engineering Handbook*, p. 44.

196- Rashid, M. H. (ed.) (2018) *POWER ELECTRONICS HANDBOOK*. Fourth Edi. Elsevier Inc.

197- 'REC 10-12' (2008) *Data sheet*, pp. 1–2.

198- Ren, G., Ma, G. and Cong, N. (2015) 'Review of electrical energy storage system for vehicular applications', *Renewable and Sustainable Energy Reviews*. Elsevier, 41, pp. 225–236. doi: 10.1016/j.rser.2014.08.003.

199- REN, Q. (2010) *Numerical Analysis and Modelling of Transmission Systems for Hybrid Electric Vehicles and Electric Vehicles*.

200- Reston Condit (2004) 'Brushed DC Motor Fundamentals', *Microchip Technology Inc.*, pp. 1–10.

201- Reston Condit and Jones, D. W. (2004) *Stepper Motor Fundamentals*. Available at: https://www.islproducts.com/designnote/stepper-motor-fundamentals/.

202- Ribeiro, P. F., Johnson, B. K., Crow, M. L., Arsoy, and Liu, Y. (2001) 'Energy storage systems for advanced power applications', *Proceedings of the IEEE*, 89(12), pp. 1744–1756. doi: 10.1109/5.975900.

203- Roberts, A., Thomas, B., Sewell, P., Khan, Z., Balmain, S. and Gillman, J. (2016) 'Current tidal power technologies and their suitability for applications in coastal and marine areas', *Journal of Ocean Engineering and Marine Energy*. Springer International Publishing, 2(2), pp. 227–245. doi: 10.1007/s40722-016-0044-8.

204- Roberts, S. (2014) *DC/DC Book of Knowledge Practical tips for the User*. First Edit, *Recom*. First Edit. Available at: https://www.schukat.com/schukat/pdf.nsf/EC53E983176DF812C1257E6200395568/$file/Recom_Book_of_Knowledge_English.pdf.

205- Rodriguez, F. and Emadi, A. (2007) 'A Novel Digital Control Technique for Brushless DC Motor Drives', *IEEE Transactions on Industrial Electronics*, 54(5), pp. 2365–2373. doi: 10.1109/TIE.2007.900312.

206- Roscher, M. A. and Sauer, D. U. (2011) 'Dynamic electric behaviour and open-

circuit-voltage modeling of LiFePO 4-based lithium-ion secondary batteries', *Journal of Power Sources*. Elsevier B.V., 196(1), pp. 331–336. doi: 10.1016/j.jpowsour.2010.06.098.

207- RS Pro Brushless DC Motor, 536-6030 *data sheet* (no date).

208- RS Pro Brushless DC Motor, 892-8779 *data sheet* (no date).

209- Saichand, K. and John, V. (2017) 'Simplified modeling of ultracapacitors for bidirectional DC-DC converter applications', Conference Proceedings - *IEEE Applied Power Electronics Conference and Exposition - APEC*, (2), pp. 3134–3141. doi: 10.1109/APEC.2017.7931145.

210- Sakka, M. Al, Gualous, H. and Omar, N. (2012) 'Batteries and Supercapacitors for Electric Vehicles', in *New Generation of Electric Vehicles*, pp. 135–164. doi: 10.5772/53490.

211- Sangdehi, S. M. M. (2015) *Optimal Design of Battery-Ultracapacitor Hybrid Source Light / Heavy Electrified Vehicle*.

212- Sangpanich, U. (2013) *Optimization of Wind-Solar Energy Systems using Low Wind Speed Turbines to Improve Rural Electrification*.

213- Sangtarash, F., Esfahanian, V., Nehzati, H., Haddadi, S., Bavanpour, M. A. and Haghpanah, B. (2008) 'Effect of Different Regenerative Braking Strategies on Braking Performance and Fuel Economy in a Hybrid Electric Bus Employing CRUISE Vehicle Simulation', *SAE International Journal of Fuels and Lubricants*, 1(1), pp. 828–837. doi: 10.4271/2008-01-1561.

214- Sawle, Y., Gupta, S. C. and Bohre, A. K. (2017) 'Review of hybrid renewable energy systems with comparative analysis of off-grid hybrid system', *Renewable and Sustainable Energy Reviews*. Elsevier Ltd, (June), pp. 1–19. doi: 10.1016/j.rser.2017.06.033.

215- Sebastián, R. and Peña-Alzola, R. (2015) 'Control and simulation of a flywheel energy storage for a wind diesel power system', *International Journal of Electrical Power and Energy Systems*, 64, pp. 1049–1056. doi: 10.1016/j.ijepes.2014.08.017.

216- Sen, B., Ercan, T. and Tatari, O. (2017) 'Does a battery-electric truck make a difference? – Life cycle emissions, costs, and externality analysis of alternative fuel-powered Class 8 heavy-duty trucks in the United States', *Journal of Cleaner Production*. Elsevier Ltd, 141, pp. 110–121. doi: 10.1016/j.jclepro.2016.09.046.

217- SEN, P. C. (2013) *PRINCIPLES OF ELECTRIC MACHINES AND POWER ELECTRONICS*. THIRD EDIT. John Wiley & Sons.

218- Senty, S. (2013) *Motor Control Fundamentals*. Delmar, Cengage Learning.

219- Serteller, N. F. O. and Ustundag, D. (2017) 'Analysis of dynamic behaviour of direct current motor with electrical braking techniques', *2017 CHILEAN Conference on Electrical, Electronics Engineering, Information and Communication Technologies, CHILECON 2017-Proceedings*, 2017-Janua, pp. 1–7. doi: 10.1109/CHILECON.2017.8229542.

220- Shan, X. Y., Wang, Y., Wang, D. W., Weng, Z., Li, F. and Cheng, H. M. (2015)

'A smart self-regenerative lithium-ion supercapacitor with a real-time safety monitor', *Energy Storage Materials*. Elsevier, 1, pp. 146–151. doi: 10.1016/j.ensm.2015.10.001.

221- Sharma, P. and Bhatti, T. S. (2010) 'A review on electrochemical double-layer capacitors', *Energy Conversion and Management*. Elsevier Ltd, 51(12), pp. 2901–2912. doi: 10.1016/j.enconman.2010.06.031.

222- Shen, J. (2016) *ENERGY MANAGEMENT OF BATTERY-ULTRACAPACITOR HYBRID ENERGY STORAGE SYSTEM*.

223- Shen, P. K., Wang, C.-Y., Xueliang, S. P. J., Sun, X. and Zhang, J. (eds) (2016) *Electrochemical ENERGY Advanced Materials and and Technologies*. Taylor & Francis Group .

224- Shi, L. and Crow, M. (2008) 'Comparison of ultracapacitor electric circuit models', in *Proceedings of the IEEE Power & Energy Society General Meeting*. Pittsburgh, PA, pp. 1–6. Available at: http://ieeexplore.ieee.org/abstract/document/4596576/ (Accessed: 18 January 2018).

225- Singh, A. (2015) *Ultracapacitor Characterization Using a Novel Dynamic Parameter Identification Modelling Technique for Electric Transportation Applications*.

226- Singh, G. K. (2013) 'Solar power generation by PV (photovoltaic) technology: A review', *Energy*. Elsevier Ltd, 53, pp. 1–13. doi: 10.1016/j.energy.2013.02.057.

227- Skvarenina, T. L. (2002) *The Power Electronics Handbook* - Industrial electronics series.

228- Solano Martínez, J. (2012) *Energy management of a hybrid electric vehicle: an approach based on type-2 fuzzy logic* .

229- Song, Z., Li, J., Han, X., Xu, L., Lu, L., Ouyang, M. and Hofmann, H. (2014) 'Multi-objective optimization of a semi-active battery/supercapacitor energy storage system for electric vehicles', *Applied Energy*. Elsevier Ltd, 135, pp. 212–224. doi: 10.1016/j.apenergy.2014.06.087.

230- Song, Z., Hou, J., Hofmann, H., Li, J. and Ouyang, M. (2017) 'Sliding-mode and Lyapunov function-based control for battery/supercapacitor hybrid energy storage system used in electric vehicles', *Energy*. Elsevier Ltd, 122, pp. 601–612. doi: 10.1016/j.energy.2017.01.098.

231- Spyker, R. L. (2000) 'Classical equivalent circuit parameters for a double-layer capacitor', *IEEE Transactions on Aerospace and Electronic Systems*, 36(3 PART 1), pp. 829–836. doi: 10.1109/7.869502.

232- Stephen L. Herman (2011) *Delmar's Standard Textbook of Electricity*. 5th Edit. Delmar, Cengage Learning .

233- *Technical guide No. 8 - Electrical Braking* (2018). Available at: http://www05.abb.com/global/scot/scot201.nsf/veritydisplay/6866afe6c69df93dc1257888004521e1/$file/abb_technical guide no.8_revb.pdf.

234- Theraja, B. L. and Theraja, A. K. (2005) *A TEXTBOOK OF ELECTRICAL TECHNOLOGY ALL VOLUME BASIC ELECTRICAL ENGINEERING IN S.I. SYSTEM OF UNITS*. S. CHAND & COMPANY LTD.

235- Thoolen, F. (1993) *Development of an Advanced High-Speed Flywheel Energy Storage System*. doi: 10.6100/IR406829.

236- Tie, S. F. and Tan, C. W. (2013) 'A review of energy sources and energy management system in electric vehicles', *Renewable and Sustainable Energy Reviews*. Elsevier, 20, pp. 82–102. doi: 10.1016/j.rser.2012.11.077.

237- Tremblay, O., Ieee, M., Dessaint, L., Ieee, S. M. and Dekkiche, A. (2007) 'A Generic Battery Model for the Dynamic Simulation of Hybrid Electric Vehicles', *Electrical Engineering*, (V), pp. 284–289. doi: 10.1109/VPPC.2007.4544139.

238- Tur, O., Ustun, O. and Tuncay, R. N. (2007) 'An Introduction to Regenerative Braking of Electric Vehicles as Anti-Lock Braking System', *2007 IEEE Intelligent Vehicles Symposium*, (5), pp. 944–948. doi: 10.1109/IVS.2007.4290238.

239- Turkenburg, W., Arent, D. J. and Bertani, R. (2010) 'Renewable Energy', in, pp. 761–900.

240- Tushnet, M. (2000) 'CAPACITOR BRAKING', in, pp. 74–91. doi: 10.5860/CHOICE.37-1220.

241- U.S. Energy Information Administration (EIA) (2019) 'Country Analysis Executive Summary: Iraq', p. 9. Available at: https://www.eia.gov/beta/international/analysis_includes/countries_long/Iran/pdf/iran_exe.pdf.

242- *Ultra-capacitors* (2019). Available at: https://www.electronics-tutorials.ws/capacitor/ultracapacitors.html.

243- Un-Noor, F., Padmanaban, S., Mihet-Popa, L., Mollah, M. N. and Hossain, E. (2017) 'A comprehensive study of key electric vehicle (EV) components, technologies, challenges, impacts, and future direction of development', *Energies*, 10(8), pp. 1–82. doi: 10.3390/en10081217.

244- UNECE (2012) *ECONOMIC COMMISSION FOR EUROPE World Forum for Harmonization of Vehicle Regulations (WP.29); How it works, how to join it*. Third edit. Available at: http://www.unece.org/trans/welcome.html.

245- Upadhyay, S. and Sharma, M. P. (2014) 'A review on configurations, control and sizing methodologies of hybrid energy systems', *Renewable and Sustainable Energy Reviews*. Elsevier, 38, pp. 47–63. doi: 10.1016/j.rser.2014.05.057.

246- 'USER GUIDE NI USB-6008/6009 Bus-Powered Multifunction DAQ USB Device' (no date) *User Guide*, pp. 1–26. Available at: http://www.ni.com/pdf/manuals/371303n.pdf.

247- *Variable Speed Drives and Motors - Installation Guidelines for Power Drive Systems* (2012).

248- Vodovozov, V. (2012) *Electric Drive Systems and Operation*.

249- 'World Oil Review' (2018) Oil & Gas, 1.

250- Wright, M. M., Daugaard, D. E., Satrio, J. A. and Brown, R. C. (2010) 'Techno-economic analysis of biomass fast pyrolysis to transportation fuels', *Fuel*. Elsevier Ltd, 89(SUPPL. 1), pp. S2–S10. doi: 10.1016/j.fuel.2010.07.029.

251- Xia, C. (2012) *Permanent Magnet Brushless DC Motor Drives and Controls*. John Wiley & Sons Singapore Pte. Ltd. doi: 10.1002/9781118188347.

252- Xie, S., Feng, J. and Zhang, G. (2012) 'Study on simulation traction load with regenerative braking', *Energy Procedia*, 14, pp. 1299–1304. doi: 10.1016/j.egypro.2011.12.887.

253- Xu, J. and Cao, B. (2015) 'Battery Management System for Electric Drive Vehicles – Modelling, State Estimation and Balancing', in *New Applications of Electric Drives*. InTech.

254- Yang, X. (2012) 'Energy recovery efficiency of flow-coupled flywheel vehicle', *Research Journal of Applied Sciences, Engineering and Technology*, 4(17), pp. 2905–2910.

255- Yang, X., Li, H., Jiang, Z., Wang, H. and Yin, Z. (2013) 'Review on Application of Hybrid Energy Storage Based on Ultracapacitor', *Proceedings of the 2nd International Conference on Systems Engineering and Modelling*, pp. 315–318. doi: 10.2991/icsem.2013.60.

256- Yedamale, P. (2003) *Brushless DC (BLDC) Motor Fundamentals, Microchip Technology Inc*.

257- Yeo, H., Hwang, S. and Kim, H. (2006) 'Regenerative braking algorithm for a hybrid electric vehicle with CVT ratio control', *Proceedings of the Institution of Mechanical Engineers, Part D: Journal of Automobile Engineering*, 220(11), pp. 1589–1600. doi: 10.1243/09544070JAUTO304.

258- Yong, J. Y., Ramachandaramurthy, V. K., Tan, K. M. and Mithulananthan, N. (2015) 'A review on the state-of-the-art technologies of electric vehicle, its impacts and prospects', *Renewable and Sustainable Energy Reviews*. Elsevier, 49, pp. 365–385. doi: 10.1016/j.rser.2015.04.130.

259- Yoong, M. K., Gan, Y. H., Gan, G. D., Leong, C. K., Phuan, Z. Y., Cheah, B. K. and Chew, K. W. (2010) 'Studies of regenerative braking in electric vehicle', *IEEE Conference on Sustainable Utilization and Development in Engineering and Technology 2010, STUDENT 2010 - Conference Booklet*, (November), pp. 40–45. doi: 10.1109/STUDENT.2010.5686984.

260- Yuan, X., Liu, H. and Zhang, J. (eds) (2011) *Lithium - Ion Batteries: Advanced Materials and Technologies*. Taylor & Francis Group .

261- ZAINI (2012) *CONTROL STRATEGIES FOR BLENDED BRAKING IN ROAD VEHICLES*.

262- Zeraoulia, M., Benbouzid, M., Diallo, D., Zeraoulia, M., Member, Student, El, M., Benbouzid, H. and Member, Senior (2010) 'Electric motor drive selection issues for HEV propulsion systems : A comparative study', *IEEE Transactions on Vehicular Technology*, 55(6), pp. 1756–1764. doi: 10.1109/TVT.2006.878719.

263- Zhang, J., Lv, C., Gou, J. and Kong, D. (2012) 'Cooperative control of

regenerative braking and hydraulic braking of an electrified passenger car', *Proceedings of the Institution of Mechanical Engineers, Part D: Journal of Automobile Engineering*, 226(10), pp. 1289–1302. doi: 10.1177/0954407012441884.

264- Zhang, L., Hu, X., Wang, Z., Sun, F. and Dorrell, D. G. (2018) 'A review of supercapacitor modelling, estimation, and applications: A control/management perspective', *Renewable and Sustainable Energy Reviews*. Elsevier Ltd, 81(February 2017), pp. 1868–1878. doi: 10.1016/j.rser.2017.05.283.

265- Zhang, Q. and Deng, W. (2016) 'An adaptive energy management system for electric vehicles based on driving cycle identification and wavelet transform', *Energies*, 9(5). doi: 10.3390/en9050341.

266- Zhang, S., Xiong, R. and Zhou, X. (2015) 'Comparison of the topologies for a hybrid energy-storage system of electric vehicles via a novel optimization method', *Science China Technological Sciences*, 58(7), pp. 1173–1185. doi: 10.1007/s11431-015-5843-y.

267- Zhang, W., Han, Y. and Li, F. (2007) 'Braking Energy Regeneration System of Buses Based on Compressed Air Energy Storage', pp. 404–412.

268- Zhang, X., Zhang, Z., Pan, H., Salman, W., Yuan, Y. and Liu, Y. (2016) 'A portable high-efficiency electromagnetic energy harvesting system using supercapacitors for renewable energy applications in railroads', *Energy Conversion and Management*. Elsevier Ltd, 118, pp. 287–294. doi: 10.1016/j.enconman.2016.04.012.

269- Zhang, Z., Zhang, X., Chen, W., Rasim, Y., Salman, W., Pan, H., Yuan, Y. and Wang, C. (2016) 'A high-efficiency energy regenerative shock absorber using supercapacitors for renewable energy applications in range extended electric vehicle', *Applied Energy*. Elsevier Ltd, 178, pp. 177–188. doi: 10.1016/j.apenergy.2016.06.054.

270- Zhao, J. and Yangwei, Y. (2011) 'Brushless DC Motor Fundamentals Application Note', *MPS, The future of Analog IC Technology*, (July 2011), pp. 7–8.

271- Zhao, X., Sánchez, B. M., Dobson, P. J. and Grant, P. S. (2011) 'The role of nanomaterials in redox-based supercapacitors for next generation energy storage devices', *Nanoscale*, 3(3), pp. 839–855. doi: 10.1039/c0nr00594k.

272- Zhao, Y. (2016) 'Characteristic Parameters Identification of Hybrid Supercapacitor with Aqueous Electrolyte Under Combined Effect of Current and Temperature', in *International Conference on Electronic Information Technology and Intellectualization (ICEITI 2016)*, pp. 354–359.

273- Zhou, T. (2009) *Control and Energy Management of a Hybrid Active Wind Generator including Energy Storage System with Super-capacitors and Hydrogen technologies for Microgrid Application*.

274- Zhou, Y. L. (2008) *Modelling and simulation of hybrid electric vehicles*.

275- Zhu, D. (2011) 'Vibration Energy Harvesting: Machinery Vibration, Human Movement and Flow-Induced Vibration', in *SUSTAINABLE ENERGY HARVESTING*

TECHNOLOGIES – PAST, pp. 25–54. doi: 10.1002/cne.23430.

276- Ziemann, V. (2018) *A Hands-On Course in Sensors Using the Arduino and Raspberry Pi*. Taylor & Francis Group, LLC.

277- Zou, Y., Hu, X., Ma, H. and Li, S. E. (2015) 'Combined State of Charge and State of Health estimation over lithium-ion battery cell cycle lifespan for electric vehicles', *Journal of Power Sources*. Elsevier B.V, 273, pp. 793–803. doi: 10.1016/j.jpowsour.2014.09.146.

278- Zuo, L. and Tang, X. (2013) 'Large-scale vibration energy harvesting', *Journal of Intelligent Material Systems and Structures*, 24(11), pp. 1405–1430. doi: 10.1177/1045389X13486707.

Appendices

Table 1: Specific parts of data extracted as it represented in Figure (5.45) shown on page 207.

X_Value	Speed (rpm)	V_{UCs} (V)	I_{UCs} (A)	X_Value	Speed (rpm)	V_{UCs} (V)	I_{UCs} (A)
0	0.061	0.097	0.192	25	1.499	0.097	0.398
0.1	0.061	0.097	1.223	25.1	1.499	0.097	0.398
0.2	0.061	0.097	1.532	25.2	1.499	0.097	0.398
0.3	0.091	0.097	3.800	25.3	1.499	0.097	0.398
0.4	0.091	0.0974	9.367	25.4	1.499	0.097	0.398
0.5	0.091	0.0974	2.460	25.5	1.499	0.097	0.295
0.6	0.214	0.0974	6.480	25.6	1.499	0.097	0.295
0.7	0.326	0.0974	8.954	25.7	1.499	0.097	0.089
0.8	0.326	0.0974	5.552	25.8	1.499	0.097	0.192
0.9	0.407	0.0974	2.563	25.9	1.499	0.097	0.295
1	0.469	0.0974	1.326	26	1.499	0.097	0.295
1.1	0.520	0.0974	4.625	26.1	1.499	0.097	0.398
1.2	0.571	0.0974	5.140	26.2	1.499	0.097	0.398
1.3	0.622	0.0974	5.759	26.3	1.499	0.097	0.398
1.4	0.662	0.0974	4.109	26.4	1.499	0.097	0.192
1.5	0.703	0.0974	7.820	26.5	1.499	0.097	0.192
1.6	0.744	0.0974	9.882	26.6	1.499	0.097	0.295
1.7	0.815	0.0974	9.264	26.7	1.499	0.097	0.295
1.8	0.836	0.0974	8.954	26.8	1.499	0.097	0.295
1.9	0.907	0.0974	2.254	26.9	1.499	0.097	0.295
2	0.938	0.0974	2.563	27	1.499	0.097	0.192
2.1	0.989	0.0974	5.759	27.1	1.499	0.097	0.192
2.2	1.040	0.0974	7.614	27.2	1.499	0.097	0.398
2.3	1.080	0.0974	4.006	27.3	1.499	0.097	0.295
2.4	1.101	0.0974	3.491	27.4	1.499	0.097	0.398
2.5	1.142	0.0974	3.078	27.5	1.499	0.097	0.398
2.6	1.172	0.0974	2.872	27.6	1.499	0.097	0.295
2.7	1.203	0.0974	3.697	27.7	1.499	0.097	0.295
2.8	1.22	0.0974	3.181	27.8	1.499	0.097	0.295
2.9	1.244	0.0974	3.491	27.9	1.499	0.097	0.192
3	1.274	0.097	2.047	28	1.499	0.097	0.192

3.1	1.284	0.097	2.666	28.1	1.499	0.097	0.192
3.2	1.305	0.097	1.841	28.2	1.499	0.097	-0.013
3.3	1.315	0.097	2.151	28.3	1.499	0.097	0.398
3.4	1.325	0.097	1.635	28.4	1.488	1.255	-7.229
3.5	1.356	0.097	1.635	28.5	1.468	1.097	-6.405
3.6	1.356	0.097	1.429	28.6	1.448	1.149	-6.405
3.7	1.366	0.097	2.047	28.7	1.407	1.149	-6.199
3.8	1.376	0.097	1.326	28.8	1.386	1.149	-6.50
3.9	1.386	0.097	1.429	28.9	1.366	1.149	-6.405
4	1.397	0.097	1.326	29	1.325	1.149	-6.199
4.1	1.407	0.097	0.913	29.1	1.305	1.149	-5.992
4.2	1.407	0.097	0.913	29.2	1.274	1.149	-5.889
4.3	1.417	0.097	0.707	29.3	1.244	1.149	-5.580
4.4	1.427	0.097	0.913	29.4	1.223	1.149	-5.889
4.5	1.427	0.097	1.017	29.5	1.203	1.149	-5.786
4.6	1.437	0.097	0.604	29.6	1.172	1.044	-5.065
4.7	1.448	0.097	1.017	29.7	1.152	1.044	-5.168
4.8	1.448	0.097	0.604	29.8	1.121	0.992	-4.755
4.9	1.448	0.097	0.913	29.9	1.101	1.044	-4.858
5	1.448	0.097	0.604	30	1.080	0.992	-4.549
0	0.071	0.097	0.192	30.1	1.060	1.044	-4.858
0.1	0.061	0.097	1.223	30.2	1.040	0.992	-4.343
0.2	0.061	0.097	1.532	30.3	1.009	1.044	-4.549
0.3	0.091	0.097	3.800	30.4	0.999	1.044	-4.549
0.4	0.091	0.097	9.367	30.5	0.978	0.939	-3.828
0.5	0.091	0.097	2.460	30.6	0.948	0.939	-3.828

Table 2: Part of the data extracted as it represented in Figure (5.50) shown on page 211.

X_Value		Speed (rpm)		Generator voltage (V)		UC voltage (V)	
Simul.	Exp.	Simul.	Exp.	Simul.	Exp.	Simul.	Exp.
0	0	3	3.008	14.765	13.765	1.834	1.834
0.099	0.072	2.994	2.99	14.735	13.712	1.836	1.992
0.200	0.123	2.986	2.998	14.690	13.660	1.838	1.992
0.299	0.222	2.976	2.987	14.640	13.607	1.840	1.99
0.400	0.323	2.966	2.977	14.587	13.660	1.842	1.992
0.500	0.425	2.956	2.967	14.533	13.554	1.844	1.992
0.599	0.523	2.946	2.957	14.479	13.554	1.846	1.992
0.700	0.624	2.936	2.947	14.426	13.449	1.847	1.992
0.799	0.722	2.926	2.947	14.373	13.396	1.849	1.992
0.900	0.824	2.916	2.936	14.321	13.29	1.851	1.992
1	0.9238	2.906	2.916	14.268	13.291	1.853	1.992
1.099	1.0518	2.896	2.916	14.216	13.291	1.855	1.992
1.200	1.125	2.886	2.906	14.163	13.291	1.857	1.992
1.299	1.223	2.877	2.896	14.111	13.291	1.859	1.992
1.400	1.324	2.867	2.885	14.058	13.185	1.861	1.992
1.500	1.423	2.857	2.875	14.00	13.132	1.863	1.992
1.599	1.522	2.847	2.865	13.954	13.132	1.865	1.992
1.700	1.623	2.837	2.865	13.902	13.132	1.867	1.992
1.799	1.724	2.827	2.855	13.850	13.080	1.868	1.992
1.900	1.823	2.818	2.845	13.800	12.974	1.870	1.992
2	1.924	2.808	2.834	13.749	12.974	1.872	1.992
2.099	2.023	2.799	2.834	13.699	12.974	1.874	1.992
2.200	2.124	2.789	2.824	13.649	12.921	1.876	2.044
2.299	2.223	2.780	2.814	13.599	12.869	1.877	2.044
2.400	2.324	2.771	2.804	13.549	12.869	1.879	1.992
2.500	2.425	2.761	2.794	13.499	12.816	1.881	2.044
2.599	2.522	2.752	2.783	13.449	12.763	1.883	2.044
2.700	2.625	2.742	2.783	13.399	12.763	1.885	1.992
2.799	2.723	2.733	2.773	13.349	12.658	1.886	2.044
2.900	2.824	2.724	2.763	13.300	12.605	1.888	1.992
3	2.922	2.714	2.753	13.250	12.658	1.890	1.992
3.099	3.022	2.705	2.743	13.202	12.499	1.892	2.0446

3.200	3.125	2.696	2.743	13.154	12.499	1.893	1.992
3.299	3.223	2.687	2.732	13.106	12.447	1.895	2.044
3.400	3.324	2.678	2.722	13.058	12.447	1.897	2.044
3.500	3.423	2.669	2.712	13.011	12.394	1.898	2.044
3.599	3.524	2.660	2.702	12.963	12.394	1.9006	2.044
3.700	3.625	2.651	2.702	12.915	12.341	1.902	2.044
3.799	3.724	2.642	2.692	12.868	12.236	1.904	2.044
3.900	3.823	2.633	2.681	12.820	12.236	1.905	2.044
4	3.922	2.624	2.671	12.773	12.288	1.907	2.044
4.099	4.024	2.615	2.671	12.725	12.183	1.909	2.044
4.200	4.125	2.606	2.66	12.678	12.183	1.910	2.044
4.299	4.224	2.597	2.651	12.631	12.025	1.912	2.044
4.400	4.325	2.589	2.641	12.585	12.077	1.914	2.044
4.500	4.423	2.58	2.630	12.540	12.025	1.915	2.044
4.599	4.523	2.572	2.630	12.494	11.972	1.9173	2.044
4.700	4.624	2.563	2.620	12.449	11.972	1.918	2.044
4.799	4.724	2.554	2.610	12.403	11.866	1.920	2.044
4.900	4.825	2.546	2.600	12.358	11.919	1.922	2.044
5	4.923	2.537	2.600	12.313	11.866	1.923	2.044
5.099	5.023	2.529	2.590	12.268	11.814	1.925	2.044
5.200	5.1240	2.520	2.579	12.223	11.708	1.926	2.044
5.299	5.224	2.512	2.569	12.177	11.761	1.928	2.044
5.400	5.323	2.503	2.569	12.132	11.708	1.930	2.044
5.500	5.424	2.495	2.559	12.088	11.603	1.931	2.044
5.599	5.523	2.486	2.549	12.0431	11.603	1.933	2.044
5.700	5.624	2.478	2.539	11.998	11.603	1.934	2.097
5.799	5.724	2.470	2.539	11.955	11.497	1.936	2.044
5.900	5.823	2.462	2.528	11.912	11.392	1.937	2.097
6	5.924	2.453	2.518	11.868	11.392	1.939	2.044
6.099	6.023	2.445	2.508	11.825	11.444	1.940	2.044
6.200	6.125	2.437	2.508	11.7828	11.392	1.942	2.044
6.299	6.224	2.429	2.498	11.739	11.339	1.943	2.044
6.400	6.323	2.421	2.488	11.697	11.286	1.945	2.044
6.500	6.422	2.413	2.477	11.654	11.286	1.946	2.044
6.599	6.523	2.405	2.477	11.611	11.181	1.948	2.097

6.700	6.624	2.397	2.467	11.568	11.181	1.949	2.044
6.799	6.724	2.389	2.467	11.526	11.181	1.951	2.097
6.900	6.823	2.381	2.457	11.483	11.181	1.952	2.097
7	6.923	2.373	2.447	11.441	11.075	1.954	2.097
7.099	7.024	2.365	2.447	11.398	11.022	1.955	2.097
7.200	7.124	2.357	2.426	11.356	11.022	1.957	2.097
7.299	7.222	2.349	2.426	11.315	10.970	1.958	2.097
7.400	7.324	2.341	2.416	11.274	10.917	1.960	2.097
7.500	7.424	2.334	2.416	11.234	10.917	1.961	2.097
7.599	7.524	2.326	2.406	11.193	10.864	1.963	2.097
7.700	7.624	2.318	2.396	11.152	10.811	1.964	2.097
7.799	7.725	2.311	2.386	11.112	10.811	1.965	2.097
7.900	7.824	2.303	2.386	11.072	10.759	1.967	2.097
8	7.922	2.295	2.375	11.031	10.706	1.968	2.097
8.099	8.023	2.288	2.365	10.991	10.706	1.970	2.097
8.200	8.124	2.280	2.365	10.951	10.600	1.971	2.097
8.299	8.223	2.273	2.355	10.910	10.653	1.972	2.097
8.400	8.323	2.265	2.345	10.870	10.600	1.974	2.097
8.500	8.423	2.258	2.345	10.830	10.548	1.975	2.097
8.599	8.524	2.250	2.335	10.790	10.495	1.977	2.097
8.700	8.625	2.242	2.335	10.750	10.442	1.978	2.097
8.799	8.723	2.235	2.325	10.712	10.442	1.979	2.097
8.900	8.824	2.228	2.314	10.673	10.337	1.981	2.097
9	8.923	2.221	2.304	10.635	9.704	1.982	2.097
9.099	9.024	2.214	2.304	10.597	9.704	1.983	2.097
9.200	9.1240	2.206	2.294	10.558	9.65	1.984	2.097
9.299	9.225	2.199	2.284	10.520	9.651	1.986	2.097
9.400	9.324	2.192	2.284	10.482	9.598	1.987	2.0972
9.500	9.423	2.185	2.274	10.444	9.493	1.988	2.097
9.599	9.524	2.178	2.263	10.406	9.493	1.990	2.097
9.700	9.623	2.170	2.263	10.368	9.493	1.991	2.097
9.799	9.723	2.163	2.253	10.330	9.493	1.992	2.097
9.900	9.824	2.156	2.253	10.292	9.440	1.994	2.097
10	9.924	2.149	2.243	10.255	9.440	1.995	2.097
10.099	10.024	2.142	2.243	10.217	9.387	1.996	2.097

10.200	10.125	2.135	2.223	10.1796	9.387	1.997	2.097
10.299	10.223	2.128	2.223	10.142	9.282	1.999	2.0972
10.400	10.323	2.121	2.223	10.104	9.334	2.000	2.097
10.500	10.423	2.114	2.212	10.068	9.334	2.001	2.097
10.599	10.523	2.107	2.212	10.032	9.282	2.002	2.097
10.700	10.624	2.100	2.202	9.996	9.282	2.004	2.097
10.799	10.725	2.093	2.192	9.960	9.282	2.005	2.097
10.900	10.824	2.087	2.182	9.924	9.176	2.00	2.097
11	10.923	2.08	2.182	9.889	9.176	2.007	2.097
11.099	11.024	2.073	2.172	9.853	9.123	2.008	2.097
11.200	11.124	2.066	2.172	9.817	9.071	2.010	2.097
11.299	11.224	2.060	2.161	9.782	9.071	2.011	2.097
11.400	11.324	2.053	2.161	9.746	9.071	2.012	2.097
11.500	11.425	2.046	2.151	9.711	9.071	2.013	2.097
11.599	11.524	2.040	2.141	9.675	8.965	2.014	2.097
11.700	11.623	2.033	2.141	9.640	8.912	2.016	2.097
11.799	11.723	2.026	2.131	9.605	8.965	2.017	2.097
11.900	11.824	2.020	2.131	9.569	8.860	2.018	2.097
12	11.924	2.013	2.121	9.534	8.860	2.019	2.097
12.099	12.024	2.006	2.121	9.499	8.860	2.020	2.097
12.200	12.123	2	2.110	9.464	8.860	2.022	2.097
12.299	12.223	1.993	2.100	9.430	8.807	2.023	2.097
12.400	12.323	1.987	2.100	9.396	8.807	2.024	2.097
12.500	12.422	1.981	2.090	9.363	8.754	2.025	2.097
12.599	12.525	1.974	2.090	9.330	8.754	2.026	2.097
12.700	12.624	1.968	2.080	9.296	8.701	2.027	2.097
12.799	12.723	1.962	2.070	9.263	8.649	2.028	2.097
12.900	12.824	1.956	2.070	9.229	8.596	2.029	2.097
13	12.924	1.949	2.059	9.196	8.649	2.030	2.097
13.099	13.024	1.943	2.059	9.163	8.543	2.032	2.097
13.200	13.123	1.937	2.049	9.130	8.596	2.033	2.097
13.299	13.223	1.931	2.049	9.097	8.596	2.034	2.097
13.400	13.324	1.924	2.039	9.064	8.490	2.035	2.097
13.500	13.424	1.918	2.039	9.031	8.543	2.036	2.097
13.599	13.524	1.912	2.029	8.998	8.438	2.037	2.097

13.700	13.623	1.906	2.029	8.965	8.438	2.038	2.097
13.799	13.723	1.899	2.019	8.932	8.438	2.039	2.097
13.900	13.823	1.893	2.008	8.899	8.332	2.040	2.149
14	13.922	1.887	2.008	8.866	8.385	2.041	2.149
14.099	14.024	1.881	1.998	8.835	8.385	2.042	2.097
14.200	14.123	1.875	1.998	8.8042	8.332	2.043	2.097
14.299	14.225	1.869	1.988	8.773	8.332	2.044	2.097
14.400	14.324	1.863	1.988	8.7419	8.279	2.045	2.097
14.500	14.423	1.858	1.978	8.710	8.174	2.046	2.149
14.59	14.523	1.852	1.978	8.679	8.227	2.0479	2.149
14.700	14.624	1.846	1.968	8.648	8.174	2.048	2.097
14.799	14.724	1.84	1.968	8.617	8.227	2.049	2.097
14.900	14.824	1.834	1.957	8.587	8.121	2.050	2.097
15	14.924	1.828	1.957	8.556	8.1744	2.051	2.1498
15.099	15.023	1.823	1.947	8.525	8.121	2.052	2.097
15.200	15.124	1.817	1.937	8.494	8.068	2.053	2.097
15.299	15.224	1.811	1.937	8.463	8.016	2.05	2.149
15.400	15.323	1.805	1.927	8.433	8.016	2.055	2.097
15.5	15.423	1.799	1.927	8.402	7.963	2.056	2.149
15.599	15.524	1.794	1.917	8.372	8.016	2.057	2.097
15.700	15.623	1.788	1.917	8.341	7.963	2.058	2.149
15.799	15.723	1.782	1.906	8.311	7.963	2.059	2.149
15.900	15.824	1.776	1.906	8.280	7.857	2.060	2.149
16	15.924	1.771	1.896	8.250	7.910	2.061	2.149
16.099	16.022	1.765	1.896	8.219	7.857	2.062	2.149
16.200	16.124	1.760	1.886	8.190	7.857	2.063	2.149
16.299	16.223	1.754	1.886	8.162	7.805	2.064	2.1496
16.400	16.323	1.749	1.876	8.133	7.752	2.065	2.1498
16.500	16.423	1.743	1.876	8.104	7.752	2.066	2.1498
16.599	16.524	1.738	1.866	8.076	7.752	2.067	2.1498
16.700	16.623	1.732	1.866	8.047	7.699	2.068	2.149
16.799	16.723	1.727	1.855	8.018	7.699	2.069	2.149
16.900	16.823	1.722	1.855	7.990	7.699	2.070	2.149
17	16.922	1.716	1.845	7.961	7.646	2.071	2.149
17.099	17.024	1.711	1.845	7.933	7.646	2.071	2.149

17.200	17.123	1.706	1.835	7.904	7.594	2.072	2.149
17.299	17.222	1.700	1.835	7.8765	7.594	2.073	2.149
17.400	17.323	1.695	1.825	7.848	7.488	2.074	2.149
17.500	17.423	1.690	1.825	7.819	7.488	2.075	2.149
17.599	17.523	1.684	1.815	7.791	7.488	2.076	2.149
17.700	17.623	1.679	1.815	7.763	7.488	2.077	2.149
17.799	17.723	1.674	1.804	7.735	7.435	2.0782	2.149
17.900	17.824	1.668	1.8049	7.707	7.435	2.079	2.149
18	17.922	1.663	1.794	7.678	7.383	2.080	2.149
18.099	18.024	1.658	1.794	7.650	7.383	2.080	2.149
18.200	18.123	1.652	1.784	7.622	7.383	2.081	2.149
18.299	18.223	1.647	1.784	7.594	7.330	2.082	2.149
18.400	18.324	1.642	1.774351	7.568	7.383	2.083	2.149
18.500	18.424	1.637	1.774	7.542	7.277	2.084	2.149
18.599	18.524	1.632	1.764	7.515	7.277	2.085	2.149
18.700	18.623	1.627	1.764	7.489	7.277	2.085	2.149
18.7998	18.723	1.622	1.764	7.463	7.277	2.086	2.149
18.900	18.825	1.617	1.753	7.436	7.224	2.087	2.149
19	18.923	1.612	1.753	7.410	7.277	2.088	2.202
19.099	19.023	1.607	1.743	7.384	7.224	2.089	2.149
19.200	19.124	1.602	1.743	7.358	7.172	2.089	2.149
19.299	19.225	1.597	1.733	7.332	7.119	2.090	2.149
19.400	19.324	1.593	1.733	7.306	7.119	2.091	2.149
19.500	19.422	1.588	1.733	7.280	7.066	2.092	2.149
19.599	19.524	1.583	1.723	7.254	7.066	2.093	2.149
19.700	19.624	1.578	1.713	7.228	7.066	2.093	2.149
19.799	19.724	1.573	1.713	7.202	7.066	2.094	2.149
19.900	19.825	1.568	1.702	7.176	7.011	2.095	2.149
20	19.923	1.563	1.702	7.150	7.066	2.096	2.149
20.099	20.023	1.558	1.702	7.124	6.961	2.097	2.149
20.200	20.124	1.553	1.692	7.098	7.013	2.097	2.149
20.299	20.223	1.549	1.692	7.073	6.855	2.098	2.202
20.400	20.324	1.544	1.682	7.047	6.908	2.099	2.202
20.500	20.424	1.539	1.682	7.021	6.908	2.100	2.149
20.599	20.524	1.534	1.672	6.996	6.908	2.101	2.202

20.700	20.623	1.529	1.672	6.970	6.855	2.101	2.202
20.799	20.723	1.525	1.662	6.946	6.802	2.102	2.202
20.900	20.824	1.52	1.662	6.922	6.855	2.103	2.149
21	20.922	1.516	1.651	6.898	6.802	2.104	2.149
21.099	21.023	1.511	1.651	6.874	6.802	2.104	2.202
21.200	21.123	1.507	1.651	6.850	6.697	2.105	2.202
21.299	21.224	1.502	1.641	6.826	6.697	2.106	2.202
21.400	21.324	1.498	1.641	6.802	6.750	2.106	2.202
21.500	21.422	1.493	1.631	6.778	6.644	2.107	2.149
21.59	21.523	1.489	1.631	6.755	6.644	2.108	2.1498
21.700	21.624	1.484	1.621	6.731	6.644	2.108	2.149
21.799	21.724	1.480	1.621	6.707	6.697	2.109	2.202
21.900	21.823	1.475	1.611	6.683	6.644	2.110	2.149
22	21.923	1.471	1.611	6.660	6.591	2.111	2.149
22.099	22.023	1.466	1.611	6.636	6.539	2.111	2.202
22.200	22.125	1.462	1.600	6.613	6.591	2.112	2.202
22.299	22.224	1.457	1.600	6.589	6.539	2.113	2.149
22.400	22.324	1.453	1.600	6.565	6.539	2.113	2.202
22.500	22.422	1.448	1.590	6.542	6.539	2.114	2.202
22.599	22.523	1.444	1.590	6.518	6.43375	2.115	2.202
22.700	22.623	1.44	1.5806	6.495	6.433	2.115	2.202
22.799	22.723	1.435	1.580	6.472	6.433	2.116	2.202
22.900	22.824	1.431	1.570	6.448	6.433	2.117	2.202
23	22.922	1.426	1.570	6.425	6.381	2.118	2.149